Responsive Polymers for Dynamic Modulation of Bio-macromolecular Transport Properties

MASSACHUSETTS INSTITUTE OF TECHNOLOGY
SEP 10 2008
LIBRARIES

by

Smeet Deshmukh

B.S. Chem. Eng., University of Institute of Chemical Technology, Mumbai (2002)

M.S.C.E.P. Chem. Eng., Massachusetts Institute of Technology, Cambridge, MA (2004)

Submitted to the Department of Chemical Engineering in partial fulfillment of the requirements for the degree of

DOCTOR OF PHILOSOPHY IN CHEMICAL ENGINEERING

at the

MASSACHUSETTS INSTITUTE OF TECHNOLOGY

August, 2008

© Massachusetts Institute of Technology, 2008. All rights reserved.

Signature of Author.....
Department of Chemical Engineering
August 29, 2008

Certified by.....
T. Alan Hatton
Ralph Landau Professor of Chemical Engineering Practice
Thesis Supervisor

Certified by.....
Kenneth A. Smith
Gilliland Professor of Chemical Engineering
Thesis Supervisor

Accepted by.....
William M. Deen
Professor of Chemical Engineering
Chairman, Committee for Graduate Students

ARCHIVES

Responsive Polymers for Dynamic Modulation of Bio-macromolecular Transport Properties

by
Smeet Deshmukh

Submitted to the Department of Chemical Engineering on August 29, 2008 in Partial Fulfillment of the Requirements for the Degree of Doctor of Philosophy in Chemical Engineering

ABSTRACT

Responsive self-assembling polymers are used in wide range of applications in the food, pharmaceutical, agricultural, electronic and environmental industries, as well as in the biomedical field. The proper design of such polymers is critical for the particular applications being considered. In this thesis, different matrices that can be modulated dynamically by the application of appropriate stimuli were designed and used for two applications: electrophoretic separation and gene transfection.

Light represents an attractive trigger to change the properties of a polymer solution because it enables structural transitions to be induced under isothermal conditions without the addition of other chemical species to the solution, and is externally reversible and hence amenable to device design and automation. Amphiphilic copolymers with azobenzene moieties are of interest because the azobenzene can undergo reversible *trans-cis* photoisomerization leading to conformational isomers with significantly dissimilar dipole moments and hydrophobicities and thus different propensities to aggregate into nanoscale structures in aqueous media. Copolymers of 4-methacryloyloxyazobenzene (MOAB) and N,N-dimethylacrylamide aggregate strongly in aqueous solutions with concentration-dependent aggregate size distributions and well-defined boundaries between the dilute and semi-dilute regimes. The copolymers are strongly surface active, an uncommon observation for random copolymers, and exhibit pronounced photoviscosity effects at higher concentrations. *Trans*-to-*cis* isomerization under UV light leads to partial dissociation of the azobenzene aggregates that form physical crosslinks, thereby significantly affecting the polymer solution rheology, with a consequent ten-fold loss of viscoelasticity upon irradiation, especially in concentrated polymer solutions.

Photo-responsive poly(N,N-dimethylacrylamide-*co*-methacryloyloxyazobenzene) (MOAB-DMA) and temperature-responsive Pluronic F127 (PF127) copolymers were blended to obtain mixed micellar systems that were responsive to both stimuli. The azobenzene groups of DMA-MOAB in the *trans* conformation self-associate and the interactions with PF127 are less pronounced when compared to those with *cis* conformation of the azobenzene groups. The *cis*- isomer of the MOAB-DMA copolymer self-associates less strongly than does the *trans* conformation, and thus the copolymer micelles dissociate upon UV irradiation. These polymeric unimers can form mixed micelles with the PF127 present. This causes the sol-gel transition temperature of the MOAB-DMA/PF127 blend to be 2-6 degrees lower upon UV irradiation than under dark conditions depending on the molar ratio of the two polymers. It has been found that

aqueous blends of PF127 (20 wt%) and DMA-MOAB (5 wt%) possess a low viscosity at room temperature when equilibrated in the dark and undergo a sol-gel transition when UV irradiated, with a 1000-fold viscosity increase. Such a transition strongly alters the transport properties of solutes such as proteins, DNA and the like within the polymer solutions. The electrophoretic mobility of proteins was measured in both the sol and the gel state obtained in dark and under UV irradiation, respectively. A fifty to seventy percent decrease in the electrophoretic mobility was obtained by UV irradiation responsive gelation, depending on the size of the protein molecules. Dynamic changes in the aggregation behavior of photoresponsive polymers enable novel opportunities for the control of viscosity and transport properties for the polymer solutions to be used as a matrix in separation processes. The binary protein mixture separations that were carried out in dynamically modulated electrophoresis experiments were found to have improved resolution as compared to the conventional electrophoresis operations. The improvement in resolution and yield, which depends on three dimensionless parameters, can be predicted using numerical simulations if the operating conditions, electrophoretic mobility of solutes and the change in electrophoretic mobility on gelation are known.

A facile, one-step synthesis of cationic block copolymers of poly(2-*N*-(dimethylaminoethyl) methacrylate) (pDMAEMA) and copolymers of poly(propylene oxide) (PPO) and poly(ethylene oxide) (PEO) has been developed. The PEO-PPO-PEO-pDMAEMA (L92-pDMAEMA) and PEO-pDMAEMA copolymers were obtained via free radical polymerization of DMAEMA initiated by polyether radicals generated by cerium(IV). Over 95% of the copolymer fraction was of molecular mass ranging from 6.9 to 7.1 kDa in size, indicating the prevalence of the polyether-monoradical initiation mechanism. The L92-pDMAEMA copolymers possess parent surfactant-like surface activity. In contrast, the PEO-pDMAEMA copolymers lack significant surface activity. Both copolymers can complex with DNA. Hydrodynamic radii of the complexes of the L92-pDMAEMA and PEO-pDMAEMA with plasmid DNA ranged in size from 60 to 400 nm, depending on the copolymer/DNA ratio. Addition of Pluronic P123 to the L92-pDMAEMA complexes with DNA masked charges and decreased the tendency of the complex to aggregate, even at stoichiometric polycation/DNA ratios. The transfection efficiency of the L92-pDMAEMA copolymer was by far greater than that of the PEO-pDMAEMA copolymer. An extra added Pluronic P123 further increased the transfecton efficacy of L92-pDMAEMA, but did not affect that of PEO-pDMAEMA.

Thesis Supervisor: T. Alan Hatton
Title: Ralph Landau Professor of Chemical Engineering Practice

Thesis Supervisor: Kenneth A. Smith
Title: Gilliland Professor of Chemical Engineering

Acknowledgements

I would like to express my gratitude to all those who have helped me to get to this stage. I am grateful to my advisors T. Alan Hatton and Kenneth A. Smith for giving me the opportunity to work in their group. Alan has helped me become a better researcher by letting me explore my ideas. I would also like to thank my thesis committee members, Prof. William Deen, Prof. Patrick Doyle and Prof. Daniel Wang for all of their contributions during my committee meetings.

I am highly indebted to Dr. Lev Bromberg for his help with my research and for lending his time and effort for discussing my research problems even amidst his long lists of other commitments. I would also like to thank Hatton group members past and present for their help. In particular, I would like to thank Lino Gonzalez for imparting me some of his knowledge of optics and Comsol, and Sanjoy Sircar and Huan Zhang for timely discussions. I am also grateful to Harpreet, Saurabh and Abhinav for all their help and chats, which were a good break from research and how could I not mention: allowing me to gorge on their home-made food. I want to extend my thanks to my collaborators Prof. Carmen Alvarez-Lorenzo and her group from Universidad de Santiago de Compostela and Dr. Valery Alakhov from Supratek Pharma Inc.. I am also appreciative of McKinley group members for allowing me to use their lab for rheological measurements.

Most importantly I would like to thank my father Prakash Deshmukh and my mother Sunanda Deshmukh without whom I would not be here. My special thanks to Shobhit Gupta for his unconditional love and support. I owe him big time for all those moments he helped me to hold it together when I felt completely lost. I would also like to extend my thanks to my friends at MIT: Anamika, Kishori, Malancha, Vikrant, Saikat, Yamini, Vijay, Vivek, Siddharth, Anjali, Manu, Jagmeet and Sushil for being there for me when I needed them. I also want to thank Janet Fischer whom I met on the very first day here as my International Student Host and since then she has always watched out for me during my stay at MIT.

Table of Contents

List of Figures

List of Schemes

List of Tables

Chapter 1

Introduction

1.1 Motivation and Approach

The self-assembly of synthetic polymers has attracted attention in research for varied applications from semiconductor microelectronics,[1] thin films,[2] separations, pharmaceuticals, and biotechnology application.[3] The ordered self-assembly of proteins, DNA and biomembranes has been known for a while but this is not the case with synthetic polymers, until recently. Synthetic polymers, generally, do not show definite folding structures in solution. Polymer chains assume random coil or simply extended conformations prevalently when dissolved in solvents. Self-assembly of polymers can take place due to associations formed by electrostatic interactions, hydrophobic interactions, or hydrogen bonding. Studies by Morishima et al.[4] and Akiyoshi et al.[5] clearly demonstrate that linear polymers with hydrophilic main chains and suitably-substituted hydrophobic side chains can assume compact conformations having definite molecular sizes and shapes leading to further exploration of such self-assembling polymers. The self-assembly of polymers can be brought about by change in concentration or by applying external stimuli. Self-assembling polymers are very popularly used in research as encapsulation vehicles for gene and drug transfection.[6] The proper design of such polymers is critical for improving the transfer/transfection efficiency and form focus of many researches.[6]

Stimuli-responsive polymers which can self-assemble in response to external stimuli, such as pH, temperature, light, electric and magnetic field, have caught attention for a decade now. These materials have wide applications in various fields such as food, pharmaceutical, agricultural, electronic and environmental industries, as well as in biomedical engineering. Photoresponsive polymers have attracted considerable interest [7,8,9,10,11] because light as an external stimuli can be controlled remotely, changed rapidly, and it is clean compared with traditional stimuli such as temperature, pH, electric field,

and ionic strength.[12,13,14,15] Azobenzene-containing photoresponsive polymers especially have been widely investigated due to their potential applications.[16,17,18,19]

Azobenzene derivatives are the most widely used chromophores alongwith stillbene. It is well known that azobenzene chromophores undergo photoinduced trans-cis isomerization under UV irradiation, while the reverse cis-trans isomerization can be induced photochemicallly or thermally. [20,21,22,23,24] Accompanied by the isomerization, both the molecular dimension and the dipole moment change dramatically. This has led to the use of azobenzene derivatives as photoresponsive "triggers" for controlling macroscopic properties of surfactants[25] and polymers[21,24,26] When azobenzene chromophores are incorporated into polymers as pendant groups, the conformational change of azobenzene would produce a concomitant change in polymer properties both in solution and bulk solid sates. [26] The change in physical properties especially viscosity upon irradiation is of importance in applications such as drug delivery, paints and separation. The change in viscosity upon irradiation termed as photoviscosity effect has been seen in various synthesized polymers with azobenzene as photoresponsive moiety.[79,80] Most of these polymers are shown to have photoviscosity effect in organic solvents such as dioxane, N,N-dimethylacetamide and THF. Very few photoresponsive polymers have been synthesized which showed photoviscosity effect in aqueous medium. There is a potential need for amphiphilic photoresponsive polymers showing few orders of magnitude viscosity changes upon irradiation which could be potentially used as a matrix for delivery and separation processes requiring aqueous medium.

There is an increasing need for the microscale separation and purification of products from microreactors used for their synthesis, and for the separation of compounds to be fed to microscale systems for analysis. Such microscale devices are an attractive option for separations whenever small quantities of specialty materials must be produced or analyzed. Gel electrophoresis and size exclusion chromatography are two separation methods that could be exploited effectively in such microscale separations, and could benefit from the development of tailored gel media that can be readily modified for specific applications. In addition, such gelation on demand can be exploited in the loading of the separation media in the microchannel, since low viscosity polymer solutions can be fed to the system, and subsequently caused to gel in-situ, thereby

avoiding the need for the pumping of viscous gel material into the small radius channels. The traditional electrophoresis requires modifying the proteins by interacting with other surfactants like SDS for separation leading to denaturation of proteins. It will be of significant advantage if the separation can be enhanced by modifying the matrix instead of solutes/proteins. Finally, the properties of responsive gels could be exploited in the dynamic tuning of the gel structure at different points within the channel in real time to aid to the focusing and enhance the resolution of protein separations. These processes would benefit from the use of imaging and feed-back control to help sharpen the separation processes as seen in Scheme 1-1 .

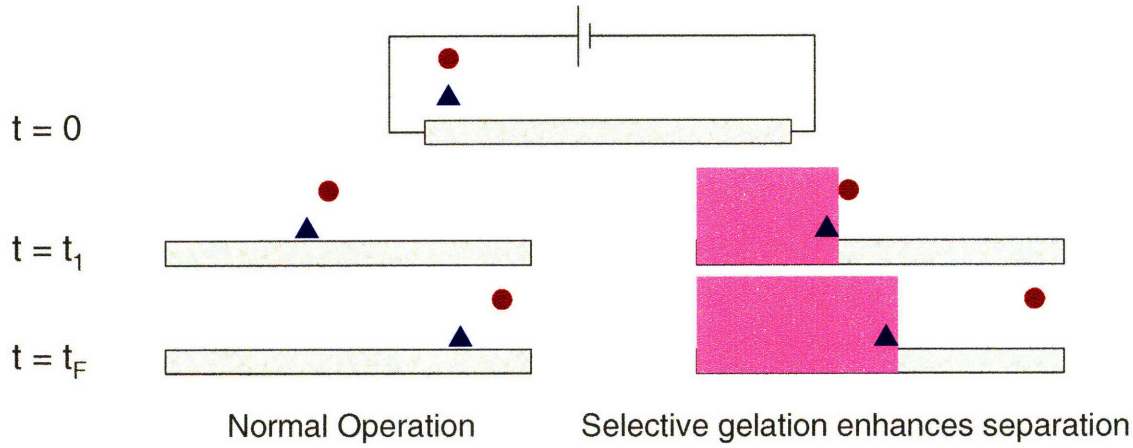

Scheme 1-1: Schematic of dynamic modulation of matrix for selective gelation for enhanced separation

The miniaturized or so-called "lab on a chip" chemical and biological separation and analysis systems enable vast improvements in their performance both in terms of the speed and in throughput, in comparison with the more traditional "full size" instrumentation.[27] Perhaps the most striking example of these improvements is the success of capillary electrophoresis (CE) in speeding up the sequencing of the first human genome project.[28] This accomplishment would have required many more years with traditional full-size slab-gel technology. The high speed, fast analysis time, resolution of the capillary electrophoresis has led to this accomplishment. The advancement of the DNA electrophoresis from slab-gels to capillary arrays represents the first step in a biotechnological revolution, which will be driven by the miniaturization of biochemical analysis platforms, in particular based on integrated micro-fluidic devices or

chips made from glass or plastic.[29,30] Miniaturized chemical and biological analysis platforms promise to serve as critical enabling technologies for the revolution in genomic and proteomic sciences, as well as in the development of sensors for chemical and biological defense. Reduction of size offers many anticipated advantages such as reduced costs, faster transport mechanism, and equivalent or perhaps improved sensitivity of the mini-sensors. The design and fabrication of the hardware and detection systems for these devices are rapidly maturing. However, the matrices for miniaturized devices are lagging behind the hardware design. Just as the astounding success of capillary electrophoresis in the human genome project was enabled to perform optimally, further miniaturized systems will require the design of materials specifically adapted for their unique features. The materials that engendered excellent performance in slab-gel electrophoresis fail in capillary-based systems.[31] Similarly, materials that are designed for high performance capillary-based systems lead to suboptimal performance in microscale systems. Full realization of the high through put and cost-saving potential of microscale systems for proteomics, genomics, sensing applications will require the development of novel, smart polymeric materials fashioned specifically for these systems.

There is a need for the development of separations media that can be easily tuned for specific applications, and regenerated. For example, when dealing with large-scale separations, it is desirable to recycle surfactants or polymers in a surfactant/gel-based separation processes, both for environmental and for economic reasons. For microscale separations, the capability to tune the separation media will permit multiple stages of separation (and thus high selectivities) to be achieved. Thus, a system in which separation media or matrices can be tuned through the manipulation of an easily controlled external variable such as temperature, an applied potential, or light, will likely be of broad utility. It would be necessary for such tunable gels to maintain their volume while changing structure, which generally cannot be anticipated for chemically cross-linked gels. In many cases physical gels do not shrink when undergoing internal structural rearrangement. There is no need for surface modification of the microchannel when sol-gel matrices are utilized.[32] Duke et al[33] showed that physical gels serve as better sieving media than chemically cross-linked gels as the separation limit for physical gels is higher than that of chemical gels for nucleic acids. As for high molecular weight molecules,

chemically cross-linked gels cannot separate molecules on basis of molecular weight. Physical gels can extend the range of fractionation, and separation limits can be extended by a factor of up to 10, or more.[33]

1.2 Photoresponsive Polymers

A photoresponsive polymer is a kind of functional polymer having photoreceptor chromophore, which can transfer the photoenergy into conformational change in polymer. The light is initially stored as chemical structure change of the chromophores and then transferred into the polymer chain, causing reversible conformation changes. The conformational change in azobenzene contained in the polymer should produce a concomitant change in physical and chemical properties of the polymer solutions and solids. This is the underlying concept behind controlling polymer chemical or physical properties by photoirradiation using the photoresponsive trigger molecules.

Many molecules, such an azobenzene [21,22,23,34], stilbene,[35,36,37] spiropyran, [34,3839] and triarylmethane[40] can be transformed into other isomers under photoirradiation. On the other hand, they can also return to the initial state thermally or photochemically. These isomerizations are termed as photochromisms. Among the many compounds available, azobenzene is the most frequently used chromophore for photoresponsive polymers.

1.2.1 Azobenzene

Azobenzene and its derivatives are compounds with the characteristic double bonded –N=N- functional groups. The stereochemistry of the double bond generally has profound consequence on the properties of molecules. It gives the molecule more rigidity and imposes geometrical restriction on the molecule, a flatness or planar configuration upon the double bond.

Azobenzene dye exists in two isomeric states, a thermodynamically stable *trans* and a metastable *cis* state. The energy difference between the ground states of the *trans* and *cis* isomers of azobenzene is about 50kJ/mol showing that *trans* form

thermodynamically stable.[23] When irradiated with light of appropriate wavelength, the azobenzene chromophores undergo a reversible *trans-cis-trans* isomerization process. The energy absorbed at a particular wavelength by the azobenzene chromophores take them to an electronically excited state. Then the excited state goes back to the ground state either in the *cis or trans* configuration through non-radioactive decay. The metastable *cis* state isomerizes to the *trans* state either by a spontaneously thermal process or a reverse *cis-trans* photoisomerization cycle. Since the *trans* state is more stable, the *cis* state can thermally isomerizes back to the *trans* state. Normally, the thermal *cis-trans* reconversion takes place without any irradiation and this process is significantly slower (orders of magnitude) than the photo reconversion isomerization.[41,43]

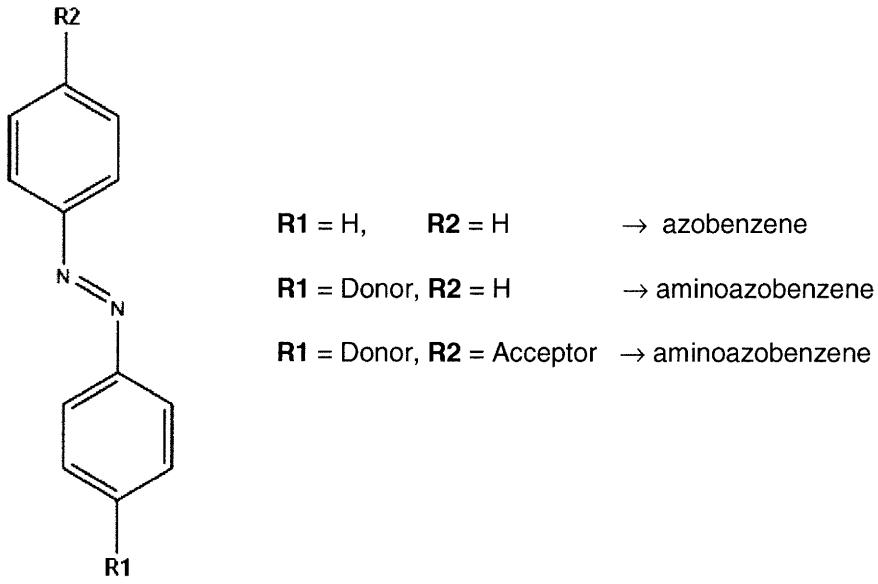

Figure 1-1: Classification of azobenzene derivatives

Azobenzene chromophores can be classified into three types based on the energetic ordereing of (n,π*) and (π,π*) states: azobenzene type, aminoazobenzene type and pseudo-stilbene type, as illustrated in Figure 1-1. [42,43,44] Azobenzene type molecules display a low intensity n-π* band in the visible region of the spectrum and a high intensity π-π* in the UV region. Amino-azobenzene type molecules are characterized spectroscopically by a close or overlapped n-π* and π-π* band in the violet or near-

visible UV region. Pseudo-stilbene type molecules, a type of the azobenzene molecules with electron-sonor and electron-acceptor (push/pull) substituents aat 4 and 4' positions, have a long wavelength π-π^* band and the sequence of (n-π^*) and (π-π^*) states are reversed on the energy scale, which is similar to stilbene.

1.2.2 Photoisomerization of Azobenzene

There are three main associated changes that take place with photoisomerization of azobenzene.[21,24]

a) A change in the absorption profile: The *trans-cis* isomerization causes a decrease in the absorption at 320nm owing to π-π^* transition.
b) A change in molecular dimension: The distance between the 4- and 4'- carbons is shortened from 9.0 A° to 5.5 A° by isomerization from the *trans* to the *cis* state, as shown in Figure 1-2.
c) A change in dipole moment. The dipole moment changes from 0.5 D (*trans*) to 3.1D (*cis*).

These photoinduced configuration changes can significantly influence the bulk and surface properties of polymers containing azobenzene chromophores. Therefore, they are of utmost value in probing conformational dynamics of macromolecules by site-specific photo-labeling, in estimating the free volume in cross-linked networks and in designing photoreactive polymers responsive to external stimuli.

Even though the isomerization of azobenzene groups has been subject of many studies, the mechanism of photoisomerization and the thermal isomerization of azobenzene are still not fully understood. The isomerization mechanism has been investigated since the early 1950s. [23] It was first suggested that the azobenzene groups isomerizes by rotation around the –N=N- bonds.[45] In this process, the π-bond is broken homolytically or heterolytically, as a result of which part of the azobenzene groups may freely rotate around the –N=N- axis. [46,47,23]

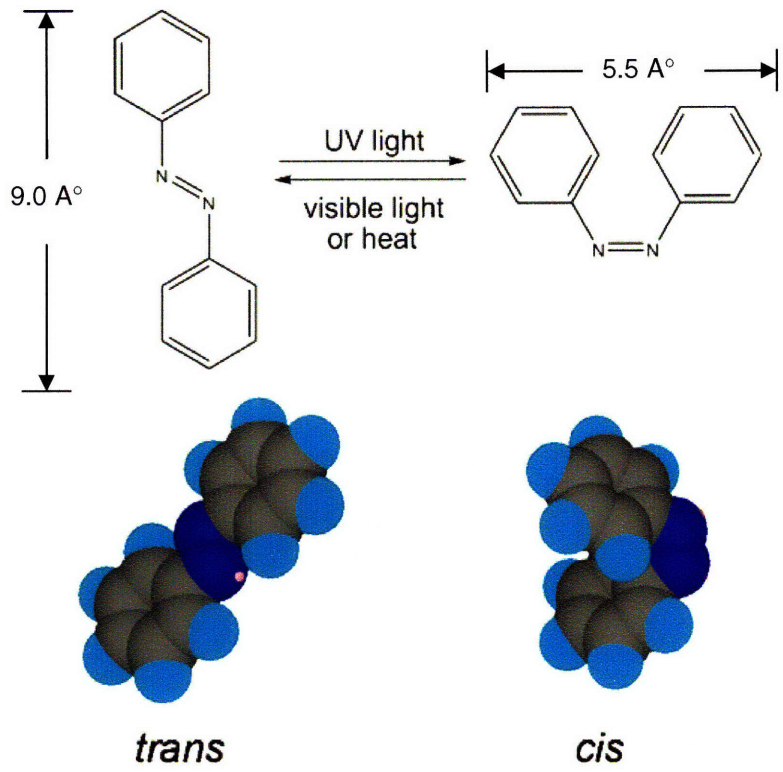

Figure 1-2: Structural geometry changes of azobenzene upon trans-cis isomerization[21]

An alternative mechanism was later where the isomerization of azobenzene group occurs via the inversion of one or both of the nitrogen through a linear *sp*-hybridized transition state in which the double bond is retained.[48,49,50] The essential difference between the two mechanisms is that the rotation mechanism proceeds via a dipole transition state accompanying a large volume change, where the inversion mechanism requires only a local movement involving hydridization of the nitrogen atom. In general, it is evident both experimentally [50] and theoretically[51,52,53] that the thermal *cis-trans* isomerization of azobenzene proceeds via the plane inversion mechanism[54] and both the inversion and rotation mechanism. [42] Rotation and inversion pathways of the *trans-cis-trans* isomerization of azobenzene groups are illustrated in Figure 1-3. The debate related to the interpretation of the mechanism is not settled and further research is carried out in this area.[53,54,55,56,57]

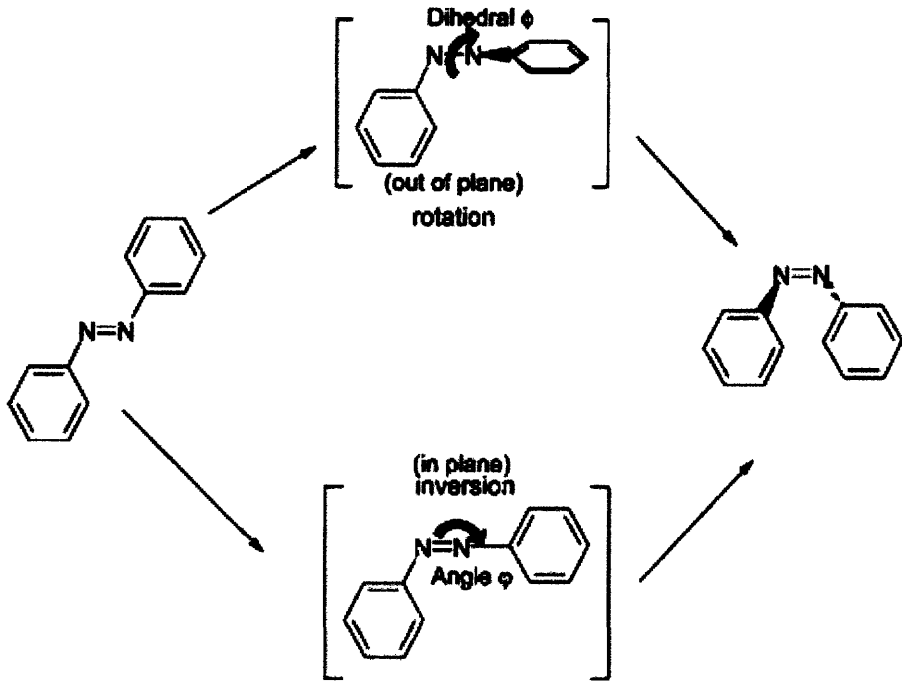

Figure 1-3: Schematic diagram of the rotation and inversion pathways of the trans cis isomerization of azobenzenes. The rotation pathway is obtained by a torsion of the azo group around the CNNC dihedral angle. The inversion pathway is obtained by an in-plane inversion of the NNC angle (angle) formed between the azo group and the attached carbon of one of the benzene rings.[58]

1.2.3 Photochemical and Thermal Isomerization of Azo Polymers

Azo polymers have attracted considerable interests in the past decade due to their various potential applications, such as photonics,[59,60] optical information storage systems[61,62] and surface relief gratings.[63] Recently, match attention has been paid to photo-switchable biomaterials for the development of optobioelectronic devices. [64,65]

The isomerization rate of *azo* polymers depends not only on the chemical structure of the azobenzene chromophores but also on the properties of polymer matrices, such as the type of attachment of the chromophores to the polymer backbone, glass transition temperature, crystalline order, etc.[21,43] It has been shown that the isomerization rate in solutions is very sensitive to the local microenvironment surrounding the

azobenzene groups, such as the polarity of the solvent, as well as the polymer concentration.[23,66,67]

The steric effect is an important factor that affects the isomerization of azobenzene moiety. Morishima et. al.[68] studied the photoisomerization of amphiphilic polyelectrolytes, in which the azobenzene moieties were compartmentalized in hydrophobic microdomains. The concentration of the polymer was kept such that there were no chromophore-chromophore interactions. It was demonstrated that the compartmentalization of azobenzene moieties significantly impedes the *trans-cis* photoisomerization as a result of compartmentalization owing to the motional restriction imposed on the *trans* isomers in the hydrophobic domains. These steric effects on the isomerization rate depend on the hydrophobic groups surrounding the azobenzene moieties. The steric constraint decreases in the order of cyclodecyl > adamantly > lauryl. Badjic et. al.[69] studied the photoisomerization kinetics of azobenzene and its derivatives within SDS and CTAB micelles. It was seen that the kinetics of azobenzene isomerization depends on electronic and steric properties of the molecules and on the environment in which the molecules are held. To this effect it was found that the isomerization is faster in solution than within micelles. It is also shown that azobenzenes are capable of undergoing isomerization in highly viscous solutions, liquid crystals, condensed monolayers, micellar solutions, polar solvents and even solids.[70,71,66,43]

1.3 Photoresponsive Behavior of Azo Polymers

When azobenzene chromophores are incorporated in the main chain or as a side chain of the polymers, the conformational changes of azobenzene induced by the isomerization will produce a concomitant change in chemical or physical properties of the azo polymers both in solution and in solid states. Table 1-1 lists the properties of azo polymers that can be controlled by photoirradiation.

Table 1-1: Physical and chemical properties of azo polymers controlled by azo photo-irradiation[26]

Solution	Solid
Viscosity	Membrane potential
pH	Membrane permeability
Solubility	Surface wettability
Metal ion capture	Shape
Capability	Miscibility of polymer blend

1.3.1 Photostimulated effects

Aggregation may be formed between azobenzene moieties in the presence of water, through hydrophobic interactions and ordered stacking of azo groups. [72,73,74,75,76] These interactions are favored in dark-adapted samples as *trans* azobenzene moieties are planar and hydrophobic. Light induces the disaggregation process, as *cis* form is more polar and not planar,[77] thus inhibiting the associative conditions. Therefore, it is likely that the different polarity and the different geometry between the *trans* and the *cis* form of the azo moieties provide the driving force for the photoinduced aggregation-disaggregation process.[78]

The viscosity of a polymer system is a direct reflection of the polymer conformation. The constitution of polymers containing azobenzene in the backbone suggests that these polymers would behave like semi-flexible rods in solution. The extended rod-like shape of the semi-flexible chain is expected to shrink rapidly to a compact conformation when the configuration of the constituent azobenzene units changes from *trans* to the *cis* form. This results in the change in viscosity of polymer solutions and is termed as the photoviscosity effect.[79] Figure 1-4 illustrate the conformational changes of polymer chains using photochromic chromophores as a tool. The mechanism utilizes the change induced in the intramolecular interaction between pendant groups by photoirradiation.

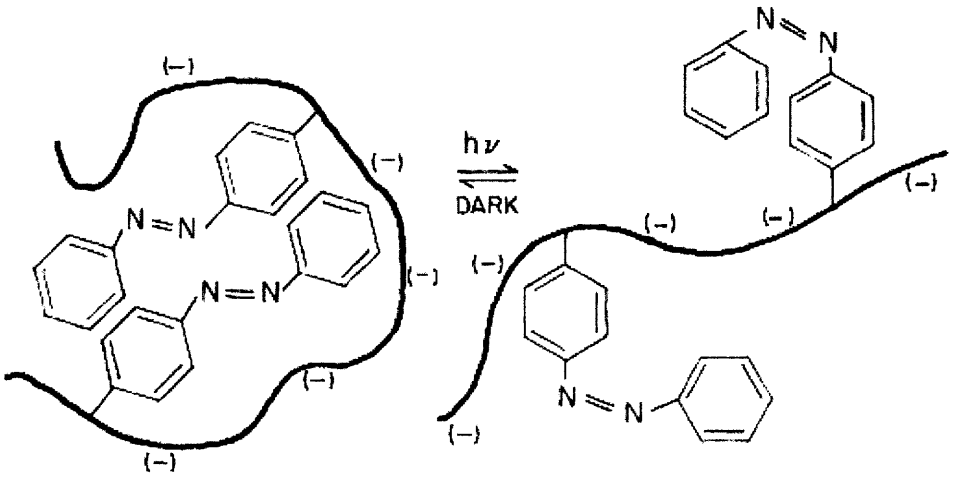

Figure 1-4: Schematic illustration of photostimulated conformational changes of polymer chains. Light energy decreases hydrophobic interaction, allowing an extension driven by coulombic repulsion (polymer being polyelectrolyte).[79]

This system of poly(methacrylic acid) with pendant azobenzene groups developed by Lovrein[79] was first to report the photoviscosity effect. In an aqueous solution, the viscosity increases by UV irradiation by about 20 percent. However, another study of a styrene-maleic anhydride copolymer with pendant azobenzene groups showed that the reduced viscosity decreased by 24-30% in dioxane solution after irradaiation with UV light.[80] Fernando et. al. investigated the photoviscosity effect of azobenzene modified poly (methylmethacrylate) copolymers in dimethylsiloxane (DMSO) solutions. A decrease of 77% of the reduced viscosity is observed after UV irradiation. The majority of previous publications on photoviscosity of azobenzene have focused on the effect of these functional groups in the polymer backbone. Irie and co-workers[81] synthesized a range of polyamides containing azobenzene groups in the backbone. All of the polyamides exhibited a degree of the photoviscosity effect. They reported a 60% specific viscosity reduction due to irradiation ($410 > \lambda > 350$ nm) of a solution in *N,N'*-dimethylacetamide. The authors investigated the influence of spacer groups in the polymer backbone and speculated that the magnitude of the photoinduced change in the viscosity decreases with the addition of flexible units such as methylene chains. Kumar and co-workers investigated a range of polyureas[82] with azobenzene groups in the

polymer backbone in DMSO at 35° C. The intrinsic viscosity was found to be about 30% lower during UV irradiation (410 > λ > 350 nm) than in the dark. The photoviscosity change was attributed to a conformational change of the polymer chain rather than interchain interactions. A study of similar polyureas was performed in DMSO at 30°C,[83] with the intrinsic viscosity reported to be about 40% lower during UV irradiation than in the dark.

1.4 Electrophoresis

Electrophoresis has been regarded as a powerful technique for the separation of charged macromolecules such as proteins based on its charge and size.[84] Electrophoresis offers high selectivity, high resolution and low cost options compared to existing techniques such as fractional precipitation and liquid chromatography, which require expensive media and reagents.[85]

1.4.1 Development in Electrophoresis

Different types of chromatography methods have been used for separation of proteins for a long time.[86] Chromatographic separations are based on interaction of an analyte with the surface of a stationary phase. However, proteins are amphiphilic and thus often surface-active molecules. They also display poor mass transfer kinetics during the chromatographic process. As a consequence, resolution is often less than desired, protein recovery may be low, and native protein may be denatured during the chromatographic process. The other alternative, which parallels chromatography, is slab-gel electrophoresis, taking into account the charged nature of the protein. But it also has its own disadvantages. It is laborious and time-consuming technique requiring preparation of gel, separation of the sample, staining and de-staining and gel-drying. The gel staining with a dye or stain may occur in a non-linear fashion, i.e., the intensity of the stained bands may be poorly correlated with the protein amount. Also, the joule heating caused by the electric field leads to band broadening and hence, low resolution. Consequently, capillary electrophoresis technique has been developed, which combined

the aspects of both gel electrophoresis and high performance liquid chromatography (HPLC). The shorter length of the capillary as compared to the slab-gel electrophoresis reduced the separation time. The capillaries of about 100-300 μm in diameter were able to effectively dissipate the energy (joule heating). This led to a large increase in the overall resolution of the separation. The use of capillaries simplifies detection and process automation, making it more quantitative and reproducible.

The efforts to adapt gels to the capillary format have been due to the gels' high resolving power compared to polymer solutions.[87] Disadvantages of these gel-filled columns include a short lifetime, low reproducibility, and poor detection sensitivity due to high UV absorption of the gel matrix. Also, the loading of the gels onto the capillary is quite difficult. A further miniaturization of the capillary format to microchannel would reduce joule-heating effect, further increasing the resolving power. The separation time in microchannel would be further reduced. The problem of the gel loading can be solved by replacing the permanent gels by responsive physical gels.

1.4.2 Matrices in different electrophoresis

For many years, electrophoresis was performed in a macroscopic slabgel format, and permanent gels such as agarose or acrylamide were used successfully for sieving. The first attempts to separate DNA by CE used capillaries filled with gel (e.g., agarose or cross-linked polyacrylamide), which was a natural adaptation of slab-gel electrophoresis to a capillary system. In spite of their excellent size selectivity, these media present serious disadvantages. Firstly, gel polymerization in the capillary involves a change in volume, which can bring about inhomogeneities, gel breakage and formation of air bubbles. In addition, gels or buffers can be degraded by hydrolysis, especially at the alkaline pH used for biopolymer separations. This leads to short-lasting gel-filled capillaries, that rarely survive more than 100 injections. The idea of substituting gel-based matrices with physical gels or solutions of (uncross-linked) polymers was fundamental for the progress and the establishment of CE as a convenient, cost reduced alternative to slab-gel electrophoresis. The very efficient heat dissipation and anticonvective properties of thin capillaries allows separation in fluids using high fields (typically 200–300 V/cm), without loss of resolution, and permanent gels are not required

anymore to prevent convection. As mentioned above, however, a sieving effect remains mandatory for most applications: polymers in solution can, in suitable conditions, act as obstacles to the migration of analytes, and provide such sieving, while avoiding most of the problems raised by permanent gels. The question of analyte-matrix interaction is at the heart of electrophoresis.

1.5 Thesis Overview

The overall goals of this research were to i) design and prepare matrices with objectives of proper encapsulation of DNA for gene transfection and for responsive photoviscosity effect ii) study the solute transport properties through the photoresponsive matrix and iii) dynamic modulation of the matrix for separation of solutes Chapter 2 details the preparation of amphiphilic nonionic photoresponsive polymer. Photokinetics and photoviscosity effect in aqueous medium were studied. Chapter 3 contains interaction of synthesized photoresponsive polymer with well-known thermoresponsive Pluronic polymeric surfactant. The effect of irradiation on the interaction was studied on their physical blends. Chapter 4 deals with solute transport properties through the physical blends of polymer. The models are considered to understand the change in the transport properties with the change in matrix physical psroperties. Chapter 5 entails the dynamic separation of solutes by modulating the matrix properties. Chapter 6 outlines details of synthesis of polycationic Pluronic polymer. Self-assembling properties and transfection efficiencies of this polymer were studied.

1.6 References

1. T. Thurn-Albrecht et al., "Nanoscopic Templates from Oriented Block Copolymer Films," Advanced Materials 12, 787 (2000).
2. Hammond, P.T., Whitesides, G.M., Macromolecules; 1995; 28(22); 7569-7571.
3. Naka. K., Ohki, A., Maeda, S., Chem. Lett. 1991, 1303
4. Morishima,Y., Nomura, S., Ikeda, T., Seki, M., and Kamachi, M., Macromolecules; 1995; 28(8) pp 2874 - 2881;

5. Akiyoshi, K., Deguchi, S., Moriguchi, N., Yamaguchi, S., and Sunamoto, J.,Macromolecules; 1993, 26(12) pp 3062 - 3068
6. Kwon, G.S., and Kataoka, K., Block-copolymer micelles as long-circulating drug vehicles, Adv. Drug Deliv. Rev. 16 (1995), pp. 295–309.
7. Suzuki, A. and Tanaka, T. (1990) Nature 346, pp. 345-347.
8. Mamada, A., Tanaka, T., Kungwatchakun, D. and Irie, M. (1990) Macromolecules 23 , pp. 1517-1519.
9. Juodkazis, S., Mukai, N., Wakaki, R., Yamaguchi, A., Matsuo, S. and Misawa, H. (2000) Nature 408, pp. 178-181.
10. Lee, H., Pietrasik, J. and Matyjaszewski, K. (2006) Macromolecules 39 , pp. 3914-3920.
11. Sumaru, K., Ohi, K., Takagi, T., Kanamori, T. and Shinbo, T. (2006) Langmuir 22 , pp. 4353-4356.
12. Xia, Y., Yin, X., Brurke, N. A. D. and Stoever, H. D. H. (2005) Macromolecules 38, pp. 5937-5943.
13. Zhang, H. and Ruehe, J. (2005) Macromolecules 38, pp. 4855-4860.
14. Lokuge, I. S. and Bohn, P. W. (2005) Langmuir 21, pp. 1979-1985.
15. Gallyamov, M. O., Tartsch, B., Khokholov, A. R., Sheiko, S. S., Boerner, H. G., Matyjaszewski, K. and Mller, M. (2004) Macromol. Rapid Commun. 25, pp. 1703-1707.
16. Shimoboji, T., Larenas, E., Fowlor, T., Kulkarni, S., Hoffman, A. S. and Stayton, P. S. (2002) Proc. Natl. Acad. Sci., USA. 99, pp. 16592-16596.
17. Pieroni, O., Fissi, A., Angelini, N. and Lenci, F. (2001) Acc. Chem. Res. 34, pp. 9-17.
18. Durr, H. and Bouas-Laurent, H. (1990) Photochromism: Molecules and Systems Elsevier , Amsterdam
19. Yuan, W., Jiang, G., Wang, J., Wang, G., Song, Y. and Jiang, L. (2006) Macromolecules 39, pp. 1300-1303.
20. Zimmerman, G., Chow, L, and Park, U., The photochemical isomerization of azobenzene, Journal of the American Chemical Society, 1958, 80(14),3528-3531.

21. Kumar, G. S., and Neckers, D.C., Photochemistry of azobenzene containing polymers, Chem. Rev., 89(8),1915-1925.
22. Kumar, G. S., Azo-functional polymers: functional group approach in macromolecular design, 1993, Lancaster, Basel, Technomic Publishing Co. Inc., 19-115.
23. Rau, H., Photoisomerication of azobenzenes, In J.F.Rabeck (Ed.), Photchemistry and photophysics, Boca Raton, FL: CRC, 1990, 2,119-141.
24. Irie, M., and Ikeda, T., Photoresponsive polymers. In K.Takemaoto P.M. Ottenbrite, M. Kamachi (Eds.), Functional monomers and polymers, New York: Marcel Dekket, 1997, pp. 665.
25. Shang, T., Smith, K.A, Hatton, T.A., Photoresponsive surfactants exhibiting unusually large,reversible surface tension changes under varying illumination conditions, Langmuir, 2003, 19 (26), 10764-10773.
26. Irie, M., Photoresponsive polymers: reversible control of polymer confirmation in solution and gel phase. In C.B. Mcardle (Ed.) Applied Photochromic Polymer Systems, Glasgow, Blackie, New York,
27. Ramsey, J.M, Nat Biotechnol. 1999, 17, pp. 1061-1062.
28. Lander, E.S., Linton, L.M., Birren, B., Nusbaum, C., Zody M.C., Baldwin, J., Devon, K., Dewar, K., Doyle, M., FitzHugh, W, Nature, 2001, 409, 860-921.
29. Sunderberg, S., Kopf-Sill, A., Nagle, R., Gallagher, S., Chow, C., Wada, G., Nikoforov, T., Parce, J.W., Am Lab 30, 1998, pp.22.
30. Sassi, A.P., Paulus, A., Cruzado, I.D., Bjornson T., Hooper, H.H., J. Chromatogr. 2000, A 894, 203-217.
31. Sartori, A., Barbier, V.,. Vivoy, J.L., Electrophoresis, 2003, 24, 421-440.
32. Rebecca, A., Zangmeister, K, Tarlov, M.J., Langmuir, 19 (17), 6901 -6904, 2003.
33. Duke T. et al, Viovy J.L., Physical Review E, vol.49, 3, 1994
34. Pieroni, O., Fissi, A., and Popova, G., Photochromic polypeptides. Progress in Polymer Science, 1998, 23, 81-123.
35. Peeler, A.M., Mahadevan, S., Hoyle, C.E., and D. Creed. Polym. Prepr., 1999,40,pp. 540
36. Yu, D., and Yu, L., Polym. Prepr., 1994 , 35,pp.32.

37. Likhtenshtein, G. I., Bishara, R., Papper, V., Uzan, B., Fishov, I., Gill, B., and Parola, A.H., J. Biochem. Biophys. Methods, 1996, 33 , p. 117.
38. Arai, K., Shitara, Y., and Ohyama, T., Preparation of photochromic spriopyrans linked to methylcellulose and photoregulation of their properties, J. Materials Chem., 1996, 6(1), 11-14.
39. Konak, C., Rathi, R. C., Kopeckova, P., Kopecek,J., Photoassociation of water-soluble copolymers containing photochromic spirobenzopyran moieties, Polymers for Advanced Technology, 1998, 9 (10-11), 641-648.
40. Bapista, M S., and Indig, G.L., Effect of BSA binding on photophysical and photochemical properties of triarylmethances dyes, J. Phys. Chem. B, 1998, 102(23), 4678-4688.
41. Durr, H., In Photochromisn: Molecules and System, Eleservier: Amsterdam, 1990, pp.173-176.
42. Xie, S., Natansohn, A., and Rochon, P., Recent developments in aromatic azo polymer research, Chem. Mat., 1993, 5, 403-411.
43. Barett, C., Natansohn, A., and Rochon, P.,Cis-trans thermal isomerization rates of bond and doped azobenzene in a series of polymers, Chemistry of Materials, 1995, 7 (5), 899-903
44. Ho, M., Natansohn, A., Barett, C., and Rocohn, P., Azo polymers for reversible optical storage, the effect of polarity of azobenzene groups. Canadian J. Chem., 1995, 73(11), 1773-1778.
45. Rodd, D., Blanc, J., and Brown, G., (Eds.), Photochromism: New York, InterScience, 1971.
46. Wides, P.O., Pacfici, J.G., Irick,G., and Whitten, D.G., Solvent and substituent on the thermal isomerization of substituted azobenzenes, a flash spectroscopic studey, J. Am. Chem. Soc., 1971, 93(8), 2004-2008.
47. Nerbonner, J.M., and Weiss, R.G., Elucidation of the thermal isomerization mechanism for azobenzene in a cholestric liquid crystal solvent, J. Am. Chem. Soc., 1978, 100(18),5953-5954.

48. Haberfield, P., Block, P. M., and Lux, M.S., Enthalpies of solvent transfer of the transition states in the cis-trans isomerization of azo-compounds, rotation vs the nitrogen inversion mechanism, J.Am. Chem. Soc., 1975, 97 (20), 5804-5806.
49. Chen, D.T., and Morawez, H., Photoisomerization and fluorescence of chromophores built into the backbones of flexible polymer chains, Macromolecules, 1976, 9(3), 463-468.
50. Rau, H., and Luddeche, E., On the rotation-inversion controversy on photoisomerization of azobenzenes, experimental proof of inversion, J. Am. Chem. Soc., 1982, 104(6), 1616-1620.
51. Ikegami, T., Kurita, N., Sekino, H., and Ishikawa, Y., Mechanism of cis-to-trans-isomerization of azobenzene: direct MD study, J. Phys. Chem. A, 2003, 107 (22), 4555-4562.
52. Cattaneo, P., and Persico, M., An ab initio study of the photochemistry of azobenzene, Phys. Chem. Chem. Phys., 1999, 1(20), 4739-4745.
53. Ishikawa, T., Noro,T., and Shoda, T., Theoretical study on the photoisomerization of azobenzene, J.Chem.Phys., 2001, 115,7503-7513.
54. Asno, T., Okada, T., Shinkai, S.,Shigematsu, K., Kusano, Y., and Manabe, O., Temperature and pressure dependences of thermal cis-to-trans isomerization of azobenzenes which evidence an inversion mechanism, J. Am. Chem. Soc., 1981, 103 (17), 5161-5165.
55. Fujino, T., Arzhantsev,S.Y., and Tahara.T., Femtosecond time-resolved fluorescene study of photoisomerization of trans-azobenzene, J. Phys .Chem. A, 2001, 105(35), 8123-8129.
56. Schultz, T., Quenneville, J., Levine, B., Toniolo, A., Martinez, T. J., Lochbrunner, S., Schmitt, M., Shaffer,J.P., Zgierski, M. Z., and Stolow, A., Mechanism and dynamics of azobenzene photoisomerization, J. Am. Chem. Soc., 2003, 125(27), 8098-8099.
57. Cembran, A., Bernardi, F., Garavelli, M., Gagliardi, L., and Orlandi, G., On the mechanism of the cis-trans isomerization in the lowest electronic states of azobenzene: S0, S1 and T1, J.Am. Chem. Soc., 126 (10), 3234-3243.

58. Crecca C.R., and Roitberg, A.E., Theoretical Study of the Isomerization Mechanism of Azobenzene and Disubstituted Azobenzene Derivatives, J. Phys. Chem. A, 2006, 110 (26), 8188 -8203

59. Ikeda, T., Sasaki, T., and Ichimura, K., Photochemical switching of polarization in ferroelectectric liquid-crystal films, Nature, 1993, 361,428-430.

60. Cheben, P., Moonte, F., Worsfold, D.J., Carlsson, D.J., Grover, C. P., and Mackenzie, J.D.A., Photorefractive organically modified silica glass with high optical grain, Nature, 2000, 408, 64-67.

61. Pedersen, M., Hvilsted,S., Holme,N.C.R., and Ramanujam, P.S., Influence of the substituent on azobenzene side-chain polyester optical storage materials, Macromolecular Symposia, 1999, 137, 115-127.

62. Hu, X., Zhao, X.Y., Gan L.H., and Xia, X.L., Synthesis, characterization and photochromic properties of PMMA functionalized with 4,4-diacryloyloxyazobenzene, J.Appl.Polym.Sci., 2002, 83(5), 1061-1068.

63. Viswanathan, N.K., Kim, D.Y., Bian, S., Williams, J., Liu, W.,, Li, L., Samuelson,L., Kumar, J., and Tripathy,S.K., Surface relief structures on azo polymer films, J. Mat. Chem., 1999, 9, 1941-1955.

64. Willne, I., Photoswitchable biomaterials: en route to optobioelectronic systems. Acc. of Chem. Res., 1997, 30 (9), 347-356.

65. Pieroni, O., Fissi, A., Angelini, N., and Lenci, F., Photoresponsive polypeptides, Acc. Chem. Res., 2001, 34(1), 9-17.

66. Paik, C. S., and Morawetz, H., Photochemical and thermal isomerization of azoaromatic residues in the side chains and the backbone of polymers in bulk, Macromolecules, 1972, 5(2), 171-177.

67. Barrett, C., Natansohn, A., and Rochon, P., Thermal cis-trans isomerization rates of azobenzenes bound in the side chain of some copolymers and blends, Macromolecules, 1994, 27 (17), 4781-4786.

68. Morishima, Y., Tsuji, M., and Kamachi, M., Photochromic isomerization of azobenzene moieties compartmentalized in hydrophobic microdomains in a microphase structure of amphiphilic polyelectrolytes, Macromolecules, 1992, 25 (17), 4406-4410.

69. Badjic, J.D., and Kostic, N. M., Reactivity of Organic Compounds Inside Micelles Embedded in Sol-Gel Glass. Kinetics of Isomerization of Azobenzene Inside CTAB and SDS Micelles Embedded in Silica Matrix, J. Phys. Chem. B,2001, 105 (31), 7482 -7489
70. Shirota, Y., Moriwaki, S., Yoshikawa, S., Ujike, T., Nakano, H., J. Mater. Chem., 1998, 8, 2579.
71. Priest, W.J., Sifain, M.M., J. Polym. Sci. Part A: Polym. Chem., 1971, 9, 3161
72. Rinnert, H.; Thirion, C.; Dupont, G.; Lamatre, J. Biopolymers 1977, 16, 241 9-2427.
73. Smerdon, J. J.; Isenberg, I. Biochem. Biophys. Res. Commun. 1973, 55, 1029-1034.
74. D'Anna, J. A., Jr.; Isenberg, I. Biochemistry 1974, 13, 4992-4997.
75. Sato, S.; Ebert, C. D.; Kim, S. W. J. Pharm. Sci. 1983, 72, 228-232.
76. Rueger, M.; Bienert, M.; Mehlis, B.; Gast, K.; Zirwer, D.; Behlke, J. Biopolymers 1984, 23, 747-758.
77. Hampson, C. C.; Monteath Robertson, J. J.Chem. Soc. 1941, 409-413
78. Pieroni, O., Fissi, A., Houben, J.L., and Ciardelli, F., J. Am. Chem. SOC. 1985, 107, 2991-2993
79. Lovrein, R., The photoviscosity effect, Proc. Nat. Acd. Sci., 1967, 57 (2), 236-242.
80. Irie, M., Adv. Polym. Sci., 1990, 94, 27-67.
81. Irie, M.; Hirano, Y.; Hashimoto, S.; Hayashi, K. Macromolecules 1981, 14, 262-267.
82. Kumar, G. S.; DePra, P.; Neckers, D. C. Macromolecules 1984, 17, 1912-1917.
83. Kumar, G. S.; DePra, P.; Zhang, K.; Neckers, D. C. Macromolecules 1984, 17, 2463-2467.
84. Ivory, C. F., Sep. Sci. Tech. 1988, 23, 875.
85. Scopes, R. K., Protein Purification: Principles and Practice, 2nd ed., Springer-Verlag: New York, 1982.
86. Wehr, T., Diaz, R.R., Zhu, M., Capillary Electrophoresis of Proteins, Marcel-Dekker, New York, 1999.

87. K.Tsuji, J.Chromatography B, 1994, 662, 291.

Chapter 2

Photoresponsive behavior of amphiphilic copolymers of methacryloyloxy-azobenzene and N,N-Dimethylacrylamide

2.1 Introduction

Photoresponsive polymers may respond to irradiation by changing their conformations in water. This, in turn, may reversibly alter the viscosity of the polymer solution and produce the *photoviscosity effect* which was first reported several decades ago.[1] It has since attracted considerable attention, partly because of its appeal as an environmentally benign, functional, photoswitchable technology.[2,3,4,5] Most photoresponsive polymers contain azo- dyes, such as azobenzene, either in their backbones or in side chains. The change in conformation is due to *cis*↔*trans* isomerization transitions in the dye, which can be followed by changes in the solution viscosity, dipole moment, and refractive index.[3] In water, a decrease in the solution viscosity upon UV irradiation can be attributed to an increase in the hydrophilicity of the azobenzene in its *cis* form relative to that in its *trans* form, which leads to fewer azobenzene-azobenzene associations.[3,4]

The present study was motivated by our interest in the design and synthesis of such materials for use as matrices in separation processes, in particular in capillary and gel electrophoresis. Photoinduced changes in polymer conformation are very attractive as triggers for modulating the separation medium or gel properties as they are not affected by any of the external mass transfer limitations associated with pH-, redox-, and other chemical triggers. Another advantage of these gels is the potential to establish sharp, spatially well-defined regions of modified gel properties, which may have benefits for the dynamic control and modulation of the separation processes; it would be difficult to sustain such spatially-resolved structural features with temperature-responsive polymers

owing to the inevitable establishment of temperature gradients between the heated and non-heated, or cooled, regions within the gel.

We have used azobenzene as the photoresponsive moiety in the polymers. Its usual water-insolubility has been overcome through the careful design of the copolymer to be water-soluble without macrophase separation even when all azobenzene groups are present in their most hydrophobic, i.e. *trans,* form. The undesirable use of additives such as surfactants[5] or cyclodextrins,[2] which can aid polymer solubility but complicate separation processes in which these polymers are to be used, was avoided, as was the use of ionic or ionizable groups of the type used thus far to create water-soluble copolymers that exhibit the photoviscosity effect.[1] Such ionic copolymers can change conformation in the strong electric fields typical of electrophoretic processes because of a decrease in the positive osmotic pressure originating from the polymer counterions, and because counterion gradients in polyelectrolyte solutions can lead to the collapse of the polymer and thus affect its ability to perform as a separation matrix. Hence, we chose a nonionic vinyl monomer, N,N-dimethylacrylamide (DMA), as one of the copolymer constituents in developing water-soluble, photoswitchable copolymers. Copolymerization of DMA with other vinyl monomers and the scaling behavior of its gels are well-known[6] and poly-DMA has been proven to be an efficient medium in capillary electrophoresis, since it is both insensitive to electric fields and capable of withstanding high voltages.[7,8] Copolymers of DMA with pendant azobenzene moieties along the backbone exhibit a significant, concentration-dependent photoviscosity effect in water, without macrophase separation. We have characterized the equilibrium and kinetic photoisomerization behavior, as well as related gelling and other photosensitive colloidal properties of these copolymers by using dynamic light scattering, surface tension, absorption spectroscopy, probe solubilization and rheological measurements.

2.2 Experimental

2.2.1 Materials

Methacryloyl chloride (97%), 4-hydroxyazobenzene (98%), N,N-dimethylacrylamide (99%), and 2,2'-azobisisobutyronitrile (initiator, AIBN, 98%), and Nile Red (fluorescence probe phenoxazone-9) were all purchased from Sigma-Aldrich Chemical Co. (St. Louis, MO) and used as received. Triethylamine (99%) was obtained from J.T. Baker (Phillipsburg, NJ) and was also used without further treatment. Deuterated solvents were obtained from Cambridge Isotope Laboratories (Andover, MA). All other solvents, buffers, and gases were obtained from commercial sources and were of the highest purity available.

2.2.2 Copolymer Synthesis

Photoresponsive polyacrylamides modified with azobenzene moieties have previously been reported in the literature.[9,10,11] They typically contain tertiary amino groups and thus behave as polyelectrolytes within the pH range of 5-8. The potential applications of stimuli-responsive polymers as gel electrophoretic separation media require neutral copolymers devoid of charges in this pH range. It was for this reason that we developed copolymers of N,N-dimethylacrylamide (DMA) and trans-4-methacryloyloxyazobenzene (MOAB), synthesized according to the route shown in Scheme 2-1and Scheme 2-2. The synthesis route was chosen such that the azobenzene in the resultant copolymer existed as the sidechain. This was done for the purpose as the interpolymer sidechains association can act as physical crosslink which could be sensitive to isomeric form. The synthetic route for formation of first monomer trans-4-Methacryloyloxyazobenzene (MOAB) can be described as follows. It was prepared by condensation of 4-hydroxyazobenzene and methacryloyl chloride in THF, with triethylamine (TEA) acting as a promoter). In brief, 4-hydroxyazobenzene (10 g, 50.0 mmol) was dissolved in 120 ml THF, to which triethylamine (acid scavenger; 7.11 ml, 50.6 mmol) and 2,6-di-tert-butyl-p-cresol (free-radical inhibitor, 5 mg) were added.[12] The resulting solution was purged with nitrogen and stirred at room temperature for 30 mins. Methacryloyl chloride (15 ml, 150 mmol) was then added gradually from a glass syringe while the solution was maintained in an ice-cooled water bath. The formation of

triethylammonium salt in the form of precipitate was observed immediately upon methacryloyl chloride addition. The reaction mixture was stirred for 48 h at room temperature. The precipitate was removed by filtration, and the solution was diluted with a mixture of chloroform and water (3:1) to convert the excess methacryloyl chloride into methacrylic acid. The organic layer was washed three times with distilled water to remove the polar compounds. Finally, the organic layer was dried by contact with anhydrous Na_2SO_4, and the residual solvent was removed ab vacuo. The product was twice purified by re-crystallization by evaporation of the n-hexane and dried under vacuum.

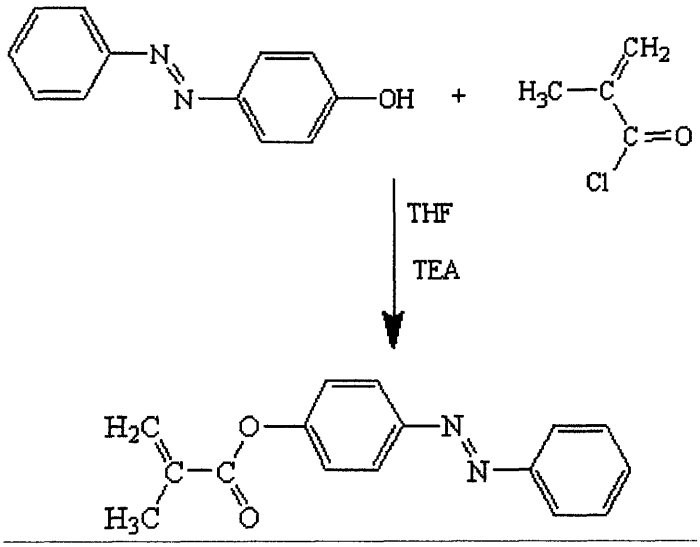

Scheme 2-1: Synthetic route to the preparation of *trans*-4-methacryloyloxyazobenzene (MOAB)

A series of copolymers with a molar MOAB fraction with respect to DMA varying from 0.1 to 0.4 was synthesized and tested for aqueous solubility at 0.001 wt% effective concentration. MOAB was copolymerized with a hydrophilic monomer, N,N-dimethylacrylamide (DMA) via free-radical polymerization with AIBN as the initiator. (Scheme 2). For MOAB molar fraction of 0.2 with respect to DMA, following procedure was carried out. A solution containing MOAB (0.1 g, 0.38 mmol), N,N-dimethylacrylamide (0.154 ml, 1.5 mmol) and 0.15 ml of THF was deoxygenated with nitrogen while in an ice-cooled water bath. A series of polymers of varying MOAB and

DMA contents were prepared. The solution was then heated to 70°C, and AIBN (5 mg, 2 wt %) was added gradually. The solution was then maintained at a temperature of 70 °C for 18 hours. To complete the polymerization, the solution temperature was raised to 90 °C and maintained there for 2 hours. The resulting polymer was dialyzed for 48 hours against deionized water using a 3500 Da MWCO membrane and then lyophilized.

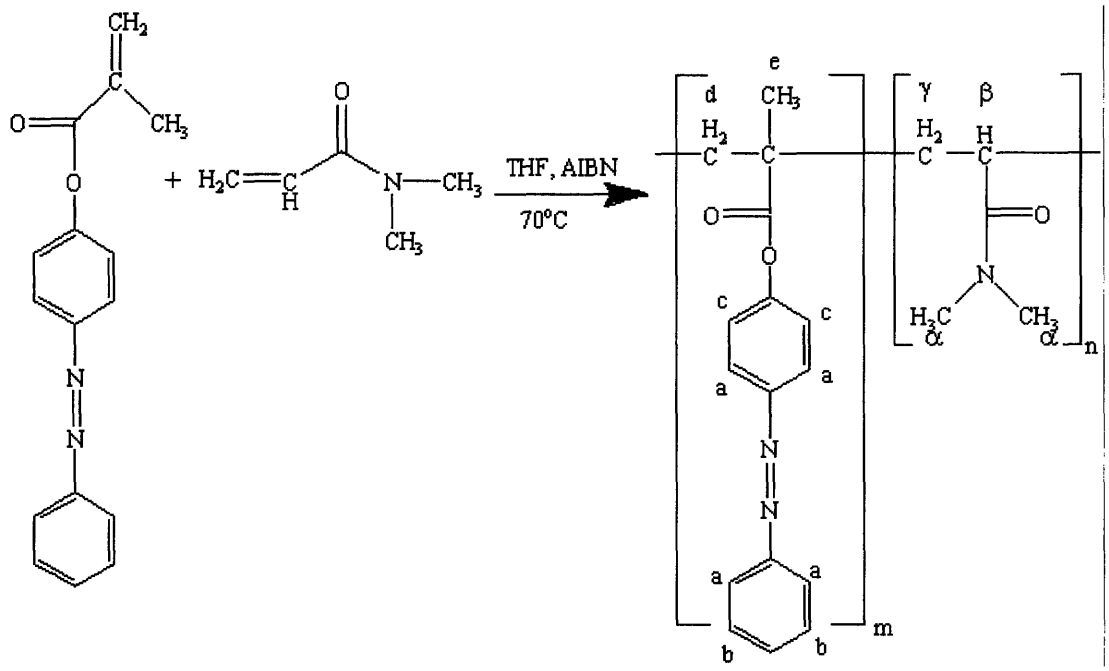

Scheme 2-2: Synthetic route toward the copolymerization of MOAB and DMA. The protons in MOAB-DMA copolymers are labeled with letters which are correspondingly characterized in NMR as seen in Figure 2-1

A polymer on the borderline of aqueous solubility had a nominal, as-synthesized MOAB molar fraction of about 0.2. The MOAB-DMA copolymer was characterized by ^{1}H NMR and GPC. The ^{1}H NMR spectra of polymer solutions in CD_2Cl_2 were acquired with a Bruker AMX400 spectrometer. Gel permeation chromatography (GPC) was carried out with THF as the mobile phase. The MOAB-DMA copolymer with nominal molar fraction of about 0.2 was found to be of a weight-average molecular weight of 24 kDa. Based on obtained molecular weight and nominal molar fraction, there are about 38 MOAB units present on the polymer chain containing 150 units of DMA. The polydispersity found by GPC was about 1.4. The actual average content of azobenzene groups was determined by NMR analysis to be 0.185, based on the ratio of the protons in

the azobenzene moiety to those of the methyl group of DMA (See Scheme 2-2 and Fig.1 for the proton designations). All analogous copolymers with nominal *molar fraction* values exceeding 0.2 appeared to be water-insoluble.

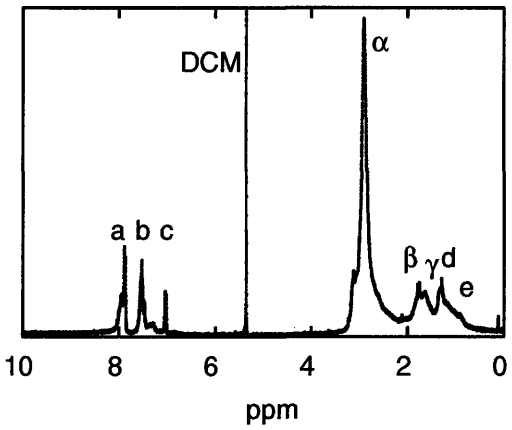

Figure 2-1: A representative 1H NMR (400 MHz) spectrum of MOAB-DMA in CD_2Cl_2. Protons are labeled as shown in Scheme 2-2.

2.3 Polymer aggregation phenomena

The colloidal properties, and in particular the aggregation behavior, of the copolymers in water as a function of concentration were characterized by surface tensiometry, probe solubilization techniques and dynamic light scattering. In all these studies, illumination was provided by a Model 6283 200-W mercury lamp (Oriel, Stratford, CT) equipped with either a 320 nm band-pass filter (Oriel Model 59800, used to obtain monochromatic UV light) or 400 nm pass filter (Oriel Model 59472, used to obtain radiation in the visible range) mounted on an arc lamp housing (Oriel Model 66902) and powered by an arc lamp power supply (Model 68910). The setup was equipped with a heat-absorbing filter (Schott KG 4 Heat Absorbing, Oriel) to remove the heat generated by the UV and IR light. The intensity of irradiation was measured by an Accu-Cal™ 30 Radiometer (Dymax, Torrington, CT) and found to be $0.1 mW/cm^2$ (325nm).

Equilibrium surface tensions were measured at a 25°C with a Kruss K10T tensiometer (Kruss USA, Hamburg, Germany) using the Wilhelmy plate method.[13]

Equilibrium surface tensions, γ, of the aqueous polymer solutions at varying polymer concentrations before and after UV irradiation are reported in Figure 2-2. It is notable that the MOAB-DMA copolymer exhibited significant surface activity, which is uncommon for random copolymers, and appeared to form micelles or aggregates above critical micellization concentrations (cmcs) of about 0.15 to 0.20 wt% for both the *trans* and *cis* forms of the copolymer. After UV irradiation, there is presence of both isomers, i.e., the establishment of a photostationary state with incomplete interconversion of the photoisomers from one state to the other, on same polymeric chain. The *trans* isomer on the polymer chain can lead to interpolymer associations via π-π stacking forming aggregates. Furthermore, the cis- isomers that are present on the chains can be incorporated into those hydrophobic aggregates. Thus both *trans* and *cis* taking part in mixed micelle-like aggregates.

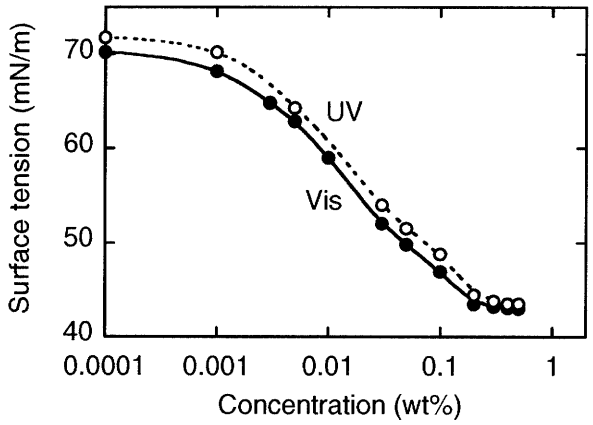

Figure 2-2: Concentration dependencies of the equilibrium surface tension in MOAB-DMA at 25°C and pH =7 before (filled points) and after (open points) UV irradiation using a Hg lamp with 0.1 mW/cm2 (325nm).

Studies[14,15] have shown that the aggregation pattern of the micelles is different between the *trans* surfactant and *trans/cis* surfactant mixture in terms of aggregation number, structure of micelles and so on. The difference in cmc of pure *trans* and *cis* is shown to depend on the design of the surfactant. For azobenzene containing ionic surfactants[14,15] it is shown that for different tail chain lengths and spacer chain lengths, the ratio of increase in cmc changes which can vary from 1.2 to 4 times but the mechanism is not explained. In accordance with their experimental observations, the

slight difference of cmc seen in our case can be attributed to the design of our polymer with a large hydrophilic part with shorter tail chain length and spacer group.

Fluorescence spectra were recorded on a TimeMaster Fluorescence Lifetime Spectrometer (Photon Technology International, PTI, Canada) in the steady-state mode (band-pass, 3 nm; integration time, 2 s). FeliX software was used for data acquisition and analysis. Properties of the aggregates formed in the polymer solutions were assessed by steady-state fluorescence studies by employing a fluorescent dye, Nile Red, as the probe. A 0.5 μM aqueous stock solution of Nile Red was prepared from which 0.02 ml aliquots were removed and added to 2ml of polymer solutions of varying concentrations. The resulting Nile Red solutions were then allowed to equilibrate for 3-4 hrs. The sample was excited at a wavelength of 570 nm and the emission scan was run from 600-700 nm.

Aggregation in the MOAB-DMA solutions was further probed by following the effect of polymer concentration on the solubilization of Phenoxazon-9 (Nile Red), a hydrophobic fluorescent dye sensitive to the lipophilicity of its environment.[16] Nile Red is especially suited to probe the MOAB-DMA solutions because its excitation wavelength maximum (λ_{ex} = 570 nm) is remote from the absorption wavelength of both *trans* and *cis*-forms of the copolymer, and thus Nile Red excitation *per se* would not cause any isomerization of the azobenzene moieties of the copolymer.

Changes in the spectra and fluorescence intensities of Nile Red with changing polymer concentration before and after UV irradiation are shown in Figure 2-3. Above a threshold value of about 0.005 to 0.01 wt%, the fluorescence intensity increased dramatically with increasing polymer concentration, indicating a molecular (and thus fluorescent) dispersion of the water-insoluble dye in the hydrophobic cores of the MOAB-DMA aggregates.[16] The significant hypochromic or blue shift of more than 40 nm in the maximum observed emission wavelength provided evidence of this less polar dye environment. The increase in fluorescence is over a broad range of concentrations as seen in most of the associative copolymers. [17,18] These observations suggest the presence of a premicellization process, i.e., the formation of di-, tri-, tetrameric aggregates, etc. at Cp < cmc, obtained from surface tension measurements.[17] At concentrations above 0.1 to 0.2 wt%, the probe fluorescence intensity reached a plateau, and no further increases in

fluorescence intensity were observed with increasing polymer concentration. This concentration range over which the fluorescence varies coincides with the range over which the surface tensions changed dramatically from those for the fully dispersed states to the fully aggregated condition (compare with Figure 2-2). It is notable that the relative increase in the fluorescence intensity of Nile Red when the majority of the azobenzene groups in the polymer were in the *cis-* conformation was about 25 percent lower than when these groups were in the *trans*-conformation, reflecting the higher solubilizing capacity and more hydrophobic environment provided by the azobenzene aggregates of the *trans*-isomers *vis-à-vis* the *cis* form.[13]

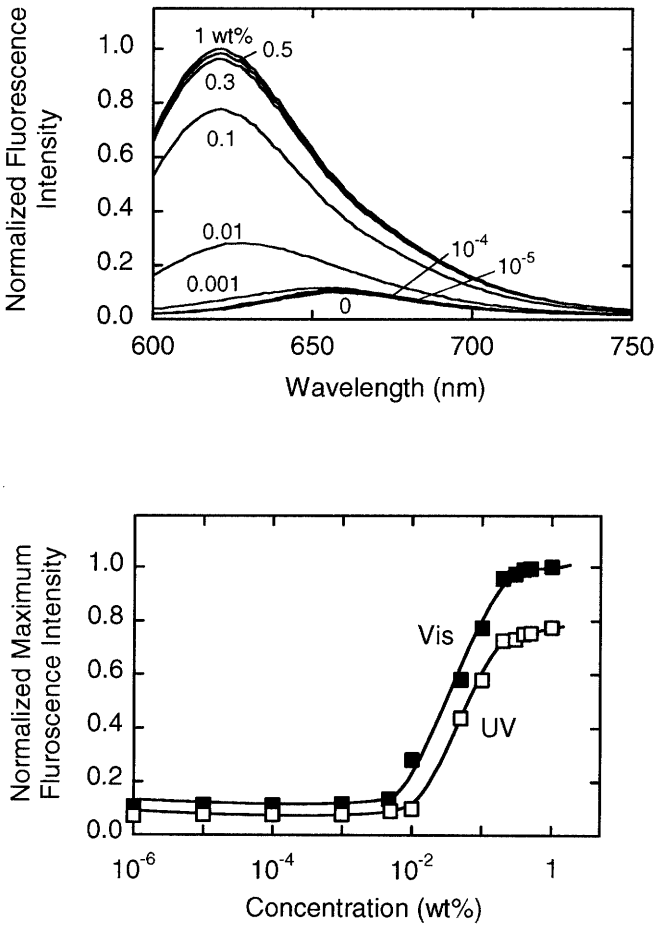

Figure 2-3: (a) Effect of polymer concentration on fluorescence emission intensity of Nile Red in aqueous solutions of MOAB-DMA. Dye concentration is 0.1mM in a solution of pH 7.0 and at a temperature of 25°C. (a) Emission spectra obtained before UV irradiation; (b) Maximum fluorescence intensity versus polymer concentration before

(filled points) and after (open points) irradiation. The irradiation intensity was 0.1mW/cm^2 (325nm), irradiation time for each sample was equal to the time required to reach UV-photostationary state.

Dynamic light scattering experiments were performed on a Brookhaven Instruments BI-200SM equipped with goniometer alignment software, a BI-9000 Correlator and a Spectra Physics He-Ne Model 127 laser operating at a scattering angle $\theta = 90°$ and a wavelength of incident light of 633 nm at a power of 50 mW. A 10 mL glass scattering cell was immersed in a bath of refractive index matching silicone oil The bath also provided temperature control within 0.02°C. Dynamic light scattering data also showed that at concentration above 0.1 wt%, hydrodynamic radius was about 30 nm in size indicating the formation of aggregates.

2.4 Copolymer photoisomerization kinetics

Photochemical isomerization of azopolymers in solutions has been extensively investigated by many researchers. Previous studies concentrated on azobenzene behavior in organic solvents where aggregation mechanisms are different from those in water.[19,20] However, only a few studies have been performed in aqueous solutions. This is partly because most azo polymers are water-insoluble. It has been shown that the isomerization of azo polymers depends not only on the azobenzene chromophores but also on the properties of polymer matrixes, such as the type of attachment of chromophores to the polymer backbone, glass transition temperature, crystalline order and so on.[21,22] In solutions the isomerization rate is very sensitive to the local environments surrounding the azobenzene chromophores, such as the polarity, pH of the solvent.[23] Previous studies concentrated on azobenzene behavior in organic solvents where aggregation mechanisms are different from those in water.[19,20] Numerous isomerization kinetics studies of azo-derivatives have been conducted on films or liquid crystals,[24,25,26] and there have been reports dealing with the isomerization kinetics of azo-surfactants in the aggregated state.[27,28] Herein, we report on photoisomerization kinetics of the azobenzene-containing

amphiphilic polymer in aqueous solutions, where concentration-dependent aggregation phenomena prevail. Hence, kinetics studies were conducted over a concentration range covering the transition from unimers to aggregated hydrophobic domains.

The kinetics of photoisomerization of the pendant azobenzene groups in aqueous solutions of these polymers were characterized by electronic absorption spectroscopy in the UV/vis region.[29] The kinetics of the copolymer isomerization were monitored by UV absorbance. UV-vis absorption spectra were obtained using a Hewlett-Packard HP 8453 spectrophotometer with a quartz cuvette (1 cm or 1 mm path lengths). The path length was chosen such that, even at the highest polymer concentrations, absorbance value was less than or equal to 2 for UV-vis spectrophotometer instrumental accuracy. As the absorbance is negative logarithm to the base 10 of transmittance, to remain within 1% transmittamce and not letting the stray light reduce the accuracy of the measurement, the absorbance value is usually kept less than or equal to 2. Figure 2-4 depicts typical absorption spectral changes due to photoisomerization after the polymer solutions had been exposed to either UV or visible irradiation for different periods of time. The strong absorption band centered at 325 nm corresponds to the $\pi \rightarrow \pi^*$ transitions of the azobenzene.[30] The value of λ_{max} for an isolated azobenzene group is typically 350 nm, but the peak shifts to shorter wavelengths when the azobenzene is derivatized with electron-withdrawing groups such as the methacryloyl moiety.[31] The band of lower intensity at 430 nm corresponds to the $n \rightarrow \pi^*$ transition. The dark-adapted state is obtained under conditions where there is no irradiation at all, and is the lowest energy state. Essentially all of the azobenzene moieties are in the *trans* form under these conditions. Under visible light irradiation, the photostationary state is a mixture of the two isomers, but with the trans form in great excess. Similarly, a photostationary state is obtained under UV irradiation, in this case with the *cis* form being in excess. The decreasing intensity of the 325-nm band following UV-irradiation corresponds to the *trans*→*cis* transition, while its increase after irradiation with visible light (λ_{max} >400 nm) indicates the *cis*→*trans* rearrangement.

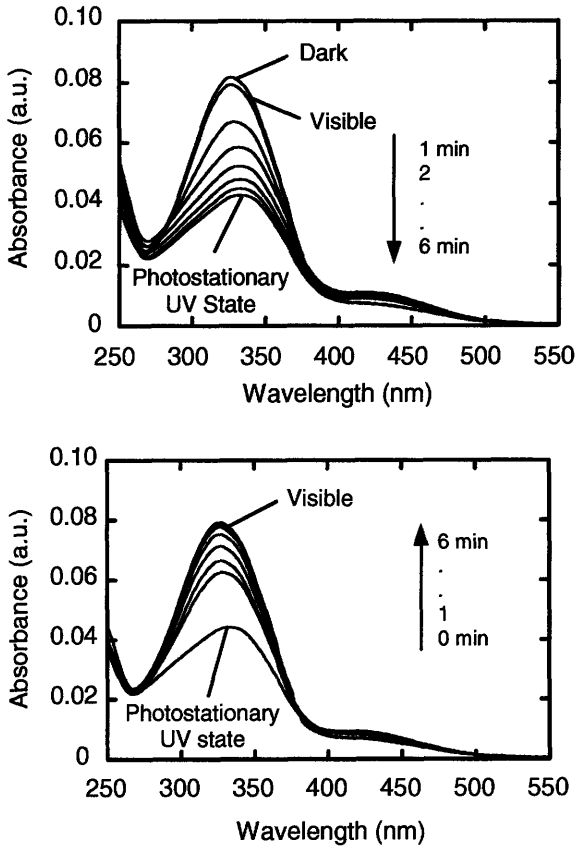

Figure 2-4: (a) UV-vis absorption spectra for 0.001 wt% MOAB-DMA solution under UV irradiation (325nm bandpass filter) for different times (b) UV-vis absorption spectra for MOAB-DMA solution after visible light (> 400nm filter) illumination for different times.

The kinetics of such rearrangements are readily monitored by following the changes in the spectra with time. The transition between the two photostationary states on exposure to alternating UV and visible illumination was completely reversible. In all experiments, only transparent solutions with absorbance below 0.003 in the 600-800 nm ranges were used.

The polymer solution was illuminated continuously with a narrow band photon flux of 0.1 mW/cm^2 and the *trans* and *cis* absorption bands were monitored until the system reached its photostationary equilibrium state (Figure 2-4). The kinetics were analyzed quantitatively by assuming that the absorption of photons of a particular

wavelength by an isomer A leads to the excitation of this species to A^*, which then either reverts back to A or transforms to the other isomer, B, according to the reaction scheme [24]

$$A \underset{k_{rA}}{\overset{\varepsilon_A I}{\rightleftarrows}} A^* \xrightarrow{k_{dA}} B$$

where ε_A is the molar absorption coefficient and I is the local illumination intensity. The rate constants of the $A^* \rightarrow A$ and $A^* \rightarrow B$ conversions are k_{rA} and k_{dA}, respectively. The reverse reaction with conversion $B \rightarrow A$ was assumed to follow a similar pathway, with the reaction scheme

$$B \underset{k_{rB}}{\overset{\varepsilon_B I}{\rightleftarrows}} B^* \xrightarrow{k_{dB}} A$$

Neither fluorescence nor phosphorescence was detected in the photoresponsive polymer solutions, consistent with literature reports to the effect that most azobenzene groups are essentially nonemitting.[32] The experimental evidence indicated that most if not all the A^* that reverts back to A does so non-radiatively. Thermal reconversion of the *cis* to the *trans* state also occurs, but the time scale of this reaction at room temperature is on the order of several hours[9] and thus it can be neglected in the kinetics analysis when the light-induced isomerization occurs within less than an hour. In most analyses of photoconversion processes, the solution is well stirred so that the concentration of each species is uniform throughout. In unstirred systems, and in rigid gels, this assumption may not be valid, since the light intensity falls as the beam traverses the solution, and the conversion rate varies across the cell. The time-dependent changes in the isomer concentrations at any particular point within the beam are:

$$\frac{d[A]}{dt} = -\varepsilon_A I[A] + k_{rA}[A^*] + k_{dB}[B^*] \qquad \text{Eq. 2-1}$$

$$\frac{d[A^*]}{dt} = \varepsilon_A I[A] - k_{rA}[A^*] - k_{dA}[A^*] \qquad \text{Eq. 2-2}$$

$$\frac{d[B^*]}{dt} = \varepsilon_B I[B] - k_{rB}[B^*] - k_{dB}[B^*] \qquad \text{Eq. 2-3}$$

$$\frac{d[B]}{dt} = -\varepsilon_B I[B] + k_{rB}[B^*] + k_{dA}[A^*] \qquad \text{Eq. 2-4}$$

where I is the light intensity at the point of interest, with spatial dependency at any given time satisfying the equation

$$\frac{dI}{dx} = -\left(\varepsilon_A[A] + \varepsilon_B([A]_0 - [A])\right)I; \qquad I(x=0) = I_0 \qquad \text{Eq. 2-5}$$

It has been shown that the concentrations of the intermediates [A^*] and [B^*] are small, and we make the quasi-steady-state assumptions that $d[A^*]/dt \approx 0$ and $d[B^*]/dt \approx 0$.[26] The rate expressions given by Eq. 2-1 to Eq. 2-4 can thus be combined to give the overall rate expression for the production or loss of isomer A:

$$\begin{aligned}\frac{d[A]}{dt} &= -\varepsilon_A\left(\frac{k_{dA}}{k_{rA}+k_{dA}}\right)I[A] + \varepsilon_B\left(\frac{k_{dB}}{k_{rB}+k_{dB}}\right)I[B] \qquad \text{Eq. 2-6}\\ &= -K\left(\left[\frac{I}{I_0}\right][A] - \left(\frac{\varepsilon_B\phi_B}{\varepsilon_A\phi_A}\right)\left[\frac{I}{I_0}\right]([A]_0 - [A])\right)\end{aligned}$$

where $K = \varepsilon_A\phi_A I_0$ is the apparent rate constant for the isomerization reaction $A \rightarrow B$ under an irradiation intensity of I_0; the quantum yield of the isomerization process $A \rightarrow B$ is $\phi_A = \frac{k_{dA}}{k_{rA}+k_{dA}}$, and that of $B \rightarrow A$ is $\phi_B = \frac{k_{dB}}{k_{rB}+k_{dB}}$.

Under photostationary conditions(ss), the conversion α_{ss} the of the isomer from A to B at a given wavelength λ, can be obtained from Eq. 2-6 by setting $d[A]/dt = 0$

$$\alpha_{ss} = 1 - \left.\frac{[A]}{[A]_0}\right|_{ss} = \left(1 + \frac{\varepsilon_B \phi_B}{\varepsilon_A \phi_A}\right)^{-1} \qquad \text{Eq. 2-7}$$

These equations indicate that while the dynamic approach to the photostationary state depends on the local light intensity I, which can vary with position, the final state is independent of the irradiation intensity, and the photostationary species concentrations are constant across the cell.

For unstirred systems and for rigid gels, the isomer concentrations $[A]$ and $[B]$ vary across the cell. The average concentration in the beam path at any given time can be related to the total absorbance, Abs, using

$$\begin{aligned} \frac{Abs}{Abs_0} &= \frac{\varepsilon_A \langle [A] \rangle + \varepsilon_B \langle [B] \rangle}{\varepsilon_A [A]_0} = \left(1 - \frac{\varepsilon_B}{\varepsilon_A}\right) \frac{\langle [A] \rangle}{[A]_0} + \frac{\varepsilon_B}{\varepsilon_A} \\ &= 1 - \left(1 - \frac{\varepsilon_B}{\varepsilon_A}\right) \langle \alpha \rangle \end{aligned} \qquad \text{Eq. 2-8}$$

provided that Beer's law holds. The initial absorbance is Abs_0, while the notation $\langle \bullet \rangle$ represents the spatial average over the beam path. This relationship provides a direct link between the experimentally accessible absorbance and the spatially-averaged photo-isomer concentrations during the dynamic experiments.

The extinction coefficient ratio $\varepsilon_B / \varepsilon_A$ was determined to be 0.45 ± 0.072 in separate experiments following published procedures and was assumed to be independent of polymer concentration described in the Appendix of this Chapter.[26] This information, together with experimental steady-state absorbance measurements, was used to estimate the quantum yield ratio ϕ_B / ϕ_A by combining Eq. 2-7 and Eq. 2-8:

$$\frac{\phi_B}{\phi_A} = \left(1 - \frac{\varepsilon_A}{\varepsilon_B}\left(\frac{Abs}{Abs_0}\right)_{ss}\right) \Big/ \left(\left(\frac{Abs}{Abs_0}\right)_{ss} - 1\right) \qquad \text{Eq. 2-9}$$

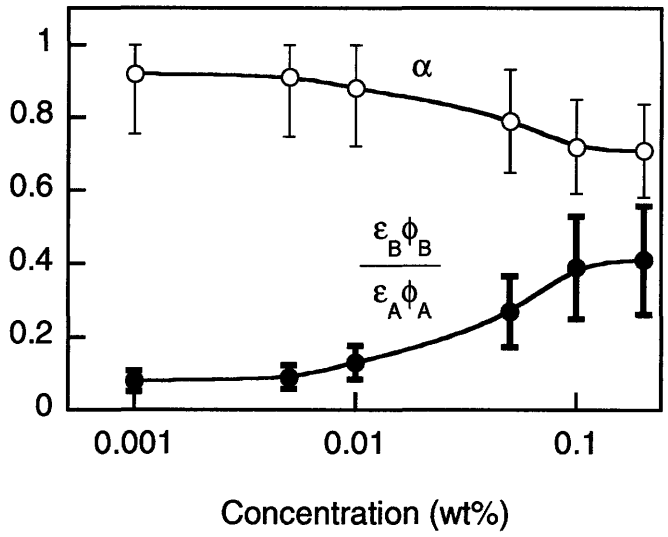

Figure 2-5: The equilibrium conversion for different concentration obtained from experimental data. The product of ratio of extcintion coefficient and quantum yield is also plotted. All the values are plotted with error bars considering 1% error in absorbance value measurement in experiments.

The variations in the equilibrium conversion and the quantum yield ratio with polymer concentration are summarized in Figure 2-5. The ratio of the quantum yields was assumed to be independent of the isomeric composition, and to depend only on the total polymer concentration. The quantum yield ratio, and hence equilibrium photoconversion efficiency, varied significantly over the polymer concentration range between 0.01 and 0.1 w%, consistent with the surface tension and fluorescence assay results, a direct result of the increasing steric confinement of the azobenzene groups as the aggregates begin to form; these effects will be discussed further below.

The value of the apparent isomerization rate constant, *K*, was obtained experimentally for our aqueous copolymer solutions from the rates at which the absorbance of the solution changed following irradiation. The kinetic scheme presented by Eq. 2-1 to Eq. 2-4 has been solved and used by other workers for conditions under which the spatial dependence of the absorbance intensity and the reverse reaction could be neglected.[9,28] In our work, however, because the azobenzene concentration, and hence absorption, are high, the light intensity falls as the beam passes through the polymer

solution, and this decrease must be accounted for in analyzing the experimental absorbance results.

The coupled Eq. 2-5 and Eq. 2-6 were integrated simultaneously using numerical methods to obtain [*A*] and *I* as functions of time and position for any given value of *K*. This enabled calculation of the spatial average concentration $\langle [A] \rangle$ as a function of time, which was then used with Eq. 2-8 to estimate the corresponding time-variation in the absorbance ratio, Abs/Abs_0. The sum of squared errors between these numerically predicted Abs/Abs_0 values and experimental results over the time course of the experiment was minimized with respect to *K* for each initial concentration, $[A]_0$, to obtain that value of *K* that gave the best fit to the data. As is seen in Figure 2-6(a), good fits of the data were obtained, with $R^2 > 0.98$ in all cases. The rate constants, *K*, determined from the fits are shown in Figure 2-6(b) to exhibit a sigmoidal dependency on polymer concentration, with values ranging from 0.006 s^{-1} at low concentrations ($C_P \leq 0.01$ wt%) to ~ 0.0006 s^{-1} at higher concentrations ($C_P \geq 0.1$ wt%) over the concentration range studied. For the non-aggregated MOAB-DMA solution, *K* was close to that reported previously for azo-polymers with electron-withdrawing groups under similar irradiation conditions.[33]

The quantum yield for isomer *A* can be calculated directly from the apparent rate constant via $\phi_A = \frac{K}{\varepsilon_A I_0}$ and that for isomer *B* using the now-known values ϕ_A and of the ratio ϕ_B/ϕ_A given in Figure 2-5. For concentrations less than 0.01 wt%, i.e., when the copolymer exists in the non-aggregated state, the quantum yield for the *trans* isomer, ϕ_{trans}, is 0.11, close to that of azobenzenes derivatized with electron withdrawing groups;[29,33] typical quantum yields have been reported to be in the range of 0.2-0.4 for underivatized azobenzene, depending on the polarity of the solvent,[34] and are known to be lowered by the presence of electron-withdrawing substituent groups. For azo-copolymers the quantum yield can be significantly smaller still ($\phi << 1$) due to the steric hindrance to isomerization presented by the neighboring groups and polymer segments.[28]

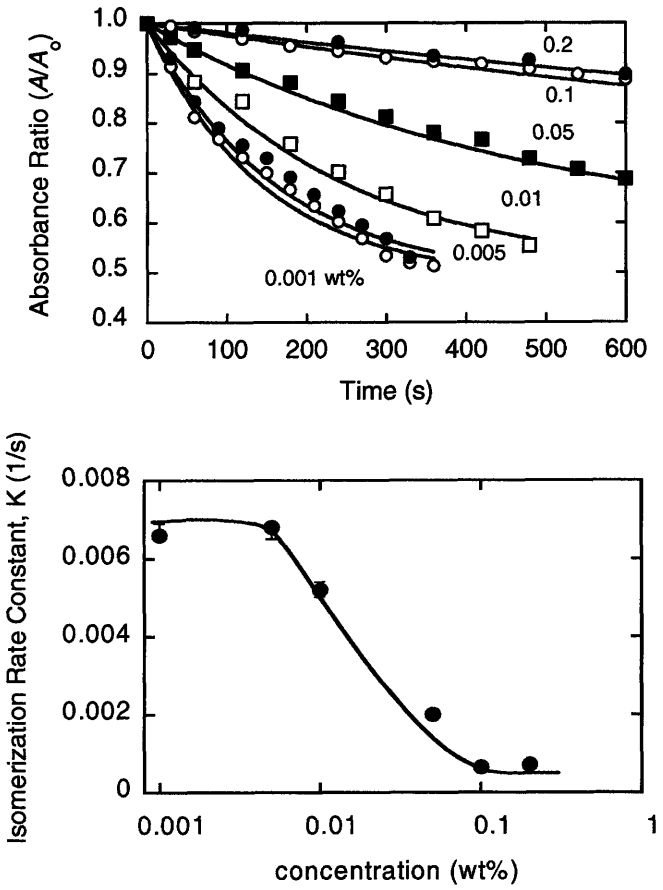

Figure 2-6: (a) Kinetic plots based on Equation (8) found from the ratio of absorbance at 325nm at different times to that at initial time (Abs_0) for varying MOAB-DMA concentrations. (b) The rate constant for the trans-cis photoisomerization, K, at 25 °C and pH 7.0 as a function of polymer concentration, obtained from the slopes of the lines in (a). The illumination was carried out at 0.1mW/cm^2 (325 nm).

Our results at the higher concentrations (C_P > 0.1 wt%) at which the azobenzene groups reside primarily in aggregates are consistent with those from the azo-copolymer studies in that the quantum yields are an order of magnitude smaller (ϕ_{trans} ~ 0.015) than at the lower concentrations. When confined within these aggregates, the groups are constrained sterically from converting efficiently from one geometric conformation to the other. Consequently, the reversion of *A* back to *A** non-radiatively is facilitated, causing a reduced efficiency of the *A*→ *B* conversion and hence a lower quantum yield. For the *cis* isomer at low concentrations, the quantum yield ϕ_{cis} = 0.021 is five-fold lower than

that for the *trans* conformation, while when in the aggregated state, the quantum efficiencies of the two isomers are essentially the same. The decrease in the rate constant or quantum efficiency of the *trans→cis*, and, to a lesser extent, of the *cis→trans* isomerization on aggregation is consistent with the reported studies by Badjic et.al.,[35] who showed a three-fold decrease in the isomerization rate of azobenzene when it was incorporated into surfactant micelles.

2.5 Photoviscosity phenomena

Rheological measurements were performed on a controlled stress Rheolyst Series AR1000 Rheometer (TA Instruments, New Castle, DE) with a cone and plate geometry system (cone: diameter, 2 cm; angle, 2°, truncation, 57 μm). Temperature control (internal resolution 0.016 °C) was provided by two Peltier plates. Steady-state flow experiments were conducted in a stepped shear rate ramp mode. Creep measurements were accomplished in a retardation mode where compliance versus time is measured under a given stress and fitted to yield zero-shear viscosity, η_o. Dynamic mechanical analysis (oscillatory rheological measurements) was carried out on polymer solutions using frequency sweep mode with constant shear of 0.6 Pa. The rate of strain amplitude was below 10^{-3} s^{-1}. The irradiation- and concentration-dependent behavior of the rheological properties of the DMA-MOAB polymer solutions in steady shear are compared with those under dynamic oscillatory shear in Figure 2-7.

A significant (up to a 20-fold) reduction in the zero shear rate (η_0) viscosity occurred on switching from visible to UV radiation, with the effect being greatest for the more concentrated solutions. Such a viscosity reduction, or *photoviscosity effect,* is due to the *trans-cis* transition of the azobenzene groups in the copolymer.[1,3,4,36,37,38] Isomerization of the azo units from their planar, apolar, *trans* form to the skewed, polar, *cis* form inhibits hydrophobic interactions and causes the azo units to dissociate from the aggregates thus reducing the number of associations, or physical junctions (cross-links), in the polymer matrix. Hence, the photoresponse can be attributed to the network-like,

elastic properties of associative polymer solutions, which are dictated by the numbers and lifetimes of the cross-links.[39,40]

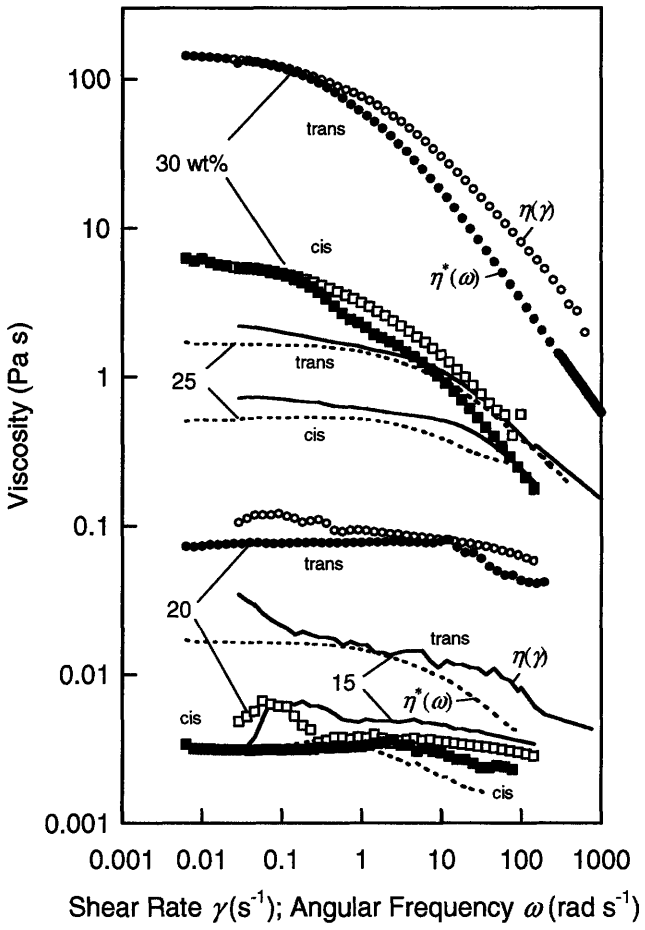

Figure 2-7: Dynamic and equilibrium viscosity of MOAB-DMA aqueous solutions before and after UV irradiation obtained in the oscillatory shear and equilibrium flow experiments, respectively. The results at some concentrations are given by open and closed symbols, while those at other concentration are given by solid and broken lines for easier identification of the curves.

Both oscillatory and steady-state flow modes of shear exhibited broad plateau viscosity ranges before shear-thinning, spanning γ and ω ranges from 0.0028 to 500 s^{-1} and 0.00628 to 100 rad/s. In some cases, an increase with shear rate prior to shear thinning could be observed in the $\eta(\gamma)$ *vs* γ curves. This is attributed to structuring of the system under the influence of large deformations.[36]

The $\eta^*(\omega)$ curves obtained at low strain amplitudes showed a monotonic decrease with increasing frequency, and deviated from the empirical Cox–Merz rule, in that $\eta(\gamma)$ was measurably greater than $\eta^*(\omega)$ over most of the range of experimentally accessible time scales. In addition, a transition to shear thinning at higher rates of shear in the steady-state flow compared to that in the oscillatory shear experiment was observed, again deviating from the Cox–Merz behavior.[41] The empirical Cox-Merz rule expects the equilibrium shear viscosity to be equal to the complex dynamic viscosity observed under oscillatory shear, and indeed many polymer melts and solutions follow this rule, although deviations are rather typical for transient networks of amphiphilic polymers.[41,42] These deviations can be attributed to the shear rate dependency of the junction dissociation rate and to a nonaffine deformation of the network.

At polymer concentrations ≤10% (not shown in Figure 2-7), the steady-state flow data exhibited significant scatter due to spindle slip at relatively low equilibrium viscosities. This limited our ability to obtain reliable data at these concentrations. Creep retardation measurements can be used in this region, however, and reproducible Newtonian viscosity data were obtained over the entire concentration range of interest from the steady-state shear compliance, J_e^o, based on the relationship

$$\Gamma(t)/\sigma_0 = J_e^0 + t/\eta_0 \qquad \text{Eq. 2-10}$$

where t is the time, $\Gamma(t)$ is the shear strain, and σ_0 is the shear stress.

The concentration dependencies of η_0 are presented in Figure 2-8. In the concentration range up to 10-15 wt %, the zero-shear rate viscosities, both before and after irradiation, grew as the square root of polymer concentration (C_P), in accordance with the empirical Fuoss law ($\eta_0 \propto C_P^{0.5}$) indicating that the polymer solution could be classified as semidilute (above the overlap concentration, C*) and unentangled. At higher concentrations (C_P > 15 wt%), viscoelastic gels evolved, characterized by a very high scaling exponent on the order of 10. It has been argued that very strong concentration dependencies of η_0 in solutions of hydrophobically modified amphiphilic polymers reflect extensive chain entanglements,[43] but in solutions of relatively low molecular

weight polymers, analogous to our case, the high scaling exponents may be better explained by a specific network topology dominated by the intermolecular associations at higher concentrations. It is interesting to observe that the effect of the UV irradiation on viscosity was magnified at the high concentrations, where the η_0 values diminished up to 20-fold after irradiation (Figure 2-8). In this concentration regime the viscosity is dominated by the associative junctions of the azobenzene aggregates, and thus is affected the most by the isomerization of the azobenzene groups. For concentrations $C_P \geq 10$ wt%, the steady shear rate viscosity measurements gave similar results, further confirming the more than an order of magnitude decrease in viscosity on UV irradiation at 30 wt% concentration.

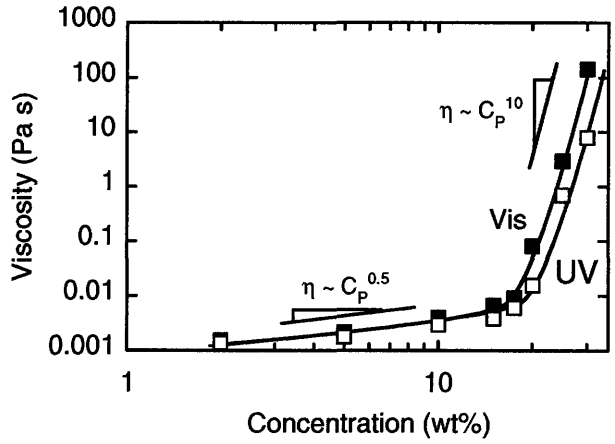

Figure 2-8: Concentration dependencies of zero-shear viscosity of aqueous MOAB-DMA solutions before (filled squares) and after (open squares) UV irradiation. The two different slopes shown indicate $\eta \sim C^{0.5}$ and $\eta \sim C^{10}$ scaling regimes as described in the text.

The frequency dependencies of the storage and loss moduli of representative DMA-MOAB solutions are depicted in Figure 2-9. These results show that even at concentrations as high as 30 wt% the solutions exhibited a dynamic response characteristic of viscoelastic fluids (G" > G' at most frequencies), consistent with the transient nature of the hydrophobic associations among the azobenzene groups. The number of these associations was lowered by the UV light, as evidenced by the drop in the moduli upon irradiation (15 times decrease for 30wt% copolymer concentration).

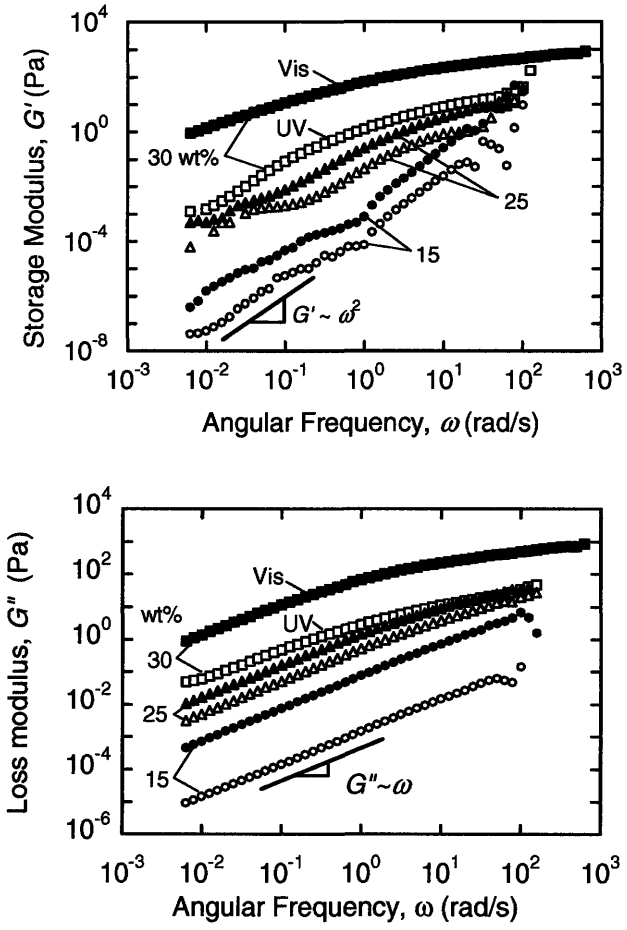

Figure 2-9: Linear viscoelastic response of MOAB-DMA copolymer solutions: (a) storage moduli and (b) loss moduli as a function of angular frequency for polymer concentrations 30, 25, and 15 wt% before and after UV illumination. pH 7.0, 25 °C.

When irradiated, the 15 wt% solution exhibited the $G' \propto \omega^2$ and $G'' \propto \omega$ relationships characteristic of network dynamics represented by a single Maxwellian unit. Such behavior is typical of polymers interacting via topological entanglements. Solutions at higher concentrations exhibited weaker frequency dependencies of the moduli, both before and after irradiation, reflecting broadening of the terminal relaxation spectrum due to the combined effects of the topological entanglements and hydrophobic-associations.[42]

2.6 Conclusion

Solutions of the MOAB-DMA copolymers exhibit a multitude of effects due to self-assembling phenomena such as dramatic changes in surface activity, micellization, and viscoelasticity previously observed in aqueous solutions of hydrophobically modified amphiphiles,[43] but with a new twist: the MOAB-DMA copolymers are also capable of photoisomerization, which alters all of these self-assembly-related properties. At low concentrations (C < 0.01 wt%), most polymer molecules are either monomeric or present in oligomeric aggregates. At polymer concentrations exceeding 0.01 wt%, small oligomeric aggregates are formed. Hydrophobic micelle-like microdomains formed at C > 0.1 wt% are evident from surface tension and fluorescence solubilization studies. A value of the critical overlap concentration, C*, ($C^* = \frac{3M_w}{4\pi N R_g^3}$, where R_g is the radius of gyration) can be estimated to be 1.2 wt% from the empirical scaling laws describing the molecular weight dependence of R_g.[44] This estimate matches the semidilute region boundary found herein (Figure 2-9). Above about a 10 wt% concentration, entanglements take place along with both intra- and intermolecular associations. The sharp rise in viscosity at concentrations above 15 wt% indicates formation of a gel network with an infinite structural correlation length and a wide distribution of aggregate sizes. A range of structures observed is shown schematically in Figure 2-10 .

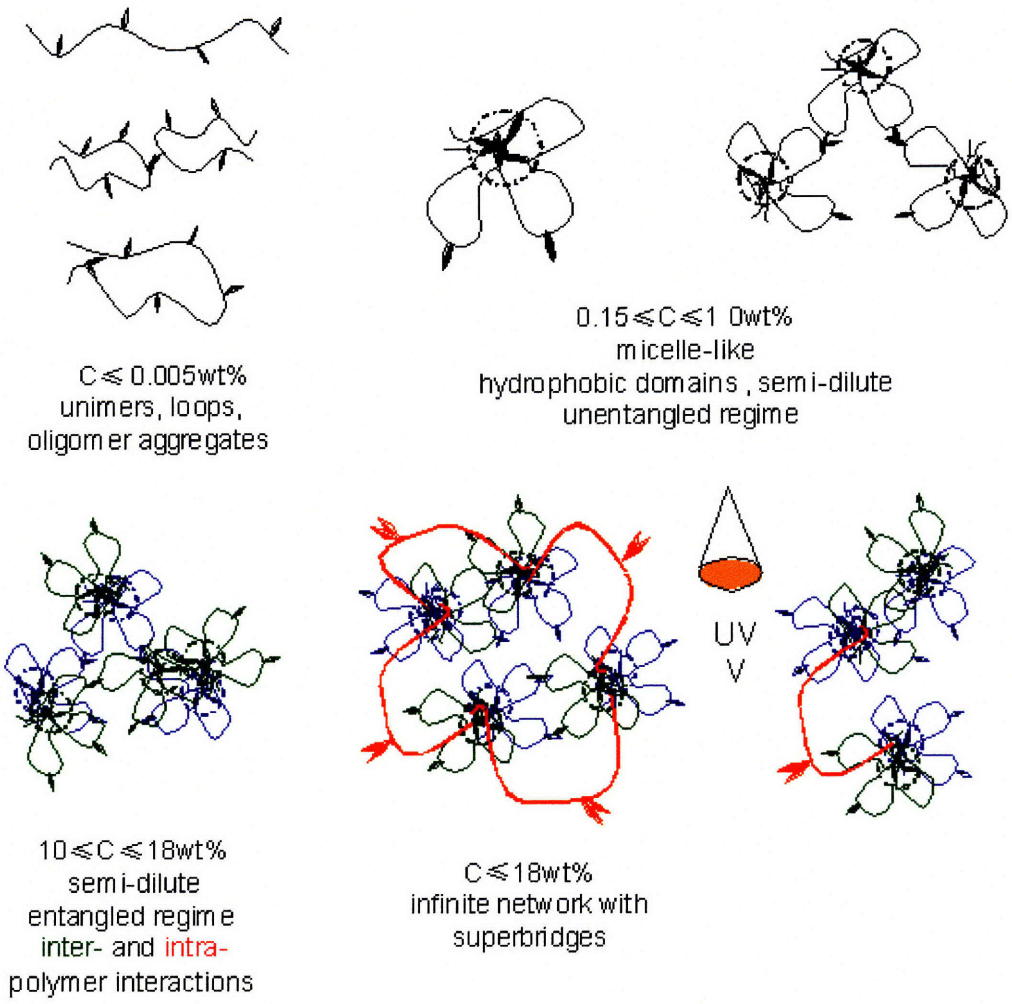

Figure 2-10: Schematic of suggested polymer solution structures as a function of polymer concentration.

Photoisomerization upon UV irradiation leads to a loss of viscoelasticity. The presence of aggregates that are impermeable to certain solutes such as proteins can alter the overall transport of those solutes through the polymer network undergoing aggregation, as the solutes negotiate a more torturous diffusional path through the aggregate-cross-linked gel.[43] We believe that such structural changes with their effects on the permeability of amphiphilic solutes such as proteins, can be exploited in the dynamic control of, for instance, protein gel electrophoretic separation processes and topical drug release.

2.6.1 Appendix

A. Calculation of Ratio of Extinction Coefficients[45]

When azobenzene is irradiated with any wavelength absorbed by both trans (A) and cis (B) isomers, a photostationary state will be established eventually.

$$A \underset{\phi_B}{\overset{\phi_A}{\leftrightarrow}} B$$

where, ϕ_A is the quantum yield of trans-cis isomerization and ϕ_B is the quantum yield of the cis-trans isomerizaton due to UV light irradiation. We have different photostationary state depending on the irradiation wavelength λ,

$$\left(\frac{[A]}{[B]}\right)_\lambda = \left(\frac{\phi_B}{\phi_A}\right)_\lambda \left(\frac{\varepsilon_B}{\varepsilon_A}\right)_\lambda = \left(\frac{\phi_B}{\phi_A}\right)_\lambda \left(\frac{A_A}{A_B}\right)_\lambda \qquad \text{Eq. 2-11}$$

where, A_A and A_B denote the absorbance, at this wavelength, of similar solutions containing only A or only B, respectively, i.e. the equilibrium A $\leftrightarrow$B is shifted completely toward either A or B.

If α is defined as the extent of conversion of A $\leftrightarrow$ B at any particular wavelength of irradiation, the concentration ratio of trans- and cis- isomers at a photostationary state can be expressed as:

$$\left(\frac{[A]}{[B]}\right)_\lambda = \left(\frac{1-\alpha}{\alpha}\right)_\lambda \qquad \text{Eq. 2-12}$$

At any particular wavelength, the absorbance at the photostationary state (A_S) of a mixture of trans- and cis- isomers is given by Eq. 2-13, where the overall concentration of [A]+[B] is constant

$$A_B = A_A + \frac{\Delta}{\alpha} \qquad \text{Eq. 2-13}$$

where, Δ is observed change in absorbance (A_S - A_A) when starting from A only. α can be calculated as shown by Fischer[12] employing the two different photostationary states, resulting from irradiation by two different wavelengths λ_1 and λ_2 respectively.

$$\alpha_{\lambda 2} = \left(\frac{\Delta_{\lambda 1}}{A_{A\lambda 1}} - \frac{\Delta_{\lambda 2}}{A_{A\lambda 2}} \right) / \left(1 - n + \frac{\Delta_{\lambda 1}}{A_{A\lambda 1}} - \frac{n\Delta_{\lambda 2}}{A_{A\lambda 2}} \right) \qquad \text{Eq. 2-14}$$

where Δ / A_A denotes the relative change of absorbance observed at a particular irradiation wavelength, λ_1 or λ_2. Eq. 2-14 contains two variables the conversion, $\alpha_{\lambda 2}$ and n, the ratio of α for the two different photostationary states obtained from irradiation at two different wavlength, $\alpha_{\lambda 1} / \alpha_{\lambda 2}$.

The factor n can be related to measurable quantities, the expression for which can be deduced with following method. UV-vis spectra used for the quantification of the conversion obtained by the irradiation experiment at two different irradiation wavelength. From Eq. 2-8 we have for any irradiation wavelength λ, if we monitor absorbance values at a certain wavelength γ from UV-vis spectra we can write following equation

$$\left(\frac{Abs}{Abs_0} \right)_\gamma = \left(1 - \left(\frac{\varepsilon_B}{\varepsilon_A} \right)_\gamma \right) \frac{[A]}{[A]_0} + \left(\frac{\varepsilon_B}{\varepsilon_A} \right)_\gamma \qquad \text{Eq. 2-15}$$

Defining in terms of conversion at the irradiation wavelength λ

$$\alpha_\lambda = \frac{\left(1 - \left(\frac{Abs}{Abs_0} \right)_{\gamma,\lambda} \right)}{\left(1 - \left(\frac{\varepsilon_B}{\varepsilon_A} \right)_\gamma \right)} \qquad \text{Eq. 2-16}$$

The ratio of conversions obtained at two different irradiation wavelength (1 and 2) can hence be given by

$$\frac{\alpha_{\lambda 1}}{\alpha_{\lambda 2}} = \frac{\left(1-\left(\frac{Abs}{Abs_0}\right)_{\gamma,\lambda 1}\right)}{\left(1-\left(\frac{\varepsilon_B}{\varepsilon_A}\right)_{\gamma}\right)} \Bigg/ \frac{\left(1-\left(\frac{Abs}{Abs_0}\right)_{\gamma,\lambda 2}\right)}{\left(1-\left(\frac{\varepsilon_B}{\varepsilon_A}\right)_{\gamma}\right)} \qquad \text{Eq. 2-17}$$

Hence,

$$\frac{\alpha_{\lambda 1}}{\alpha_{\lambda 2}} = \frac{\left(1-\left(\frac{Abs}{Abs_0}\right)_{\gamma,\lambda 1}\right)}{\left(1-\left(\frac{Abs}{Abs_0}\right)_{\gamma,\lambda 2}\right)} \qquad \text{Eq. 2-18}$$

If we are looking at same solution and same wavelength then Abs_0 will be same in both irradiation case and so,

$$\frac{\alpha_{\lambda 1}}{\alpha_{\lambda 2}} = \frac{\left((Abs-Abs_0)_{\gamma,\lambda 1}\right)}{\left((Abs-Abs_0)_{\gamma,\lambda 2}\right)} \qquad \text{Eq. 2-19}$$

The ratio n thus can be related to measurable absorbance values by following expression.

$$n = \frac{\alpha_{\lambda 1}}{\alpha_{\lambda 2}} = \frac{\Delta_{\gamma,\lambda 1}}{\Delta_{\gamma,\lambda 2}} \qquad \text{Eq. 2-20}$$

Using this value of n in Eq. 2-14, we can obtain the value of $\alpha_{\lambda 2}$. The value of $\alpha_{\lambda 1}$ can then be found using Eq. 2-20. The ratio of extinction coefficients can then be calculated using Eq. 2-21 which is obtained by rearranging Eq. 2-11 and Eq. 2-13 . Plugging this

$$\left(\frac{\varepsilon_B}{\varepsilon_A}\right)_{\lambda 1} = \left(\frac{A_B}{A_A}\right)_{\lambda 1} = \left(1+\frac{\Delta_{\lambda 1}}{\alpha_{\lambda 1}}\frac{1}{A_{A\lambda 1}}\right) \qquad \text{Eq. 2-21}$$

In the present study, photoisomerization experiment was carried out for aqueous solution of MOAB polymer with UV irradiation at two different irradiation wavelength of 325nm and 360 nm respectively. The $\varepsilon_B/\varepsilon_A$ ratio is determined using the above method and is found to be 0.45 at 325 nm and 0.73 at 360 nm.

B. Calculation of the ratio of quantum yield at a given wavelength

We assume here that the ratio of extinction coefficients of *trans-* to *cis-* form $\varepsilon_B/\varepsilon_A$ to be constant for a given wavelength for different concentration and states as extinction coefficients are primarily function of the photochemical properties of the compound.

From the UV photo-stationary state, we can calculate the conversion as

$$\frac{[A]}{[A]_0} = (1-\alpha) = \frac{\left(\frac{A}{A_0} - \frac{\varepsilon_B}{\varepsilon_A}\right)}{\left(1 - \frac{\varepsilon_B}{\varepsilon_A}\right)} \qquad \text{Eq. 2-22}$$

The ratio of quantum yield for a particular concentration can then be obtained using Eq. 2-11

Table 2-1: : Equilibrium conversions of A to B and the ratio of quantum yields for different concentrations are summarized

Conc. (wt%)	Conversion (α)	$(\varepsilon_B\phi_B)/(\varepsilon_A\phi_A)$	ϕ_B/ϕ_A
0.001	0.92	0.08	0.18
0.005	0.91	0.09	0.20
0.01	0.88	0.13	0.29
0.05	0.79	0.27	0.60
0.1	0.72	0.39	0.87
0.2	0.71	0.41	0.91

C. Does there exist an analytical solution for obtaining the value of K? If not, then special cases where analytical solution can exist!!!

The Eq. 2-6 can be written in following form with average and dimensionless concentration and intensity

$$\frac{d\overline{[A]}}{dt} = -K\bar{I}\overline{[A]} + k_2 K\bar{I}\,(1-\overline{[A]}) \qquad \text{Eq. 2-23}$$

where k_2 is the ratio of product of extinction coefficient and quantum yields of *trans-* and *cis-* form which is assumed to be constant . Non-dimensionalizing concentration using $\overline{[A]} = {}^{[A]}\!/_{[A]_0}$, which can be related to A/A_0, the ratio of the absorbance at a given time t to that at the commencement of the kinetics experiment ($t = 0$) for a given polymer concentration by equation 16. Also, $\bar{I} = {}^{I}\!/_{I_0}$ is the ratio of the intensity at a given location x in the cell to that of the incident intensity ($x = 0$).

The fractional changes in $[A]$ across the cell are small even when the changes in I are not, so it can be treated as being constant at the average value, <[A]> and <[B]>, in the cell. Hence, integration of Eq. 2-5 over the path length of the cell yields the intensity of light absorbed by the molecules

$$I = I_0 e^{(-\varepsilon_A <[A]> + \varepsilon_B <[B]>)x} \qquad \text{Eq. 2-24}$$

The time dependence of the average absorbent concentration is obtained by averaging Eq. 2-5 over the cell, and approximating the average of the product $<[A]I>$ as the product of the averages, i.e.:

$$\frac{d<\overline{[A]}>}{dt} = -K<\bar{I}><\overline{[A]}> + k_2 K<\bar{I}>(1-<\overline{[A]}>) \qquad \text{Eq. 2-25}$$

The average light intensity within the cell is

$$< I >= \frac{I_0}{(\varepsilon_A < [A] > + \varepsilon_B < [B] >) l} \left(1 - e^{-(\varepsilon_A < [A] > + \varepsilon_B < [B] >) l}\right) \qquad \text{Eq. 2-26}$$

where l is the path length within the cell.

Substituting Eq. 2-8 and Eq. 2-26 in Eq. 2-25, we get

$$\frac{d\,A/A_0}{dt} = -K \frac{1}{A_0 (\frac{A}{A_0})} \left[1 - e^{-A_0 \left(\frac{A}{A_0}\right)}\right] \left[\frac{A}{A_0} - \frac{\varepsilon_B}{\varepsilon_A}\right] + k_2 K \frac{1}{A_0 (\frac{A}{A_0})} \left[1 - e^{-A_0 \left(\frac{A}{A_0}\right)}\right] \left[1 - \frac{A}{A_0}\right] \qquad \text{Eq. 2-27}$$

This equation can be written in general form as

$$\frac{dy}{dt} = -\frac{K}{k_3} \left(\frac{1}{y}\right) \left[1 - e^{-k_3 y}\right] [y - k_4] + \frac{k_2}{k_3} K \left[\frac{1}{y}\right] \left[1 - e^{-k_3 y}\right] [1 - y] \qquad \text{Eq. 2-28}$$

The analytical solution to this general form of differential equation does not exist. The equation is analytically solvable only for specific case of $k_2 = 0$ and $k_4 = 0$. This case is true when there is no reverse isomerization reaction B $\rightarrow$ A taking place and also when the ratio extinction coefficient of *cis-* and *trans-* form is quite small ($k_4 = 0$). For this case, the equation 22 reduces to

$$\frac{dy}{dt} = -\frac{K}{k_3} \left[1 - e^{-k_3 y}\right] \qquad \text{Eq. 2-29}$$

Integrating above equation we get,

$$\frac{1}{k_3} \ln \left[\frac{e^{-k_3 y} - 1}{e^{-k_3} - 1}\right] = -Kt \qquad \text{Eq. 2-30}$$

The expression can be hence used for cases where the designed azo-containing surfactant or polymer satisfies the above conditions.

2.7 References

1. Lovrien, R., Proc. Natl. Acad. Sci., U.S.A. 1967, 57, (2), 236-242.
2. Zheng, P., Hu, X., Zhao, X., Li, L., Tam, K. C., Gan, L.H., Macromol. Rapid Commun., 2004, 25, 678-682.
3. Moniruzzaman, M.; Sabey, C. J.; Fernando, G. F., Macromolecules, 2004, 37, (7), 2572-2577.
4. Matejka, L.; Dusek, K., Makromolek. Chem.-Macromol. Chem. Phys., 1981, 182, (11), 3223-3236.
5. Lee, C. T.; Smith, K. A.; Hatton, T. A., Macromolecules, 2004, 37, (14), 5397-5405.
6. Bromberg, L.; Grosberg, A. Y.; Matsuo, E. S.; Suzuki, Y.; Tanaka, T., J. Chem. Phys., 1997, 106, (7), 2906-2910.
7. Olsen, K. G.; Ross, D. J.; Tarlov, M. J., Anal. Chem., 2002, 74, (6), 1436-1441.
8. Chiari, M.; Cretich, M.; Horvath, J., Electrophoresis, 2000, 21, (8), 1521-1526.
9. Sin, S. L.; Gan, L. H.; Hu, X.; Tam, K. C.; Gan, Y. Y., Macromolecules, 2005, 38, (9), 3943-3948.
10. Desponds, A.; Freitag, R., Langmuir, 2003, 19, (15), 6261-6270.
11. Barret, C., Natasohn, A., and Rochon, P., Chem. Mater, 1995, 7, (5), 899-903.
12. Moniruzzaman, M.; Sabey, C. J.; Fernando, G. F., Macromolecules, 2004, 37, (7), 2572-2577.
13. Pallas, N. R.; Pethica, B. A., Colloids Surf., 1983, 6, (3), 221-227.
14. Bromberg, L. E.; Barr, D. P., Macromolecules, 1999, 32, (11), 3649-3657.
15. Szczubialka, K., Ishikawa,K., and Morishima, Y., Langmuir, 16 (5), 2083 -2092, 2000
16. Gosselet, N.M. , Beucler, F., Renard, E., Amiel, C., and Sebille, B., Colloids and Surfaces A: Physicochemical and Engineering Aspects, (1999), Vol. 155,pp. 177-188
17. Lednev, I. K.; Ye, T. Q.; Hester, R. E.; Moore, J. N., J Phys. Chem., 1996, 100, (32), 13338-13341

18. Zimmerman, G., Chow, L.,Y., Paik, U.,N., J. Am. Chem. Soc., 1958, 80, (14), 3528-3531.
19. Kumar, G.S., & Neckers, D.C. (1989)., Chemical Reviews, 89 (8), 1915-1925.
20. Barrett, C., Natansohn, A., & Rochon, P. Chemistry of Materials, 1995, 7(5), 899-903
21. Rau. H., In Photochromism: Molecules and Systems. 1990, (Elservier,
22. Amsterdam), 165-191.
23. Matczyszyn, K., Sworakowski, J., J. Phys. Chem. B, 2003, 107, (25), 6039-6045.
24. Kanbara, T., Oshima, M., Imayasu, T., Hasegawa, K., Macromolecules, 1998, 31, (25), 8725-8730.
25. Bobrovsky, A. Y., Pakhomov, A. A., Zhu, X. M., Boiko, N. I., Shibaev, V. P., Stumpe, J., J. Phys. Chem. B, 2002, 106, (3), 540-546.
26. Sin, S. L.; Gan, L. H.; Hu, X.; Tam, K. C.; Gan, Y. Y., Macromolecules, 2005, 38, (9), 3943-3948.
27. Shang, T., Smith, K. A., Hatton, T. A., Langmuir, 2003, 19, (26), 10764-10773.
28. Durr, H., In Photochromism: Molecules and Systems. Elsevier: Amsterdam, 1990; p 1-14.
29. Kang, H. C., Lee, B. M.; Yoon, J.; Yoon, M., J. Colloid Interface Sci., 2000, 231, (2), 255-264.
30. Forber, C. L., Kelusky, E. C., Bunce, N. J., Zerner, M. C., J. Amer. Chem. Soc.,1985, 107, (21), 5884-5890.
31. Rau. H., In Photochromism: Molecules and Systems. 1990, (Elservier, Amsterdam), 165-191.
32. Nakayama, K.; Endo, M.; Majima, T., Bioconjugate Chem., 2005 16 (6), 1360 - 1366.
33. Durr, H., In Photochromism: Molecules and System. Elservier: Amsterdam, 1990; p 173-176.
34. Badjic, J. D.; Kostic, N. M., J. Phys. Chem. B, 2001, 105, (31), 7482-7489.
35. Pieroni, O., Fissi, A., Ciardelli, F., Photochem. Photobiol.,1986, 44, (6), 785-791.
36. Kumar, G. S.; Neckers, D. C., Chem. Rev., 1989, 89, (8), 1915-1925.

37. Fissi, A.; Pieroni, O.; Balestreri, E.; Amato, C., Macromolecules, 1996, 29, (13), 4680-4685.
38. Green, M. S., J. Chem. Phys., 1946, 15, 80-89.
39. Bromberg, L., Macromolecules, 1998, 31, (18), 6148-6156.
40. English, R. J.; Gulati, H. S.; Jenkins, R. D.; Khan, S. A., J. Rheol., 1997, 41, (2), 427-444; Cox, W.P., Merz, E.H., J.Polym.Sci., 1958, 28, 619-625.
41. English, R. J.; Raghavan, S. R.; Jenkins, R. D.; Khan, S. A., J. Rheol., 1999, 43, (5), 1175-1194.
42. Bromberg, L., In Handbook of Surface and Interfaces of Materials. 2001, Vol. 4: Solid Thin Films and Layers, (Chapter 7), 369-404
43. Gennes, P. G. , Scaling Concepts in Polymer Physics. 1979, (Cornell University Press, Ithaca, New York).
44. Fischer, E., The Journal of Physical Chemistry, 1967, 71(11), 3704-3706.

Chapter 3

Dually responsive system with blends of Pluronic F127 and MOAB-DMA

3.1 Introduction

Stimuli-sensitive materials find a wide range of applications in the food, pharmaceutical, agricultural, electronic and environmental industries, as well as in the biomedical field, in which they are used as cell scaffolds and site-specific drug delivery systems.[1] In particular, temperature-responsive polymers may provide liquid systems with in-situ-gelling ability to form solid drug depots once in a contact with the living tissues.[2] The temperature responsiveness is due to conformational changes caused by an entropy-driven association of moieties on the polymer chains with temperature-dependent water solubility.[3] The appearance of associations with resulting aggregates acting as physical cross-links between polymer chains leads to a gelation or to a complete phase separation.[4] Pluronic or poloxamer copolymers, consisting of poly(ethylene oxide) (PEO) and poly(propylene oxide) (PPO) blocks (PEO-b-PPO-b-PEO), are prevalent representatives of temperature-responsive copolymers used as pharmaceutical excipients. In aqueous solution, the copolymer molecules aggregate forming spherical micelles with a PPO core and a hydrated PEO shell. If the concentration is sufficiently high, an increase in temperature causes an ordered packing of the micelles and their entanglement, inducing gelation of the system.[5] A number of studies on the performance of Pluronic F127 (F127) as a micellar carrier of drugs or as a component of *in-situ* gelling systems, [6] which is approved for intravenous, inhalation, oral solution, suspension, ophthalmic, and topical formulations,[7] have been reported. It is known that the polymer-polymer and polymer-water interactions can be altered by the addition of cosolvents or other polymeric components, which strongly modify the sol-gel transition temperature and the

gel strength and, as a consequence, modify any property dependent on the micro- and macroviscosity of the system, such as solute diffusion or release.[8,9,10]

Photoresponsive systems have been used as sensors or actuators in various fields.[11] Some recent papers have demonstrated ain interest in these systems as membranes able to control the transfer of ions or the flow of monatomic gases or liquids through microchannels.[12] The development of suitable new materials and the study of the photoregulation of the permeation of larger molecules may open new possibilities for photoresponsiveness in separation and drug delivery. Light can be applied externally to the body to switch on and off drug release at a specific site, offering a potential for controlling the release that can be difficult to achieve using other stimuli.[13] Research in this field has been mainly focused on copolymer micelles or liposomes that can be dissociated by the action of light.[14] Photoinduced conformational changes are typically due to the photoisomerization of a dye molecule such as azobenzene bonded to the polymer. The trans-cis isomerization of azobenzene groups alters the polarity and conformation of the polymer chains in a rapid and reversible fashion. The self-association of the azobenzene groups that occurs in the trans conformation is lost when, upon exposure to UV light, the relatively more hydrophilic cis conformation is adopted which causes a decrease in the viscosity as seen in Chapter 2.

Implementation of temperature-induced gel systems with photoregulation may open new approaches for enhancing the performance of matrices that can be started as a free flowing fluid that gels *in-situ* upon exposure to light enabling external tuning using an adequate light source in field of separations and delivery. Hence, the goal of this work is to develop temperature- and light-responsive solutions based on blends of F127 and poly(N,N-dimethylacrylamide-co-methacryloyloxyazobenzene)(MOAB-DMA) polymer. Herein, we are interested in exploring the effect of conformational changes in MOAB-DMA in response to changes in irradiation wavelength on the temperature-responsive behavior of Pluronic solutions.

3.2 Pluronic F127 micelles and gels

Copolymers of poly(ethylene oxide)-poly(propylene oxide)-poly(ethylene oxide) (PEO-PPO-PEO, commercially known as Pluronics, generic name poloxamers) are water soluble and exhibit low toxicity. Certain molecular weight classes of Pluronics have been approved by the Food and Drug Administration (FDA) for clinical use,[15,16] including Pluronic F127. Nonionic polymer surfactant Pluronic F127 has the molecular formula of ($EO_{97}PO_{69}EO_{97}$). These compounds are surface active and form micelles and liquid lyotropic crystalline phases.[17,18] Ultrasonic and light-scattering measurements [19,20,21] have indicated a micellar association for Pluronic F127 over the temperature range 10-40°C. Other techniques such as NMR,[22] rheology, and fluorescence have also shown the micellar arrangement of block copolymers. At low concentrations they form monomolecular micelles, but higher concentrations result in multimolecular aggregates consisting of a hydrophobic central core with the surrounding hydrophilic polyoxyethylene chains facing the aqueous medium. Micellization occurs in dilute solutions of block copolymers in selected solvents above the critical micellar concentration, at a given temperature. The spherical micelle consists of a core of mainly the hydrophobic PPO blocks with a low water content surrounded by a water-swollen corona of PEO blocks. At higher concentrations, above a critical gel concentration, the micelles can order into a lattice. These scenarios are illustrated in Figure 3-1

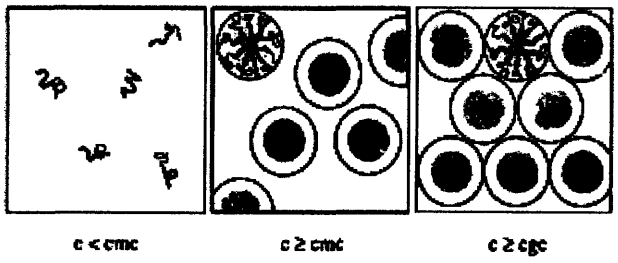

Figure 3-1: Illustration of the critical micelle concentration (cmc) and critical gel concentration (cgc) in a block copolymer solution.[23]

An increase in hydrophobicity of the PPO block and a lower degree of PEO hydration occur at higher temperature or concentration. This leads to a compact packing

of copolymer molecules at higher temperatures in agreement with experimental results showing that the hydrodynamic radius is roughly constant while the aggregation number and the volume fraction of the micelles increases with temperature.[24,25,26] A liquid micellar phase is stable at low temperatures but transforms into a face-centred cubic structure by increasing the temperature for concentrations higher than 17wt% (Figure 3-2).[27] The formation of a gel at higher temperatures is due to an ordered three-dimensional structured state or network. Neutron scattering studies have showed that the observed change in viscosity is due to a "hard sphere crystallization" as the micelle volume fraction approaches the critical volume fraction of 0.53 (micelles close-packed).[28,29] A Pluronic F127 (C> 17wt%) gel is a self-forming liquid-crystalline gel phase, consisting of large, spherical micelles of Pluronic F127 that becomes so crowded that the micelles are forced to pack together into a semiregular lattice (cubic lattice).[30,31,32] The phase is gel-like because the micelles cannot easily slip past one another, despite the absence of crosslinks. The micelles of Pluronic F127 are packed with local face-centered cubic symmetry.[30] The hydrophobic PPO micelle core has a diameter of about 6 to 9nm, whereas the surrounding brush of hydrated PEO chains has an effective diameter that decreases from about 9 to 7nm as the polymer concentration is increased. [33,34,35,36] At even higher temperatures, the gel structure breakdown resulting in a solution of low viscosity.

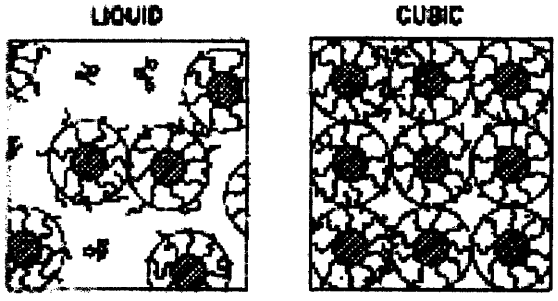

Figure 3-2: Schematic illustration of micellar phases formed by the Pluronics® with increasing temperature. [37]

3.3 Physical blends of Pluronic F127 and photoresponsive polymer MOAB-DMA

Physical blends were made instead of grafting or co-polymerizing Pluronic F127 with MOAB-DMA as it then gives flexibility of changing the composition of the mixture. Lower molecular weight MOAB-DMA (4kDa) was used for this study.

DLS experiments

The DLS measurements were performed using an ALV-5000F optical system equipped with CW diode-pump Nd:YAG solid-state laser (400 mW) operated at 532nm (Coherent Inc., Santa Clara CA, USA). The intensity scale was calibrated against scattering from toluene. The 0.1% DMA-MOAB solutions were filtered (Millipore 0.45 mm, Ireland) into the quartz cell (previously washed with condensing acetone vapour) and maintained at normal light or irradiated at 325 nm. The diffusion coefficient was deduced from the standard second-order cumulant analysis of the autocorrelation functions measured at 90° angle. The apparent hydrodynamic radius ($r_{h,app}$) of the micelles was calculated from the apparent diffusion coefficients. The hydrodynamic radius of the micelles is around 10-15 nm for the *trans* isomer as compared to 2-6nm for the *cis* form. The most interesting result of these experiments was the evolution in the number of counts of the irradiated samples when the UV irradiation finished caused due to the power visible light emitted by the laser. The UV irradiated sample showed a lower number count relative to the non-irradiated sample immediately after UV irradiation for 10 minutes but progressively increased to reach the number of counts observed with the non-irradiated sample over a period of about 15 minutes. This may indicate that UV irradiation causes the number and/or size of micelles/aggregates to decrease. When UV irradiation is stopped, the system recovers its initial state with visible irradiation. This behaviour was found for both MOAB-DMA solutions and MOAB-DMA/Pluronic 1:1 solutions.

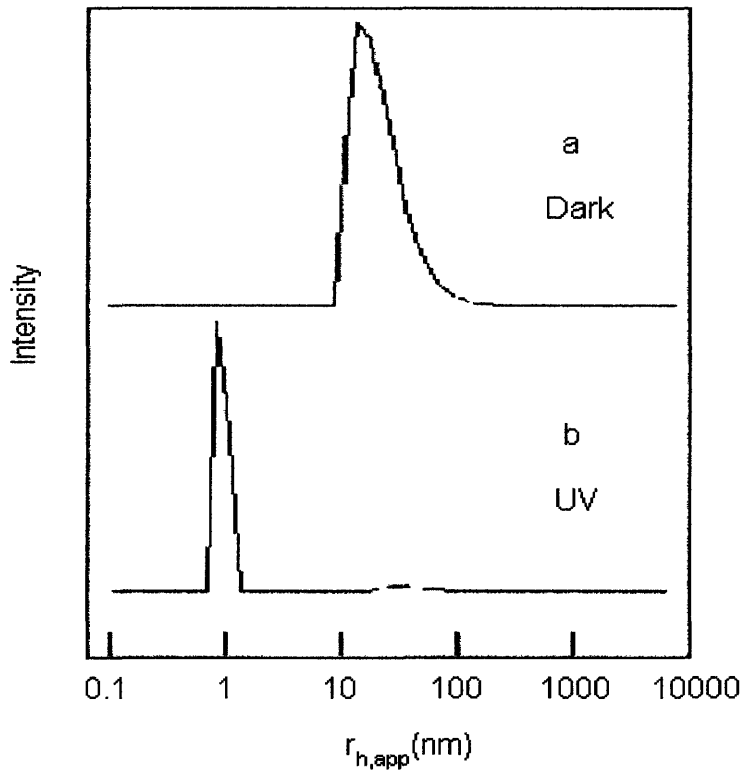

Figure 3-3: Intensity fraction distribution of the apparent hydrodynamic radius for 0.1% MOAB-DMA solution (a, b) under different irradiation conditions

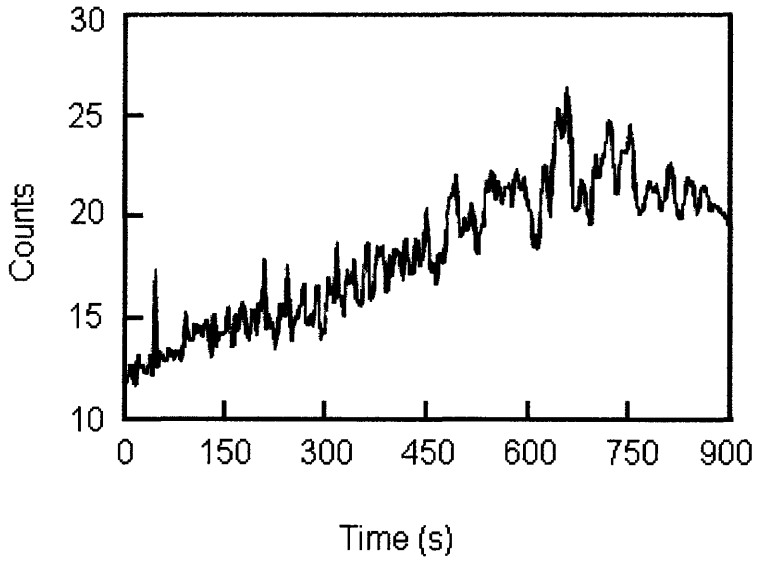

Figure 3-4: Evolution of the count number as a function of time for MOAB-DMA solution (0.1%) UV irradiated for 10 min. The increase in counts is related following the progressive self-aggregation of the azobenzene groups as they recover to the trans conformation.

The UV-vis spectra of MOAB-DMA in the presence and absence of Pluronic F127 is the same indicating the trans- to cis- isomerization is not affected by the presence of F127. The isomerization is completely reversible in the presence of Pluronic F127.

To obtain a homogeneous blend, different ratios of MOAB-DMA and F127 were dissolved in excess THF and the solvent was removed under vacuum. The solutions with different total copolymer concentrations were then prepared (keeping the F127:MOAB-DMA weight ratio constant) by adding appropiate amounts of the dried mixture to cold water under shaking and then stored at 4°C for complete dissolution.

3.3.1 Effect of MOAB-DMA on Pluronic F127 micelles: mixed aggregates

Mixed amphiphile systems (including surfactants, polymers, and copolymers) are fascinating from a scientific standpoint because of the complex ways in which they can associate into "supramolecular", "nanoscale", and "self-assembled" structures. They are technically important because mixtures provide a way of tailoring microdomain properties through simple composition variations; new structures may thus be obtained by changing the system composition, rather than through synthesis of new materials. Formation of mixed micelles or aggregates in case of hydrophobically modified polymers and nonionic surfactants have been observed in past for different systems for which the mixed micelle theory described below can be used.[38]

3.3.1.1 A pseudo-phase model for mixed micellization/ aggregation

The thermodynamic formulation for the mixed micellization process of noninonic surfactants in terms of the phase model is simple because nonionic mixed micelles do not suffer from the complications of the micellar counterion binding and electrostatic effects observed with the charged systems. This formulation can be extended to the aggregation

of nonionic surface active polymer mixture, here we use the model described by Clint.[39] The following symbols are used.

μ_1^b, μ_2^b: chemical potentials of monomeric surfactants 1 and 2 in bulk.

μ_1^{0b}, μ_2^{0b}: standard chemical potentials.

μ_1^m, μ_2^m: chemical potentials of surfactants 1 and 2 in mixed micelles.

μ_1^{0m}, μ_2^{0m}: standard chemical potentials in micelles.

C_{Mmix} : CMC of mixed micelles.

C_{M1}, C_{M2} : CMCs of pure surface active polymer 1 and 2.

y: mole fraction of surfactant 1 in the total polymer mixture.

x: mole fraction of surfactant 1 in the mixed micelles.

C: total concentration of mixed polymers.

C_1^m, C_2^m: concentrations of monomeric surfactants polymer 1 and 2.

Below the CMC ($C \leq C_{Mmix}$), the monomer concentrations are

$$C_1^m = yC \qquad \text{Eq. 3-1}$$

$$C_2^m = (1-y)C \qquad \text{Eq. 3-2}$$

Above the CMC ($C \geq C_{Mmix}$), the micellar mole fraction is expressed by

$$x = \frac{yC - C_1^m}{C - C_1^m - C_2^m} \qquad \text{Eq. 3-3}$$

The chemical potential for surfactant i in a mixed micellar system can be given as follows.[40]

$$\mu_i^m = \mu_i^{0m} + RT \ln x_i \gamma_i \qquad \text{Eq. 3-4}$$

$$\mu_i^b = \mu_i^{0b} + RT \ln C_i^m \qquad \text{Eq. 3-5}$$

$$\mu_i^{0m} = \mu_i^{0b} + RT \ln C_{Mi} \qquad \text{Eq. 3-6}$$

The difference in the standard states $(\mu_i^{0m} - \mu_i^{0b})$ is identical to ΔG_{mic}^0 since it describes the difference per mole between the free energy of surfactant in a micelles and in water, which id equal to $RT \ln C_{Mi}$.[41]

Case 1: Ideal binary mixed surfactant system

If solution ideality can be assumed, then activity coefficient $\gamma_i = 1$ and from the condition of the micellization phase equilibrium, $\mu_i^m = \mu_i^b$ $(i = 1, 2)$, we obtain

$$C_1^m = xC_{M1} \qquad \text{Eq. 3-7}$$

$$C_2^m = (1-x)C_{M2} \qquad \text{Eq. 3-8}$$

Eliminating x from these equations gives

$$C_2^m = \left(1 - \frac{C_1^m}{C_{M1}}\right) C_{M2} \qquad \text{Eq. 3-9}$$

and from Eq. 3-3 and Eq. 3-7

$$C_1^m = \frac{(yC - C_1^m)C_{M1}}{C - C_1^m - C_2^m} \qquad \text{Eq. 3-10}$$

At the CMC, we have

$$yC_{Mmix} = xC_{M1} \qquad \text{Eq. 3-11}$$

$$(1-y)C_{Mmix} = (1-x)C_{M2} \qquad \text{Eq. 3-12}$$

Re-arranging Eq. 3-9 and Eq. 3-10 and combining with Eq. 3-11 and Eq. 3-12, we get

$$C_{Mmix} = \frac{1}{y/C_{M1} + (1-y)/C_{M2}} \qquad \text{Eq. 3-13}$$

$$C_{Mmix} = xC_{M1} + (1-x)C_{M2} \qquad \text{Eq. 3-14}$$

Thus, Eq. 3-13 can be used to calculate the cmc of an ideal mixed surfactant system provided the pure surfactant CMCs are known. Eq. 3-9 and Eq. 3-10 enable calculation of the concentrations of monomeric surfactants C_1^m and C_2^m above the CMC in such a system. If the monomer concentrations are evaluated at a certain concentration C above the CMC, the micellar/aggregate composition x can be calculated by means of Eq. 3-3, as a function of the concentration C. In addition, one can predict solution properties primarily depending on monomeric surfactant/polymer concentrations under certain conditions.

Case 2: Nonideal binary mixed surfactant system

The preceding equations have been derived for systems containing ideal mixed micelles composed of nonionic surfactants. However, the equations Eq. 3-4 to Eq. 3-6 can be applied to systems of nonideal mixed micelles by not eliminating the activity coefficient for surfactant i in the mixed micelles. For a binary surfactant system, applying the condition for micellization equilibrium ($\mu_i^m = \mu_i^b$), we get

Eq. 3-15

$$C_i^m = x_i \gamma_i C_{Mi} \quad (i = 1,2) \qquad \text{(a,b)}$$

At the CMC, Eq. 3-15 (a,b) become

$$yC_{Mmix} = x\gamma_1 C_{M1} \qquad \text{Eq. 3-16}$$

$$(1-y)C_{Mmix} = (1-x)\gamma_2 C_{M2} \qquad \text{Eq. 3-17}$$

Eq. 3-16 and Eq. 3-17 lead to the expression for the cmc of the non-ideal mixed surfactants,

$$C_{Mmix} = \frac{1}{\frac{y}{\gamma_1 C_{M1}} + \frac{(1-y)}{\gamma_2 C_{M2}}} \qquad \text{Eq. 3-18}$$

The micellar activity coefficients under the regular solution approximation[42] are

$$\gamma_1 = \exp(\beta(1-x)^2 \qquad \text{Eq. 3-19}$$

$$\gamma_2 = \exp(\beta x^2) \qquad \text{Eq. 3-20}$$

where β is an interaction parameter. The single parameter β is expressed in terms of the molecular interactions in the mixed micelles:

$$\beta = \frac{N_A(w_{11} + w_{22} - 2w_{12})}{RT} \qquad \text{Eq. 3-21}$$

where w_{11} and w_{22} are the energies of interaction between the same kinds of surfactant molecules in the pure micelles; w_{12} is the interaction energy between the different kinds of molecules in the mixed micelles; and N_A is the Avagardo number. If the value of β is

obtained from the experiment, one can discuss the mixed micellization in terms of molecular interactions.

Using Eq. 3-19 and Eq. 3-20, we can get $\ln\gamma_1 / \ln\gamma_2$ which can be further equated to those obtained from Eq. 3-16 and Eq. 3-17 leading to two expressions,

$$\frac{x^2 \ln\left(C_{Mmix}\, y / C_{M1}\, x\right)}{(1-x)^2 \ln\left(C_{Mmix}(1-y) / C_{M2}(1-x)\right)} = 1 \qquad \text{Eq. 3-22}$$

From experimental measurements of the CMC of a binary mixed surfactant system, C_{Mmix}, as a function of the monomer composition in bulk, y, and the CMCs of pure surfactants, C_{M1} and C_{M2}, Eq. 3-22 can be used to determine the compositions, x and $(1-x)$, of the mixed micelle formed at the C_{Mmix}. The interaction parameter β can then be fit using the values of y, C_{M1} and determined value of x in Eq. 3-18 by comparing it with the observed C_{Mmix}. The value of C_{Mmix} can in turn, be calculated by using Eq. 3-18, Eq. 3-19 and Eq. 3-20 using the determined value of β and x as a function of monomer (bulk) composition. From Eq. 3-22, it can be seen that if β is large and negative, the interaction between the two surfactants in the mixed micelles is strong and the mixed micelles are stabilized.

Fluorescence spectroscopy has often been commonly used to obtain critical micelle concentration in case of Pluronics[43] and is similarly used to determine the CMCs of the lower molecular weight (~4000 kDa) MOAB-DMA, the other surface active polymer used in this study. The fluorescence spectroscopy was also used for measuring cmc for high molar ratio MOAB-DMA solutions for two reasons (i) consistency of the technique used and (ii) that we are using smaller molecular weight polymer here as compared to the one discussed in Chapter 2, the formation of pre-micellar aggregates would not exist over long range of concentration as in case of low-molecular weight surface-active polymer the n-mers forming aggregates will be low in number. The

transition from unimers to micelles/aggregates in both cases is found to be narrow enough for the cmc/cac can be obtained from intersection of the tangent to the transition line with the baseline as shown in Figure 3-5.[26]

3.3.1.2 Experimental

Fluorescence spectroscopy was used to obtained the critical micelle/aggregate concentration of the mixture of Pluronic F127 and the photoresponsive polymer, MOAB-DMA. Solutions containing Pluronic F127 and MOAB-DMA were prepared at different molar ratios ranging from 0 to 1. Nile red was used as a probe in the study. Nile Red is a positive solvatochromic dye and shows one of the largest shifts in excitation and emission maxima in going from nonpolar solvents (λ_{max}^{ex} ~ 484 nm, λ_{max}^{em} ~ 529 nm) to polar solvents (in water, λ_{max}^{ex} ~ 591 nm, λ_{max}^{em} ~ 657 nm). All three of the absorption, excitation, and emission maxima shift to the lower energies when the polarity of the medium surrounding Nile Red is increased. Nile Red has photochemical stability and strong fluorescence nature and has been extensively used in many different applications where the dipolarity of the medium needs to be explored.[44] Nile Red was chosen as a probe also for the reason that its absorption curve in water does not overlap with that of MOAB-DMA in constrant to the absorption spectra of pyrene, DPH.

A concentrated solution of Nile Red in methylene chloride solvent was prepared (2.65μM). About 0.02 ml of this concentrated solution was added to 1 ml of the solution under study. The methylene chloride from the resultant mixture was removed via evaporation. The emission scan over the wavelength range from 600 to 700 nm was recorded using TimeMaster Fluorescence Lifetime Spectrometer (Photon Technology International, PTI, Canada) in the steady-state mode (band-pass, 3 nm; integration time, 2 s) with excitation wavelength, λ^{ex} = 570nm for Nile Red. The fluorescence intensity was measured for different polymer concentrations of a given molar ratio.

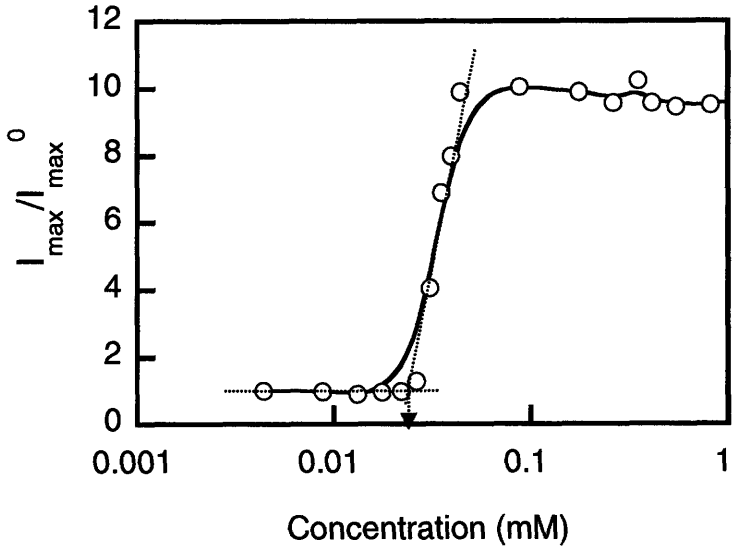

Figure 3-5: Maximum fluorescence intensity normalized by the fluorescence intensity of Nile Red in a non-aggregated state as affected by the concentration of the mixture of Pluronic F127 and MOAB-DMA (molar ratio 80:20). The estimation of critical micelle/aggregation concentration from the data is shown by the dotted line.

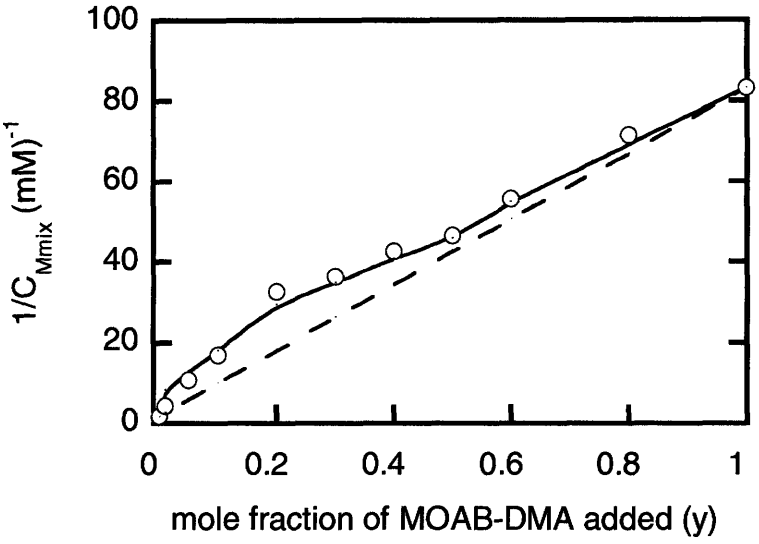

Figure 3-6: Experimental values of the cmcs (o) of the F127/ MOAB-DMA mixtures at different MOAB-DMA mole fraction from fluorescence measurements at 25°C plotted in inverse form; calculated cmc's for ideal mixed micelles according to Eq. 3-13 (dashed line); and calculated cmc's according to regular solution theory with β value of -5.5(solid line).

The critical micelle/aggregation concentration for physical blends of different molar ratios is given in Figure 3-6. Very good fit of regular solution theory to experimental values was found to be with $R^2 \geq 0.99$. The interaction parameter β provides a useful way to identify synergistic ($\beta < 0$) and and antagonist behavior ($\beta > 0$) between two surfactants in a mixture. The value of β =-5.5 fits the data well with R^2 close to 1. These results show that there is synergy between F127 and MOAB-DMA at 25°C. For comparison purposes a β of -3.4 was reported for $C_{12}EO_6$ / SDS mixed micelles in presence of NaCl[45] and a value of -2.7 for $C_{12}EO_6$ / Pluronic F127 mixed micelles.[46] This all shows that in all cases mixed micellar aggregates are formed in the mixture of Pluronic F127 and MOAB-DMA. The mixed micellar aggregates are formed with inclusion of azobenzene side chains of MOAB-DMA within the PPO core of Pluronic F127 micelles.

Table 3-1: Critical Micelle Concentrations of Aqueous Mixtures of F127/MOAB-DMA at 25°C deduced from fluorescence measurements. $x_{MOAB-DMA}$ is the mole-fraction of MOAB-DMA in the mixed micelles and γ is the activity coefficient. The values of activity coefficient calculated using β of -5.5.

Overall Molar fraction of MOAB-DMA	CMC_{mix} (mM)	$x_{MOAB-DMA}$	$\gamma_{MOAB-DMA}$	γ_{F127}
0	0.550	-	-	-
0.01	0.239	0.40	0.14	0.84
0.05	0.093	0.59	0.40	0.68
0.1	0.059	0.67	0.54	0.61
0.2	0.031	0.71	0.62	0.58
0.3	0.028	0.79	0.78	0.51
0.4	0.024	0.84	0.87	0.46
0.5	0.022	0.91	0.96	0.40

0.6	0.018	0.90	0.94	0.41
0.8	0.014	0.93	0.98	0.38
1	0.012	-	-	-

The value of activity coefficient of both F127 and MOAB-DMA is close to 1 when they are close to pure state as expected. The large mole-fraction of MOAB-DMA in mixed micelles even at total lower molar ratio of MOAB-DMA can be attributed to the fact that the short hydrophobic azobenzene-containing side chain can be easily solubilized in the PPO core of the Pluronic F127 surfactant micelles. On the other hand the mole fraction of F127 in mixed micelles is smaller (less than 0.1) even at a molar ratio of 0.5 and less. The reason can be that the azobenzene core formed by MOAB-DMA is smaller and can only accommodate a lower mole-fraction of F127 in mixed micelles.

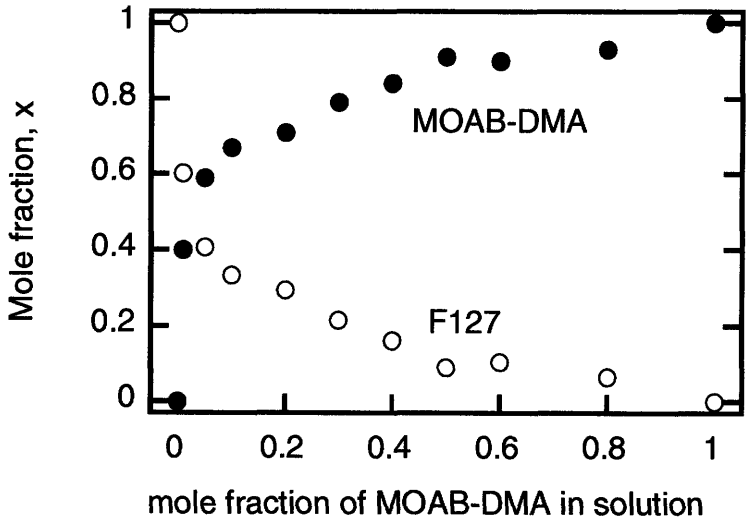

Figure 3-7: Plot of mole-fraction of F127 and MOAB-DMA in mixed micelles with respect to added mole fraction of MOAB-DMA in the total surfactant solution

3.4 Thermodynamics of physical blends of Pluronic F127 and MOAB-DMA

A micro DSC III instrument (SETARAM, France) with an ultralow background noise (< 0.2μW) was employed in the conventional differential scanning calorimetry (DSC) measurements. Liquid samples weighing 100 mg were placed in a fluid-tight batch vessel and run against distilled water as a reference. Multiple heating – cooling cycle scans were performed with scan rates of 1K/min.

In the DSC experiments a well-defined endothermic peak characteristic of the micellization of triblock copolymers was obtained. The concentration of Pluronic F127 used in this study was 10wt%; at higher concentrations it was not possible to obtain a complete peaks within the range of the equipment capability (e.g. for 12-15 wt% the onset temperature with addition of MOAB-DMA is below -5°C). The transition from unimers to micelles results in a broad endothermic transition. The determination of the critical micelle temperature from DSC experiments has been of debate. The transition can be characterized either by the temperature of the peak transition at maximum heat flow (T_p) or by the onset temperature (T_{on}), which is determined from the intercept of the base-line prior to the transition and the tangent to the increasing part before the peak defining the CMT.[47,48] In this study both the temperature at the onset of the peak and peak temperature will be analyzed.

Typical DSC peaks for 10% wt% F127 in the presence of various amounts of MOAB-DMA ranging from 0.1 to 3.5 wt% are shown in Figure 3-8. These endothermic transition peaks occur as a result of heating, and from the peak area the micellization enthalpy ΔH_{mic} can be evaluated for each composition. The narrow peak of F127 alone is broadened on addition of MOAB-DMA as the population of micelles is diversified. From Figure 3-8, it can also be seen that both T_p and T_{on} are shifted to left, i.e. a decrease in T_p and T_{on} as the amount of MOAB-DMA is increased in the mixture with F127.

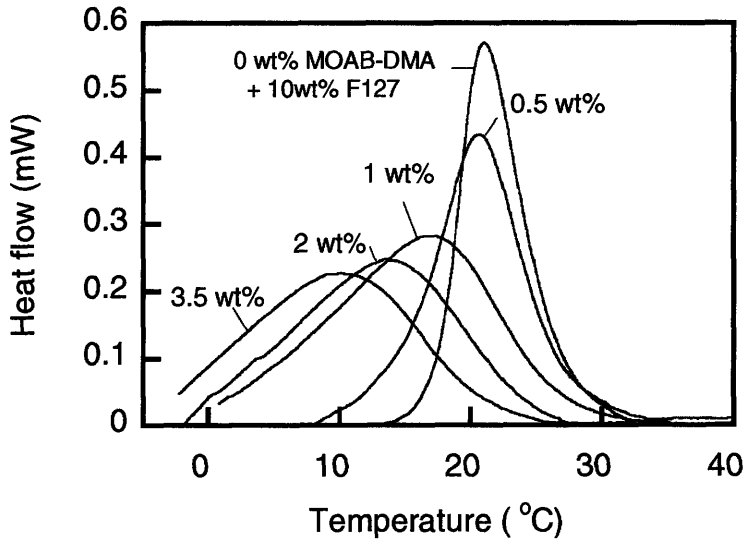

Figure 3-8: Change of the peak temperature and CMT of F127 caused by the addition of different amounts of MOAB-DMA. DSC data in which heat flow is plotted as a function of temperature for 10wt% F127 in the presence of different amounts of MOAB-DMA

The addition of MOAB-DMA to a fixed amount of F127 seems to stabilize the mixed micelles in the sense that the CMT moves to lower temperatures (cmc is decreased). The solubilization of azobenzenes present as sidechains in the MOAB-DMA polymer in Pluronic F127 micelles leads to a stabilization of the micelle and thus lowers the critical micellization temperature (cmt), analogously to the well-documented effect of solubilization of other non-polar solutes.[49]

The heat of micellization for an ideal surfactant binary mixture can be given by

$$\Delta H_{mic} = x\Delta H_{mic,1} + (1-x)\Delta H_{mic,2} \qquad \text{Eq. 3-23}$$

The excess molar enthalpy of micellization can be given by

$$H^E = x(1-x)\beta RT \qquad \text{Eq. 3-24}$$

and hence

$$\Delta H_{mic} = x\Delta H_{mic,F127} + (1-x)\Delta H_{mic,MOAB-DMA} + x(1-x)\beta RT \qquad \text{Eq. 3-25}$$

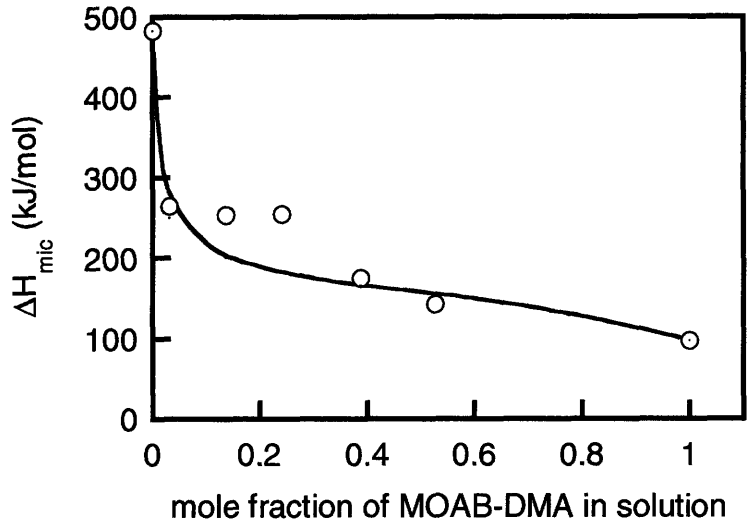

Figure 3-9: The heat of micellization of mixed micelles of F127 and MOAB-DMA for different mole fraction of MOAB-DMA in solution. The (o) shows the values obtained experimentally from DSC whereas solid line represents the calculated heat of micellization using Eq. 3-25 with $\beta = -5.5$

The heat of micellization obtained for 10wt% F127 in our study is close to that reported by Shishido et. al.[50]From Figure 3-9 it can be seen that the regular solution theory for mixed micelles can be applied to our system of Pluronic F127 and MOAB-DMA. These data clearly indicate that the interaction of MOAB-DMA and F127 causes mixed micellization process with an enthalpy of the micellization that is very sensitive to the composition of the mixed micelles.

3.5 Effect of MOAB-DMA on gelation of Pluronic F127 solutions

Rheological measurements on higher concentration of F127 solutions were performed using a controlled stress Rheolyst Series AR1000 Rheometer (TA Instruments,

New Castle, DE) with a cone and plate geometry system (cone: diameter, 2 cm; angle, 2°, truncation, 57 μm). Temperature control (internal resolution 0.016 °C) was provided by two Peltier plates. Dynamic experiments were carried out in a controlled stress mode (temperature ramp ca. 2.5 deg/min). With increases in the amount of MOAB-DMA copolymer added to a Pluronic F127 30wt% solution, the gelation temperature decreases as shown in Figure 3-10. The trans- isomers are in their planar, apolar form that is extremely hydrophobic and promotes formation of aggregates which can localize Pluronic unimers and the unassociated trans- azobenzene can be solubilized in the PPO core.[51] The solubilized azobenzene in the PPO core leads to a reduction in the gelation temperature for any given Pluronic F127 concentration.[52]

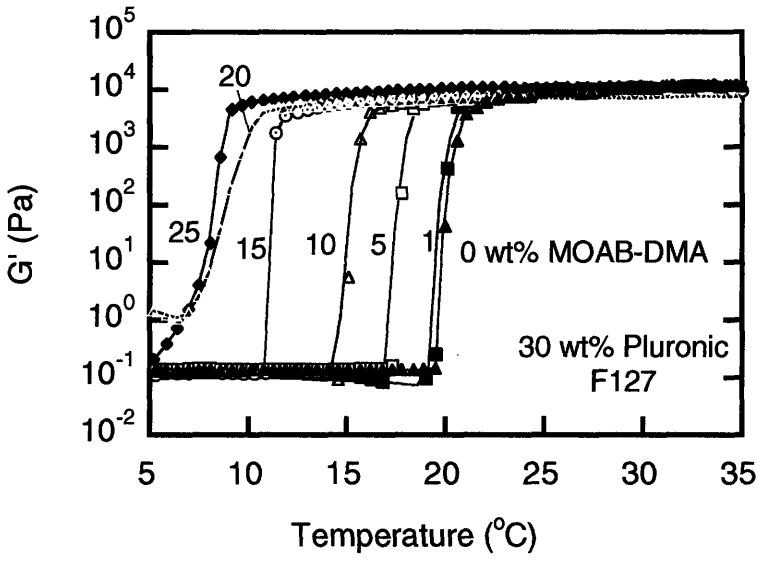

Figure 3-10: Plot of storage modulus with respect to temperature of 30 wt% Pluronic solution with different composition of MOAB-DMA copolymer added (added MOAB-DMA wt%s' shown as legends next to its respective plot) under dark-adapted state.

3.5.1 Gelation temperature dependence on UV irradiation for the blends of Pluronic F127 and MOAB-DMA

Similar to the effect of lowering the critical micellization temperature, solubilization of azobenzene in PPO core can lead to increases in micelle volume fraction to exceed the critical and form ordered three-dimensional gel. Also the backbone of the

MOAB-DMA can help in bridging the Pluronic micelles to induce the gelation of micellar suspension. The schematic of the association is shown in Figure 3-11 A.

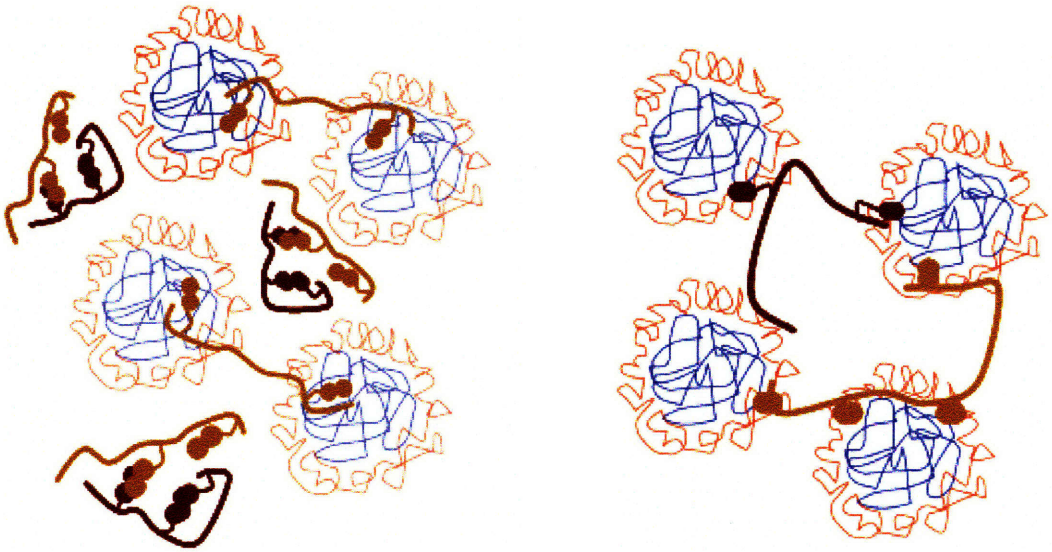

A B

Figure 3-11: Schematic of association of MOAB-DMA with Pluronic F127 micelles. The spherical micelles are of Pluronic F127 and the polymer with sidechains is representative of MOAB-DMA polymer (azobenzene shown by filled circles), (A) represents trans-isomer whereas (B) represents cis-isomer

The temperatures at which the storage moduli increased, which indicate massive formation of micelles that crowd the system thus dramatically enhancing its viscoelasticity, corresponded to the gelation temperatures (further referred to as T_{gel}). The gelation point was taken to be the temperature at which $G'=G''$. T_{gel} declined systematically with the concentration of the added MOAB-DMA, resulting in a decrease of over 15°C at the highest concentration studied. Figure 3-12 shows the gelation temperature for the mixture of 30wt% Pluronic F127 with varying mole fraction of MOAB-DMA under dark-adapted state as well as after UV irradiation. The effect of UV irradiation i.e. conversion of the trans- to cis- on gelation temperature can be seen clearly from Figure 3-12. Notably, the UV irradiation of the blends resulted in measurable and systematic shifts in the T_{gel}, which was observed to be lower in the solutions where the majority of the azobenzene groups were in their cis- conformation. Trans moieties associate with each other forming aggregates that incorporate Pluronic unimers while the

unassociated moieties are incorporated into the Pluronic micelles (PPO core) leading to the reduction of gelation temperature. The formation of the mixed micelles dramatically impacts the T_{gel}. The findings in Figure 3-12 are likely due to a less persistent formation of MOAB-DMA aggregates upon UV-irradiation with more unassociated cis-azobenzene groups becoming available for incorporation within the Pluronic micelles to form mixed micelles, as can be seen in Figure 3-11.On the other hand, the persistence of the DMA-MOAB aggregates in the dark reduces the availability of the azobenzene moieties for incorporation in the Pluronic micelles, and thus T_{gel} changes to comparatively lower extent.

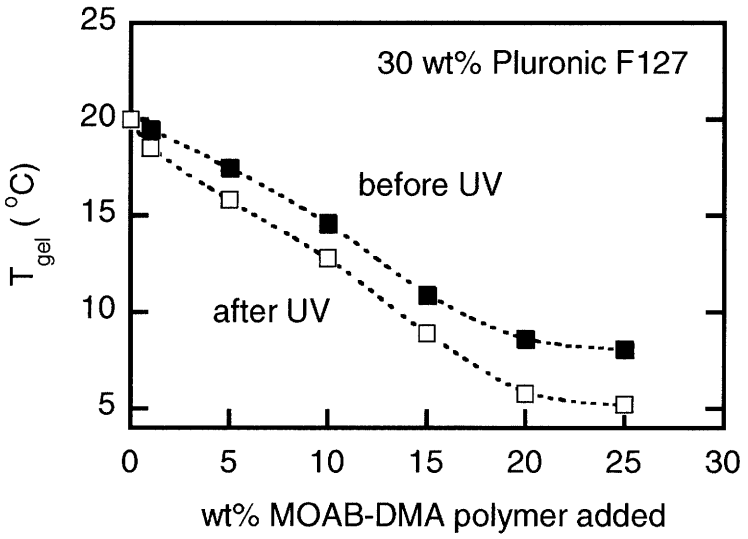

Figure 3-12: Plot of gelation temperature with respect to the composition of MOAB-DMA copolymer added. The shift in gelation before UV (filled squares) and that after UV (open squares) shows that there is 2-3° C decrease in gelation temperature upon irradiation.

Additional experiments were done to confirm that the interaction of the azobenzene and the micelles caused the above effects. It is known that cyclodextrins may form complexes with azobenzene groups, altering their self-associative behavior,[53] the effects of the hydroxypropyl-β-cyclodextrin (HP-βCD) addition to the MOAB-DMA solutions were also investigated. The DLS analysis of F127: MOAB-DMA 2:1 weight ratio solutions stored at dark with addition of HP-βCD showed two populations with

diameters centered at 0.6 and 7 nm, respectively (Figure 3-13 a). The first peak at 0.6nm can be attributed to the free HP-βCD units.[54] After UV irradiation, the peak at 0.6 nm disappeared, which indicates that as self-association of the azobenzene groups decreases, complexation with cyclodextrin units becomes more favorable (Figure 3-13 b).

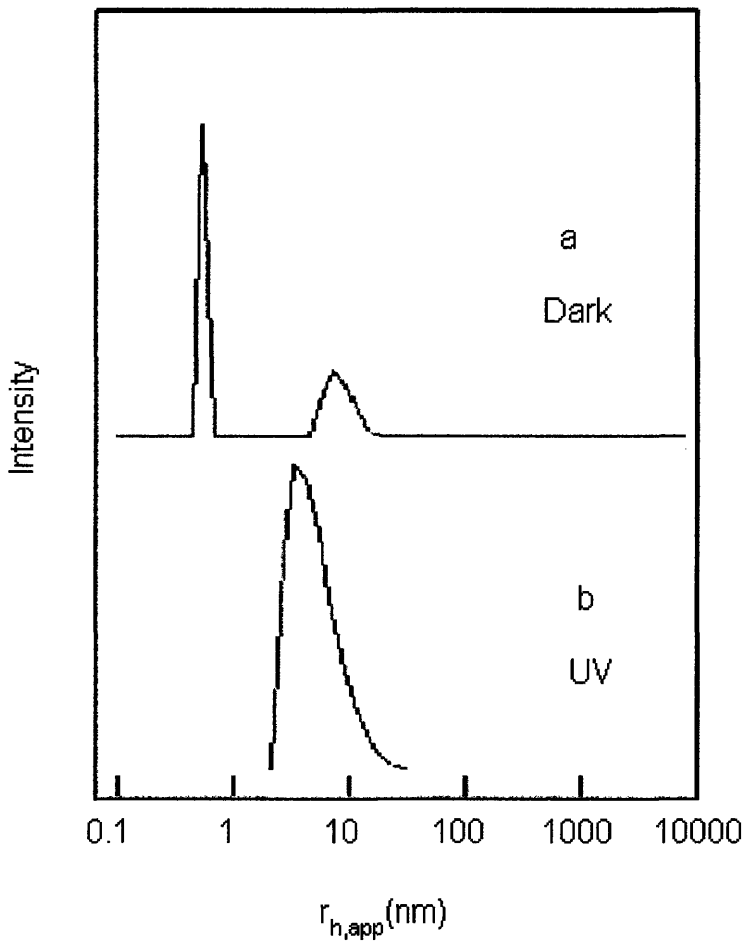

Figure 3-13: Intensity fraction distribution of the apparent hydrodynamic radius for 0.05% DMA-MOAB solution in presence of F127 and cyclodextrin such that F127:MOAB-DMA:HP-βCD 2:1:1 solution (a, b) under different light conditions. In sample a, the peak at 0.6 nm, which corresponds to free HP-βCD units, disappeared after UV irradiation for 10 min mostly due to complexation of the azobenzene groups of MOAB-DMA with HP-βCD.

This means that the self-association of the azobenzene groups at trans conformation makes the complexation with HP-βCD difficult despite of being energetically more

favorable than when they are at cis conformation. The isomerization to the cis conformation, with the consequent rupture of the aggregates, was needed to enable the cyclodextrin to complexate the azobenzene group.

To test the hypothesis of the hydrophobic interaction of the aromatic groups of the MOAB- DMA with Pluronic F127 micelles, additional rheological experiment was carried out by adding HP-βCD to the solutions. The DLS data indicated that complexation of azobenzene with HP-βCD indeed occurs. The addition of HP-βCD to F127:DMA-MOAB 2:1 solutions for F127 concentration greater than 17wt% caused the system to lose the light-induced gelation; i.e., T_{gel} remained constant regardless of the irradiation conditions. The lack of light-responsiveness can be explained by the greater proportion of MOAB groups that form complexes with the cyclodextrin units. Thus, the gelation temperature of the system becomes independent of the irradiation conditions when there are insufficient extra free azobenzene groups to interact with the F127 micelles. These results indicate that the effect of light on the T_{gel} of the blend system is due to its influence on the extent of the hydrophobic interactions between both copolymers.

3.5.2 Sol-gel transition using photo-stimuli

The lowering of the gelation temperature with UV irradiation indicates that there will be a small range of temperature for which sol to gel transition can be carried out using only light as stimuli converting trans- to cis-. It was found that with 20 wt% Pluronic F127 with 5wt% azobenzene, the gelation temperature under trans- state was close to room temperature. The gelation temperatures from storage modulus plot can be seen from Figure 3-14 for the composition described above for both trans- and cis-dominant states. At intermediate temperature of T=23°C, sol-gel transition can be obtained by shining UV irradiation (Figure 3-14). It was observed that the viscosity changed from 2x 10^2 cP to 3x 10^5 cp for this composition (~ 1500 fold increase) upon UV irradiation at this blend composition.

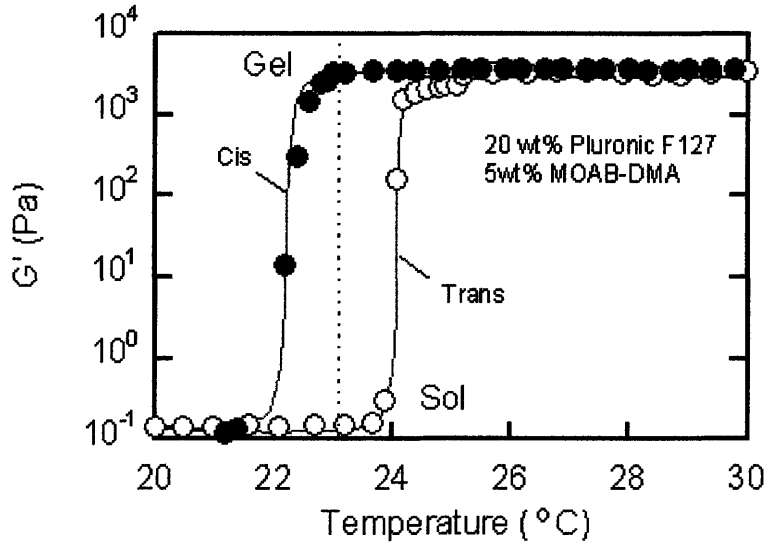

Figure 3-14: Plot of storage moduli (G') with respect to temperature for 20wt% Pluronic F127 solution with 5wt% MOAB-DMA copolymer before UV (open circles) and after UV (filled circles).

3.6 Conclusion

Surface-active polymer mixtures are widely used in many different commercial formulations. [55,56] One of the fundamental requirements in understanding the behavior of these systems is the knowledge of the equilibrium concentrations during the binding process. During the course of these studies it is discovered that the nonionic surfactant MOAB-DMA interacts strongly with the triblock copolymer F127. This is a surprising observation in the sense that under normal circumstances it is generally accepted that nonionic surface-active polymers have little or no affinity toward nonionic polymers, particularly at room temperature.[57,.58] But the strong interaction is due to the azobenzene solubilizing in the PPO core of the Pluronic F127 micelles. The light-induced trans-cis isomerization of DMA-MOAB alters the interaction of this copolymer with F127 micelles and, as a consequence, modifies the sol-gel temperature of the system. Therefore, it is possible to prepare a liquid system of low viscosity in the dark and to increase the viscosity rapidly when light is applied at room temperature. The dual light-

and temperature-responsiveness of the DMA-MOAB:F127 blend can be used as matrix for delivery as well as for separations.

3.7 References

1. Packhauser, C. B.; Schnieders, J.; Oster, C. G.; Kissel, T. Eur. J. Pharm. Biopharm. 2004, 58, 445-455.
2. Ruel-Gariepy, E.; Leroux, J-C. Eur. J. Pharm. Biopharm. 2004, 58, 409-426.
3. Tanaka, T. ACS Symp. Ser. 1992, No. 480, 1-21.
4. Chevillard, C.; Axelos, M. A. V. Colloid Polym. Sci. 1999, 275, 537-545.
5. Dumortier, G.; Grossiord, J. L.; Agnely, F.; Chaumeil, J. C. Pharm. Res. 2006, 23, 2709-2728.
6. Rowe, R.; Sheskey, P.; Weller, P.J. Handbook of Pharmaceutical Excipients, 4th ed.; Pharmaceutical Press and American Pharmaceutical Association: London, Washington, DC, 2003; p 447.
7. Kabanov, A. V.; Batrakova, E. V.; Alakhov, Yu, V. J. Controlled Release 2002, 82, 189-212.
8. Gilbert, J. C.; Richardson, J. L.; Davies, M. C.; Palin, K. J. J. Controlled Release 1987, 5, 113-118.
9. Eeckman, F.; Amighi, K.; Moes, J. Int. J. Pharm. 2001, 222, 259-270.
10. Pisal, S. S.; Paradkar, A. R.; Mahadik, K. R.; Kadam, S. S. *Int. J. Pharm.* 2004, *207*, 37-45.
11. Barrett, C.; Mermut, O. PMSE Prepr. 2005, 92, 51-52.
12. Rosario, R.; Gust, D.; Hayes, M.; Jahnke, F.; Springer, J.; Garcia, A. A. Langmuir 2002, 18, 8062-8069.
13. Jiang, J.; Tong, X.; Morris, D.; Zhao, Y. Macromolecules 2006, 39, 4633-4640.
14. Bisby, R. H.; Mead, C.; Morgan, C. C. Biochem. Biophys. Res. Commun. 2000, 276, 169-173.
15. Escobar-Chávez1, J. J., López-Cervantes, M., Naïk2, A., Kalia, Y. N., Quintanar-Guerrero, D., Ganem-Quintanar, A., Applications Of Thermo-Reversible Pluronic

F-127 Gels In Pharmaceutical Formulations; J. Pharm. Pharmaceut. Sci., 2006, 9(3):339-358.

16. Miller S. C., and Drabik, B. R., Rheological properties of poloxamer vehicles, Int. J. Pharm., 18, 269-276, 1984.
17. Attwood, D., Collet, J. H., and Tait, C., The micellar properties ofn the poly(oxyethylene)–poly(oxypropylene) copolymer Pluronic F-127 in water and electrolyte solution, Int, J. Pharm., 26, 25-33, 1985.
18. Chen-Chow, P., Drug Release from Pluronic F-127 Gels, Diss. Abstr. Int., 340, 4751, 1980.
19. Schmolka, R., Physical basis for poloxamer interactions, Ann. N. Y. Acad. Sci.,720, 92-97,1994.
20. Almgren, M., Bahadur, P., Jansson, M., Li, P., Brown, W., Bahadur, A., J. Colloid Interface Sci., 151, 157, 1992.
21. Rassing, J., and Atwood, D., Ultrasonic velocity and ligth scattering studies on polyoxyethylene-polyoxypropylene copolymer Pluronic F-127 in aqueous solution, Int. J. Pharm., 13, 47-55, 1983.
22. Zhou, Z., and Chu, B., Light scattering study on the association behavior of triblock polymers of ethylene oxide and propylene oxide in aqueous solution, J. Colloid interface Sci., 126, 171-180, 1988
23. Yu, G., Deng, Y., Dalton, S., Atwood, D., Price, C., Booth, C., J. Chem. Soc. Faraday Trans., 25, 2537, 1992.
24. Rassing, J., Mackenna, W., Bandopadhyay, S., and Eyring, E., Ultrasonic and 13C-nmr studies on gel formation in aqueous solutions of the ABA block polymer Pluronic-127, J. Mol. Liquid., 27, 165-178, 1984.
25. Rassing, J., Mackenna, W., Bandopadhyay, S., and Eyring, E., Ultrasonic and 13C-nmr studies on gel formation in aqueous solutions of the ABA block polymer Pluronic-127, J. Mol. Liquid., 27, 165-178, 1984.
26. Escobar-Chávez1, J. J., López-Cervantes, M., Naïk2, A., Kalia, Y. N., Quintanar-Guerrero, D., Ganem-Quintanar, A., Applications of Thermo-Reversible Pluronic F-127 Gels in Pharmaceutical Formulations; J. Pharm. Pharmaceut. Sci., 2006, 9(3):339-358.

27. Mortemsem, K,, Brown, W., and Noeden, B., Inverse melting transition and evidence of three dimensional cubatic structure in a block copolymer micellar system. Phys. Rev. Lett., 68, 2340-2343.
28. Linse, P., Phase behavior of poly(ethylene oxide)-poly(propylene oxide) block copolymers in aqueous solution, J. Phys. Chem., 1993, 97, 13896-13902.
29. Mortensen, K, and Talmco, Y., Cyro-TEM and SANS microstructural study of Pluronic® polymer solutions, Macromoleciles, 1995, 28, 8829-8834.
30. Wu, C., Liu, T., Chu, B., Schneider,D.K., and Graziano,V., Characterization of the PEO-PPO-PEO triblock copolymer and its application as separation medium in capillary electrophoresis, Macromolecules, 1997, 30, 4574-4583.
31. Wu, C., Liu, T., Chu, B., Schneider, D.K., and Graziano,V., Characterization of the PEO-PPO-PEO triblock copolymer and its application as separation medium in capillary electrophoresis, Macromolecules, 1997, 30, 4574-4583.
32. Mortemsem, K,, Brown, W., and Noeden, B., Inverse melting transition and evidence of three dimensional cubatic structure in a block copolymer micellar system. Phys. Rev. Lett., 68, 2340-2343.
33. Wanka, G., Hoffman, H, and Ulbricht, W., Phase diagrams and aggregation behavior of poly(oxyethylene)-poly(oxypropylene)-poly(oxyethylene) triblock copolymers in aqueous solution, macromolecules, 1994, 27, 4145-4149.
34. Mortensen, K, and Talmco, Y., Cyro-TEM and SANS microstructural study of Pluronic® polymer solutions, Macromoleciles, 1995, 28, 8829-8834.
35. Kaler, E. W.; Herrington, K. L.; Miller, D. D.; Zasadzinski, J. A. *NATO ASI Ser. C* 1991, *369*, 571.
36. J.H. Clint, J. Chem. Soc. Faraday I,1975, 71,1327
37. D.N. Rubingh in Solution Chemistry of Surfactants, (K.L. Mittal, ed.), Plenum, New York, 1979, Vol. 1 , pp. 337
38. J.F. Scamehorn in Phenomena in Mixed Surfactant Systems (J.F. Scamehorn, ed.), ACS Symp. Ser. 311, American Chemical Society, Washington, D.C., 1986, p.1.
39. P.M. Holland in Structure / Performance Relationship in Surfactants (M.J. Rosen, ed.) ACS SYmp. Ser. 253, American Chemical Society, Washington, D.C., 1984, p. 141

40. M.J.Hey, J.W. MacTaggart, and C.H.Rochester, J. Chem. Soc. Faraday I 81: 207 (1985)
41. C.M. Ngyugen, J.F. Scamehorn, J. Colloid Interface SCi, 112: 438 (1986)
42. R.F. Kamrath and E.I. Franses, Ind. Eng. Chem. Fundam. 22:230 (1983)
43. N.Nishikido, J. Colloid Interface Sci, 60: 242 (1977)
44. F. Tokiwa and K. Agiami, Kolloid Z.Z. Polym., 239: 687 (1970)
45. J. F. Deye, T. A. Berger and A. G. Anderson, Anal. Chem., 1990, 62,615
46. Goloub, T.P., Pugh, R.J., Zhmud, B.V., J. Colloid Interface Sci. 2000, 229, pp-72
47. S. Couderc, Y.Li, D.M. Bloor. J.F. Holzwarth, and E. Wyn-Jones, Langmuir, 2001, 17, 4818-4824
48. Nixona, S.K., Hvidtb, S., and Bootha, C., Journal of Colloid and Interface Science, 2004, 280(1), 219-223
49. Hecht, E.; Mortensen, K.; Gradzielski, M.; Hoffmann, H. J. Phys. Chem. 1995, 99, 4866
50. N. Plucktaveesak, L.E. Bromberg, and R.H. Colby, XIIIth International Congress on Rheology, Cambridge, UK, 2000
51. Shishido,S.M., Seabra, A.B., Loh, W.,and Ganzarolli de Oliveira,M., Biomaterials, 2003,24(20), 3543-3553
52. Gille, K., Knoll, H., Rittig, F., Fleisher, G., and Karger, J., Langmuir , 15 (4), 1999, pp. 1059-1066
53. Zheng, P.; Hu, X.; Li, L.; Tam, K. C.; Gan, L. H. Macromol. Rapid Commun. 2004, 25, 678-682.
54. Wu, A.; Shen, X.; He, Y. J. Colloid Interfacial Sci. 2006, 297, 525-533.
55. Brackman, J. C.; Engberts, J. B. F. N. Chem. Soc. Rev. 1993, 22, 85.
56. Polymer-Surfactant Systems; Kwak, J. C. T., Ed.; Surfactant Science Series Vol. 77; Marcel Dekker: New York, 1998; pp 239-477.
57. Goddard, E. D. Interactions of Surfactants with Polymers and Proteins; Goddard. E. D., Ananthapadmanabhan, K. P., Eds.; CRC Press: Boca Raton, FL, 1993.
58. Saito, S.; Anghel, D. F. In Polymer-Surfactant Systems; Kwak, J. C. T., Ed.; Surfactant Science Series Vol. 77; Marcel Dekker: New York, 1998; pp 357-408

Chapter 4

Solute transport properties in physical blends of Pluronic F127 and MOAB-DMA

4.1 Introduction

The change in the rheological and structural properties of the matrix on application of light stimuli have led us to explore whether the change in the solute transport properties within the matrix also take place during the process. The change in solute transport properties upon irradiation can be exploited in applications like separations, drug delivery, encapsulation of solutes, and so on.Solute transport properties in a polymer matrix have been an important subject of study from theoretical as well as practical points of view. A large number of investigations have been carried out since the publication of the classical book of Crank and Park.[1] Hindered transport of macromolecules through a polymer matrix occurs in a wide range of systems, such as gel chromatography, ultrafiltration, gel electrophoresis and controlled release drug delivery systems. In the case of electrophoresis through a polymer matrix, in gels and in non-gel systems, the electrophoretic mobility is solute transport parameter of importance. The reduction in electrophoretic mobility due to hindrance in solute transport in electrophoresis through polymer matrices has been discussed theoretically in large body of work. [2,3,4,5] Sieving polymers or gels that have been commonly used are polyacrylamide (PAAm), polysaccharides, poly(ethylene oxide), cellulose derivatives and agarose.[6] Models of molecular sieving within polymer solutions or gels described the solute transport as being through a matrix comprised of cylindrical fibrous obstacles, as first formulated by Ogston.[19] Since then, various models have been proposed based on three different approaches, as described below in Section 4.3. There has not been much attention paid to to describe the matrices which are micellar or colloidal in nature; such models are needed to understand and predict the changes in the solute mobility due to changes in matrix properties. The effect of change in viscosity does not translate directly into an equivalent

amount of change in diffusion or electrophoretic mobility of solutes as defined by Stokes equation. In this chapter we examine the transport properties of proteins in associative polymeric surfactant systems. In particular, we probe the electrophoretic mobility of proteins in the low-viscosity (sol) and high-viscosity (gel) states of the matrix developed in Chapter 3. Models for the electrophoretic mobility of proteins in both states of the matrix are developed and compared to simulation data available from the literature and to our experimental data.

4.2 Experimental

Pluronic F127 and photoresponsive polymer (MOAB-DMA) blend solutions were made in 1X TBE buffer solution to increase ionic strength to enhance the passage of ions through the polymer matrix. Fused-silica capillaries were coated with polyvinylalcohol (PVA) to mask the negative charge on the glass capillaries so as to avoid electro-osmosis and also protein adsorption.[17] Since fluorescein dye does not fluoresce in the presence of azobenzene, which absorbs strongly at its excitation wavelength (480 nm), the proteins for the study were labeled with red dye (TRITC) with an excitation wavelength of 550 nm and emission wavelength of 580 nm. The labeling reaction was that of isothiocyanate with the terminal amine group of the proteins. The labeling procedure used for this process is described below and the reaction scheme is shown in Scheme 4-1. The TRITC dye (1mg) of was added to a 1ml protein solution in 0.1 M sodium carbonate, pH9, at a concentration of 2mg/ml in dry DMSO. This mixture was stirred at 4°C for around 10-12 hrs in the dark. The reaction was quenched by the addition of ammonium chloride to a final concentration of 50mM. It was further reacted for 2hr to block the remaining isothiocyanate groups. The obtained derivative was then dialyzed using a membrane with MWCO 1000. The unreacted TRITC and the side products were removed by dialysis in de-ionized water. The dilute dialyzed derivative was then lyophilized to obtain dry TRITC-labeled proteins.

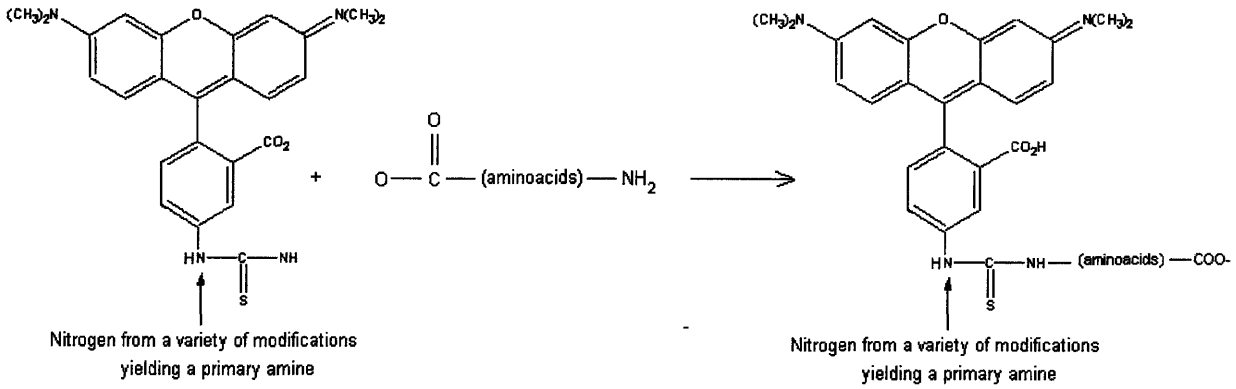

Scheme 4-1: Generic protein labeling reaction with red dye TRITC

4.2.1 Electrophoresis experiments

The electrophoresis experiments were conducted in a a fused-silica capillary of 13cm in length with I.D. of 340μm. The device was machine shopped within MIT facility to meet the requirements and the setup can be seen in Figure 4-1 . The capillary was capped on both ends by buffer cell custom-made of polyacrylic with holes made in the center at the top forming port for adding buffer. An additional hole was drilled on the side of the buffer cell for inserting Platinum wire used for the electrodes. The Platinum wires were then connected to a high voltage potientometer (Fischer Biotech Electrophoresis Systems, FB650) for carrying electrophoresis experiments. A rectangular casing was machined such that it can be assembled to surround the capillary with connections available to connect it to water bath for temperature control. The polymer blends in low-viscosity state were filled into the capillary using syringe. The buffer cell was filled the same working buffer TBE. 5mg/ml protein solution is injected into the capillary using a syringe. A small volume of a solution was injected hydrodynamically and the buffer was added slowly at equal rates to both buffer cells. A microscope was placed distance of 6 cm from the injection end to detect the fluorescently labeled proteins as they migrated along the channel.

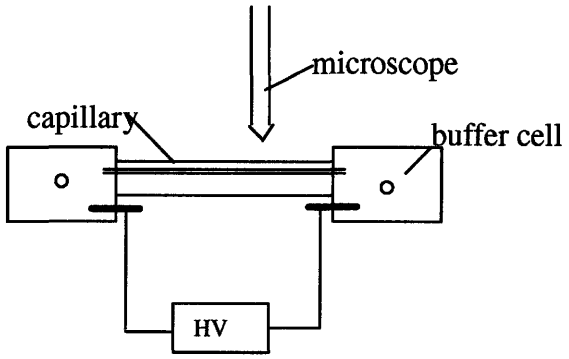

Figure 4-1: Schematic of electrophoresis setup and the fluorescence output of the labeled protein at a given location.

The electrophoretic mobility data obtained for different proteins under the sol and gel states are shown as function of charge to mass ratio in Figure 4-2. Since the electrophoretic mobility (μ) of a protein in a buffer varies approximately as $\mu \propto \frac{Z}{M^{2/3}}$. The estimation of charge to mass ratio for the common proteins used in the study was done in combination with the process described by Gao et. al.[7] and other documented research.[8,9] From the Figure 4-2, it can be seen that the electrophoretic transport of proteins/peptides in the presence of our matrix in the background electrolyte occur on the charge/mass ratio basis with molecular sieving effects acting as a secondary mechanism.

The electrophoretic mobility of proteins at the concentration of 5mg/ml and pH 8.3 were in gels were lower than those in sols by about 30 to 60%. The reduction in protein electophoretic mobility correlated well with protein size, with increasing protein radius, as shown in Figure 4-3. It indicates that the sieving/obstruction mechanism also plays a role in mediating the transport of proteins through polymer matrix. The decrease in the electrophoretic mobility is not directly proportional to the increase in the viscosity as anticipated.

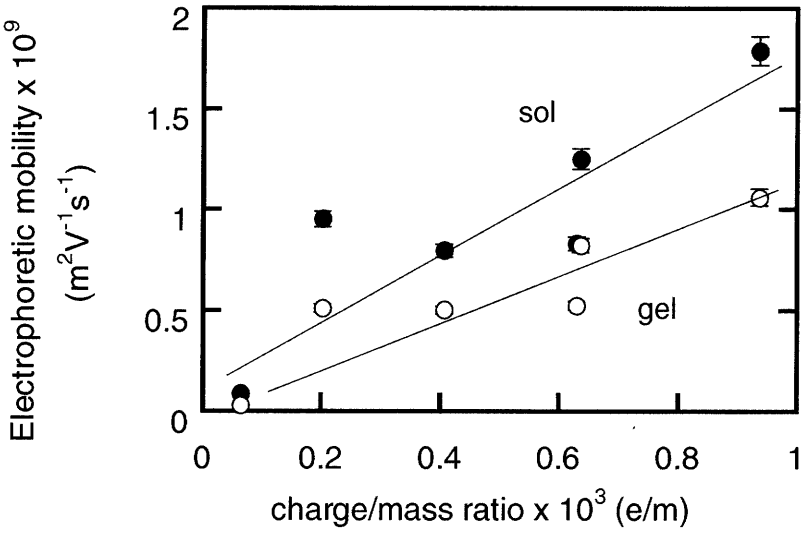

Figure 4-2: Electrophoretic mobility of proteins varies with charge/mass ratio in both sol (before UV) and gel state (after UV) polymer blend used as matrix in a 13 cm long capillary column.

	Proteins	radius (nm)
1	Cytochrome c	1.4
2	Lysozyme	1.6
3	Myoglobin	1.7
4	Insulin	1.9
5	Pepsin	2.2
6	BSA	3.4
7	ConA	6.0

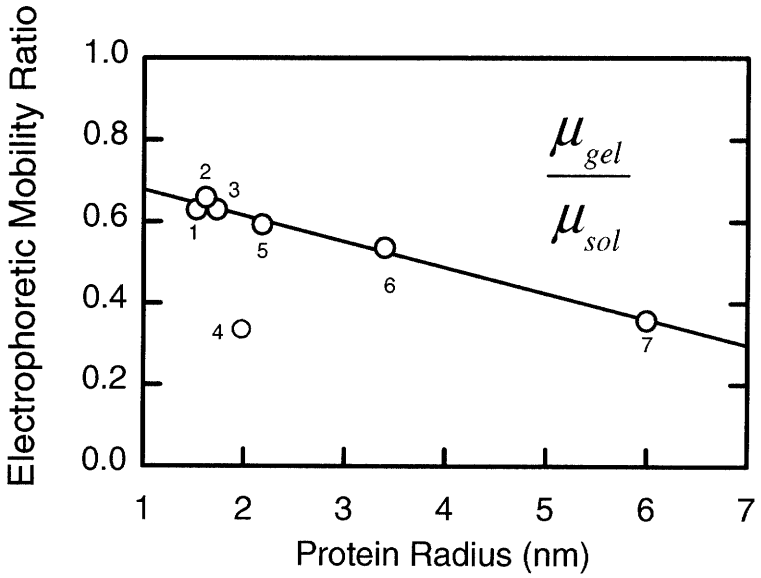

Figure 4-3: Plot of protein's electrophoretic mobility ratio (in gel and sol state) with respect to their size. List of proteins used in electrophoresis study are tabulated on the left and the data points are respectively marked.

4.3 Mechanisms and Models in Literature

The electrophoretic mobility μ and diffusion coefficient D are related through the Einstein relation.[10] The reduced electrophoretic mobility and diffusion, which is the ratio in the presence of obstacles to that in free solution, can be equated even in semi-dilute and concentrated regions.[11,12] In many studies they have been considered as one and the same and represented as the retardation factor, $R = \frac{\mu_m}{\mu_0} = \frac{D_m}{D_0}$.[13,14] Numerous models that have been developed for diffusion in polymer solutions and hydrogels can be applied to electrophoretic mobility in the same systems. Diffusion in polymer solutions and gels have been studied for decades by the use of various techniques such as gravimetry,[15] membrane permeation,[16] fluorescence recovery after photobleaching,[17]and dynamic light scattering.[18] In modeling diffusive hindrance in polymer solutions and hydrogels, it is usually assumed that a single type of cylindrical fiber, of radius r_f is arranged in either a random or spatially periodic array. [19,20,21,22,23,24] The various mechanisms and models available to describe the solute diffusion within such polymer solutions and in hydrogels are described well in the review article by Amsden.[23] There is lack of combination models to describe transport in micellar solution or gel such as those offered by the Pluronic family of copolymers. In the section that follow, we summarize the literature on the modeling of solute transport in various matrices, and use this information to interpet electrophoretic mobilities of proteins in sols and gels determined experimentally.

Free volume theory. These models are based on the theory put forward by Cohen and Turnbull to explain the process of solute diffusion in a pure liquid.[25] In this theory the solute diffuses by jumping into voids formed in the solvent space by the redistribution of the free volume within the liquid. It is assumed that the free volume can be distributed without any energy change. The voids are pictured as being formed by a general withdrawal of the surrounding liquid molecules due to random thermal motion. These holes are then filled in by reverse process.[26]

Solute diffusion is dependent on the jumping distance, the thermal velocity of the solute, and the probability that there is a hole free volume adjacent to the molecule. At a

given temperature, the rate of diffusion is determined by the probability of a void being formed of sufficient volume to accommodate the solute molecule. The diffusion coefficient of the solute in the liquid at infinite dilution, D_0, is then expressed as

$$D_0 \propto V\lambda \exp(-\frac{\gamma v^*}{v_f}) \qquad \text{Eq. 4-1}$$

in which V is the average thermal velocity, λ is the jump length roughly equivalent to the solute diameter, v^* is the critical local hole free volume required for a solute molecule to jump into a new void, γ is a numerical factor used to correct for the overlap of free volume available to more than one molecule ($0.5 \leq \gamma \leq 1$) and v_f is the average hole free volume per molecule in the liquid. Based on this basic theory with variations, Peppas and Reinhart[27] suggested the form

$$\frac{D_m}{D_0} = k_1\left(\frac{\overline{M}_c - \overline{M}_c^*}{\overline{M}_n - \overline{M}_c^*}\right)\exp\left[-k_2 r_s^2\left(\frac{\phi}{1-\phi}\right)\right] \qquad \text{Eq. 4-2}$$

in which k_1 and k_2 are undefined structural constants for a given polymer-solvent system, r_s is the radius of the solute, $\overline{M}_c$ is the number average molecular weight between polymer cross-links, $\overline{M}_n$ is the number average molecular weight of the uncrosslinked polymer, and $\overline{M}_c^*$ is a critical molecular weight between crosslinks required for the solute transport. This model was used to describe solute diffusion in poly(vinyl alcohol)/poly(acrylic acid) interpenetrating networks.[28]

Another version of the free volume theory was given by Lustig and Peppas,[29] who introduced the concept of scaling to determine the correlation length between crosslinks, similar to mesh size ξ. By considering that a solute will pass through the polymer chains only if its effective radius is smaller than ξ, they assumed that the sieving factor expression should be $(1 - r_s / \xi)$. Applying this concept to the free volume theory, they derived the expression

$$\frac{D_m}{D_0} = \left(1 - \frac{r_s}{\xi}\right) \exp\left[-Y\left(\frac{\phi}{1-\phi}\right)\right] \qquad \text{Eq. 4-3}$$

where $Y = \frac{\gamma \pi \lambda r_s^{\,2}}{v_{f,w}}$ is the ratio of the critical volume required for the successful transport of the solute molecule to the average free volume per molecule of the liquid. The correlation length is related to the polymer volume fraction, the functionality of the dependence varying with polymer-volume fraction and polymer-solvent interaction.[30] The diffusion models that are based on these free volume theories are summarized below in Table 4-1.

Table 4-1: Summary of the diffusion models based on the free volume theories

Authors	Applications	Limitations
Fujita [31]	Solvents and small-sized diffusants	Large diffusants
	Semi-dilute polymer solutions	Concentrated polymer solutions
Yasuda et. al.[32]	Semi-dilute polymer solutions	Concentrated polymer solutions
	Various solutes and solutes	Determination of numerous parameters
Vrentas and Duda[26]	Both semi-dilute and concentrated polymer solutions	Dilute polymer solutions
	Various solutes and solvents	Diffusants with size closer to or greater that mesh size
Peppas and Reinhart[27]	Chemically cross-linked gels and hydrogels	Diffusion in non-crosslinked polymers

Hydrodynamic Theory. Hydrodynamic descriptions of solute transport through solutions and gels are based on the Stokes-Einstein equation for solute diffusivity. In the Stokes-Einstein derivation, the solute molecule is assumed to be a hard sphere which is large compared to the solvent in which it moves.[33] The solute is considered to move at a constant velocity in a continuum composed of the solvent and is resisted by a frictional drag. The diffusion at infinite dilution, D_0 is expressed as,

$$D_0 = \frac{k_B T}{f} \qquad \text{Eq. 4-4}$$

in which k_B is Boltzmann's constant, T is the temperature and f is the frictional drag coefficient. Almost all hydrodynamic and obstruction theories assume an idealized polymer structure. In a sense, the polymer chains are considered to be centers of hydrodynamic resistance, fixed in place relative to the moving solute by entanglements and physical crosslinks. The polymer chains enhance the frictional drag on the solute by slowing down the fluid near them. Hydrodynamic models for solute diffusion through polymer solutions and hydrogels are therefore concerned with describing f.

For homogenous systems, Cukier[34] proposed an equation based on scaling concepts,

$$\frac{D_m}{D_0} = \exp(-k_c r_s \phi^{0.75}) \qquad \text{Eq. 4-5}$$

in which k_c is a constant for a given polymer-solvent system.

Phillips et. al.[35] calculated the frictional coefficient by using Brinkman's equation for flow through a porous medium, assuming no slip at the solute surface and constant fluid velocity far from this surface. The medium is considered to be composed of straight, rigid fibers, oriented in a random three-dimensional fashion. They thereby obtained an expression

$$\frac{D_m}{D_0} = \left[1 + \left(\frac{r_s^2}{k}\right)^{1/2} + \frac{1}{3}\frac{r_s^2}{k}\right]^{-1} \qquad \text{Eq. 4-6}$$

in which k is the hydraulic permeability of the medium. A number of other models have been developed too,as summarized in Table 4-2.

Table 4-2: Summary of the diffusion models based on hydrodynamic theories with their applicability and limitations

Authors	Applications	Limitations
Cukier[36]	Solvents and small-sized diffusants	Large diffusants
	Semi-dilute polymer solutions and highly swollen gels	Concentrated polymer solutions
Philies[37,38,39]	Semi-dilute polymer solutions	Concentrated polymer solutions
	Solvents, small-sized diffusants and macromolecules	Significance of the scaling parameters

de Gennes[40]	Diffusion in solution-like regimes	Diffusion in melt-like regime ($M>10^6$)
	Diffusion in gels and concentrated polymer solutions	Molecular significance of entanglements
Gao & Fagerness[41]	Diffusion of small-sized diffusants in multicomponent systems	Significance of the main parameters

Obstruction theory. The models based on obstruction theory assume that the presence of impenetrable polymer chains causes an increase in the path length for diffusive transport. The polymer chains act as a sieve, allowing transport of a solute molecule only if it can pass between polymer chains. Initially obstruction models were developed assuming considered that the reduction in diffusion in gels as compared to free solution was only function of volume fraction. But since then, there have been lot of changes trying to incorporate this sieving behavior of polymer chains in the free volume theory. Lustig and Peppas[29] assumed that the probability of a solute passing through a given hole in the mesh can be given as follows:

$$p(r_s) = 1 - \frac{r_s}{\xi} \qquad \text{Eq. 4-7}$$

This expression is based on the argument that solutes of equal cross-sectional area could have different hydrodynamically equivalent radii.

A more phenomenological approach was taken by Ogston et. al..[19] They assumed that the solute diffusion in the hydrogel occurs by a succession of directionally random unit steps and that a unit step does not take place if the solute encounters a polymer chain. The cross-linked polymer is assumed to exist as a random network of straight, long fibers of negligible width, and the solute is considered as a hard sphere. The unit step is taken to be the root-mean-square average diameter of spherical spaces residing between the fiber network. From such an analysis, they expressed the ratio of the diffusion coefficient in gel to that in infinte dilution in water as

$$\frac{D_m}{D_0} = \exp\left[-\frac{(r_s + r_f)}{r_f}\sqrt{\phi}\right] \qquad \text{Eq. 4-8}$$

There are been various modifications made to the equation based on the system used as mentioned in Table 4-3.

Table 4-3: Summary of the diffusion models based on obstruction models with their applicability and limitations

Authors	Applications	Limitations
Maxwell-Fricke[42]	Solvents and small-sized diffusants	Large diffusants
	Very dilute polymer solutions	Semi-dilute and concentrated polymer solutions
Mackie and Meares[43]	Semi-dilute polymer solutions	Concentrated polymer solutions
	Solvents and small-sized diffusants	Large diffusants
Ogston et. al.[19]	Semi-dilute polymer solutions	Large diffusants
	Solvents and small-sized diffusants	
Hard-sphere theory[44,45]	Semi-dilute polymer solutions	Concentrated polymer solutions

4.4 Physical models for Pluronic F127/MOAB-DMA physical blends

The matrix composition considered in this study is mostly Pluronic F127 and we wish to represent the system as being close to that observed for 20wt% Pluronic F127 solely. A good way of representation of the system in the sol state is that of randomly placed spherical micelles which can be represented as randomly placed spherical obstacles (with radius r_p). The gel state in the case of Pluronic F127 can be represented by face centered cubic crystal[46] i.e. the system can be viewed as hard impenetrable spherical obstacles present in ordered structure of cubic symmetry. The mixed micelles made with low molecular weight polymers or drugs and Pluronic F127 have been shown to have a structure similar to that of Pluronic F127.[47] The values for r_p and ϕ for Pluronic F127 sol and gel state are given by Moretensen et. al.[46,48] and Song et. al. reported in Table 4-4 [49].

Table 4-4: Values of micelles radius and volume fraction for 20wt% Pluronic F127 solution close to gelation point[46,47]

State	r_p (nm)	ϕ
Sol	5.5	0.51
Gel	6	0.56

It has been proposed by Brady[50] that the diffusivity in a gel or concentrated suspension can be written as the product of two factors F and S, where F accounts for hydrodynamic effects and S for steric or tortuosity effects. The steric factor which is similar to an inverse tortousity, is the relative diffusivity in the absence of hydrodynamic interactions between the spherical obstacles and the macromolecular solute. That is, it describes the effect of excluding the center of a spherical solute molecule (with radius r_s) from a region of radius $r_p + r_s$ centered on the spherical obstacles.

$$\frac{D}{D_0} = FS(\upsilon) \qquad \text{Eq. 4-9}$$

Hence the effective diffusivity representation with respect to diffusivity in a pure fluid (i.e. infinite dilution) can be given in Eq. 4-9. Here, υ is the adjusted volume fraction of obstacles in the system.

4.4.1 Hydrodynamic factors

Effective medium approach: The Hydrodynamic factor can be calculated by reciprocal of the ratio of the friction coefficient f in the flow case in the presence of obstacles to that in a pure fluid; f is equal to $6\pi\eta r_s$ for a sphere of radius r_s in a pure fluid with viscosity η.

For the case considered here, the value of f can be determined by using Brinkman's equation[51] for flow in a porous medium.

$$\eta\nabla^2 v - \nabla p = (\eta / k)v \qquad \text{Eq. 4-10}$$

Here p is the pressure and v is the velocity averaged over both the fluid and the spherical obstacles. Eq. 4-10 can be seen as Stokes' equations with an additional term to account for the force exerted on the fluid by the obstacles or, alternatively, it can be seen as Darcy's law with an additional term that account for viscous stresses in the fluid phase. The only structural information included in this effective medium model is contained in k, the hydraulic permeability.[20]

The value of f obtained by solving Eq. 4-10 subject to no-slip boundary conditions at the sphere surface and constant velocity far from the sphere center is[51,52]

$$F = \left[\frac{f}{6\pi\eta r_s}\right]^{-1} = \left(1 + \left(\frac{r_s^2}{k}\right)^{1/2} + \frac{1}{3}\left(\frac{r_s^2}{k}\right)\right)^{-1} \qquad \text{Eq. 4-11}$$

The hydraulic permeability parameter can be estimated using different models available in literature.

Hydraulic permeability in sol state:

The Stokes' law for a dilute bed of spheres[53] is

$$k = \frac{2}{9(1-\phi_1)} r_p^{\,2} \qquad \text{Eq. 4-12}$$

where r_p is the inclusion sphere radius.

The empirical Kozeny-Carmen relation in the general case[54] can be written as follows

$$k = \frac{1}{180}\frac{\phi_1^3}{(1-\phi_1)^2} r_p^{\,2} \qquad \text{Eq. 4-13}$$

The above equations are for dilute systems and hence cannot be applied to concentrated systems/suspensions of spheres.

Brady et. al.[55] derived an analytical expression for dimensionless hydraulic permeability for the case of a concentrated suspension of spheres, taking into account pair-wise interactions between spheres. The expression is obtained using the Percus-Yevick hard-sphere distribution.

$$k = \left[1+\phi-\frac{1}{5}\phi^2-\frac{6}{5}\phi\left(\frac{5-\phi+\frac{1}{2}\phi^2}{1+2\phi}\right)\right] r_p^{\,2} \qquad \text{Eq.4-14}$$

For completely disordered concentrated systems, Richardson and Zaki[56], showed that the hydraulic permeability can be related to volume fraction using an empirical form as follows

$$k = (1-\phi)^{\alpha} r_p^2 \qquad \text{Eq. 4-15}$$

By comparison of this form to their experimental data, they obtained a coefficient α, equal to 4.65. Maude and Whitmore[57] also investigated the problem for highly concentrated systems of spherical particles. They evaluated a wide range of experimental data available in the literature and found that Eq. 4-15 holds true for whole range of volume fractions. They determined that the coefficient α ranged from approximately from 5-9 for the different systems tested.

Happel and Brenner[53] and Ohshima[58] have derived expressions for hydraulic permeability for an ordered concentrated suspension of spheres given by Eq. 4-16 and Eq. 4-17 respectively

$$k = \left(\frac{1-\frac{3}{2}\phi^{1/3}+\frac{3}{2}\phi^{5/3}-\phi^2}{1+\frac{2}{3}\phi^{5/3}}\right) r_p^{\,2} \qquad \text{Eq. 4-16}$$

$$k = \left(1+\phi-\frac{9}{5}\phi^{1/3}-\frac{1}{5}\phi^2\right) r_p^{\,2} \qquad \text{Eq. 4-17}$$

Hydraulic permeability in gel state:

The expression for hydraulic permeability can be derived for face centered cubic systems (fcc) using the analysis of slow flow through a fcc array of spheres given by Sangani et.al.[59] The modification of Hasimota treatment of finding the drag force exerted by the fluid on a representative sphere in a fixed assembly as a function of volume fraction of the spheres (ϕ) was done to cover up the complete range of ϕ.The solution for the velocity components is periodicand is written in form of spherical harmonics near r=0. This leads to the following series expression

$$K = \sum_{s=0}^{30} q_s \left(\frac{\phi}{\phi_{\max}} \right)^{s/3} \qquad \text{Eq. 4-18}$$

with ϕ_{max}, the volume fraction of the spheres in the touching configuration. The coefficients in the series expansion are obtained from lengthy calculations[59] from the series representation of the periodic form structure using spherical harmonics. The hydraulic permeability (k) can be derived using the relation[60]

$$k = \frac{V_0}{6\pi r_p K} \qquad \text{Eq. 4-19}$$

where, V_0 is the volume of a unit cell in the lattice.

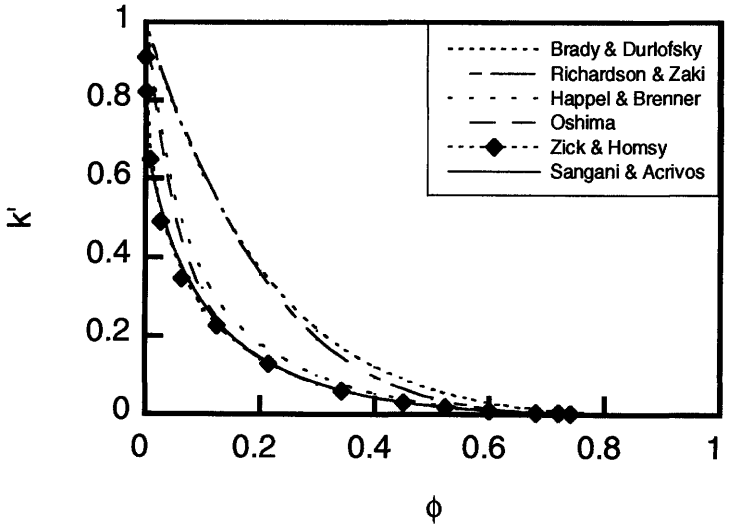

Figure 4-4: Dimensionless hydraulic permeability constant vs volume fraction of spherical obstacles. Predictions from different papers for different arrangement of the

spheres are plotted here. Hydraulic permeability is non-dimensionalized by l^2 (characteristic length = radius of spheres)

Figure 4-4 shows a comparison of the various models for the dimensionless hydraulic permeability (k') in different concentrated systems of spheres.The estimates given by Brady et.al[55] and Richardson et.al.[56] for disordered concentrated suspensions of spheres are very close. Happel et.al.[53]and Oshima et.al[58] for ordered systems (simple cubic lattice) predictions shows that the hydraulic permeability is smaller than in case of disordered systems. The ordering of the systems will have the effect of reducing the permeability of the fluid through the system. The Zick and Homsy[61] data as well as the analytical expression derived by Sangani and Acrivos[59] fit well and it can also be seen that the permeability is further reduced when the structure is face-centered cubic lattice rather than a simple cubic lattice for the same volume fraction of spheres.

4.4.2 Steric factor

Sol system. Using Amsden[62] results and the procedure presented based on the premise of Lustig and Peppas[29] that the solute can move through the matrix only if it finds a succession of openings within the polymer chains of diameter greater than the solute diameter, a probability function can be derived based on similar line as presented in above.

As solute movement within the matrix is a randomly directed process, the transport of the molecule through the hydrogel is governed by the probability of the solute finding a succession of holes of sufficiently large enough diameter. The average steric factor can be expressed as

$$S(v) = \int_{r^*}^{\infty} g(r)dr \qquad \text{Eq. 4-20}$$

in which g(r) is the distribution of opening radii within the matrix, and r^* is the critical radius required to allow solute passage. By picturing the matrix as a random network of spheres, the distribution of spaces between these spheres can be expressed as

$$g(r) = \frac{4\pi r^2}{R^3} \exp(-\frac{4\pi}{3}\frac{r^3}{R^3}) \qquad \text{Eq. 4-21}$$

The expression in Eq. 4-21 is found by extending an analogy with the Ogston model for random fiber systems to spherical obstacles. Substitution of Eq. 4-21 in Eq. 4-20 and carrying out the integration, we obtain

$$S(\upsilon) = \exp\left[-\frac{4\pi}{3}\left(\frac{r^*}{R}\right)^3\right] \qquad \text{Eq. 4-22}$$

To account for the radius of the obstacles, we rewrite Eq. 4-22 to include the average radius of space between the obstacles, $\bar{r}$, and radius of the spherical obstacles, r_p

$$S(\upsilon) = \exp\left[-\frac{4\pi}{3}\left(\frac{r_s + r_p}{\bar{r} + r_p}\right)^3\right] \qquad \text{Eq. 4-23}$$

The average radius of the opening between the obstacles can be expressed in terms of r_p and ϕ using the pore size distribution for randomly packed spheres given by Torquato et.al.[63]

$$\bar{r} = r_p \phi^{-1/3} \Gamma(0.33, \phi) \qquad \text{Eq. 4-24}$$

Substituting Eq. 4-24 in Eq. 4-23 results in

$$S(\upsilon) = \exp\left[-\frac{4\pi}{3}\left(1 + \frac{r_s}{r_p}\right)^3 \left(\frac{\phi^{1/3}}{\Gamma(0.33, \phi) + \phi^{1/3}}\right)^3\right] \qquad \text{Eq. 4-25}$$

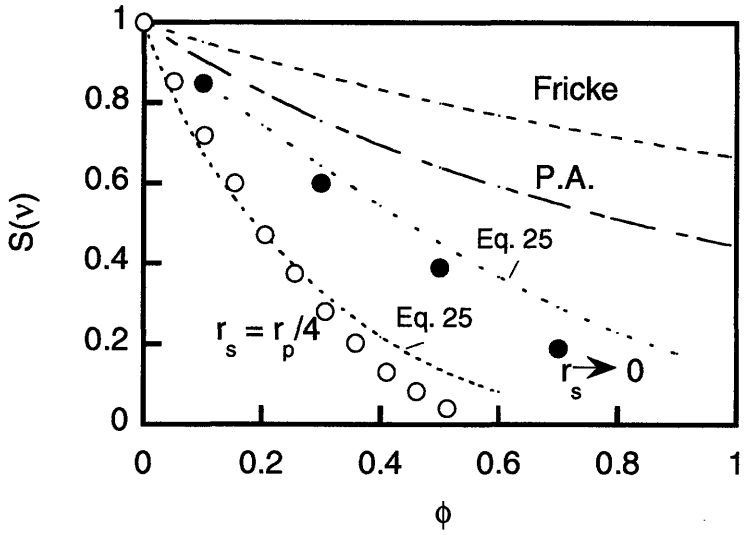

Figure 4-5: Comparison of our model equation Eq. 4-25 for the steric factor of particles in a medium consisting of randomly placed spherical obstacles with simulation data and other models in literature. The (•) represents the Brownian motion simulation data[64] for both point solute and (o) a solute with $r_s=r_p/4$; P.A. represents model obtained by the phenomenological model[65] whereas Fricke represents Fricke equation[66]. P.A. and Fricke equation can be applied only for point solute molecules and hence can be compared with case one of point solute ($r_s \rightarrow 0$).

The prediction given by our model compared with Brownian motion simulation data for a similar system shows a very good agreement for both point solute molecules as well as solute with comparable radius.

Gel system. A similar approach was attempted to apply on the fcc ordered spheres but as the g(r), the distribution of radii within this matrix is of the form

$$\frac{A_1}{r}\exp(-A_2 r)\cos(-A_3 r + A_4)$$

The integration of this form lead to very complicated analytical expression with exponential integrals and complex numbers. Hence modification of the expressions available on the literature was done. There are few studies done on self-diffusion of spheres in ordered suspensions. [67,68,69] The effective translational diffusion coefficient of molecules based on steric factor in colloid crystals studied in above papers are obtained assuming the colloidal particles as immobile spheres with centers located on the lattice points of a cubic array. The mathematical expression describing the self-diffusion in fcc

ordered colloidal crystals of spherical particles given by Blees and Leyte[70] shown in Eq. 4-26.

$$S(v)\big|_{r_s \to 0} = \frac{1}{(1-\phi)}\left(\frac{1-2K\phi}{1+K\phi}\right) \qquad \text{Eq. 4-26}$$

where,

$$K = \sum_i m_i (\phi / \phi_{\max})^{i/3} \qquad \text{Eq. 4-27}$$

with ϕ_{max} defined as the volume fraction of the sphere at dense packing for the given lattice ordered structure.The coefficients m_i appearing in Eq. 4-27 are well correlated and tabulated by Blees and Leyte[70]

The analytical expression in Eq. 4-26 is compared with the steric factor obtained by random walk simulation approach. The case considered in there study for small solutes. The analytical form fits quite well with the simulation studies. It is well evident that the steric effect is enhanced at higher volume fraction. The matrix steric asymptotically increase at $\phi > 0.9$, as the matrix is so crowded that hindrance is high even for small molecules. The expression need to be modified to include the solute diffusion taking into account the radius of the solutes and obstacles. Most of the approaches to do so involve increasing the effective radius of the particle by adding the solute radius to it and recalculating the modified/adjusted volume fraction.[71] But this approach still only holds for small solute molecules especially at higher volume fraction (as then the adjusted volume fraction can be greater than ϕ_{max} for $r_s \sim r_p$ and Eq. 4-26 would no longer hold) for Eq. 4-26.

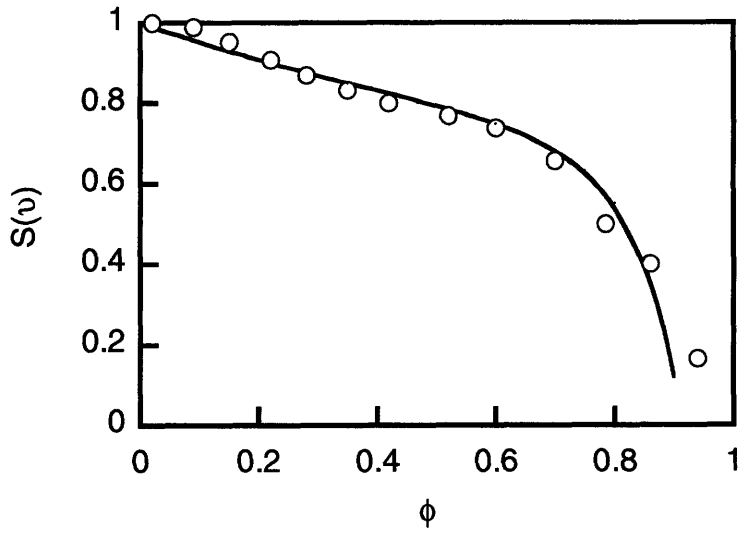

Figure 4-6: Tortuosity or Steric factor reciprocal with respect to volume fraction (ϕ) of spherical obstacles in face centred cubic array. The legend (o) shows the values for FCC structures obtained by random walk simulation approach[71]; the steric factor is described as recripocal tortuosity in their study. The dotted line represents the values obtained from Eq. 4-26

Hence to incorporate solute size effect, we tried to derive the effect of structural changes for given volume fraction for point solute molecules by comparing Eq. 4-25 with $r_s \rightarrow 0$ and Eq. 4-26. The ratio of these equations for point solute molecule was assumed to be the structural effect and considered constant for different solute sizes. The modified expression is represented in

$$S(\upsilon)=\frac{1}{(1-\phi)}\left(\frac{1-2K\phi}{1+K\phi}\right)\exp\left[-\frac{4\pi}{3}\left[\left(1+\frac{r_s}{r_p}\right)^3-1\right]\left(\frac{\phi^{1/3}}{\Gamma(0.33,\phi)+\phi^{1/3}}\right)^3\right] \qquad \text{Eq. 4-28}$$

4.5 Comparison with experimental data

The combined equations can be used to describe the electrophoretic mobility both in sol and gel state by Eq. 4-9. The ratio of electrophoretic mobility in gel state to that in sol state can be obtained from these and compared to the experimental values obtained in our case.

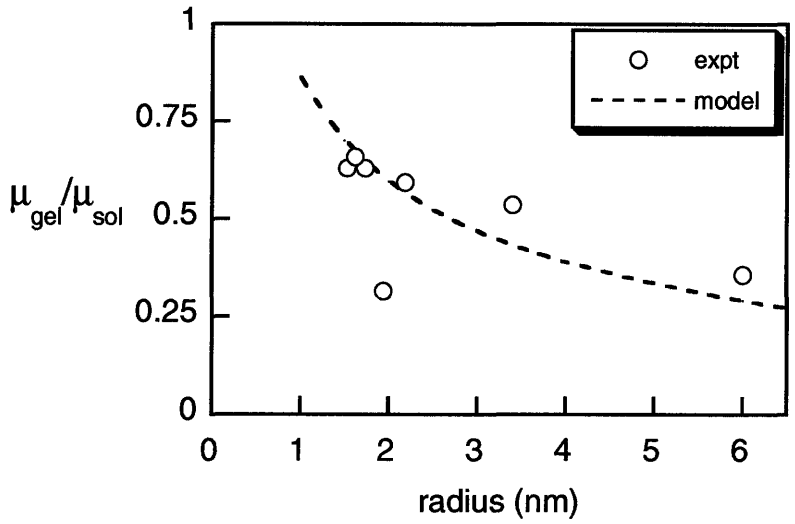

Figure 4-7: Plot of ratio solute transport properties in gel state to sol state using combined model with respect to solute size

The values determined from the combined model using parameters listed in Table 4-4 agree well with the experimental values. The model helps to predict the change in electrophoretic mobility for different solute size. The experimental data and the model help us understand that the reduction in solute (<10nm) mobility would not be of equal order of magnitude as compared to the change of viscosity if there is no specific interaction of solutes and the matrix involved. The use of the model can be extended to similar sol-gel system such as different Pluronic systems or Pluronic-PAA systems.[72]

4.6 References

1. J. Crank, G.S. Park (Eds.), Diffusion in Polymers, Academic Press, London, 1968.
2. Slater ,G., Guo, H., Electrophoresis, 1996, 17,1407-1415
3. Viovy JL, Duke T. Electrophoresis. 1993 Apr;14(4):322-9.
4. Slater G.W.1; Treurniet J.R., Journal of Chromatography A,1997, 772(1), 39-48
5. Mercier,J-F., Slater, G.W., Macromolecules, 34 (10), 3437 -3445, 2001.
6. Kitagishi, K., In Handbook of Capillary Electrophoresis Applications, Blackie Academy and Professional, Ed.1, 1997, 75-80.

7. Gao, J., Gomez,F.A., Harter, R., and Whitesides, G.M., Proceedings of National Academy of Sciences of United States Of America, 1994, Vol., 91, No. 25, 12027 - 12030
8. Gauthier-Manuel, B.; Gallinet, J. P. Langmuir 1997, 13, 2541.
9. Reeke, G. N.; Becker, J. W.; Edelman, G. M. J. Biol. Chem. 1975, 250, 1525.
10. Yeh, I-C, and Hummer, G.,Biophysical Journal, 2004, 86,681-689
11. Mercier,J-F, and Slater,G.W., Macromolecules,2001, 34 (10), 3437 -3445
12. Odijk,T., Biophys J, November 2000, 79,(5), 2314-2321
13. Ogston, A. G. Trans. Faraday Soc. 1958, 54, 1754.
14. Rodbard, D.; Chrambach, A. Proc. Natl. Acad. Sci. U.S.A. 1970, 65, 970.
15. Hu, D.S.G., Chou, K.J.N., Polymer, 1996, 37, p.1019
16. Smith, B.A.H., Sefton, M.V.,J. Biomed Mater Res., 1988,22,673
17. Wisnudel, M.B., and Torkelson, J.M., Macromolecules, 1996, 29, p.6193
18. van Asten,A.C.,Kok, W.T., Tilssen,R., and Poppe, H.,J. Polym. Sci,1996, 34, p. 283
19. Ogston, A,G., Preston, B.N., and Wells, J.D., " On Transport of Compact Particles through solutions of Chain Polymers, " Proc. R. Soc. Lond. A.,333, 297 (1973).
20. Phillips, R.J., Deen, W.M., and Brady, J.F., " Hindered Transport of Spherical Macromolecules in Fibrous Membranes and Gels", AIChE J., 35, 1761 (1989)
21. Clague, D.S. and Phillips, R.J., " Hindered Diffusion of Spherical Macromolecules through Dilute Fibrous Media," Phys. Fluid, 8, 1721 (1996)
22. Johnson, E.M., Berk, D.A., Jain, R.K., and Deen, W.M., " Hindered Diffusion in Agarose Gels: Test of the Effective Medium Model", Biophys. J., 70, 1017 (1996)
23. Amsden, B., "Solute Diffusion in Hydrogels. Mechanism and Models", Macromolecules, 31, 8382 (1998)
24. Phillips, R.J., " A Hydrodynamic Model for Hindered Diffusion of Proteins and Micelles in Hydrogels", Biophys. J.,79, 2250 (2000)
25. Cohen, M.H., Turnbull, D., J. Chem. Phys., 1959, 31, 1164
26. Vrentas, J.S., Duda, J.L., J. Polym, Sci, 1977, 15, 403
27. Peppas, N.A., Reinhart, C.T., J. Membr. Sci., 1983, 15,275
28. Peppas, N.A., Wright, S.L., Macromolecules, 1996, 29(27), 8798

29. Lustig, S.R., Peppas, N.A., J. Appl. Poly,. Sci.,1988, 36(4), 735
30. Schaefer, D.W., Polymer, 1984, 25,387
31. H. Fujita. Adv Polym Sci 3 (1961), p. 1-47
32. H. Yasuda, C.E. Lamaze and L.D. Ikenberry. Die Makro Chem 118 (1968), p. 19.
33. Bird, R.B., Stewart, W.E., Lightfoot, E.N., Transport Phenomena; John and Wiley and Sons: Toronto, 1960
34. Cukier, R.I.,Macromolecules,1984,17,252
35. Phillips, R.J., Deen, W.M., and Brady, J.F., AIChE J., 1989,35,5 (11), 1761
36. R.I. Cukier. Macromolecules 17 (1984), p. 252
37. G.D.J. Phillies. Macromolecules 20 (1987), p. 558.
38. G.D.J. Phillies. J Phys Chem 93 (1989), p. 5029.
39. G.D.J. Phillies. Macromolecules 19 (1986), p. 2367
40. P.G. de Gennes. Macromolecules 9 (1976), p. 594.
41. P. Gao and P.E. Fagerness. Pharm Res 12 (1995), p. 955.
42. H. Fricke. Phys Rev 24 (1924), p. 575
43. J.S. Mackie and P. Meares. Proc R Soc London A 232 (1955), p. 498
44. J.E. Löfroth, C. Elvingson and L. Johansson. Proc Int Symp Control Rel Bioact Mater 18 (1991), p. 146
45. L. Johansson, C. Elvingson and J.E. Löfroth. Macromolecules 24 (1991), p. 6024.
46. Mortensen, K., and Talmon, Y., Macromolecules, 1995, 28, 8829-8834
47. Sharma, P.K., Bhatia, S.R.,Bioengineering Conference, 2004. Proceedings of the IEEE 30th Annual Northeast,17-18 April 2004 Page(s):228 - 229
48. Mortensen, K., Pedersen, J.S., Macromolecules, 1993, 26, 805-812.
49. Song, M.J., Lee, D.S., Ahn, J.H., Kim, D.J., and Kimi, S.C., Polymer Bulletin, 2000,43, 497-504.
50. Brady, J.F., Hindered diffusion. In Extended Abstracts, American Institute of Chemical Engineers Annual Meeting, San Franciso, CA, 320.
51. Brinkman, H.C., "A Calculation of the Viscous Force Exerted by a Flowing Fluid in a Dense Swarm of Particles," Appl. Sci. Res. A, 1, 27 (1947)
52. Howells, I.D..,"Drag Due to the Motion of a Newtonian Fluid through a Sparse a Random Array of Small Fixed Rigid Objects", J.Fluid Mech., 64, 449 (1974).

53. J.Happel and H. Brenner, Low Reynolds Number Hydrodynamics, Noordhoff International Leyden, The Netherlands,1973
54. M.J. MacDonald, C.-F.Chu, P.P. Guilloit, and K.M. Ng, " A generalized Blake-Kozeny equation for multisized spherical particles,", AICHE J., 37 (10), 1583 (1991)
55. Brady, J.F., and Durlofsky, L.J., Phys. Fluids, 1988, 31(4), 717-727
56. Richardson, J.F., and Zaki, W.N., "The sedimentation of a suspension of uniform spheres under conditions of viscous flow, Chem. Eng. Sci.,1954, 3, 65-73
57. Maude, A.D., and Whitmore, R.L., " A generalized theory of sedimentation", British Journal of Applied Phys., 9, 477-482.
58. Ohshima, H., "Sedimentation potential in a concentrated suspension of spherical colloidal particles", J, Coll. Int. Sci., 1998, 208, 295-301
59. Sangani,A.S., and Acrivos, A., " Slow flow through a periodic array of Spheres", Int. J. Multiphase Flow, 1982, 8 (4), pp. 343-360
60. Larson,R.E., and Higdon, J.J.L., " A periodic grain consolidation model of porous media", Phys. Fluids A, 1989, 1 (1) pp. 38-46
61. Zick,A.A., and Homsy, G.M., "Stokes flow through periodic arrays of spheres", J.Fluid.Mech, 1982,115,13-26
62. Amsden, B., Polym. Gels and Networks, 1996, 6, p. 14
63. Torquato,S.,and Avellaneda, J.Chem.Phys.1991,95(9),6477-6489.
64. Kim, I.C.,and Torquato,S., J.Chem. Phys., 1992, 2,15, 1498-1503
65. Muhr,A.H., and Blanshard,J.M.V., Polymer, 1982, 23,1012
66. Fricke,H., Phys. Rev., 1924, 24, 575
67. Reeder,D.H.,Carr, P.W., Flickinger,M.C., and McCormick, A.V., J. Coll. Int. Sci., 2000, 226, 277-285
68. Kang, K.,Gapinski, J., Lettings, M.P., Buitenhuis, J., and meier, G., Ratajcyzk, M., and Dhont, J.K.G., and patkowski, A., J. Chem. Phys., 2005, 122, 044905
69. Banks, D.S., and Fradin, C., Biophys. J., 2005, 89, 2960-2971
70. Blees,M.H., and Leyte, J.C., J. Coll. Int. Sci., 1994, 166, 118-127
71. Kim, A.S., and Chen, H., J. Membrane Science, 2006,279,129-139

72. Ho, A.K., Bromberg, L.E., O'Connor, A.J., Perera, J.M., Stevens, G.W.,Hatton, T.A, Langmuir, 17 (12), 3538 -3544, 2001.

Chapter 5

Dynamically modulated matrix for electrophoretic separation

5.1 Introduction

The protein electrophoretic mobility was observed to be different in sol and gel states of polymer blends of F127 and MOAB-DMA obtained by using light stimuli. The reduction in proteins electrophoretic mobility on gelation of the matrix has led us to explore these blends as a matrix in electrophoretic separation where we could modulate the properties by applying UV light stimuli in a defined manner. In this chapter, the potential of using dynamically modulated matrix for enhancement of resolution of separation was studied. The optimum method for applying the stimuli was discussed and the expressions are developed for the location and the time of light stimuli. The theoretical simulations for two solutes electrophoretic separation in dynamically modulated matrix were done at different operating conditions. The separation obtained in this case was compared to the case of convential non-modulated matrix. The separation experiments were carried using the UV light stimuli to modulate the matrix and the change in the separation resolution was measured.

5.2 Concentration Distribution

In order to fully describe the peaks resulting from a capillary electrophoresis (CE) separation or microchip separation, we need to develop an expression that describes the concentration of a solute as a function of its position in the channel and time. Such an equation can be derived starting from the convective diffusion equation[1]

$$\frac{\partial C_i(x,t)}{\partial t} = D_i \frac{\partial^2 C_i(x,t)}{\partial x^2} - v_i \frac{\partial C_i(x,t)}{\partial x} \qquad \text{Eq. 5-1}$$

where C_i is the concentration, D_i is the diffusion coefficient and v_i is the net migration velocity of species i. It assumed that the diffusion coefficient is not a function of solute concentration.

Eq. 5-1 can be solved using the method of Fourier transorms using the boundary conditions: (1) $t > 0$, $x = \infty$, $C = 0$; (2) $t > 0$, $x = 0$, $dC/dx = 0$. The first boundary condition states that far from the initial pulse, the solute concentration is zero, whereas the second boundary condition states that because diffusion occurs at the same speed in both direction, the pulse remains symmetrical throughout the separation. The initial condition is that at t=0, $C = C_0$ or $(M/S)\delta(x)$, where S is the cross-sectional area of the capillary, M is the initial mass of the solute and $\delta(x)$ is the Dirac delta function. This states that the pulse is initially present as an infinitely thin zone. The solution to Eq. 5-1 is

$$C_i(x,t) = \frac{M}{S\sqrt{4\pi D_i t}} \exp\left\{-\left(\frac{x-\mu_i E t}{4D_i t}\right)\right\} \qquad \text{Eq. 5-2}$$

When the diffusion coefficient and electrophoretic mobility are functions of both location and time, the convective-diffusion equation is

$$\frac{\partial C_i(x,t)}{\partial t} = \frac{\partial}{\partial x}\left[D_i(x,t)\frac{\partial C_i(x,t)}{\partial x}\right] - \frac{\partial}{\partial x}\left[v_i(x,t)\cdot C_i(x,t)\right] \qquad \text{Eq. 5-3}$$

A general analytical solution does not exist for this equation, which must be solved numerically to get the solute concentration profiles.

5.3 Modelling of electrophoretic separation of 2 solutes using dynamic matrix modulation

The transport of solute through the electrophoretic device can be given by diffusion-convective equation.

Governing equations:

$$\frac{\partial C}{\partial t} = \frac{\partial}{\partial x}\left(D\frac{\partial C}{\partial x} - vC\right)$$

$$I.C. \quad C(x,0) = C_0 \quad or \quad \overline{C}(x,0) = 1 \qquad \text{Eq. 5-4}$$

$$B.C. \quad \left(D\frac{\partial C}{\partial x} - vC\right)\Big|_{x=0,l} = 0$$

5.3.1 Methodology for Numerical Simulation

The *pdepe* function in Matlab was used to obtain time-dependent axial concentration profiles.

The function: sol = pdepe(*m,pdefun,icfun,bcfun,xmesh,tspan*) solves initial-boundary value problems for systems of parabolic and elliptic PDEs in one space variable and time; pdefun, icfun, and bcfun are function handles. The ordinary differential equations (ODEs) resulting from discretization in space are integrated to obtain approximate solutions at times specified in tspan. The pdepe function returns values of the solution on a mesh provided by xmesh.

pdepe solves PDEs of the form:

$$c\left(x,t,u,\frac{\partial u}{\partial x}\right)\frac{\partial u}{\partial t} = x^{-m}\frac{\partial}{\partial x}\left(x^m f\left(x,t,u,\frac{\partial u}{\partial x}\right)\right) + s\left(x,t,u,\frac{\partial u}{\partial x}\right) \qquad \text{Eq. 5-5}$$

In Eq. 5-5, $f\left(x,t,u,\frac{\partial u}{\partial x}\right)$ is a flux term and $s\left(x,t,u,\frac{\partial u}{\partial x}\right)$ is a source term. The coupling of the partial derivatives with respect to time is restricted to multiplication by a diagonal matrix $c\left(x,t,u,\frac{\partial u}{\partial x}\right)$. The diagonal elements of this matrix are either identically zero or positive. An element that is identically zero corresponds to an elliptic equation while non-zero elements correspond to a parabolic equation. There must be at least one parabolic equation in the equation set. An element of c that corresponds to a parabolic equation can vanish at isolated values of x if those values of x are mesh points. Discontinuities in c

and/or s due to material interfaces are permitted provided that a mesh point is placed at each interface.

For $t = t_0$ and all x, the solution components satisfy initial conditions of the form $u(x,t_0) = u_0(x)$ .For all t and either x=a or x=b, the solution components satisfy a boundary condition of the form $p(x,t,u) + q(x,t) f\left(x,t,u,\frac{\partial u}{\partial x}\right) = 0$

5.3.1.1 Electrophoretic separation of solutes

We have m = 0 and u = C (concentration of solutes). The length of the column is considered to be 10 cm. The flux term, f, can be given as $f = D\frac{\partial C}{\partial x} - vC$ whereas the source term in our case is 0, where D is the effective diffusion coefficient of solute in the medium and v is the electrophoretic velocity of the solute in the medium. The finite difference method which Matlab uses for the x-dimension profiling require $D/(v \cdot \Delta x) \sim 1$ as otherwise there are destabilizing effects leading to oscillations in the solution. The order of magnitude of diffusion coefficients, D in our study is 10^{-9} to 10^{-10} m^2/s and that of electrophoretic velocity; v is 10^{-4} to 10^{-5} m/s. Hence the mesh size required is very small which takes long time for the concentration profile evolution. The mesh size chosen (also keeping in mind that the time required for the program to be of reasonable order) was 0.001 -0.0001. The initial condition for the concentration cannot be given as the pulse function as that led to further destabilization of the solution. Hence the initial condition was given as a Gaussian distribution with 1-2mm width as is the case in the real situation for microfluidic electrophoretic separation.

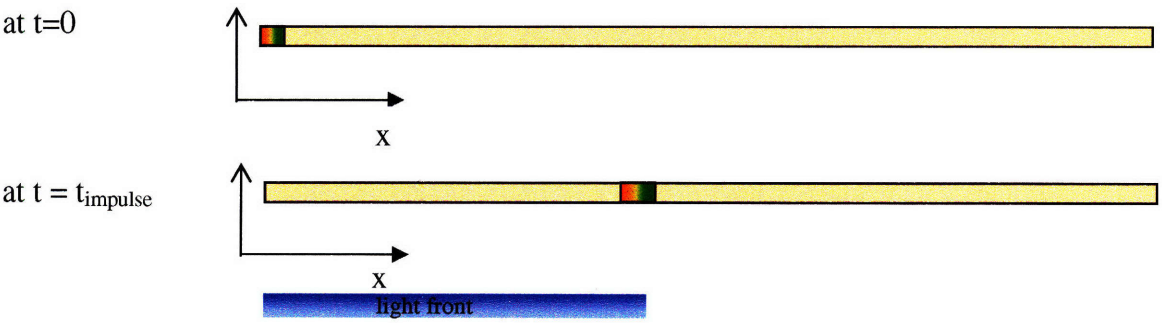

Figure 5-1: Schematic of application of light front on the electrophoretic column in case of dynamically controlled matrix

At $t=t_{impulse}$, the light front is established with a certain velocity (v_L).The concentration profiles are tracked without and with the light front. The UV light leads to a sol-to-gel transition of the medium and hence the transport properties of the solute through the medium will change in the illuminated region. In the given simulation, the parameters considered as follows

Simulation parameters:

2 solute separation

In sol state	In gel state
v_1 = 2e-4 m/s;	v1` = 1e-4 m/s;
v2 = 2.2e-4 m/s;	v2 `= 1.2e-4 m/s;
D_1 = 5e-9 m^2/s;	D_1`= 2.5e-9 m^2/s;
D_2 = 8e-9 m^2/s;	D_2` = 4e-9 m^2/s;

The basic methodology used here was that the simulations were run normally until t= $t_{impulse}$ and then the transport parameters were changed for the illuminated region. If the step function is used, then the discontinuity is imposed in the PDE formulation. Hence, the smoothed heaviside function (*flchs*) by Comsol was used instead as it is continuous function which is close to the practical case. The variables for the separation with medium modulation are velocity of the light front (v_L) and the time of the impulse ($t_{impulse}$). But varying both the parameters together in the simulation requires high computational power and time. Hence, for any particular trial simulation, $t_{impulse}$ was fixed but v_L was varied.

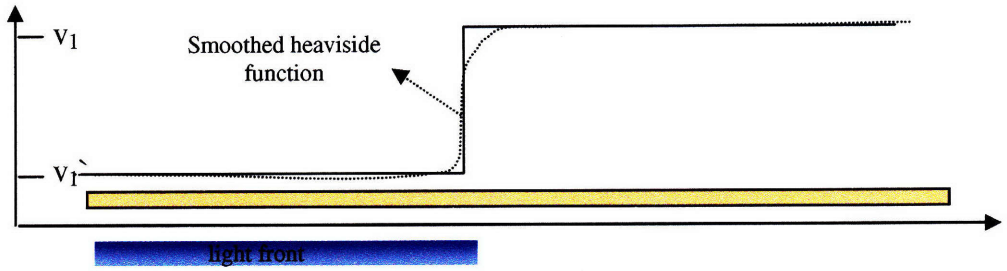

Figure 5-1b: Smoothed Heaviside function for representing the application of light front on the electrophoretic column

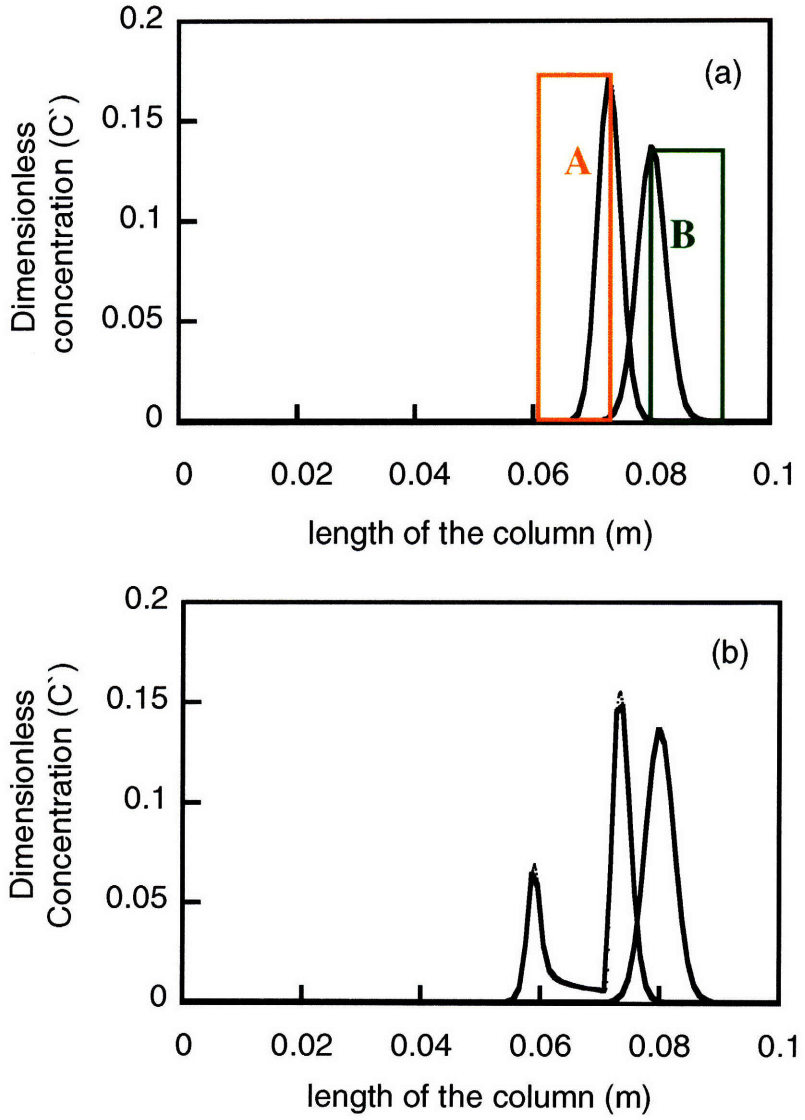

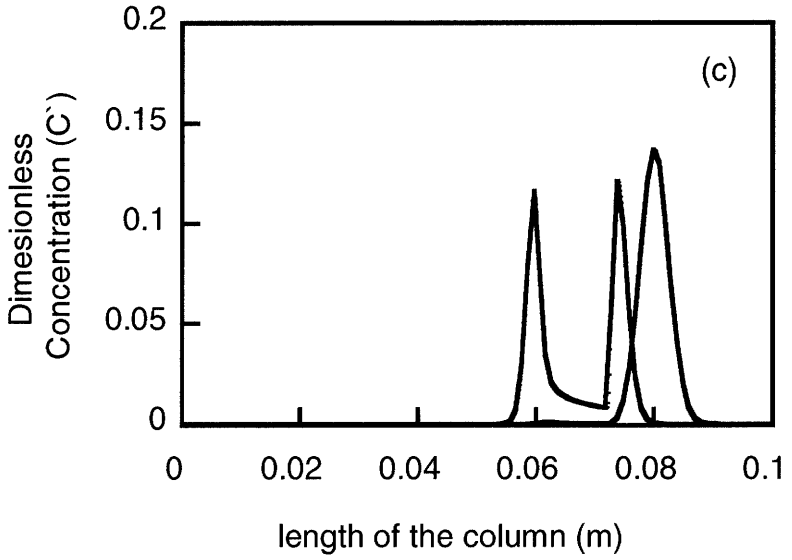
(c)
Dimesionless Concentration (C`)
0.2
0.15
0.1
0.05
0
0
0.02
0.04
0.06
0.08
0.1
length of the column (m)

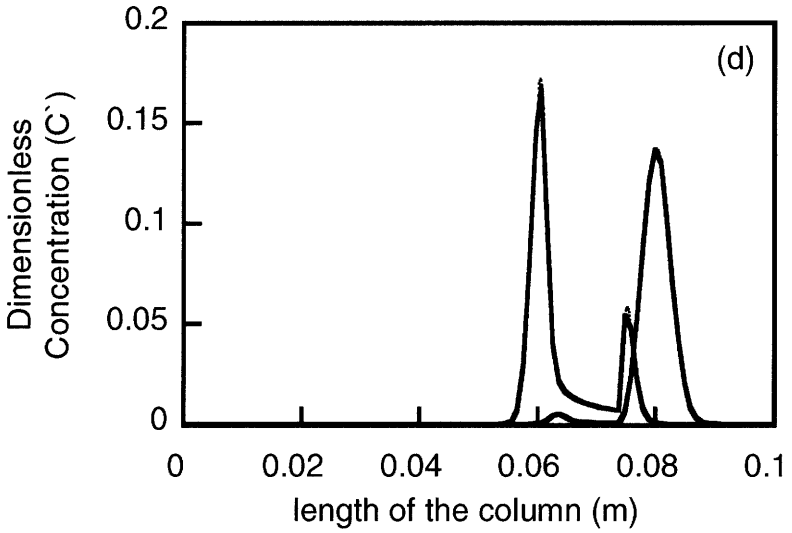
(d)
Dimensionless Concentration (C`)
0.2
0.15
0.1
0.05
0
0
0.02
0.04
0.06
0.08
0.1
length of the column (m)

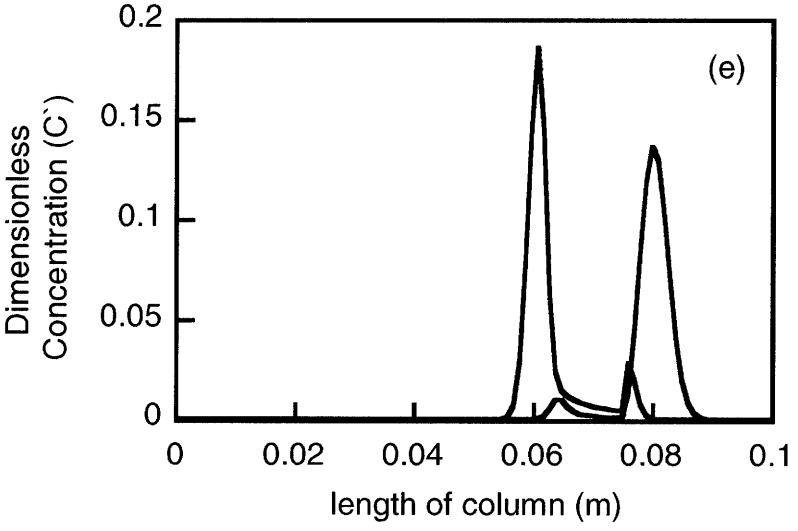
(e)
Dimensionless Concentration (C`)
0.2
0.15
0.1
0.05
0
0
0.02
0.04
0.06
0.08
0.1
length of column (m)

Figure 5-2: Concentration profile of solutes at time t = 400 secs (a) when no light front/stimuli is applied (b) when the velocity of the light front, v_L = 1.98 x 10^{-4} m/s and time of impulse, $t_{impulse}$ = 240s (c) when the velocity of the light front, v_L = 2.01 x 10^{-4} m/s and time of impulse, $t_{impulse}$ = 240s. (d) when the velocity of the light front, v_L = 2.06 x 10^{-4} m/s and time of impulse, $t_{impulse}$ = 240s. (e) when the velocity of the light front, v_L = 2.09 x 10^{-4} m/s and time of impulse, $t_{impulse}$ = 240s

Figure 5-2 (a) shows the separation of two solutes molecules moving through the matrix with constant physical properties. The curves are purely Gaussian in nature as predicted by the analytical expression given by Eq. 5-2. Figure 5-2 b to e shows the concentration profile evolution at t = 400s where the light front is started at $t_{impulse}$ = 240s and moved with different velocity v_L.It can be seen from these figures that the retardation of the solutes occurs where the UV light stimuli is applied. The location i.e. velocity of light front is critical to define how much percentage of solute A and B will be under UV light stimuli. Different amount of solutes will be retarded for different velocity of light front. It can be seen in Figure 5-2 b and c that the velocity of light front is such that only solute A is retarded. The further increase in the velocity of light front retards the solute B velocity too as seen in Figure 5-2 d and e.

In the standard/conventional case as shown above, the recovery of both solutes can be assumed to be done in the above way which will lead to high purity but the recovery of the solutes will be less. The numbers computed lead to purity =99.7 for both solutes with recovery of 46 and 54% for solute A and B respectively. This standard case is compared with our dynamic modulation method of separation to see how the purity and the recovery for both solutes are affected per pass.

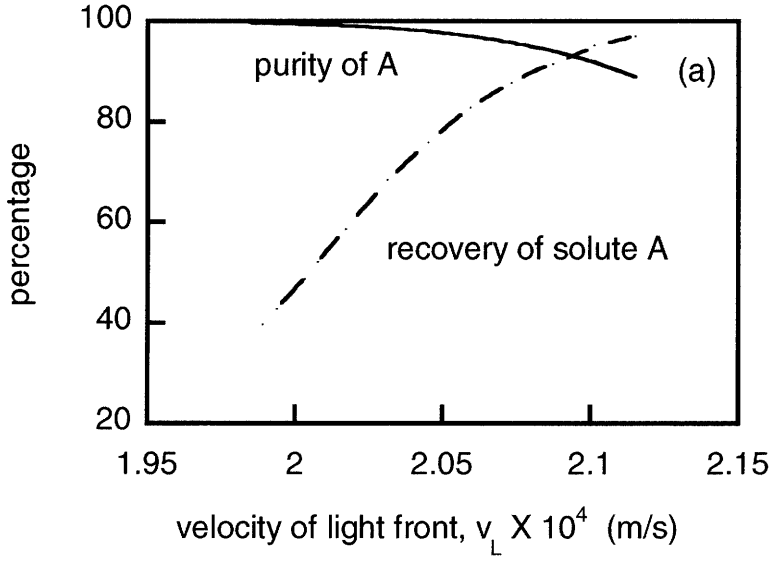
100
80
60
40
20
percentage
purity of A
(a)
recovery of solute A
1.95
2
2.05
2.1
2.15
velocity of light front, v_L X 10^4 (m/s)

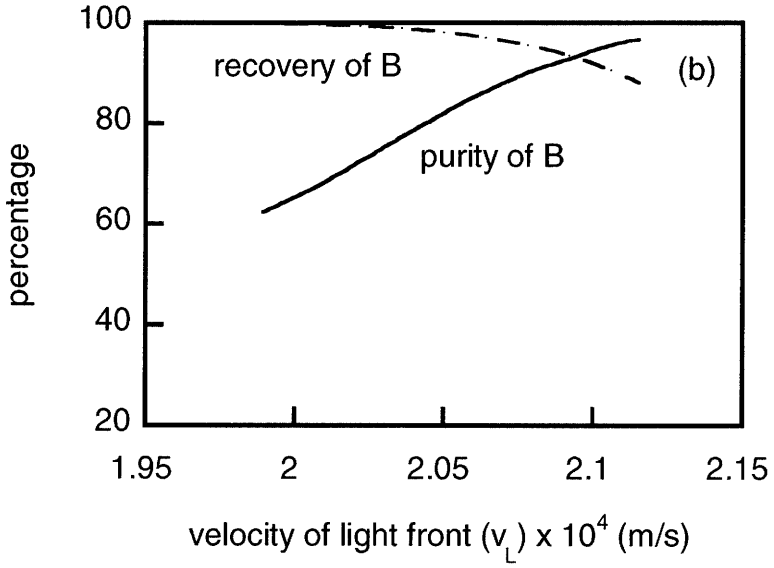
100
80
60
40
20
percentage
recovery of B
(b)
purity of B
1.95
2
2.05
2.1
2.15
velocity of light front (v_L) x 10^4 (m/s)

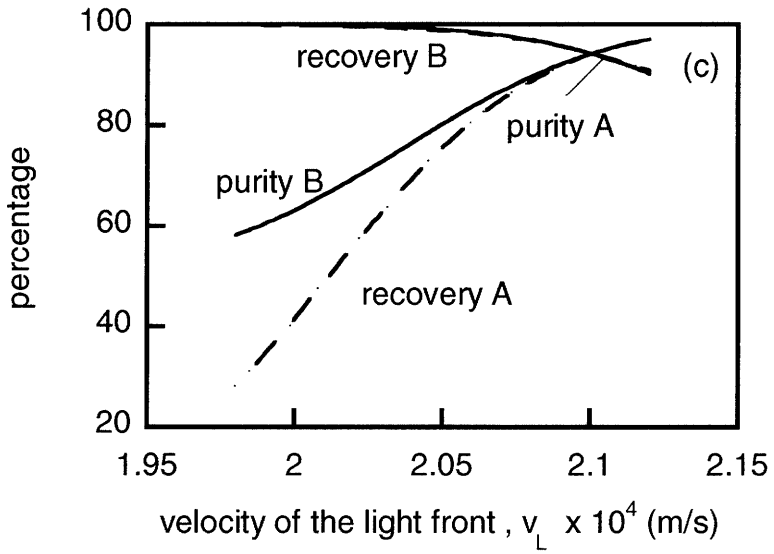

Figure 5-3: Percentage (a) recovery and purity of solute A obtained with different velocity of light front when the time of impulse, $t_{impulse}$ = 240 s, (b) recovery and purity of solute B obtained with different velocity of light front when the time of impulse, $t_{impulse}$ = 240 s, (c) recovery and purity of both solute A and B obtained with different velocity of light front when the time of impulse, $t_{impulse}$ = 300 s.

It can be seen as expected that there is a trade-off between the purity and recovery for both solutes A and B. The promising fact from this simulation is that from Figure 5-3 a combination of higher purity and recovery can be obtained as compared to conventional method in one pass itself on using dynamic matrix modulation technique.

5.4 Parameteric Analysis

Governing equations:

$$\frac{\partial C}{\partial t} = \frac{\partial}{\partial x}\left(D\frac{\partial C}{\partial x} - vC\right)$$

$$I.C. \quad C(x,0) = C_0 \quad or \quad \overline{C}(x,0) = 1 \qquad \text{Eq. 5-6}$$

$$B.C. \quad \left(D\frac{\partial C}{\partial x} - vC\right)\Big|_{x=0,l} = 0$$

The modulated gel system can lead to following equations for 2 solutes

$$\frac{\partial C_1}{\partial t}=\frac{\partial}{\partial x}\left(D_1\frac{\partial C_1}{\partial x}\right)-v_1\frac{\partial C_1}{\partial x} \qquad t<t_m \quad for\ all\ x$$

$$\frac{\partial C_1}{\partial t}=\frac{\partial}{\partial x}\left(D_1\frac{\partial C_1}{\partial x}\right)-v_1\frac{\partial C_1}{\partial x} \qquad t>t_m \quad and \quad x>x_m$$

$$\frac{\partial C_1}{\partial t}=\frac{\partial}{\partial x}\left(D_1\frac{\partial C_1}{\partial x}\right)-v_1'\frac{\partial C_1}{\partial x} \qquad t>t_m \quad and \quad x<x_m$$

$$\frac{\partial C_2}{\partial t}=\frac{\partial}{\partial x}\left(D_2\frac{\partial C_1}{\partial x}\right)-v_2\frac{\partial C_2}{\partial x} \qquad t<t_m \quad for\ all\ x$$

$$\frac{\partial C_2}{\partial t}=\frac{\partial}{\partial x}\left(D_2\frac{\partial C_1}{\partial x}\right)-v_2\frac{\partial C_2}{\partial x} \qquad t>t_m \quad and \quad x>x_m$$

$$\frac{\partial C_2}{\partial t}=\frac{\partial}{\partial x}\left(D_2'\frac{\partial C_1}{\partial x}\right)-v_2'\frac{\partial C_2}{\partial x} \qquad t>t_m \quad and \quad x<x_m$$

Eq. 5-7

Non-dimensionalizing the equations in time and length alongwith concentration

$\overline{C}=\frac{C}{C_0}$; $\tau=\frac{t}{L/v_1}$ *and* $X=\frac{x}{L}$, we get

$$\frac{\partial \overline{C}_1}{\partial \tau}=\left(\frac{D_1}{v_1L}\right)\frac{\partial}{\partial X}\left(\frac{\partial \overline{C}_1}{\partial X}-\overline{C}_1\right)=\left(\frac{1}{Pe_1}\right)\left(\frac{\partial^2 \overline{C}_1}{\partial X^2}-\overline{C}_1\right) \qquad \tau<T_m \quad for\ all\ X$$

$$\frac{\partial \overline{C}_1}{\partial \tau}=\left(\frac{1}{Pe_1}\right)\left(\frac{\partial^2 \overline{C}_1}{\partial X^2}-\overline{C}_1\right) \qquad \tau<T_m \quad and \quad X>X_m$$

$$\frac{\partial \overline{C}_1}{\partial \tau}=\left(\frac{1}{Pe_1'}\right)\left(\frac{\partial^2 \overline{C}_1}{\partial X^2}\right)-\left(\frac{\phi_1}{Pe_1'}\right)\overline{C}_1 \qquad \tau>T_m \quad and \quad X<X_m$$

$$\frac{\partial \overline{C}_2}{\partial \tau}=\left(\frac{1}{Pe_2}\right)\left(\frac{\partial^2 \overline{C}_2}{\partial X^2}\right)-\left(\frac{\phi}{Pe_2}\right)\overline{C}_2 \qquad \tau<T_m \quad for\ all\ X$$

$$\frac{\partial \overline{C}_2}{\partial \tau}=\left(\frac{1}{Pe_2}\right)\left(\frac{\partial^2 \overline{C}_2}{\partial X^2}\right)-\left(\frac{\phi}{Pe_2}\right)\overline{C}_2 \qquad \tau>T_m \quad and \quad X>X_m$$

$$\frac{\partial \overline{C}_2}{\partial \tau}=\left(\frac{1}{Pe_2'}\right)\left(\frac{\partial^2 \overline{C}_2}{\partial X^2}\right)-\left(\frac{\phi\cdot\phi_1}{Pe_2}\right)\overline{C}_2 \qquad \tau>T_m \quad and \quad X<X_m$$

Eq.5-8

where, $Pe_1=\frac{v_1L}{D_1}$; $Pe_2=\frac{v_1L}{D_2}$; $Pe_1'=\frac{v_1L}{D_1'}$; $Pe_2'=\frac{v_1L}{D_2'}$;

$\phi=\frac{v_2}{v_1}$; $\phi_1=\frac{v_1'}{v_1}$ *and* $\phi_2=\frac{v_2'}{v_2}$

Based on the dimensionless analysis, there are seven parameters influencing the solute concentration profile. These parameters are not all independent as they can be written in terms of others if we assume $\frac{D_i}{D_j} = \frac{\mu_i}{\mu_j}$ (based on Stokes equation and Debye-Huckel-Henry theory), then for same the applied potential $\frac{D_i}{D_j} = \frac{v_i}{v_j}$ for which we can deduce that

$$\frac{Pe_1'}{Pe_1} = \frac{D_1'}{D_1} = \frac{v_1'}{v_1} = \phi_1$$
$$\frac{Pe_2}{Pe_1} = \frac{D_2}{D_1} = \frac{v_2}{v_1} = \phi \qquad \text{Eq.5-9}$$
$$\frac{Pe_2'}{Pe_1} = \frac{D_2'}{D_1} = \frac{v_2'}{v_1} = \phi \cdot \phi_2$$

This reduces to four independent parameters affecting the solute profile. We can further assume that if v_2 and v_1 are close enough (or in other words, the solutes are similar in nature) then the change in matrix structure would affect both solutes to same extent leading to an assumption $\phi_1 = \phi_2$, leaving us with three independent parameters: Pe_1, ϕ and ϕ_1. Note that this ($\phi_1 = \phi_2$) is the worst case scenario for improvement in the resolution of separation, as both solutes are equally retarted by UV light and hence we have considered if for our simulation to find out the lower limit for the improvement.

The moving UV light front changes the electrophoretic mobility and diffusion coefficient which can be specified using the following Heaviside function, given by flchs in Matlab. The Heaviside function was used instead of step function due to the continuous nature of the function which does not destabilize the system as is the case of step function.

$$v_1 = v_1 + flc1hs(t - t_{impulse}, 5e-6) * ((v_1 - v_1') * (1 - flc2hs(x - v_l * t, 3e-4))) \qquad \text{Eq.5-10}$$
$$D_1 = D_1 + flc1hs(t - t_{impulse}, 5e-6) * ((D_1 - D_1') * (1 - flc2hs(x - v_l * t, 3e-4)))$$

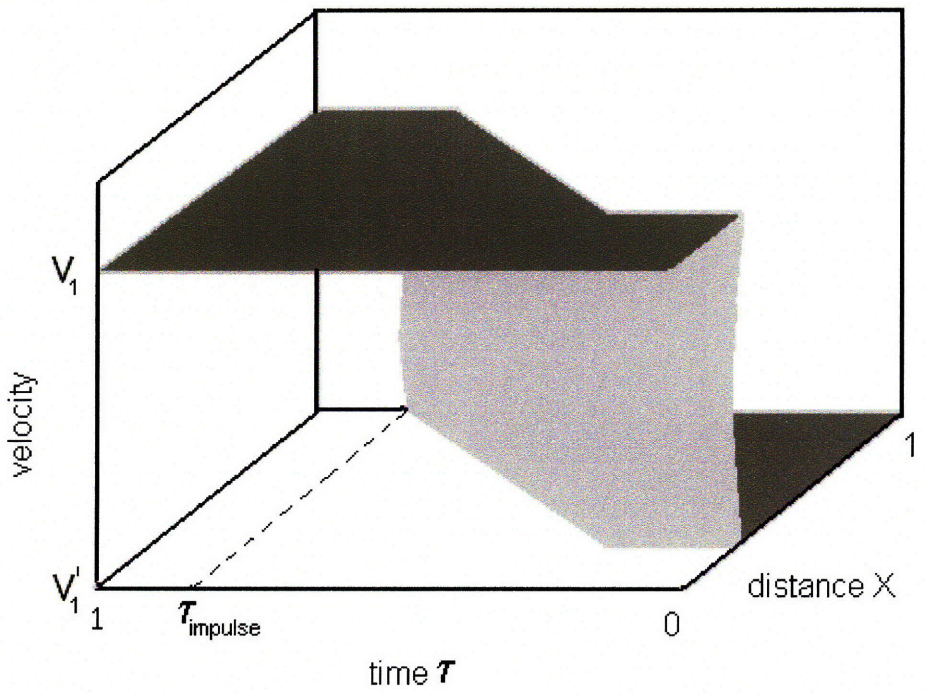

Figure 5-4: Schematic plot of velocity of solutes in dynamically modulated matrix with respect to distance and time using Eq.5-10.

The concentration profiles for the different operating strategies (i.e. no modification and with the moving UV illumination front) were obtained for a given dimensionless time τ_1. The impulse was given at $\tau = 0.5\ \tau_1$, where $\tau_1 = 0.4$. The Pe range was chosen such that even the overlapped profiles were obtained to have a complete range of conditions for the parametric study. To find out Peclet number for each ϕ such that the overlap exists following method was used.

The solution to the general governing equations results in concentration profile with Gaussian distribution as shown in Figure 5-5.

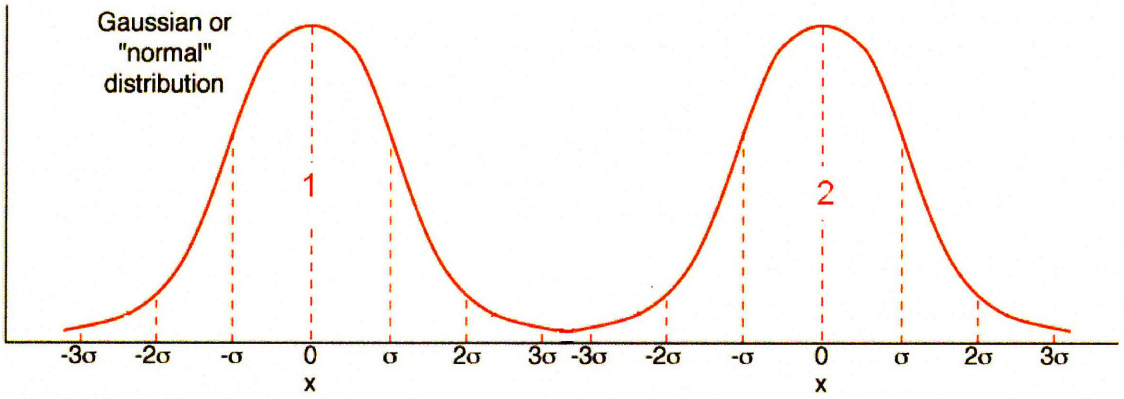

Figure 5-5: Concentration profiles obtained in case of the non-modulated matrix electrophoretic separation. The concentration profiles have Gaussian distribution as seen in Eq. 5-2.

For the given values of v_1 and v_2 and at a given time t, the overlap condition is taken to be when

$$x_1 + 3\sigma_1 \leq x_2 - 3\sigma_2$$

$$\text{where, } x_1 = v_1 t;\ x_2 = v_2 t;\ \sigma_1 = \sqrt{2D_1 t} \text{ and } \sigma_2 = \sqrt{2D_2 t}$$

Non-dimensionalizing the equation using $\tau = t/(L/v_1)$ we get Eq.5-11

$$Pe \leq \frac{(3\sqrt{2}(1+\sqrt{\phi}))^2}{(\phi - 1)^2 \tau}$$

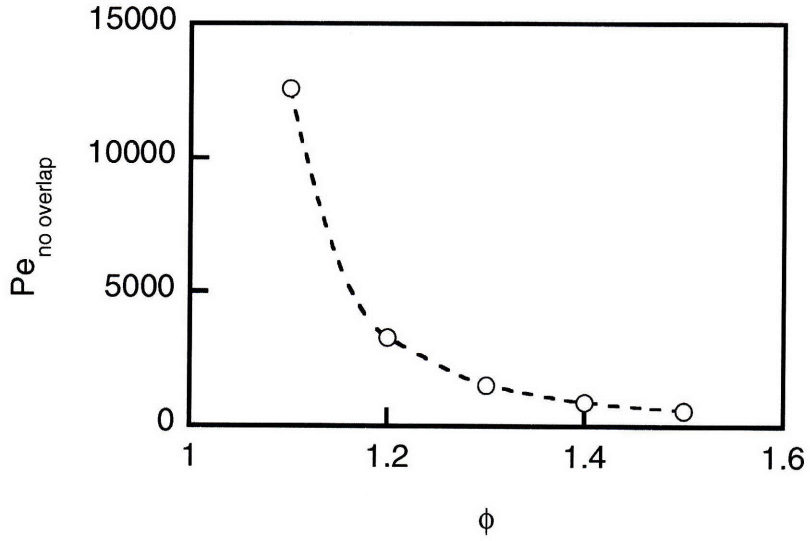

Figure 5-6: Plot of higher limit of Pe number, i.e. above which no overlap exists for a given value of ϕ.

Based on this analysis Eq.5-11 for $\tau_1 = 0.4$, the parameter ranges selected for parametric study were as follows:

ϕ : 1.1 to 1.5
ϕ_1 : 0.25 to 0.67
Pe : 400 to 8400

From Figure 5-5, it can be seen that the improvement in separation is dependent on the velocity of the light front, v_L. Qualitatively, the velocity of the light front should be such that it only specifically and selectively hinders the velocity of solute 1 and not solute 2. This case can be found by finding the length of the column where no overlap of solutes exists, which can be expressed as following condition.

$$x_{impulse} \in \{x_1 - 3\sigma_1, x_2 - 3\sigma_2\}$$

$$\left.\frac{v_L}{v_1}\right|_{low} = 1 - 3\sqrt{\frac{2}{Pe \cdot \tau_{impulse}}} \qquad \text{Eq.5-12}$$

$$\left.\frac{v_L}{v_1}\right|_{high} = \phi - 3\sqrt{\frac{2\phi}{Pe \cdot \tau_{impulse}}}$$

Eq.5-12 provides the lower and the higher limit of the velocity of light front. The lower limit of the light front velocity will be close to the case of non-modulated or conventional matrix case whereas the higher limit is the case where maximum improvement is expected. The validity of the result in Eq.5-12 can be well seen with the simulations done in the above section 5.2. The optimized v_L/v_1 of 1.03 found in the study is exactly the same as the one predicted by this equation.

There are two performance variables that characterize the quality of the separation, the yield of solute A and the separation resolution.The Y_A is defined here as the yield of solute 1/A where purity of A is at 0.99.

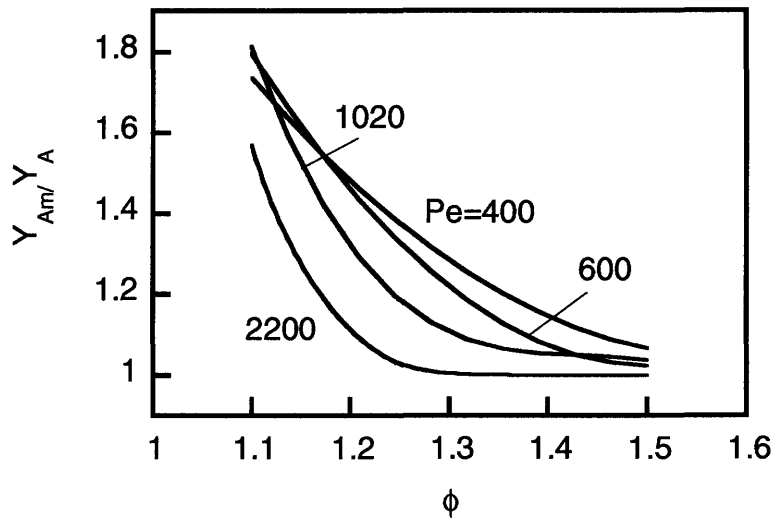

Figure 5-7: Plot of the ratio of yield of solute A in modulated gel case to that of in the general case with respect to the parameter ϕ for different values of Pe for the value of ϕ_1=0.67

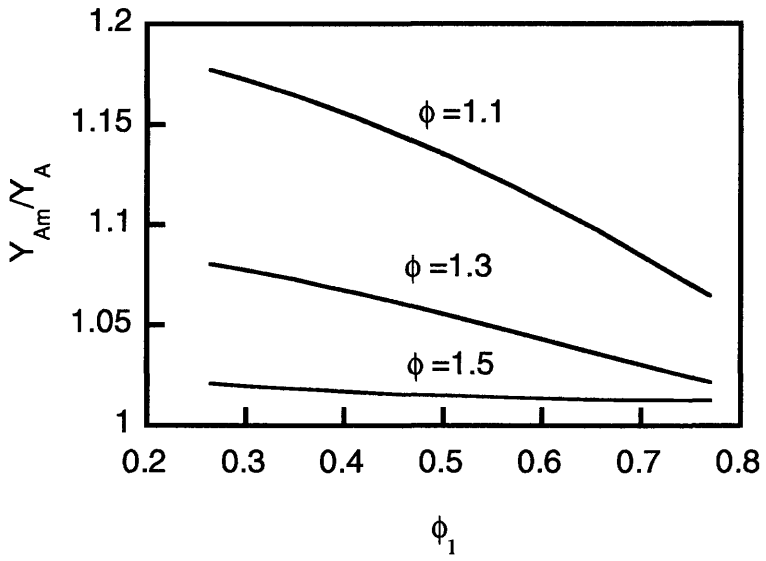

Figure 5-8: Plot of the ratio of yield of solute A in modulated gel case to that of in the general case with respect to the parameter ϕ_1 for a constant Pe = 400.

The yield ratio increases with decrease in ϕ_1 for a given value of Pe^{-1} and ϕ. The separation does improve even for higher ϕ but the improvement is not able to be captured in the response variable, yield. Hence, the modified resolution is used as another response

variable and both yield and resolution should be taken into account for looking for improvement in separation for a given parameter values.

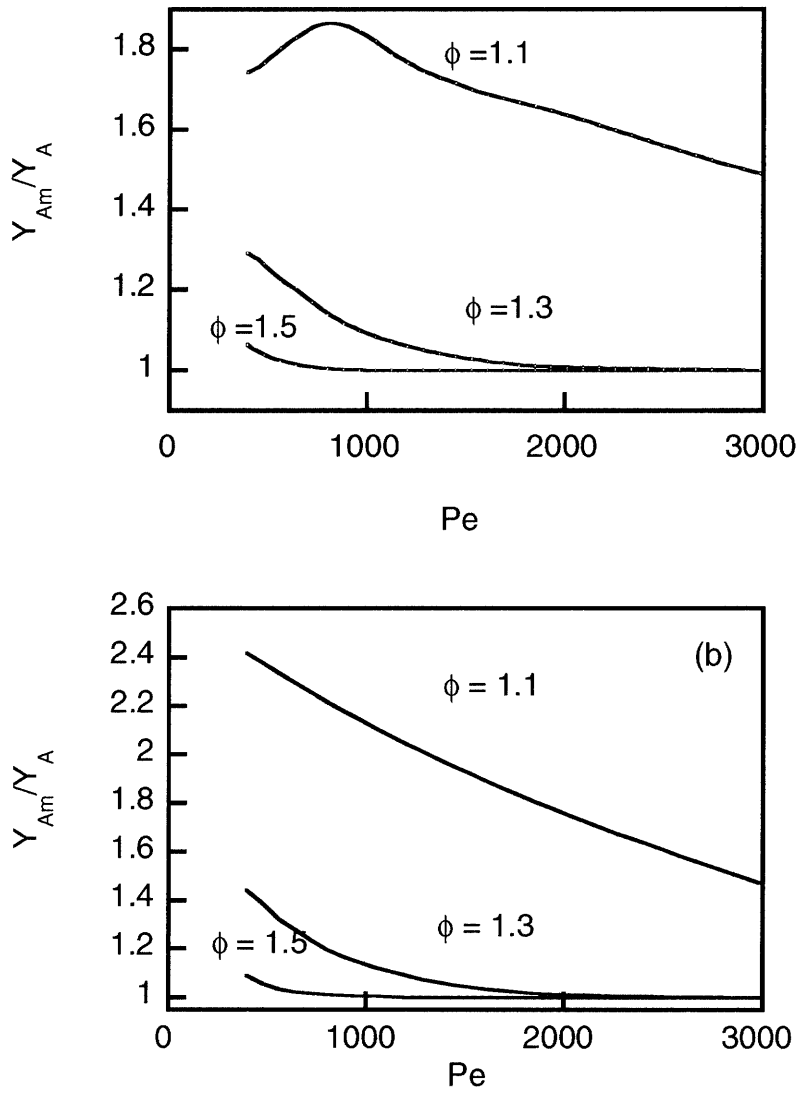

Figure 5-9: Plot of the ratio of yield of solute A in modulated gel case to that of in the general case with respect to the parameter Pe^{-1} for different values of ϕ for the value of (a) ϕ_1=0.67 and (b) ϕ_1= 0.25.

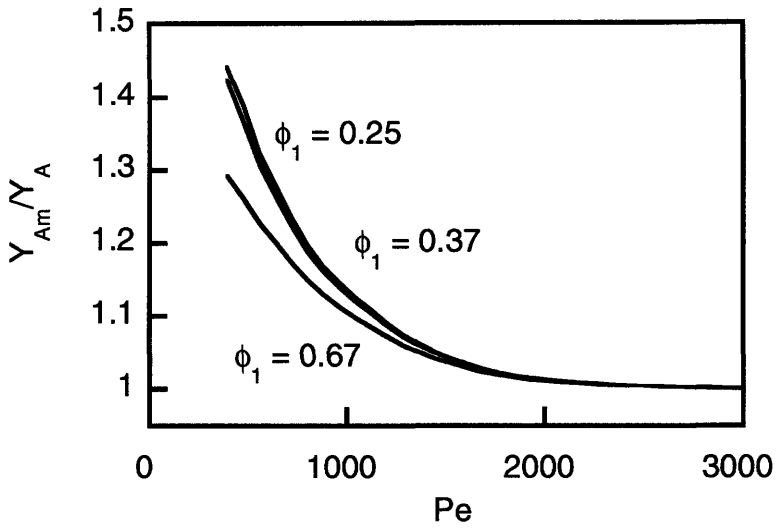

Figure 5-10: Plot of the ratio of yield of solute A in modulated gel case to that of in the general case with respect to the parameter Pe^{-1} for different values of ϕ_1 for the value of ϕ=1.3

RESOLUTION RATIO

In general, the resolution of separation of two solutes is given by equation

$$Res = \frac{(x_{peak2} - x_{peak1})}{2\sqrt{\pi} \cdot (\sigma_1 + \sigma_2)} \qquad \text{Eq.5-13}$$

This definition cannot be used directly for our modulated matrix case in case of overlap and hence we tried to redefine the resolution such that we could be able to compare the values with and without modulation of the matrix.

The modified resolution definition was done in terms of areas instead of sigmas as the peaks after the modulation may or may not be Gaussian in nature.

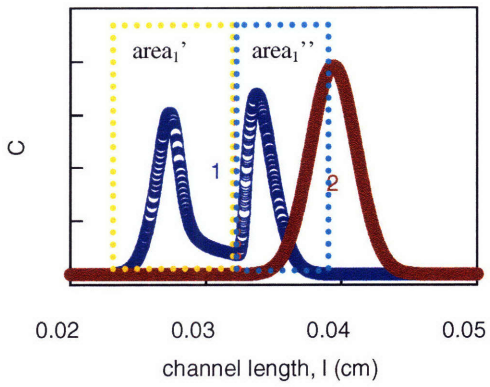

Figure 5-11: Schematic showing two solute separation in dynamically modulated matrix system. The areas are marked which are used in Eq.5-14 for weighing the resolutions of the split peaks.

Hence, in case of modulated gel, resolution was weighted average as follows:

$$\frac{\mathrm{Re}\,s_{\mathrm{mod}}}{\mathrm{Re}\,s} = \frac{\dfrac{(x_{peak2}-x_{peak1}')}{(area_2+area_1')}\cdot\dfrac{(area_1')}{(area_1'+area_1'')} + \dfrac{(x_{peak2}-x_{peak1}'')}{(area_2+area_1'')}\cdot\dfrac{(area_1'')}{(area_1'+area_1'')}}{\dfrac{(x_{peak2}-x_{peak1})}{(area_2+area_1)}} \qquad \text{Eq.5-14}$$

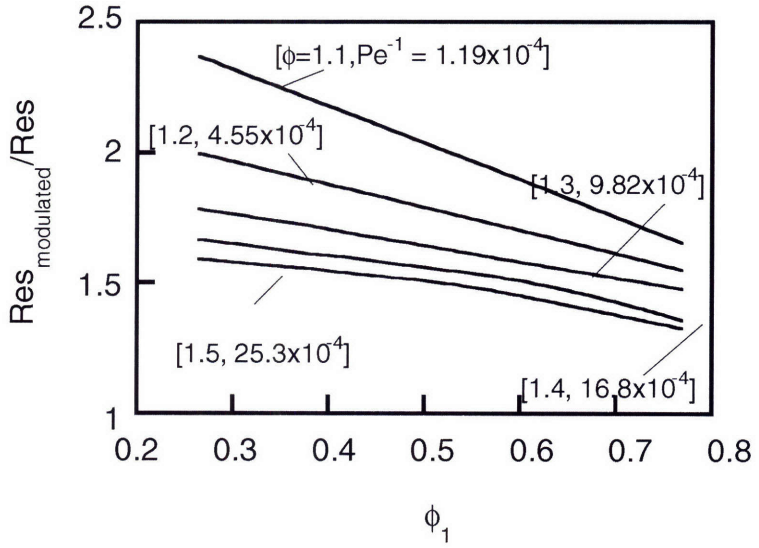

Figure 5-12: Plot of the ratio of resolution of two solutes in modulated gel case to that of in the general case with respect to the parameter ϕ_1. The corresponding values of ϕ and inverse Pe number are labeled next to the curves.

The ratio R increases with the increase in reduction of transport properties in gel. The dependence is almost linear in nature. Depending on Pe number for a given ϕ, the overlap exists or not. When the overlap exists, it is seen that the enhancement is higher.

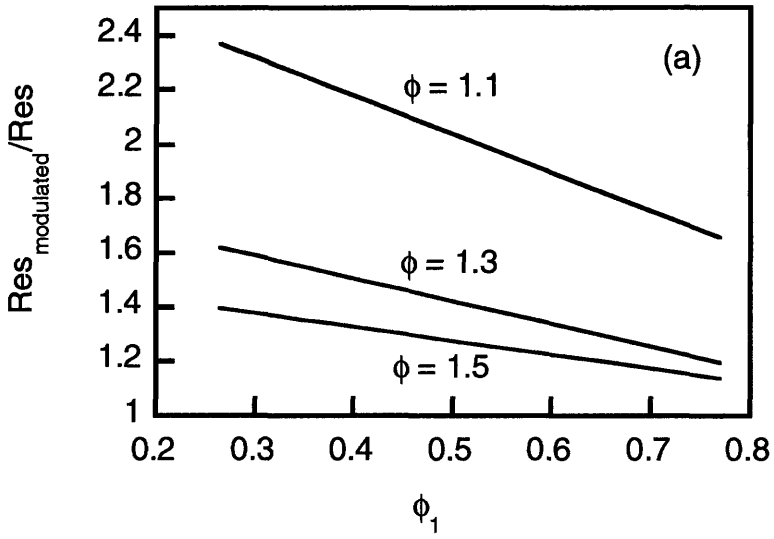

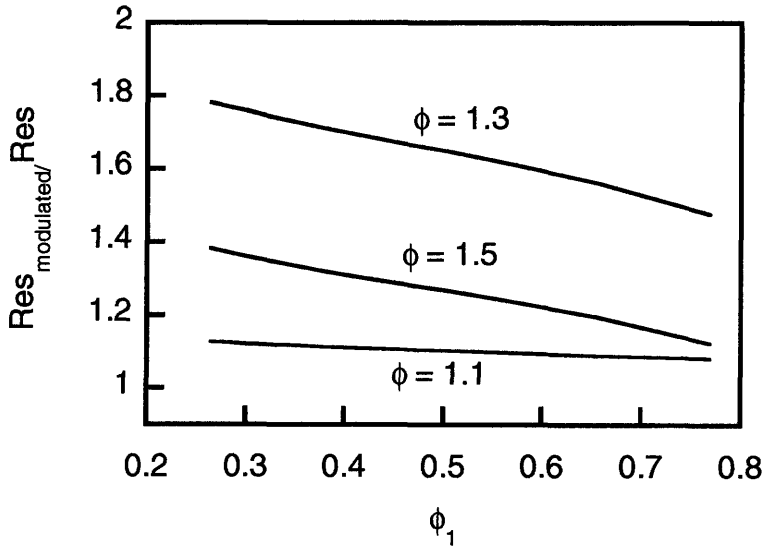

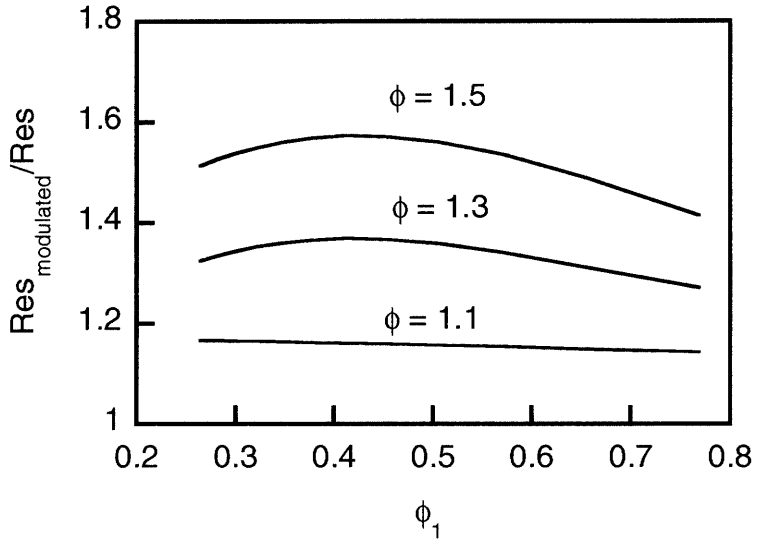

Figure 5-13: Plot of the ratio of resolution of two solutes in modulated gel case to that of in the general case with respect to the parameter ϕ_1 for different values of ϕ but at same Pe number, (a) 8400, (b) 1020 and (c) 400.

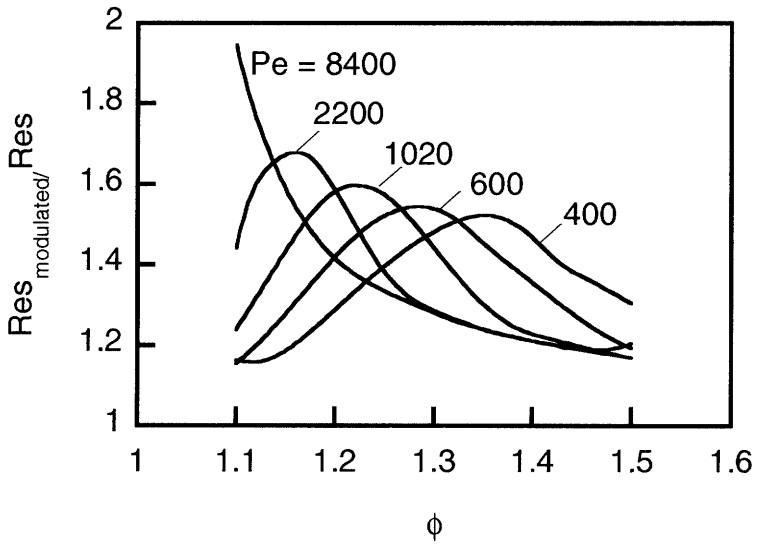

Figure 5-14: Plot of the ratio of resolution of two solutes in modulated gel case to that of in the general case with respect to the parameter ϕ for different values of Pe for the value of $\phi_1 = 0.67$.

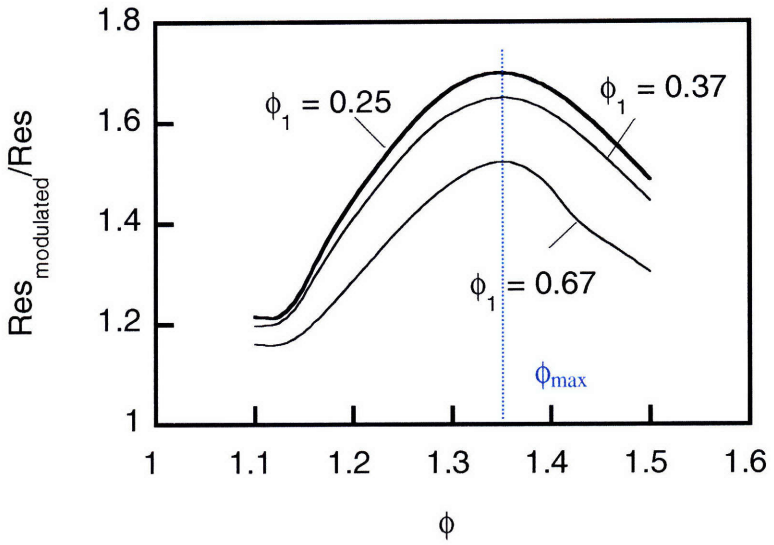

Figure 5-15: Plot of the ratio of resolution of two solutes in modulated gel case to that of in the general case with respect to the parameter ϕ for different values of ϕ_1 for the value of Pe= 400.

For a given Pe, after there is no overlap between 2 solutes ($\phi > \phi_{max}$) , the ratio of modified resolution to the conventional case can be given as

$$R = \frac{Res_{modulated}}{Res} \alpha \frac{(\phi - \phi_1) - (1 - \phi_1) \cdot (\tau / \tau_{impulse})}{(\phi - 1)} \qquad \text{Eq.5-15}$$

which is a decreasing function and hence we see the values dropping down with increase of ϕ in the described range (after ϕ_{max}). After ϕ_{max}, R is a continuously decreasing function but its value is always greater than 1.

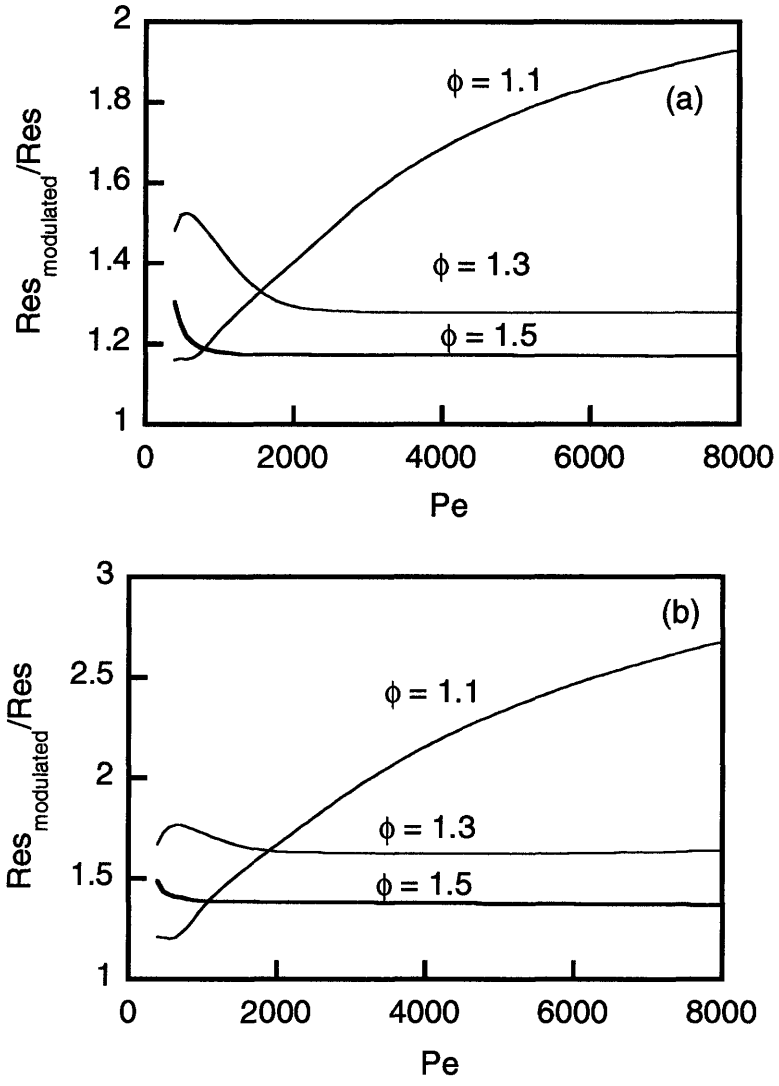

Figure 5-16: Plot of the ratio of resolution of two solutes in modulated gel case to that of in the general case with respect to the parameter Pe for different values of ϕ for the value of ϕ_1=0.67 and ϕ_1= 0.25.

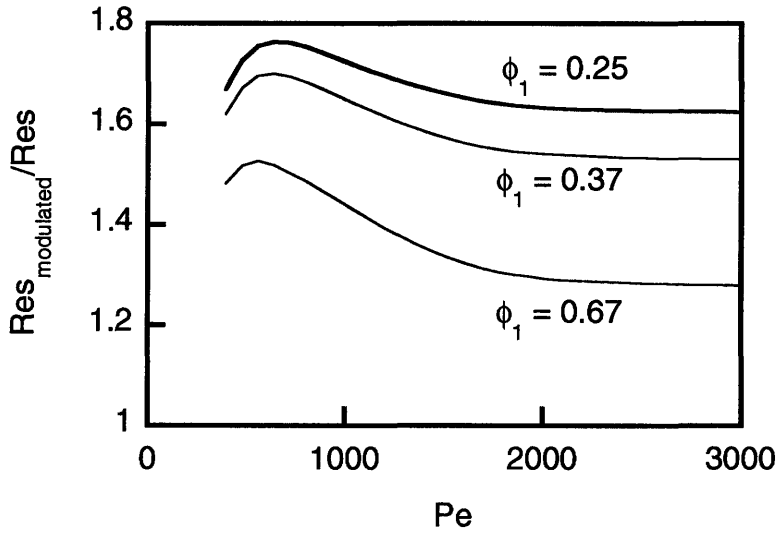

Figure 5-17: Plot of the ratio of resolution of two solutes in modulated gel case to that of in the general case with respect to the parameter Pe for different values of ϕ_1 for the value of ϕ=1.3

All the combined results obtained in the figures above shows that the yield and recovery of solutes can be improved by using the dynamically modulated matrix and the magnitude of the improvement will depend on the operating conditions, nature of the solute and the reduction of solute transport properties in gel state.

5.5 Electrophoretic separation experiments

Electrophoresis separation experiments were carried out to show the practical proof of concept of enhancement of separation in dynamically modulated system as seen in theoretical simulations. Microfluidic electrophoresis device was constructed for th e purpose as miniaturizated electrophoresis devices has shown to lead to faster and high resolution separation. The electrophoresis setup built for electrophoretic mobility could not be used for the separation directly as there provision for small width injection and also effective temperature control alongwith capability for photostimuli is difficult to obtain. Hence, device modification was carried out taking these issues in mind. A critical parameter in high resolution electrophoresis is the sample injection. Usually, two injection methods are used. The first is electro-kinetic injection, which is based on the

application of a high voltage for pumping the sample solution by generation of an electro-osmosic flow.[2] The second method of injection is pressure induced. We chose pressure induced injection as the electro-kinetic injection requires a complicated and expensive setup we wish to minimize electro-osmosis in our device. Pressure induced injection method as optimized by Bai et.al.[3] was performed by means of a multi-port two-way valve system where sample was injected after the solution was filled into the column, by switching the valve. This method enabled injection of the sample with a minimal perturbation of the flow. This method did not work for our system due to viscosity difference between injection fluid and the matrix. A simple device is described below that exploits the dually responsive polymer nature of the polymer our matrix system for sample injection.

5.5.1 Microfluidic device

A simple microfluidic channel containing device was constructed with arrangement for reservoirs at each end. The microfluidic channel was made by molding polydimethylsiloxane (PDMS) on the master consisting of plastic slides (Isaac Tech, P11011P, 1"x3" and height of 500 μm) cut into required dimension of 0.4 cm width and about 5 cm in length. The procedure for making PDMS device was based on conventional methods[4] as described below. About 30 gms of PDMS pre-polymer was used along with the curing agent (which is $1/10^{th}$ of the final pre-polymer weight) per plastic Petri dish of dimension 9 cm diameter and 1.3 cm height (see device layout below).The mixture was stirred for 5 minutes before the vacuum was drawn to remove all the bubbles. The PDMS mixture was then poured on the master placed in the Petri dish containing 4 cut plastic slides in the oven for 2.5 hours at 65°C. After PDMS was cured, it was peeled off the dish leaving the thin slides behind. The cured PDMS slab was then cut into pieces, each of which contained a single channel and holes are punched at each end. The cut piece was cleaned using Scotch tape before being plasma-bonded to glass slides of dimensions 5cm x 7.5 cm using Plasma Cleaner for 25 secs. Small 2.5ml plastic centrifuge tubes cut to fit the holes punched on the PDMS device were epoxied to the

device to act as reservoirs and for insertion of the platinum electrodes. A small hole for the sample injection was punched in the PDMS device using small needle (BD 26G3/8).

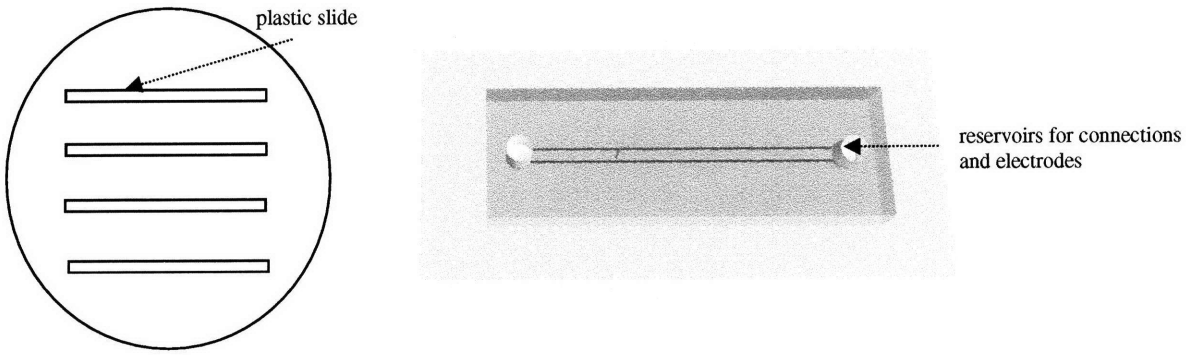

Figure 5-18: The device layout for making the channels in Petri dish is shown on the left. The microfluidic device is shown on the right made of a channel in PDMS plasma bonded to glass slide. The centrifuge tubes were used for the reservoirs for buffer and for electrical connections.

The light stimulus was applied using a fiber optic cable of 2.54 mm diameter provided on UV lamp (Dymax® Bluewave 200, intensity 40 W/cm^2). The selective gelation can be seen with this specific experiment described below. The matrix (about 0.4 ml) was placed in the 4.5 ml plastic cuvette with a lid. The cuvette was turned 90° for the matrix to rest on the long side, the fiber optics cable held close to the cuvette, which was irradiated with UV light for 10 secs and then was turned back allowing the non-gelled liquid to flow back to the bottom. The circular gelled area remains stuck to the cuvette long side due to its higher viscosity.

Figure 5-19a shows the Dymax® lamp used for photostimuli whereas part b shows the circular area formed due to selective gelation of the matrix equal to the diameter of the fiber optics seen within the dotted circle. It was difficult to get better contrast pictures as both the sol and gel are transparent and too similar in color to be able to capture a sharp difference by the camera. The width of the stimulated zone can be easily controlled by making a slit of the required dimensions by covering the rest of the illuminated surface with thick black electrical tape.

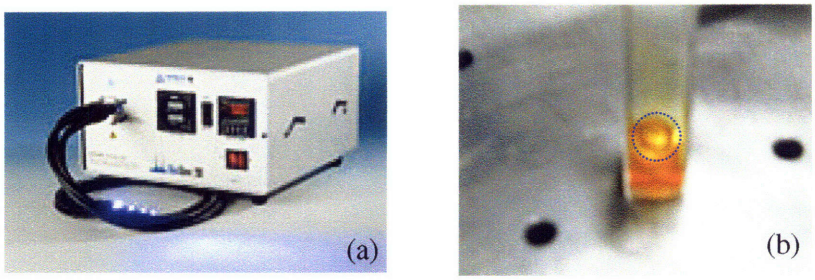

Figure 5-19: (a) Dymax® lamp used for UV irradiation and (d) Selective gelation of the physical blend matrix carried out using fiber optics of the Dymax lamp. The dotted circle is shown to help guide the eyes to see the gel circular area formed with size same as the fiber optic diameter.

The procedure used for sample injection is described below.The F127/MOAB-DMA polymer blend solution prepared in TBE buffer was poured into one of the reservoirs and the device was placed in the refrigerator for it to flow through the channel and the levels in both reservoirs were allowed to equilibrate. The device was placed in the refrigerator as the viscosity of blend decreases with temperature as described in Chapter 3. The lids to the reservoirs holding Platinum wire were then closed and the device is then placed on the thermostage (Linkam with PE94 control module with precision of 0.1°C) at T = 26°C for the matrix to be in gel state.

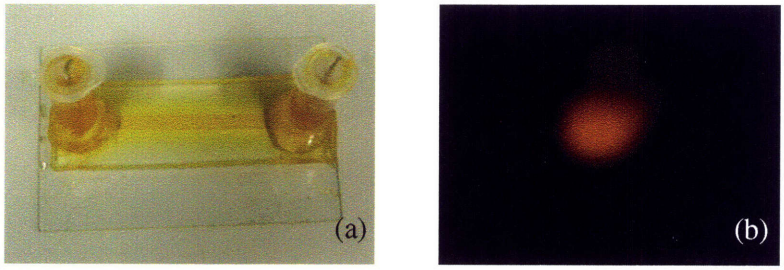

Figure 5-20: (a) Fabricated electrophoresis device on glass slide with the reservoirs on each side holding the Platinum wire. (b) Typical injection via punctured hole in PDMS seen under microscope with 2.5 X lens.

The sample injection in high viscosity polymer solution is more defined than low-viscosity solution. The sample containing protein solution was injected through the punctured hole using 10µl syringe with injection volume of 0.5 to 1µl. The temperature was then brought back to 23°C for the electrophoresis experiment to be carried out.

The possible experimental errors which led to failure of some of the electrophoresis runs are described below. The manual syringe injection was prone to producing bubbles on the insertion or removal of the syringe from the hole. The bubbles formed in the highly viscous and surface active fluids were difficult to break or remove and hence the device had to be cooled again and the bubble had to be carefully removed. Another problem arose due to the hydrogen evolved at cathode. The tiny bubbles formed at the cathode could make their way into the channel leading to a decrease in the applied voltage. A third possible cause of error was dried polymer at the Platinum electrode providing resistance to the current flow through the system, reducing it to zero and stopping the electrophoresis experiment.

The electrophoresis experiment was carried out for a mixture of TRITC labeled chymotrypsin and Texas red labeled bovine serum albumin. In the top of each frame in Figure 5-21, the gradual separation of the peaks for the two proteins is evident, but the resolution is not significant until after the photostimulus is applied and the BSA mobility is retarded even further. The bottom of each frame shows the movement of BSA by itself, which tracks equally with that of the BSA in the mixture upto the point where the stimulus is applied to the mixture case only. The retardation of the BSA due to the UV irradiation is clear on comparison of the BSA traces.

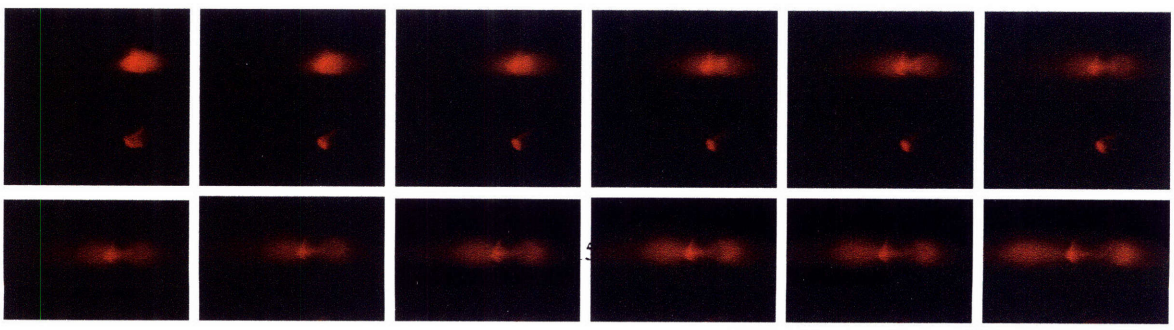

Figure 5-21: The sequence of electrophoretic separation of bovine serum albumin/solute1 (BSA) and chymotrypsin/solute2 in the physical blend of Pluronic F127 and MOAB-DMA is shown on the top. The electrophoretic transport of BSA in the same matrix is shown at the bottom under same conditions and time. The UV light irradiation was applied at $\tau_{impulse} = 0.5\tau_1$ moving with velocity, $v_L/v_{1front} = 1$. The rightmost point on the top of each picture is the injection point and hence is constant in each picture can be seen as the reference point.

Electrophoretic experiments were done for separation of Texas red-labeled bovine serum albumin (66 kDa) and ovalbumin (45 kDa). Both proteins are of similar nature with varying size and charge. Figure 5-22 shows the separation achieved after same fixed period of time in different type of matrix system (a) sol state, (b) gel state, (c) dynamic modulation of matrix at $\tau_{impulse} = 0.5\ \tau$. The parameters for this two proteins are $\phi = 1.5$, $\phi_1 \sim 0.5$, $Pe \sim 10^5$ (indicating no overlap as shown by Eq.5-11). Four similar runs were done to get resolution in different cases (a) 1.1 ± 0.2, (b) 1.2 ± 0.1 and (c) 1.7 ± 0.2. The resolution was calculated using the usual resolution of separation definition given by Eq.5-13.

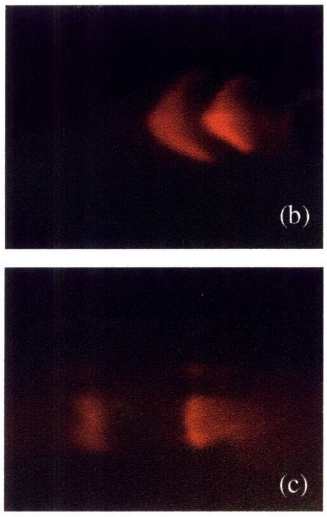

Figure 5-22: Electrophoretic separation of bovine serum albumin and ovalbumin in physical blends of Pluronic F127 and MOAB-DMA under 600 V, similar conditions and starting point shown in three different state of matrix (a) sol state, (b) gel state and (c) dynamically modulated state at $\tau_{impulse} = 0.5\ \tau_1$ at same time t = 300s.

It can be seen from Figure 5-22 as well as calculated numbers that resolution is improved about 1.3 to 1.4 times using dynamic modulation of the matrix properties. This improvement is close to that theoretically predicted value of 1.4 for the above parameters as shown in Figure 5-15. The electrophoretic separation of ovalbumin and BSA in conventional non-denaturing polyacrylamide is well studied and documented by Barton[5]. For similar conditions the resolution in a polyacrylamide strong gel (7 to 11.25%) is 1.2 to 1.4. Thus, it can be seen that there is 0.5 times enhancement than the traditional method used for BSA and ovalbumin separation. Alongwith this, the traditional matrix used polyacrylamide are chemically crosslinked gels unlike the polymer matrix used in our case, which is easily replaceable and reuseable.

5.6 Conclusion

In this chapter, the potential for exploiting dynamically modulated gel matrix to enhance electrophoretic protein separations. The proper method of applying stimuli is discussed and it is found out to be the moving light front with respect to one of the solutes. Three independent parameters governing the dynamic modulated separation process have been identified and the separation process has been simulated numerically

simulated for over appropriate ranges of their values. The equation for the optimized velocity of the light front is obtained to be applied to the system once the three governing parameters are known. The two performance variables studied were the yield or recovery of solutes with 99.0% purity and resolution of solutes normalized by their respective non-modulated matrix cases. The enhancement ratio is seen to be greater than one for all combinations of parameters. Dynamically modulated matrix electrophoresis was seen to be more effective in enhancement of separations when resolution is poor to begin with. Experiments done to demonstrate the proof of concept showed enhancement in resolution as predicted by the simulations. The responsive matrix has theadvantages that it is easy to load and replace in microfluidic devices, and that we have the ability to alongwith its capability to change solute transport properties allowing for the enhancement in protein separation.

5.7 References

1. Fahien, R.W., (1983). "Fundamentals of Transport Phenomena", McGraw-Hill, New York
2. G.J.M. Bruin, Electrophoresis, 2000, 21, 3931-3951
3. Bai, X., Lee, H.J., Rossier,J.S., Reymond, F., Schafer, H., Wossner, M., and Girault, H.H., Lab Chip, 2002,2,45-49
4. Duffy,D., McDonald,J., Schueller, O., and Whitesides, G., Anal. Chem.,1998, 70 (23),pp- 4974-4984
5. Barton, R.J., Biochem. J., 1972, 129, 983-985

Chapter 6

Gene Transfection Studies using Pluronic Copolymers with Cationic Polymer

6.1 Motivation and Approach

The development of gene therapy relies on designing optimal systems for nucleic acid transfer and expression, cationic polymers being a promising alternative to viral vectors.[1] Because the latter are toxic and immunogenic, nonviral strategies toward gene transfection are becoming more and more attractive. A variety of synthetic, polycationic polymers have become available; they demonstrate adequate safety profiles and can complex large plasmids, forming polymer-DNA complexes (polyplexes). Some of the polyplexes have superior transfection efficiency and serum sensitivity compared to the lipid-DNA complexes (lipoplexes). [2,3,4] These considerations make polycations a compelling target for future exploration in nonviral gene delivery.[5] Polycations bind to nucleic acids due to the formation of cooperative systems of salt bonds between the cationic groups of the polycation and phosphate groups of the DNA. Great efforts have been undertaken to improve the efficiency of the polycations, but, as yet, satisfactorily effective polymer systems have still to be achieved. One of the promising strategies toward creating more effective polycationic systems that complex DNA forming polyplexes[6] involves attachment of hydrophilic polymers such as poly(ethylene oxide) (PEO).[7,8] The modification of the polyplexes with PEO shields positive surface charges and creates a steric barrier against self-aggregation and unfavorable interactions with albumin, complement factors, or cellular components in the bloodstream. The modification of such polyplexes may reduce the potential of nonspecific interactions, such as opsonization or deposition due to cationic surface charges. Block copolymers of cationic polymers and PEO form complexes with DNA that are more acceptable to systemic administration than complexes of the unmodified polycations and DNA.[9,10]

Furthermore, the incorporation of propylene oxide group with polyethylene oxide when bonded to polycations, provide additional advantages to the resulting copolymers from the efficiency standpoint.[11,12,13,14,15] The problem with these copolymers that they are produced by a complex and poorly controlled conjugation chemistry. Traces of unwanted side-reaction product or unreacted monomer can prove dangerous when considered the fact that these copolymers will be used in-vivo for gene therapy.

This work focuses hence on the simple synthesis of the copolymers of PEO and poly(propylene oxide) (PPO) such as PEO-PPO-PEO (tradename Pluronic) with polycationic for gene therapy. Also, trying to understand how PPO groups in these copolymers play a role in transfection by comparing it with similar copolymers with just PEO. Different Pluronic are considered and tried to understand how they are affecting the transfection efficiency. The transfection capability for plasmid DNA using synthesized copolymers as vectors will be compared with a routinely used Lipofectamine (cationic lipid marketed by Invitrogen).

6.2 Background

6.2.1 Overview of Gene Therapy

Gene therapy is an experimental technique that uses genes to treat or prevent disease. In the future, this technique may allow doctors to treat a disorder by inserting a gene into a patient's cells instead of using drugs or surgery. Researchers are testing several approaches to gene therapy, including:

- Replacing a mutated gene that causes disease with a healthy copy of the gene.
- Inactivating, or "knocking out," a mutated gene that is functioning improperly.
- Introducing a new gene into the body to help fight a disease.

Each of us carries about half a dozen defective genes. We remain blissfully unaware of this fact unless we, or one of our close relatives, are amongst the many millions who suffer from a genetic disease. About one in ten people has, or will develop at some later stage, an inherited genetic disorder, and approximately 2,800 specific conditions are

known to be caused by defects (mutations) in just one of the patient's genes. Some single gene disorders are quite common - cystic fibrosis is found in one out of every 2,500 babies born in the Western World - and in total, diseases that can be traced to single gene defects account for about 5% of all admissions to children's hospitals.[16] Much attention has been focused on the so-called genetic metabolic diseases in which a defective gene causes an enzyme to be either absent or ineffective in catalyzing a particular metabolic reaction effectively. A potential approach to the treatment of genetic disorders is gene therapy. Using gene therapy, the absent or faulty gene is replaced by a working gene, so that the body can make the correct enzyme or protein and consequently eliminate the root cause of the disease. The most likely candidates for future gene therapy trials will be rare diseases such as Lesch-Nyhan syndrome, a distressing disease in which the patients are unable to manufacture a particular enzyme. This leads to a bizarre impulse for self-mutilation, including very severe biting of the lips and fingers. The normal version of the defective gene in this disease has now been cloned.

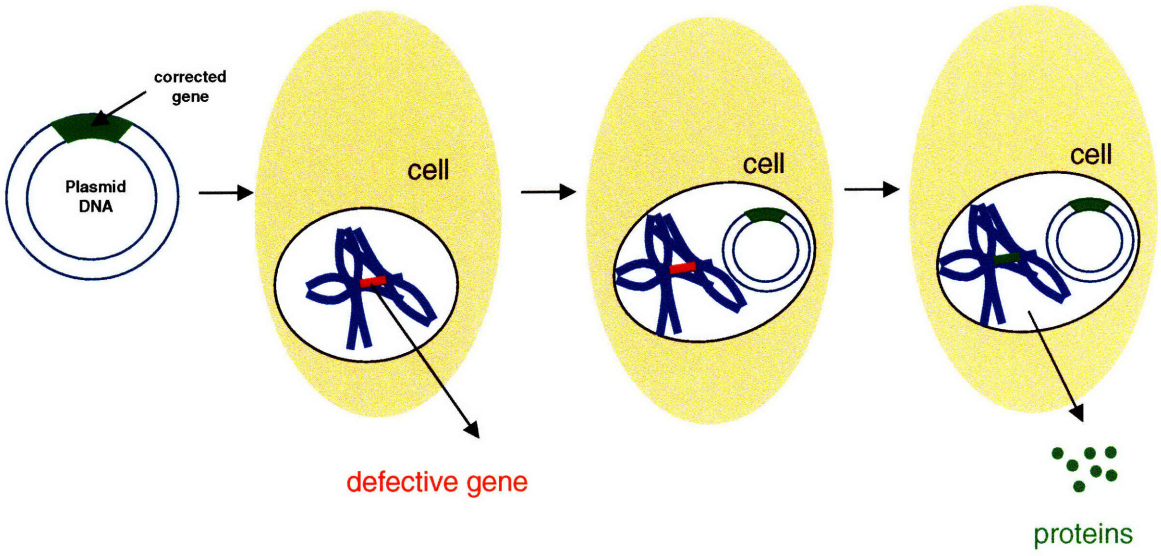

Figure 6-1: Schematic of Gene therapy using plasmid DNA for producing therapeutic proteins

If gene therapy does become practicable, the biggest impact would be on the treatment of diseases where the normal gene needs to be introduced into only one organ. One such disease is phenylketonuria (PKU). PKU affects about one in 12,000 white children, and if

not treated early can result in severe mental retardation. The disease is caused by a defect in a gene producing a liver enzyme.

Before treatment for a genetic disease can begin, an accurate diagnosis of the genetic defect needs to be made. It is here that biotechnology is also likely to have a great impact in the near future. Genetic engineering research has produced a powerful tool for pinpointing specific diseases rapidly and accurately. Short pieces of DNA called DNA probes can be designed to stick very specifically to certain other pieces of DNA. The technique relies upon the fact that complementary pieces of DNA stick together. DNA probes are more specific and have the potential to be more sensitive than conventional diagnostic methods, and it should be possible in the near future to distinguish between defective genes and their normal counterparts, an important development.

6.2.2 Vectors for Gene therapy

A gene that is inserted directly into a cell usually does not function. Instead, a carrier called a vector is genetically engineered to deliver the gene. Certain viruses are often used as vectors because they can deliver the new gene by infecting the cell. The viruses are modified so they can't cause disease when used in people. Some types of virus, such as retroviruses, integrate their genetic material (including the new gene) into a chromosome in the human cell. Other viruses, such as adenoviruses, introduce their DNA into the nucleus of the cell, but the DNA is not integrated into a chromosome. The vector can be injected or given intravenously (by IV) directly into a specific tissue in the body, where it is taken up by individual cells. Alternately, a sample of the patient's cells can be removed and exposed to the vector in a laboratory setting. The cells containing the vector are then returned to the patient. If the treatment is successful, the new gene delivered by the vector will make a functioning protein. The problem with the use of viruses as vector is that they are toxic and can cause the disruption of immune response of the body. Also, it is extremely technically challenging and time-consuming to genetically alter the virus to carry normal human DNA.

Viral vectors show excellent transfection efficiencies. However, they develop a high immunogenicity after repeated administration since the mammalian immune system

has developed strategies to eliminate viral invaders as well. Other problems associated with viral vectors are their potential oncogenicity due to insertional mutagenesis and the limited size of DNA that can be carried. Furthermore the inclusion of a targeting moiety in order to transfect specific cell types or tissues is problematic. Despite these problems, still more than two-thirds of clinical gene therapy trials use viral vectors. Because of these concerns non-viral vectors are emerging as a viable alternative. The focus has hence shifted to synthesize lipids and polymers as vectors. This first led to development of using cationic lipids for gene transfection. It does have advantage of preventing the degradation of naked DNA alongwith the ease of manufacture and control of vector size. But the surface positive charge on cationic lipids leads to their inactivation in blood, non-specific interactions with various negatively charged components of serum. Another shortcoming of lipids as vectors is that if administered intravenous (which is the most common form) being oil based formulations they are shown to have side-effects to patients. Duncan et al.[17] and Ernst et al.[18] warn that pulmonary surfactants may inhibit cationic liposome-mediated gene delivery to respiratory epithelial cells.

Non-viral systems, especially polymers, show significantly lower safety risks and can be tailored to specific therapeutic needs. They are capable of carrying large DNA molecules and can be produced in large quantities easily and inexpensively. Polymers display striking advantages as vectors for gene delivery. They can be specifically tailored for the proposed application by choosing appropriate molecular weights, coupling of cell or tissue specific targeting moieties and/or performing other modifications that confer upon them specific physiological or physicochemical properties. After identifying a suitable polymer structure a scale-up to the production of large quantities is rather easy as well. A weakness of gene therapy with cationic polymers is our limited knowledge regarding the formation of electrostatic complexes with DNA and their biological effects. Many other factors play crucial roles in this context, for example concentration of the polymer and DNA solutions, ionic strength of the solvents[19] and speed of mixing. Thus, gene therapy with cationic polymers is still rudimentarily understood and ongoing investigations will provide avenues to more sophisticated approaches. Figure 6-2 gives an overview of frequently used cationic polymers for non-viral nucleic acid delivery. The review by Smedt et. al.[20] gathers information on existing cationic polymer polyplexes

system for gene transfection. The major disadvantage of these non-viral vectors is their low transfection efficiency. Great efforts have been undertaken to improve the efficiency, however we are still far away from a system that could be considered as satisfactory.

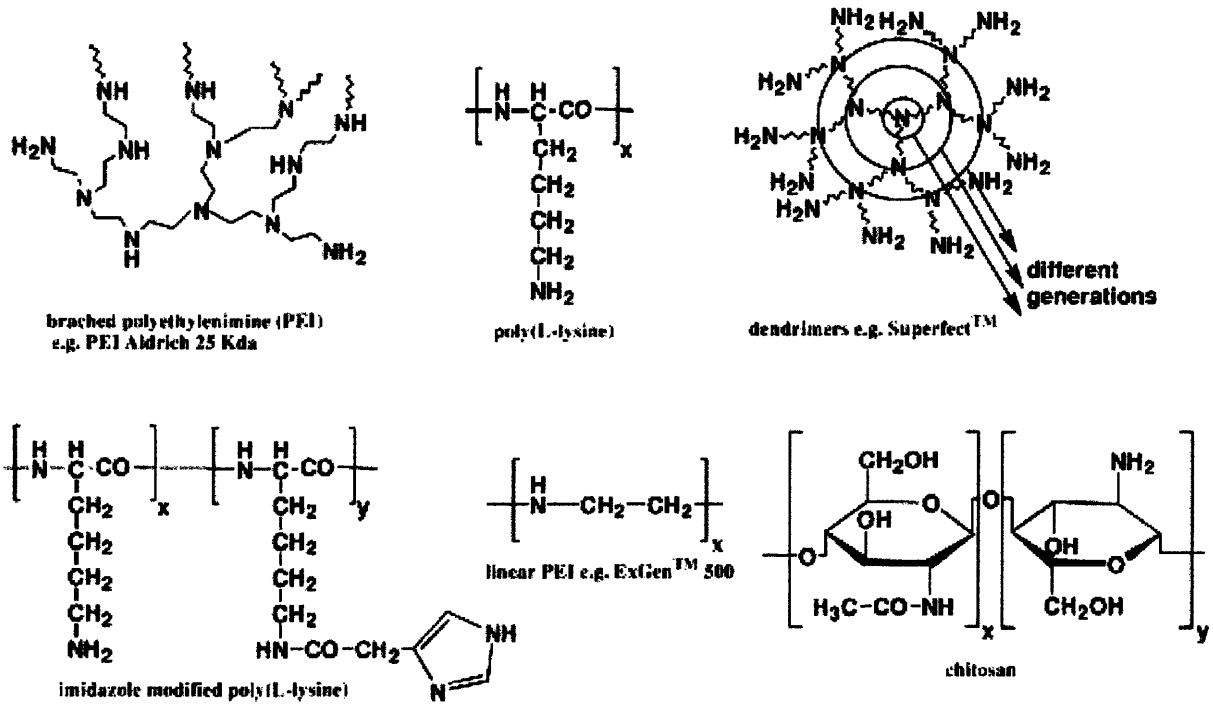

Figure 6-2: Cationic polymers most frequently used for nucleic acid delivery.[21]

The Pluronic-polycation copolymers and oligonucleotides spontaneously associate into polyion complex micelles with a hydrophobic core formed by neutralized polyions and a hydrophilic shell formed by PEO. Such complexes are sufficiently stable in solution despite complete neutralization of charge and exhibit elevated levels of transgene expression.[11] Thus far, the synthetic route toward the polycation-Pluronic copolymers involved chemical activation of the hydroxyl termini of Pluronic followed by conjugation with the primary amino groups of the polycation and separation of the conjugated copolymer from the parent Pluronic.[6] Such a synthetic route involves several steps, each followed by purification of products, and results in fairly polydisperse copolymers and hence maybe shown to have low transfection efficiency. In the present work, we aimed at development of a more straightforward synthetic route that would enable one-step synthesis of a wide range of polyether-polycation copolymers, wherein

the polycation may be optionally devoid of the primary amino groups. The synthesis we opted to use involved the generation of polyether radicals that act as an initiator for the free radical polymerization of a cationic monomer, 2-(dimethylamino)ethyl methacrylate (DMAEMA). The DMAEMA possesses tertiary amino groups, and its polymers are known for their capacity to complex and transfect DNA.[22] An analogous "oxyanionic polymerization" involving the use of potassium alcoholates such as monohydroxy-capped poly(alkylene oxide)s in the role of macroinitiators for the polymerization of DMAEMA resulting in PEO-pDMAEMA copolymers has been reported.[17] Such a polymerization proceeds in rigorously dry THF, which is oftentimes an experimental hurdle. Instead, in the synthetic route explored herein we used free radical polymerization of DMAEMA initiated by the Pluronic radicals generated by the redox reaction of the Pluronic with cerium(IV) in water. The major thrust of the present work has been the development of a facile, one-step synthetic route resulting in desired block copolymers of well-defined molecular weight. This synthetic route is applicable to a variety of vinyl monomers as well as hydroxyl-terminated polyethers. Herein, a relatively hydrophobic Pluronic L92 (PPO content of 80%) was chosen as a representative example of the Pluronic family of the surface-active copolymers because of its high modification activity toward cell membranes. The resulting L92-pDMAEMA copolymers were demonstrated to possess a good transfection capability for plasmid DNA when compared with a routinely used Lipofectamine and were much more active compared to their PEO-pDMAEMA counterparts.

6.3 Experimental

6.3.1 Materials

Pluronic L92 (average composition, $EO_8PO_{52}EO_8$) and P123 (average composition, $EO_{19}PO_{69}EO_{19}$) were received from BASF Corp. (Mount Olive, NJ) and used without further treatment. 2-(Dimethylamino)ethyl methacrylate (DMAEMA, 98%), ammonium cerium(IV) nitrate (98.5%), 2,2'-azobisisobutyronitrile (AIBN, 98%), nitric acid (70%), poly(ethylene glycol) (average M_n = 3350) were all obtained from Sigma-Aldrich Co. (St. Louis, MO) and were used without further purification. Plasmid DNA

encoding β-galactosidase (pCMV-β) was obtained from Clontech BD Biosciences (Palo Alto, CA), whereas Lipofectamine 2000 reagent was purchased from Invitrogen (Carlsbad, CA). Deuterated solvents were obtained from Cambridge Isotope Laboratories (Andover, MA), and all other chemicals were received from commercial sources and were of the highest purity available.

6.3.2 Polymer Synthesis

The polymerization with the cerium ion redox system and DMAEMA monomer was carried out in a three-neck flask equipped with a stirrer, a reflux condenser, and a nitrogen inlet/outlet. In a typical polymerization procedure, DMAEMA (5.0 g), Pluronic L92, or poly(ethylene glycol) (5.0 g) and 1 mL of 70% nitric acid were dissolved in 70 mL of deionized water, and the solution was deoxygenated by nitrogen flow and thermostated at 55 °C with stirring for 1 h. The reaction was started by injecting 3.278 g (6 mmol) of cerium(IV) ammonium nitrate dissolved in 3 mL of 0.5 M HNO_3. The reaction was allowed to proceed for 4 h under nitrogen flow and stirring. The resulting polymer was repeatedly precipitated by the addition of 1 M NaOH, redissolved in 0.01 M HCl, and dialyzed against a large excess of 0.01 M HCl solution in deionized water using dialysis tubing (Spectrum Laboratories, Inc., molecular weight cutoff, 3500). The overall yields of the polyether copolymer were 91 and 94% in the cases of L92-pDMAEMA and PEO-pDMAEMA, respectively. To prove the suggested mechanism of polymerization via formation of polyether radicals due to the presence of cerium(IV), a control experiment without Ce^{4+} was conducted. Namely, polymerization in a mixture of DMAEMA and Pluronic L92 identical to the described above was induced by the addition of 1 mmol of AIBN in acetone. A viscous solution was obtained after the polymerization conducted at 55 °C for 8 h. The solution was precipitated using 1 M NaOH, and the precipitate and the supernatant were separated. The precipitated polymer was dissolved in 0.1 M HCl, and the procedure of precipitation was repeated twice. The resulting polymer was analyzed by ^1H NMR, which found no presence of the polyether. This proved that to obtain the L92-pDMAEMA copolymer the Pluronic radicals must be generated. It was also observed that on the addition of Ce^{4+} solution to DMAEMA in the

same range of concentrations used in the above polymerization, no polymer was formed within 8 h at 55 °C, indicating the absence of homopolymerization.

6.3.3 Copolymer Characterization

The polymerization of DMAEMA was carried out using a redox system consisting of Ce^{4+} ions and Pluronic or PEO. The cerium ion-alcohol redox reaction leads to the formation of a radical on the carbon atom linked with the hydroxyl group.[23] It has been shown that in the case of a polymeric alcohol, PEG, as a reducing agent the formation of the radicals takes place at the terminal carbon atom and not along the polyether chain.[24] Drawing an analogy between PEO and PEO-PPO-PEO copolymers, we depicted the polymerization as shown in Scheme 6-1. In the first step, a redox reaction occurs between Ce^{4+} and the $-CH_2OH$ terminal group of the PEO segment, generating a free radical in a position of the hydroxide. The radical thus formed is transferred from the polymer chain to the DMAEMA monomer, and the polymerization propagates. Formation of diradicals is possible, but their relative content is minor, according to the literature data. [25,26,27,28]

The presence of diradicals, if any, can lead to the formation of copolymers of higher molecular weight. In the study, we were able to validate the polymerization mechanism by size-exclusion chromatography and NMR. Molecular weight (MW) determination was accomplished using size exclusion chromatography. Polymer samples were precipitated in 1 M NaOH, dried, and redissolved in dimethylformamide (DMF) at 1 mg/mL. The MW of the copolymers was measured in DMF using a Hewlett-Packard series 1100 HPLC system with a refractive index detector and two PLgel Mixed E columns (Polymer Laboratories, Inc., Amherst, MA). Run parameters were as follows: injection volume, 100 μL; flow rate, 1 mL/min; temperature, 40 °C. Calibration curves were developed using a PEG calibration kit (Polymer Laboratories, Inc.).

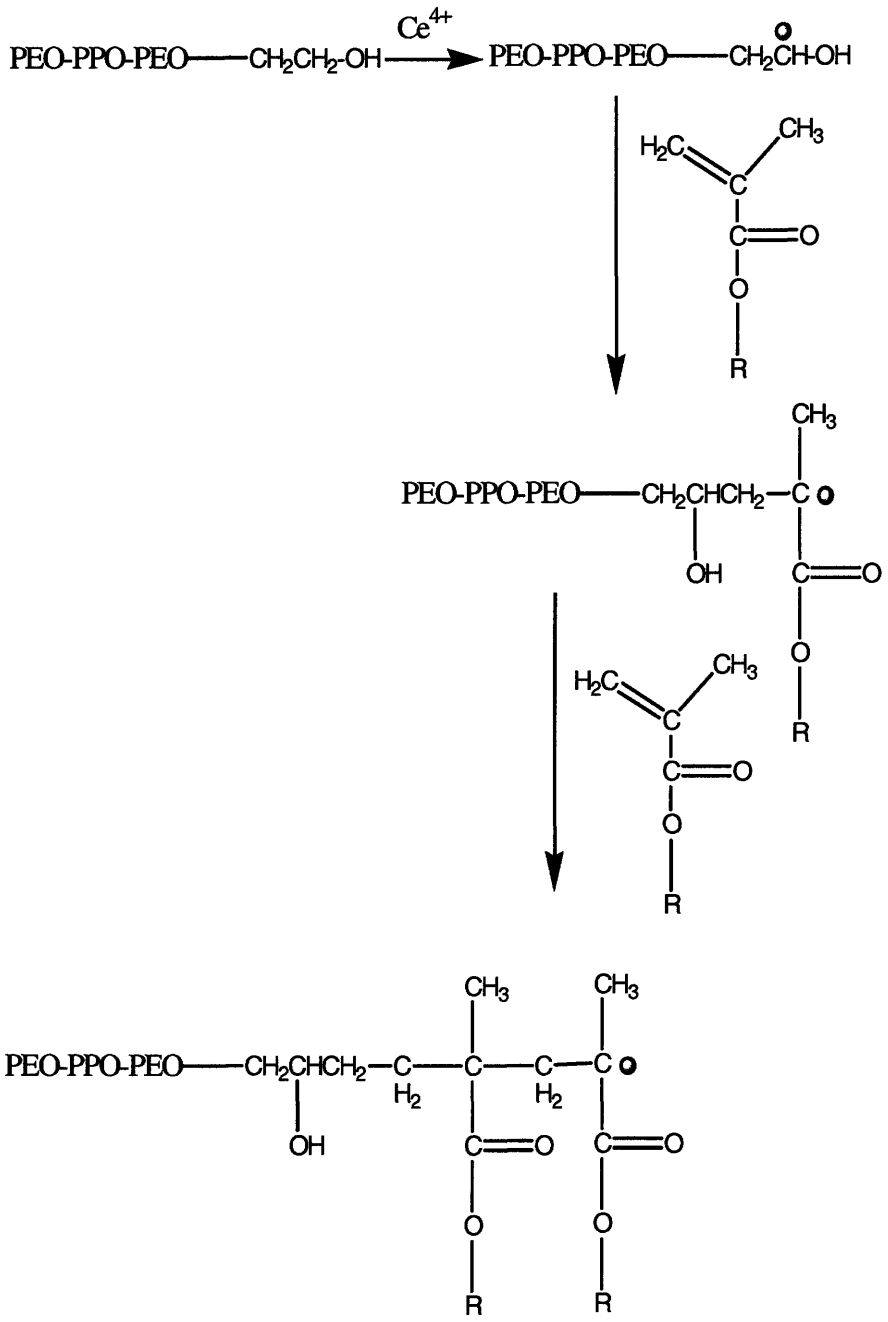

Scheme 6-1: Initiation and propagation steps in the free-radical polymerization leading to pDMAEMA-Pluronic block-copolymers.

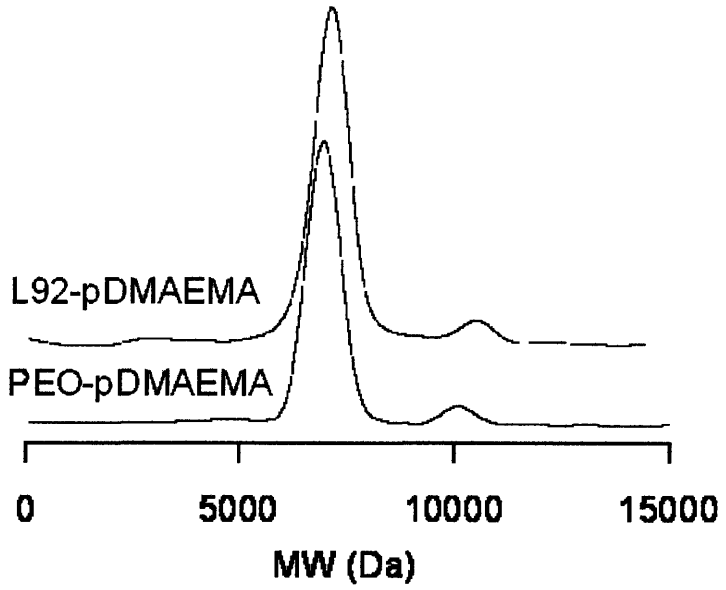

Figure 6-3: Typical size-exclusion chromatographs of L92-pDMAEMA and PEO-pDMAEMA copolymers in DMF solvent.

Figure 6-3 depicts typical SEC chromatograms of L92-pDMAEMA and PEO-pDMAEMA copolymer samples, calibrated in molecular weights. Peaks centered at 7100 (94.7% total area) and 10500 (5.3%) Da as well as 6950 (94.7%) and 10100 (5.2%) Da were observed in the case of the L92-pDMAEMA and PEO-pDMAEMA copolymers, respectively. The polydispersity index calculated by the instrument's software using an absolute MW calibration curve was in the range 1.22-1.25, in accord with the previously observed formation of relatively monodisperse copolymers resulting from polyoxyethylene-radical-induced polymerization of DMAEMA.[25,29,30] Based on the average MW of the Pluronic L92 and PEO being 3720 and 3350 Da, respectively, about 95% of either copolymer is a product of polyether-monoradical formation, resulting in "diblock" Pluronic-pDMAEMA or PEG-pDMAEMA structure. About 5% of the resulting polymers of either species are the result of the polyether-diradical formation, resulting in the bonding of two polyether segments to the forming pDMAEMA chain, with corresponding peaks observed in the 10 kDa area in the SEC chromatograms (Figure 6-3). The length of the pDMAEMA block is 22 and 23 units in L92-pDMAEMA and PEO-pDMAEMA, respectively, in the main fractions of these copolymers. These

calculations are supported by the nitrogen content measurements: N found, 4.15% (calctd, 4.26%) for the L92-pDMAEMA and N found, 4.75% (calctd, 4.61%) for the PEO-pDMAEMA copolymer, respectively

Proton NMR spectra of polymer solutions in D_2O/DCl were acquired on a Bruker AMX400 spectrometer. Using ^1H NMR spectroscopy, we were able to verify the structure of the pDMAEMA-L92 copolymers resulting from polymerization (Scheme 6-2).

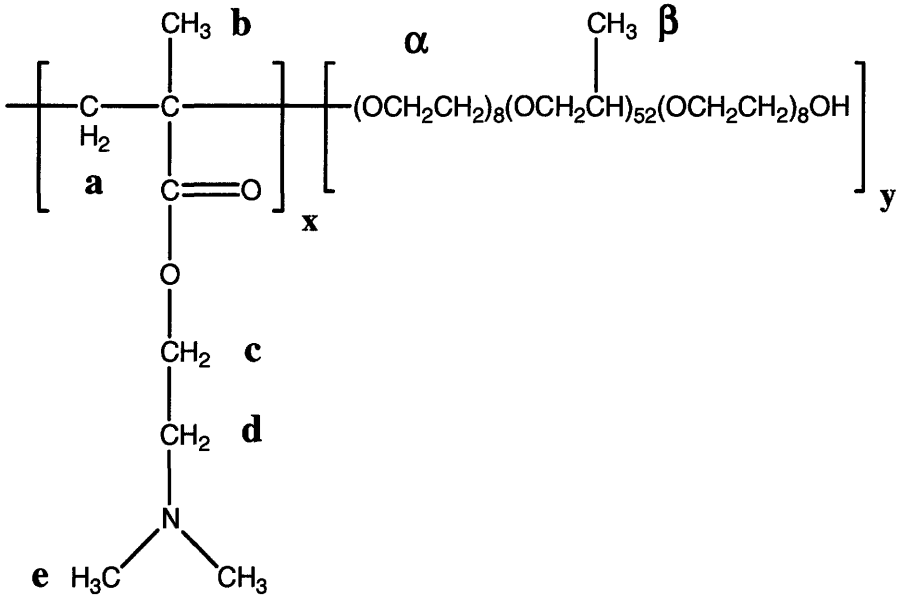

Scheme 6-2: Structure of the pDMAEMA-L92 copolymer. Labeling of the distinctive free protons in the structure are shown

As is seen in Table 6-1, the proton ratios measured by NMR corresponded to the proposed structure quite well. The average number of DMAEMA units bonded to the one L92 segment was calculated from the ratio of the backbone methylene protons in these units, respectively. At y=1 (one Pluronic segment), we obtained the expression x/84=0.9/3.3, and thus x=23, i.e., one Pluronic segment is bound to 23 DMAEMA units on average. This is in excellent agreement with the x=22 found from SEC. Importantly, no protons belonging to the methylene or methyl groups of the polyether were observed in the NMR spectrum of the sample synthesized in the absence of Ce^{4+} followed by the Pluronic removal by dialysis (see spectrum C in Figure 6-4). These observations further

confirm the mechanism of the copolymer formation via cerium (IV)-induced initiation (Scheme 6-1).

Table 6-1: Structure/ composition of copolymers obtained from ^{1}H NMR.

Structural Element	Protons[a]	Calculated	Found from NMR
DMAEMA	a:b:c:d:e	1.0:1.5:1.0: 1.0:3.0	1.0:1.1:1.1:1.0:3.2
L92	α:β	1.08:1.00	1.06:1.00
DMAEMA/ L92, mol/mol	a:α	x:84y	0.9:3.3 x=22.9 y=1

[a] For proton designations, see Scheme 2.

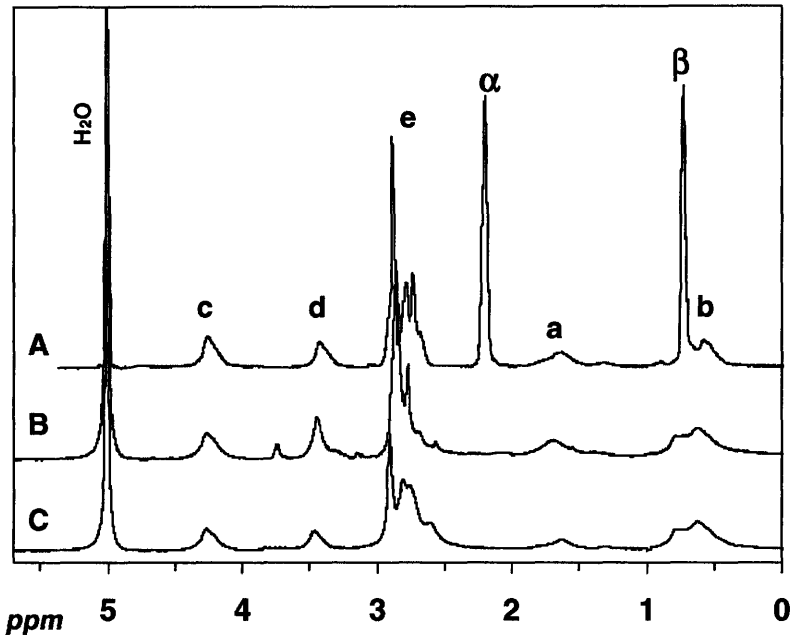

Figure 6-4: ^{1}H NMR (400 MHz) spectra of pDMAEMA-L92 (A), pDMAEMA (B), and pDMAEMA/L92 blend after dialysis (C) in D_2O/5 mM DCl. Protons are labeled as shown in Scheme 1.

6.3.4 Self-Assembling Properties of the Copolymers

Having confirmed the structure of the copolymers resulting from the cerium-initiated copolymerization of polyethers with DMAEMA, we embarked on the study of their properties that are of importance for complexation with DNA and transfection. To assess the polyelectrolyte properties of the novel copolymers, potentiometric titration of their aqueous solutions was conducted. For obtaining the apparent pK_a of the polymers, a titration was performed at 25 °C using a 736 GP Titrino potentiometric titration system (Metrohm Ltd., Herisau, Switzerland). Titration of the copolymers in their acidic form was carried out in a degassed 75 mM NaCl solution with 0.1 M NaOH as a titrant, at 0.5 wt % polymer concentration. The titration was carried out slowly for several hours to allow for proper equilibration. The apparent dissociation constant (pK_a) and the degree of ionization (α) were calculated from experimental potentiometric titration data using the Henderson-Hasselbach expression.[31] The titration curves yielded the apparent pK_a and ionization degree (α) of the titratable (tertiary amino) groups. The intrinsic dissociation constant (K_o) was found by extrapolating pK_a to α= 0 in the pK_a versus αcurves.[32] The pK_o values of the L92-pDMAEMA and PEO-DMAEDMA were found to be 7.1 and 7.4, respectively. A shift to lower pK_o in the case of the L92-pDMAEMA can be explained by the effect of Pluronic lowering the dielectric constant of the microenvironment of the amino groups. In contrast, the pK_o of the PEO-pDMAEMA copolymer roughly corresponded to the pK_a = 7.4-7.8 reported for the pDMAEMA polymer,[33] indicating that PEO block alone has a lesser effect on the ionization of the pDMAEMA than PEO-PPO-PEO when bonded with the polycation. The DMAEMA monomer possesses a notably higher pK_a of 8.0-8.4 than its homo- and copolymers because of the neighboring effect;[34] that is, the presence of some protonated side chains reduces the ability of the remaining dimethylamino groups to become protonated.

Surface tension measurements of the copolymer solutions at certain pH values were accomplished using a Kruss USA model K11 tensiometer applying the Wilhelmy plate method. In the surface tension measurements, the L92-pDMAEMA copolymers were additionally purified by repeated precipitation in 1 M NaOH followed by the

removal and drying of the polymer and redissolution in deionized water. No traces of unattached Pluronic copolymers in these species were detected by HPLC.

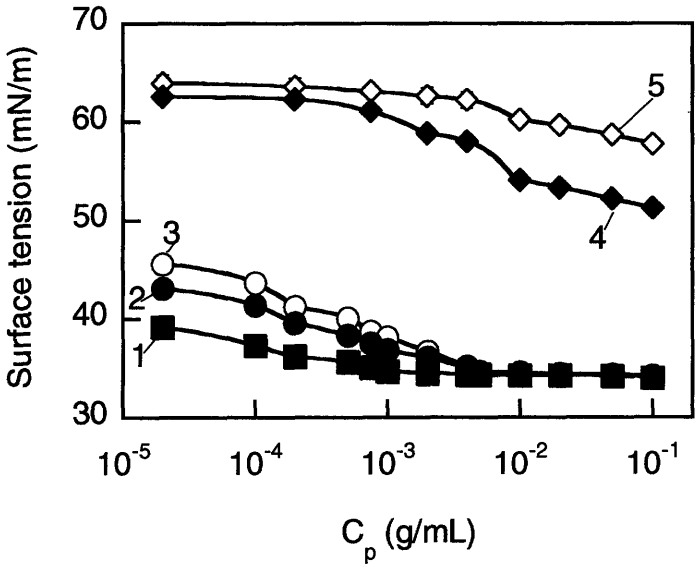

Figure 6-5: Equilibrium surface tension of the Pluronic L92 (1), L92-pDMAEMA (2,3), and PEO-pDMAEMA (4,5) copolymers as a function of the copolymer concentration (C_p) at 25°C. The dependencies 1,3, and 5 were obtained at pH 5.0 and dependencies 2 and 4 were measured at pH 7.0

The presence of the hydrophobic PPO segments in the structure of the polyether segments of the copolymers leads to profound differences in the surface activity of the L92-pDMAEMA and PEO-pDMAEMA copolymers in aqueous solutions (Figure 6-5). The surface activity of the L92-pDMAEMA copolymers was comparable to that of the parent L92 surfactant, with the critical micellization concentrations (cmc) of 5×10^{-3} and 2×10^{-3} g/mL measured for the L92-pDMAEMA and L92 copolymers, respectively. The obtained cmc of the Pluronic L92 corresponded well with the literature data, previously reported for 37 and 15 ° C.[35,36,37] Higher ionization of the copolymer at pH 5.0 resulted in lower surface activity than at pH 7.0 throughout the concentration range. The PEO-pDMAEMA copolymers possessed dramatically lower surface activity than their L92-pDMAEMA counterparts at both pH values studied. At pH 5.0, where the copolymer is highly ionized, a very minimal surface activity was observed. At pH 7.0, which is closer to pK_a of the copolymer, the pDMAEMA segment becomes more hydrophobic and, thus, more of the copolymer adheres to the air-water interface, lowering the measured surface

tension. Similar effects of pH on surface activity have been observed with block copolymers of DMAEMA and methyl methacrylate.[38] The apparent cmc of the PEO-pDMAEMA was ~0.01 g/mL at pH 7.0 and could not be measured at pH 5.0. We hypothesized that the observed differences in the surface activity of the PEO- and Pluronic-based polycations could have an effect on the ability of the copolymers to serve as nonviral transfection agents, because surfactants such as Pluronics can fuse with the cell membranes, thus decreasing their microviscosity, which leads to an enhancement of the transmembrane transport that is likely involved in the transfection mechanism.[39] As shown in the forthcoming parts of the work, we indeed observed enhanced transfection with the L92-pDMAEMA copolymers.

6.4 Complexes of polycationic copolymer with plasmid DNA

Complexation of the polycationic copolymers with plasmid DNA was studied by assessing the average hydrodynamic diameter as well as ζ-potential of the particles of the formed complexes (Figure 6-6). The ratio of the copolymer to DNA in the complex (N/P) was expressed via the ratio of equivalents of DMAEMA units to the number of nucleotides in DNA. The nucleotide average molecular mass was assumed to be 324 g/mol.[40] Within the range of concentrations studied, no precipitation was observed at any N/P ratio. A significant increase in the average particle size was observed upon neutralization of the complexes when a 1:1 stoichiometry was reached, and then the particle size gradually decreased and leveled off as particles became positively charged. The complexes of the L92-pDMAEMA with pCMV-βgal plasmid DNA had larger hydrodynamic diameters than any other complexes throughout the N/P range studied (Figure 6-6), with the solution at N/P = 1.0 being faintly opaque.

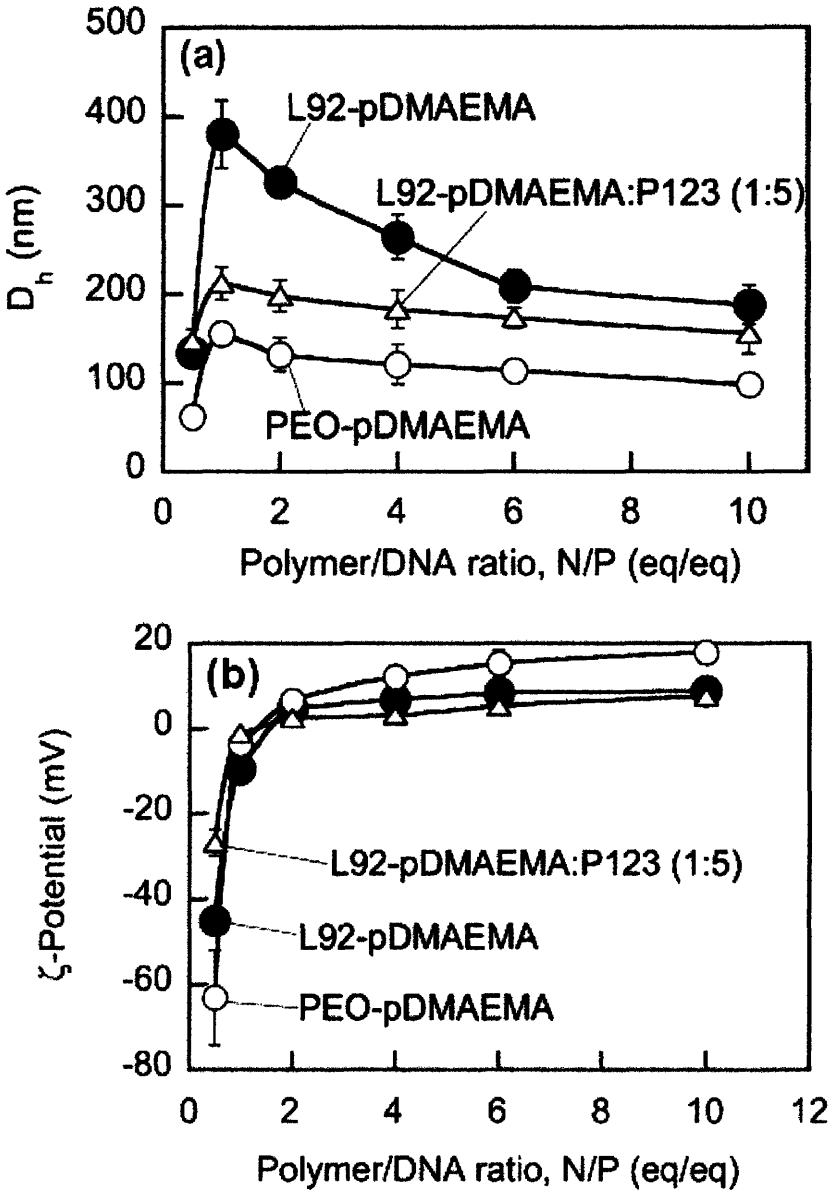

Figure 6-6: Hydrodynamic diameter (D_h) (a) and ζ-potentials (b) of the complexes formed between pCMV-βgal plasmid DNA and polycationic copolymers L92-pDMAEMA and PEO-pDMAEMA as well as a mixture of L92-pDMAEMA and Pluronic P123 (1:5 wt/wt) as a function of the polymer/DNA (N/P) ratio. The N/P ratio is expressed via the ratio of the equivalents of DMAEMA units in the copolymer to the nucleotide units in the DNA. Measurements were conducted in triplicate at 25 °C in 10 mM HEPES solution at pH 7.0.

Intermolecular associations of the hydrophobic segments of the complexes were evidently more prevalent with the L92-pDMAEMA copolymer. Notably, the addition of the relatively hydrophilic Pluronic P123, which forms mixed micelles with L92, reduced

the size of the aggregates and their electrokinetic mobility (Figure 6-6). The excess of Pluronic P123 masked the charges of the particles as compared to the L92-pDMAEMA/DNA complexes without Pluronic addition. No opacity in the solutions with P123 was observed, even at the stoichiometric N/P = 1.0. Such a stabilizing effect of the presence of the Pluronic P123 on the stabilization of the polycation/DNA complex has been previously reported with other polycationic systems.[41,42] Within the range of concentrations studied, the apparent viscosity of the solutions was between 1 to 8 mPa·s, which is small enough to ensure a good syringeability if they were parenterally administered.[43]

6.4.1 Preparation and Characterization of Copolymer/Plasmid DNA Complexes

The DNA/copolymer complexes were prepared by adding 3.1 μL of 3.2 mg/mL pCMV-βgal plasmid DNA solution in water to 997 μL of an appropriate copolymer solution in 10 mM *N*-2-hydroxyethylpiperazine-*N'*-2-ethanesulfonic acid (HEPES) buffer (pH 7.0) followed by vortexing and equilibration of a sample overnight. Series of samples containing L92-pDMAEMA and PEO-pDMAEMA copolymers, as well as L92-pDMAEMA+Pluronic P123 (1:5 weight ratio), were thus prepared. The resulting DNA/copolymer solution was filtered using a 0.2 μm membrane filter (Pall Gelman Labs).

Measurements of the potential at the surface of shear (ζ-potential) and dynamic light scattering experiments of the copolymer as well as DNA/copolymer complex solutions were performed at 25 ± 0.1 °C using a ZetaPals zeta potential analyzer and a BI-200SM goniometer, a BI-9000 correlator, and a Spectra Physics He-Ne model 127 laser operating at a scattering angle of 90 ° and a wavelength of incident light of 633 nm at a power of 50 mW. All of the above instruments were from Brookhaven Instruments Co. Measurements were performed at least in triplicate, and intensity-average hydrodynamic diameter (D_h) and Smoluchowski ζ-potential values calculated by the built-in software are reported herein.

6.4.2 Characterization of copolymer/DNA interactions

The presence of DNA did not modify the surface tension profiles of Pluronic L92 or PEO-pDMAEMA solutions (the values were around 60 mN/m in the whole range), but slightly decreased the surface tension values of L92-pDMAEMA solutions. Vinogradov et al.[44] found that PEI-PEG and its complex with DNA behaves as a surfactant with a low CMC, and related this fact to the greater stability of DNA against nuclease degradation in the presence of PEI-PEG. The fact that the self-assembly of L92-pDMAEMA is promoted in the presence of DNA makes these systems particularly attractive as non-viral vectors.

Calorimetric experiments were performed using a Tronac-450 isoperibol microcalorimeter and Tronac FS101 calorimetry software (Tronac Inc., Orem, Utah). In each experiment, a 47.5 μL DNA solution with a concentration of 0.03% (w/w) was placed in a Dewar reaction vessel, and a relatively concentrated copolymer solution (4%) was loaded into a 2 mL calibrated buret. The entire assembly was then immersed into a constant temperature water bath (298.0 K). After thermal equilibration, the copolymer solution was delivered at a constant rate of 0.3332 mL/min into the reaction vessel, in which a stirrer mixed the two solutions rapidly. The rise or decrease in the temperature of the system was monitored using a thermistor, and later reproduced using a heating coil in the reaction vessel. The apparent enthalpy was calculated from the applied current and voltage and the heating time. As a blank, a buffer solution was used instead of DNA dispersion. Calibration of the system was assured by titration of tris(hydroxymethyl)aminomethane with HCl.

The integral binding heat for the polymer/DNA interaction (Q_{int}) process was estimated by subtracting from the measured heat produced by addition of the copolymer to the DNA dispersion (Q_p), the heat effects due to the dilution/demicellization of the copolymer in the buffer solutions used as a blank (Q_d).[45]

$$Q_{int} = Q_p - Q_d \qquad \text{Eq. 6-1}$$

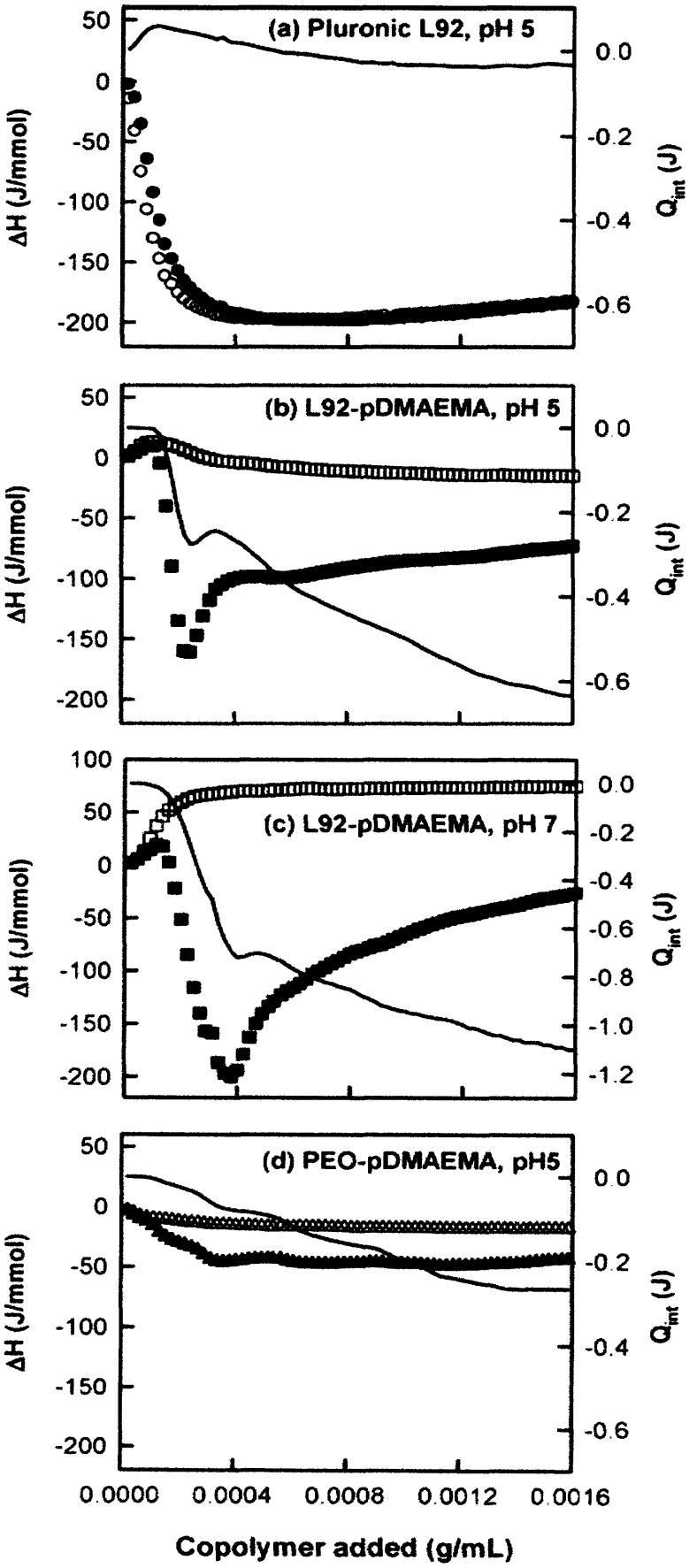
(a) Pluronic L92, pH 5
(b) L92-pDMAEMA, pH 5
(c) L92-pDMAEMA, pH 7
(d) PEO-pDMAEMA, pH5
ΔH (J/mmol)
Q_{int} (J)
Copolymer added (g/mL)

Figure 6-7: Calorimetric titration curves observed during the addition of 4% copolymer solutions into a dewar containing just phosphate buffer (open symbols) or a 0.03% DNA solution in phosphate buffer (close symbols). Polymer/DNA interaction heat, Qint, was estimated as the difference between the heat evolved in the presence and absence of DNA (continuous lines). (a) Pluronic L92, pH 5; (b) L92-pDMAEMA, pH 5; (c) L92-pDMAEMA, pH 7; (d) PEO-pDMAEMA, pH 5.

The enthalpy of DNA dilution (final concentration 3% lower) was negligible. Similar experiments were carried out with L92-pDMAEMA/Pluronic P123 1:1 and 1:5 w/w mixtures (in the buret), keeping the concentration of L92-pDMAEMA constant at 4%. Figure 6-7 shows the apparent enthalpies associated with the dilution and/or demicellization processes of Pluronic L92 (a), L92-pDMAEMA (b,c), and PEO-pDMAEMA (d) in phosphate buffer, and those of the interaction processes with DNA. The concentration of the polymers (0.04 g/mL) in the buret, before being added to the Dewar, was sufficient to be above their CMC, if any. Therefore, when the polymer solution was slowly added to an aqueous medium without DNA, the micelles of Pluronic L92 and L92-pDMAEMA broke up until the concentration in the Dewar reached the CMC.

For the Pluronic L92, the demicellization process was exothermic (negative enthalpy change), while for the L92-pDMAEMA an endothermic process was observed. The exothermic dilution process of Pluronic solutions has been attributed to the hydrogen bond formation between the triblock copolymer and water molecules after breakage of water-water and surfactant-surfactant hydrogen bonds.[32] The apparent enthalpy change observed for the demicellization of Pluronic L92 (ΔH_d= -198 J/mmol) was significantly lower than that obtained for other more hydrophilic Pluronics, such as F127 (ΔH_d= -410 J/mmol).[45] The chemical linking of pDMAEMA to L92 significantly changes the thermodynamic parameters of the demicellization; the process being endothermic but entropically favorable, as for many other typical ionic surfactants.[46] No significant interaction with DNA was observed for Pluronic L92 (Table 6-2), for which the demicellization process was not altered by the presence of DNA. In contrast, the association of L92-pDMAEMA with DNA was extraordinarily intense at both pH 5 and 7 (Figure 6-7 b and c). When the L92-pDMAEMA solution was added to the DNA

solution, an initial endothermic demicellization process was observed. However, this process stopped when L92-pDMAEMA concentration in the Dewar reached $1.1x10^{-4}$ g/mL, and a new exothermic process began. This concentration can be identified as the critical associative concentration (CAC) and corresponds to a N/P ratio of 0.3; being similar for both pHs evaluated.

Table 6-2: Thermodynamic parameters of the interaction of the copolymers with DNA at 298K. Values are within ±5%. (*J/ mmol of L92-pDMAEMA in the mixture)

Copolymer	pH	ΔH_{int} (J/mmol)
Pluronic L92	5	-3.4
	7	+6.4
L92-pDMAEMA	5	-165.4
	7	-205.5
PEO-pDMAEMA	5	-31.1
P123	5	+45.0
P123:L92-pDMAEMA 1:1	5	-40.7 (-131.8*)
P123:L92-pDMAEMA 5:1	5	-35.1 (-237.3*)

The peak in enthalpy was observed when the L92-pDMAEMA concentration reached $2.4x10^{-4}$ g/mL at pH 5 or $3.7x10^{-4}$ g/mL at pH 7, which correspond to N/P ratios of 0.82 and 1.27, respectively. Therefore, the maximum in heat evolved is achieved at cationic: anionic molar ratio close to 1. The effect of pH is related to the lower ionization degree of pDMAEMA groups at pH 7. The process of interaction was exothermic up to $6x10^{-4}$ g/mL of cationic polymer in the Dewar. This finding suggests that the saturation of the binding was reached at a N/P ratio close to 2, i.e. nonstoichiometric polyplexes could be formed. In previous studies with other cationic molecules, formation of polyplexes and lipoplexes with a N/P ratio above 1 was observed. [47,48] In the case of PEO-pDMAEMA, the dilution process in pH 5 phosphate buffer (Figure 6-7d) was exothermic, but did not show the characteristic profile of a demicellization. The interaction with DNA was significantly more exothermic, although the energy evolved in

the process was notably lower than for L92-pDMAEMA. The CAC can be established at ca. $1.13x10^{-4}$ g/mL, while the interaction process was completed when the polymer concentration was $3.63x10^{-4}$ g/mL. Considering that the polymer contains a 4.75% N, these values correspond to N/P ratios of 0.43 and 1.37, respectively. The greater CAC, lower saturation concentration and lower interaction energy observed with POE-pDMAEMA, compared to L92-pDMAEMA, clearly indicate a lower affinity for DNA. The contents of the Dewar after the experiments were cloudy in the case of L92-pDMAEMA titrations.

The enthalpies of interaction (Table 6-2) were calculated considering the average energy involved in the process up to theoretical neutralization of charges. Taking into account that each chain of copolymer contains approximately 23 units of DMAEMA, the enthalpies of interaction (Table 6-2) expressed per mol of cationic unit can be estimated as –7.2 kJ/mol and –8.9 kJ/mol for L92-pDMAEMA at pH 5 and at pH 7, respectively, and –1.3 kJ/mol for PEO-pDMAEMA at pH 5. Therefore, the microenvironment of the cationic DMAEMA units, provided by the nature and structure of polymer to which they are attached, plays an important role in the binding process. Although L92 itself show a low affinity for DNA, both molecules can act as both hydrogen-bond donor and acceptor and, also, can interact hydrophobically.[49,50] Neutral amphiphilic polymers, such as polyvinylpyrrolidone (PVP) or Tetronics (tetrafunctional block copolymers of PEO-PPO bound to ethylenediamine), can form polyplexes with DNA via hydrogen bonding as well as hydrophobic interactions.[50] This kind of association is shown as an endothermic process in which the entropic contribution occurs via release of water and/or counterions from both PVP and DNA upon their mixing.[50] Binding of DNA (both plasmid and total DNA from salmon testes) to cationic lipids was found to be endothermic or exothermic depending on the composition of the lipids and pH of the medium.[51,48] Rungsardthong et al.[17] observed that the interaction of DNA with pDMAEMA was exothermic and that the enthalpy increased from pH 4 to pH 7.4. This effect is attributed to the proton abstraction from the buffer by the nonionized amino groups of the polymer in order to interact with the anionic phosphate groups of DNA (i.e. there is a proton transference from the hydrogen phosphate of the buffer to the amino groups of pDMAEMA). Protonation changes have been also observed for PEI during complex formation with DNA.[52]

Similarly, L92-pDMAEMA showed a greater binding enthalpy at pH 7 than at pH 5. The observed interaction enthalpy at pH 7 is coincident with the value reported by Rungsardthong et al.[53] for pure pDMAEMA at pH 6.6 phosphate buffer (-8.9 kJ/mol). Therefore, it appears that the copolymerization with L92 did not modify the thermodynamic parameters of the copolymer interaction with DNA significantly. Nevertheless, since the data reported for pDMAEMA and that obtained with L92-pDMAEMA were not recorded under exactly the same pH (6.6 *vs.* 7.0), the possibility that L92 can strengthen the association through hydrogen bonding and hydrophobic interactions cannot be disregarded. In contrast, the process was significantly less exothermic for PEO-pDMAEMA. In this sense, Nisha et al.[47] have recently observed that the binding enthalpy of DNA to copolymers made of methoxy(polyethylenglycol) monomethacrylate and (3-(methacryloylamino)propyl) trimethylammonium chloride decreased proportionally to the content in poly(ethyleneglycol) in these copolymers. The enthalpy per cationic unit was measured to be ca. -2.5 kJ/mol for the most hydrophilic copolymer (we obtained an enthalpy even lower for PEO-pDMAEMA, –1.3 kJ/mol). Compared to the L92-pDMAEMA (pK_a 7.1), the PEO-pDMAEMA (pK_a 7.4) is more hydrophilic and has a greater ionization degree at pH 5. Thus, contribution of the ionic component to the interactions of the PEO-pDMAEMA with DNA (exothermic) should be considerably greater than the other weak noncovalent interactions such as hydrogen bonding and hydrophobic (endothermic). However, the extended PEO chains may impede the ionic groups of the two macromolecules from approaching each other, as close as in the case of L92-pDMAEMA.[47]

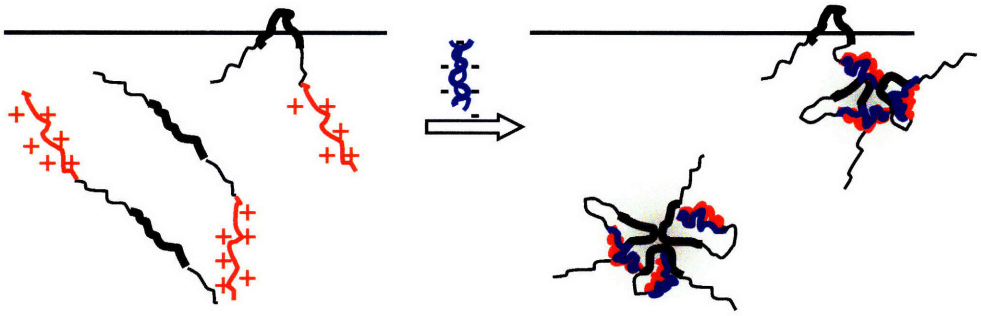

Figure 6-8: Schematic drawing of the association of DNA with L92-pDMAEMA. L92-pDMAEMA keeps its surface activity even after DNA binding. The amphiphilic character prompts the formation of polyplexes with a core (PPO and neutralized complexes) and shell (PEO and non-neutralized pDMAEMA groups) structure.

In Figure 6-8, a schematic drawing of the changes in conformation of L92-pDMAEMA molecules (below CMC) when DNA is added to the solution is shown. The amphiphilic character of L92-pDMAEMA facilitates the formation polyplexes with a core-shell structure in which PPO comprises the cores and neutralized DNA-pDMAEMA complexes and the shells are composed of extended PEO chains and some ionized pDMAEMA groups. In the case of PEO-pDMAEMA, the interaction with DNA is less energetically favorable owing to the more hydrophilic character of the copolymer. Polyplexes with compact, neutralized cores and extended PEO chains forming a shell have been reported.[54]

Since the transfection efficiency of cationic copolymers of Pluronics has been shown to be improved by Pluronic P123,[55,56] the next step was to evaluate how the presence of Pluronic P123 could modify the energetic aspects of the interaction with DNA. Previously, we have shown that the addition of P123 to the L92-pDMAEMA and DNA complexes diminished the size of the complex aggregates and masked the charges.[18] We thus assayed mixtures of P123:L92-pDMAEMA at weight ratios of 1:1 and 5:1. The demicellization processes of Pluronic P123 and its mixtures with L92-pDMAEMA were also characterized. Figure 4 shows the energy recorded in the calorimeter during the addition of concentrated P123 and P123:L92-pDMAEMA solutions to phosphate buffer at pH 5. The demicellization of P123 alone was strongly exothermic (ΔH_d= -150 J/mmol), similarly to the analogous process in L92 solutions. The demicellization of the mixtures P123:L92-pDMAEMA was even more exothermic; being above the energy expected assuming an additive contribution of the demicellization heat of both components (continuous line). This observation suggests formation of mixed micelles of P123 and L92-pDMAEMA.[57]

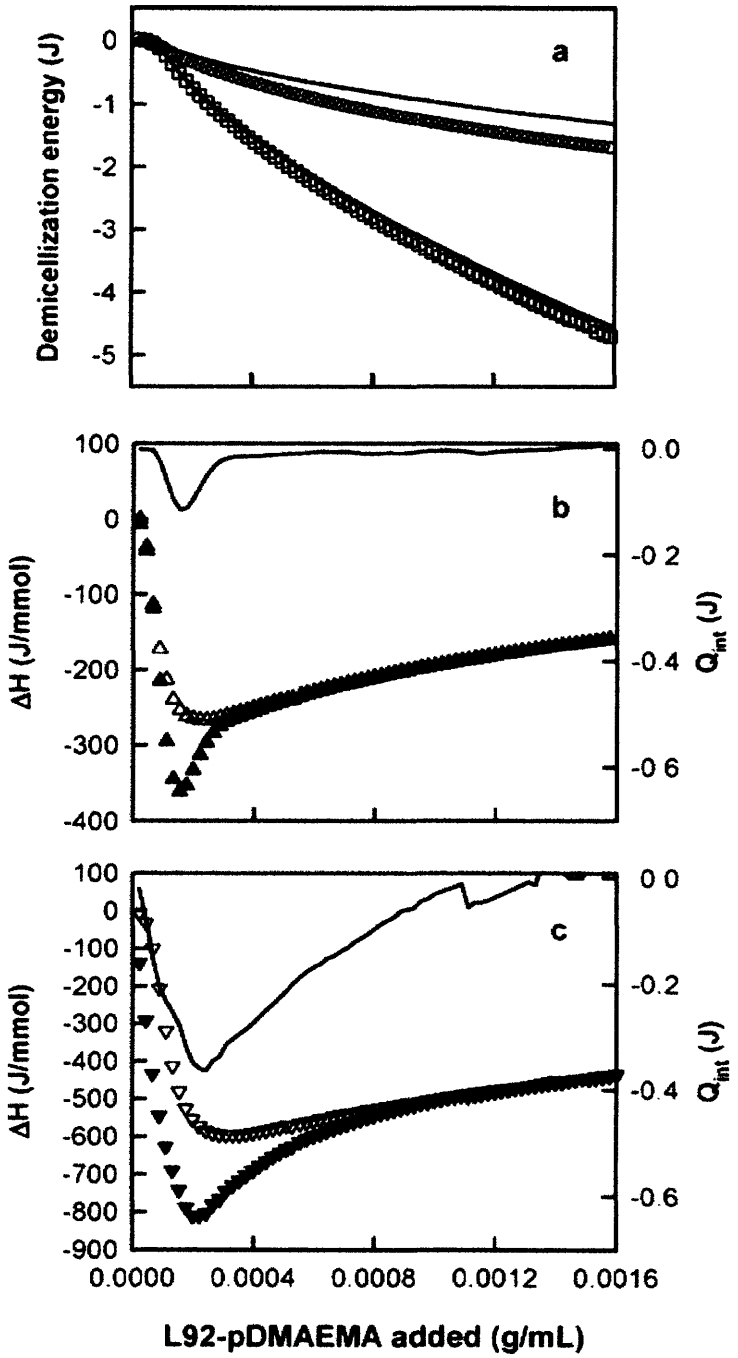

Figure 6-9: (a) Demicellization energy recorded for L92-pDMAEMA (4%) + P123 (4%) solution (open circles) and L92-pDMAEMA (4%) + P123 (20%) solution (open squares) compared to the values theoretically predicted (continuous lines, Table 2). Calorimetric titration curves observed during the addition of (b) a L92-pDMAEMA (4%) + P123 (4%) solution or (c) a L92-pDMAEMA (4%) + P123 (20%) solution into a Dewar containing just pH 5 phosphate buffer (open symbols) or a 0.03% DNA solution in pH 5 phosphate buffer (close symbols). Polymer/DNA interaction heat, Q_{int}, was estimated as the difference between the heat evolved in the presence and absence of DNA (continuous lines). The enthalpy values are referred to the molar amount of L92-pDMAEMA added to the Dewar.

Compared to the demicellization process, when P123 solution (0.04 or 0.20 g/mL) was added to the DNA solution, an endothermic event was observed (ΔH_{int} ~ +45.0 J/mmol; Table 6-2), which suggests an entropy-driven association owing to some hydrophobic and hydrogen bonding interactions between P123 and DNA (which is accompanied by a gain in entropy of the water molecules). This phenomenon may be more intense than in the case of L92 due to the greater molecular weight and the more similar content in both PPO and PEO groups (i.e. hydrogen-bond donors and acceptors).[58,59] The calorimetric profiles of the interaction of the L92-pDMAEMA:P123 with DNA (Figure 6-9) were similar to those recorded for the L92-pDMAEMA solutions without P123 added. However, the initial endothermic process was not observed, which indicates that the interaction with DNA began at slightly lower cationic polymer concentrations, especially in the P123/L92-pDMAEMA 1:1 system.The energy of interaction with DNA (Q_{int}) was lower for the 1:1 copolymer mixture (-0.12 J) than for the 5:1 one (-0.36 J). When referring the energy to the mol of L92-pDMAEMA in the mixture, the enthalpy values were in the range of those obtained with L92-pDMAEMA alone system (Table 6-2). The maximum in heat evolved was achieved for approximately a N:P ratio equals to 1.

6.5 Cell transfection studies

Chinese hamster ovary cells (CHO-K1) obtained from the American Type Culture Collection (Manassas, VA) were grown in F-12 nutrient mixture supplemented by 10% FCS (both from Invitrogen). The cells were seeded in a 24-well plate (Nunc, Roskilde, Denmark) 1 day prior to the transfection at a density of 1×10^5 cells/cm^2 in 500 μL of the growth medium. The cells were 90-95% confluent at the time of transfection. The cells were then transfected with a pCMV-β for the β-galactosidase expression following the manufacturer's protocol developed for Lipofectamine 2000. Lipofectamine 2000 is a liposome-containing formulation combining two lipids such as cationic(2,3-dioleyloxy-*N*-[2(sperminecarboxamide)ethyl]-*N*,*N*-dimethyl-1-popanaminiumtrifluoroacetate) (DOSPA) and neutral dioleyl phosphatidylethanolamine (DOPE). Lipofectamine is

frequently used as an industry standard to compare transfection efficiencies of synthetic vectors.[60] The L92-pDMAEMA and PEO-pDMAEMA were used at different copolymer/DNA weight ratios ranging from 0.6 to 35. The complex of L92-pDMAEMA with Pluronic P123 was also used as a transfection reagent at a ratio of copolymer to P123 of 1:5, 1:50, or 1:500 (w/w). This complex was prepared by mixing (1:1 dilution, v/v) L92-pDMAEMA, 0.1% aqueous solution (pH 7.5), with an aqueous solution of P123, pH 7.5. Dilution of copolymers and copolymer-Pluronic complexes was performed in microcentrifuge tubes of a serum-free medium (50 μL), so that concentration of the transfection reagents ranged from 10 μg/mL to 1 mg/mL. Plasmid DNA solution was also diluted in serum-free medium to a concentration of 16 μg/mL. After a 5-min incubation at room temperature, the DNA solution (50 μl) was added to each tube containing solution of transfection reagents and mixed gently, and after 20 min of equilibration at room temperature, 100 μL of either Lipofectamine/DNA, polycation/DNA, or polycation and P123/DNA complexes was added to each well containing cells with 500 μL of fresh growth medium supplemented with the appropriate amount of FCS. The cells were exposed to the transfection mixture for 3 h. The transfection medium was then removed and replaced with F12 supplemented with 5% FCS. Cells were incubated at 37 °C in a CO_2 incubator (Revco Technologies, Asheville, NC) for 24-72 h.

The effects of the L92-pDMAEMA and Pluronic P123 on the CHO cell growth were further examined by the cell viability tests. The 50% confluent CHO cells were incubated with polymer at final concentrations ranging from 1 μg/mL to 10 mg/mL. After 3 days of incubation at 37 °C, the number of viable cells was measured to determine the concentration of L92-pDMAEMA or Pluronic P123 leading to the death of 50% of the cell population (LD_{50}). The LD_{50} determined for the L92-pDMAEMA was 50 μg/mL, whereas the Pluronic P123 did not show any toxic effects on the CHO cells even at concentrations up to 10 mg/mL. All of the experiments described herein were conducted at polycation concentrations below the LD_{50}.

The β-galactosidase Enzyme Assay System kit (Promega, Madison, WI) combined with a BCA Protein Assay Reagent kit (Bio-Rad Laboratories, Inc., Richmond, CA) was used for assaying β-galactosidase activity in lysates prepared from the

transfected cells following the assay protocol from the manufacturer. In brief, after 24-72 h of transfection, the cells were rinsed twice with PBS and lysed for 15 min at room temperature by a lysis buffer, containing 25 mM Tris (pH 7.8), 2 mM CDTA, 2 mM dithiothreitol, 10% glycerol, and 1% Triton X-100. The resulting cell lysate was scraped from all areas of the plate surface, transferred to a microcentrifuge tube, vortexed, and centrifuged at top speed (20000*g*) for 2 min at 4 °C. The cell lysate (150 μL) was then mixed with 150 μL of Assay 2X buffer, containing 200 mM sodium phosphate (pH 7.3), 2 mM $MgCl_2$, 100 mM β-mercaptoethanol, and 1.33 mg/mL of *o*-nitrophenyl-β-D-galactopyranoside (ONPG) substrate. β-Galactosidase converts the colorless ONPG substrate into galactose and the chromophore *o*-nitrophenol, yielding a bright yellow solution. The mixtures were incubated at 37 °C until a yellow color developed (within ~1 h), and then the reaction was stopped by the addition of 1 M sodium carbonate solution (500 μL). Electronic absorbance was read at 420 nm in a quartz spectrophotometer cuvette using a SpectraMax Plus[384] high-throughput microplate spectrophotometer (Molecular Devices Corp., Sunnyvale, CA). The β-galactosydase activity was calculated as nanomoles of β-galactose formed per minute per milligram of lysate at 37 °C, according to the instruction manual. The electronic absorbance units were also used as a measure of the β-galactosidase expression.

As shown in Figure 6-10, the L92-pDMAEMA copolymer significantly enhances cell transfection in the N/P ratio ranging from 2 to 34, exhibiting a maximum level of β-gal expression at the N/P ratio of 4. Pluronic P123 significantly increased the level of transfection when added to the L92-pDMAEMA composition, resulting in 1.7- and 1.3-fold higher β-gal expressions when compared to the effects of L92-pDMAEMA alone and Lipofectamine, respectively. In contrast to the effects of the L92-pDMAEMA copolymer, the PEO-pDMAEMA copolymer resulted in only very weak β-galactosidase expression, and Pluronic 123 when added to this formulation did not increase the transfection efficacy (Figure 6-10b).

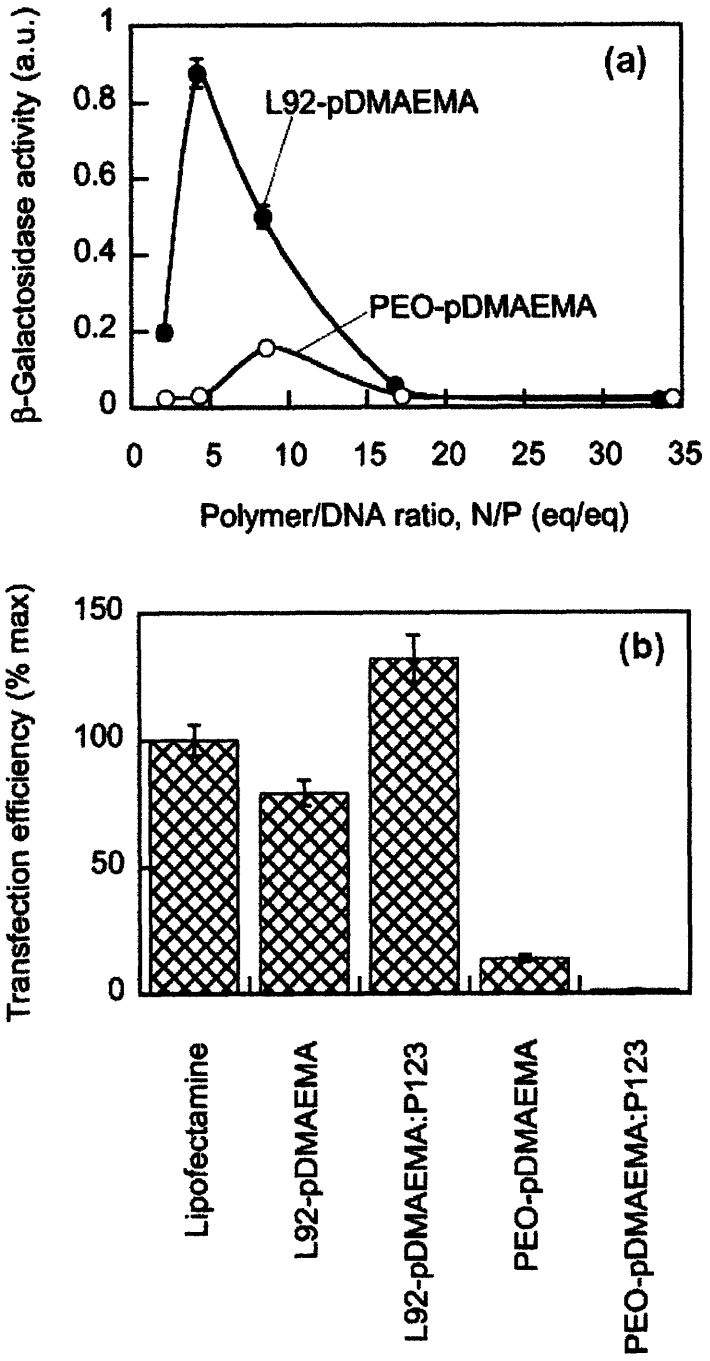

Figure 6-10: Transfection of CHO cells by pCMV-βgal using L92-pDMAEMA and PEO-pDMAEMA copolymers, mixtures of L92-pDMAEMA or PEO-pDMAEMA with 0.005% Pluronic P123 and Lipofectamine as transfection agents (TA). In (a), the 95% confluent CHO cells were transfected with the complexes of L92-pDMAEMA and plasmid DNA at different polymer/DNA (N/P) ratios. The β-galactosidase activity was assayed 48 h after the transfection using the ONPG assay. In (b), the effect of the transfection agents was calculated as the maximum β-galactosidase activity relative to the maximum enzyme activity achieved with the Lipofectamine. All assays were conducted under identical conditions 72 h after the transfection. Measurements were performed in

triplicate, and standard deviations are shown. Statistical significance of the results for each experiment was calculated using Student's t-test (all reported data were characterized by $P<0.01$).

The efficacy of cell transfection by means of cationic polymers is often diminished by serum. However, it has been demonstrated [61] that conjugation of polycations such as poly(ethylene imine) (PEI) with polyethers results in copolymers capable of forming stable complexes in serum. Furthermore, addition of Pluronics to PEI-DNA complexes has been shown to alleviate the reduction of serum-mediated gene transfer to murine fibroblasts.[62]

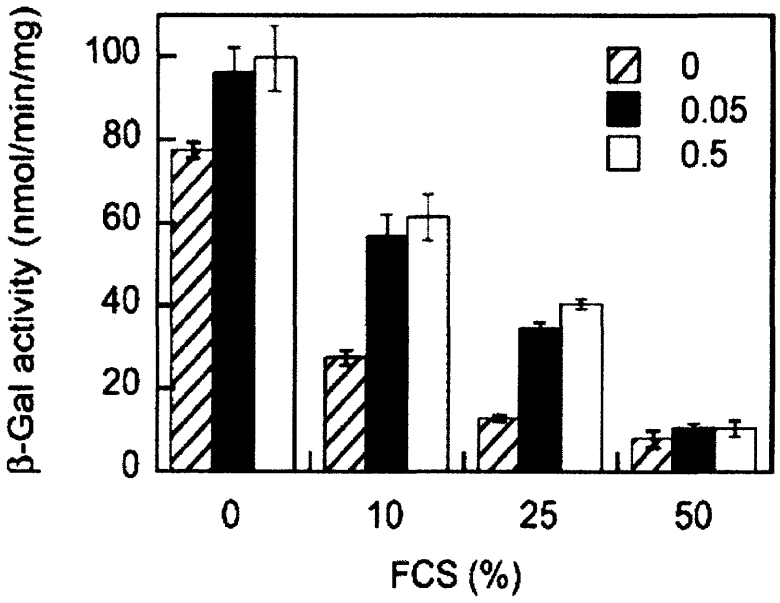

Figure 6-11: Effect of FCS concentration in the medium on β-galactosidase transfection activity. The CHO cells were transfected with L92-pDMAEMA/pCMV β-gal (4:1, w/w) complexes with or without Pluronic P123, added at0.05 or 0.5%. The media contained increasing levels of serum from 0 to 50% FCS. The β-galactosidase activity was calculated as nmoles of β-galactose formed per minute per mg of lysate at 37°C by using ONPG as a substrate. All data were obtained from triplicate. Numbers stand for 0, 0.05, and 0.5% of Pluronic P123 added.

We reasoned that the addition of Pluronic P123 that we observed to significantly enhance the efficiency of transfection (Figure 6-10 b) can help in reducing the deleterious effects of serum. Therefore, the ability of L92-pDMAEMA to mediate DNA transfer at various serum concentrations in the transfection medium was studied. The media tested

contained increasing levels of serum from 0 to 50% and Pluronic P123 from 0 to 0.5%. As is seen in Figure 6-11, the L92-pDMAEMA copolymer alone is more serum-sensitive than the L92-pDMAEMA-P123 complex, when used as a transfection reagent. Addition of FCS to the transfection medium at a 10% level resulted in 2.8- and 1.3-fold lower β-gal expressions when compared to the serum-free medium, when L92-pDMAEMA alone or L92-pDMAEMA-P123 complex was used, respectively. Pluronic P123 increased the transfection activity dramatically and at the same time reduced the serum-mediated inhibition of the DNA transfer.

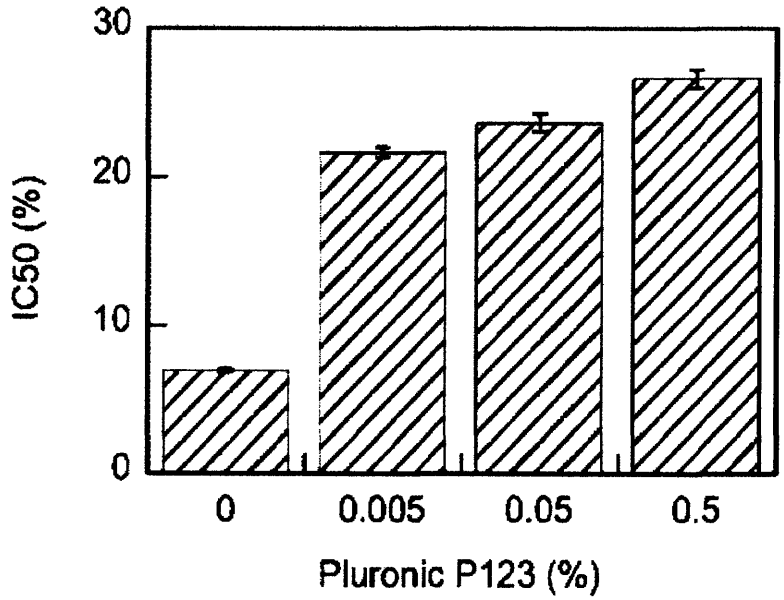

Figure 6-12: Effect of Pluronic P123 on reduction of the serum-mediated inhibition of transfection. The CHO cells were transfected with L92-pDMAEMA/pCMV β-gal (4:1, w/w) complexes with or without added Pluronic P123 (0.005; 0.05 or 0.5%). The results are presented via FCS concentration resulting in 50 % inhibition of transfection activity of L92-pDMAEMA-pCMV-β-gal complex without adding P123 in serum-free conditions (IC50, %)

Figure 6-12 shows the effect of Pluronic P123 on the transfection activity of the L92-pDMAEMA-DNA complex in the serum-containing medium. The results were reported as the percentage of FCS in the transfection medium necessary to cause 50% inhibition of the transfection activity of L92-pDMAEMA-DNA without Pluronic in serum-free conditions (IC_{50}). Remarkably, as little as 0.005% Pluronic P123 helped to increase the IC_{50} from 7 to 22%. This certainly proves shielding of the copolymer-DNA

complexes from the serum by added Pluronic species. One might attribute this protective effect to a steric barrier that Pluronic assemblies with the copolymer-DNA complex create toward the complex-serum interaction.[63]

6.6 Conclusion

A simple synthetic procedure for the free radical polymerization of DMAEMA initiated by polyether radicals that are generated by cerium(IV) has been developed. The procedure results in block copolymers of pDMAEMA and polyethers with high yields. The copolymers of Pluronic L92 with pDMAEMA are highly surface-active at pH 5.0 and 7.0, whereas the PEO-pDMAEMA copolymer is slightly surface-active only at pH 7.0, at which it is sufficiently hydrophobic. The complexes of the L92-pDMAEMA are larger than those of the PEO-pDMAEMA throughout the polymer/DNA range studied. The new block copolymer L92-pDMAEMA combines the surface activity of Pluronic L92 and the strong affinity for DNA of pDMAEMA. The self-assembly of L92-pDMAEMA is promoted in the presence of DNA. Judging by the lower CAC and greater saturation concentration and interaction energy (e.g., –7.2 kJ/mol *vs.* –1.3 kJ/mol at pH 5), the L92-pDMAEMA copolymer is more prone of forming polyplexes with DNA than its more hydrophilic counterpart, PEO-pDMAEMA copolymer. Therefore, the microenvironment of the cationic DMAEMA units, provided by the nature and structure of the polymer to which they are attached, plays an important role in the DNA binding process. Since the ionization of L92-pDMAEMA is pH-dependent, the copolymer affinity for DNA can be modulated in the physiological range, the interaction being stronger at pH 5 than at pH 7. The presence of P123 promotes the interaction process and enhances the solubility of the polyplexes. In the polyplexes, the neutral pDMAEMA-DNA complexes and PPO segments may form a core; the PEO and protonized pDMAEMA segments being oriented towards the aqueous interface. These results explain the high in vitro efficiency of L92-pDMAEMA based-polyplexes, compared to the PEO-pDMAEMA ones, as non-viral gene vectors.

The results shown in Figure 6-10 demonstrate that the L92-pDMAEMA enables transfection efficacy of the plasmid DNA comparable to that achieved with lipid-based

formulations such as Lipofectamine. Furthermore, the addition of Pluronic P123 further increases the carrier efficacy and reduces serum-mediated inhibition of DNA transfer. The new L92-pDMAEMA carrier evaluated in this study has demonstrated analogous or better in vitro properties compared to cationic polymers conjugated with nonionic amphiphilic polymers such as PEI-Pluronic. In addition to this, our polymer is a product of a one-step, robust polymerization procedure, which represents a significant advantage compared to the PEI-Pluronic carriers that are produced by a complex and poorly controlled conjugation chemistry.

Acknowledgements

This research was done in collaboration with Dr. Lev Bromberg from MIT, Prof. Carmen Alvarez-Lorenzo from Universidad de Santiago de Compostela and Dr. Valery Alakhov from Supratek Pharma Inc. The research done at MIT was funded by Cambridge-MIT-Alliance.

6.7 References

1. Ilies, M. A., Seitz, W. A., and Balaban, A. T., Cationic lipids in gene delivery: principles, vector design and therapeutical applications. Curr. Pharm. Des, 2002, 8 (27), 2441-2473.
2. Gebhart, C. L., and Kabanov, A. V., Evaluation of polyplexes as gene transfer agents. J. Controlled Release, 2001, 73, 401-416.
3. Merdan, T., Kopecek, J., and Kissel, T., Prospects for cationic polymers in gene and oligonucleotide therapy against cancer. Adv. Drug Deliv. Rev., 2002, 54 (5), 715-758.
4. Kabanov, A. V., and Kabanov, V. A., Interpolyelectrolyte and block ionomer complexes for gene delivery: physiochemical aspects. Adv. Drug Deliv. Rev., 1998, 30 (1-3), 49-60.
5. Thomas, M., and Klibanov, A. M., Non-viral gene therapy: polycation-mediated DNA delivery. Appl Microbiol Biotechnol., 2003, 62, 27-34.
6. Wagner, E., Strategies to improve DNA polyplexes for in vivo gene transfer: will "artificial viruses" be the answer? Pharm. Res., 2004, 21 (1), 8-14.

7. Nguyen, H. K., Lemieux, P., Vinogradov, S. V., Gebhart, C. L., Guerin, N., Paradis, G., Bronich, T. K., Alakhov, V. Y., and Kabanov, A. V., Evaluation of polyether-polyethyleneimine graft copolymers as gene transfer agents. Gene Ther. 2000, 7 (2), 126-138.
8. Tan, J. F., Ravi, P., Tool, H. P., Hatton, T. A., and Tam, K. C. (2005) Association behavior of biotinylated and non-biotinylated poly(ethylene oxide)-b-poly(2-(diethylamino)ethyl methacrylate). Biomacromolecules, 2005, 6 (1), 498-506.
9. Toncheva, V., Wolfert, M. A., Das, P. R., Oupicky, D., Ulbrich, K., Seymour, L. W., and Schacht, E. H., Novel vectors for gene delivery formed by self-assembly of DNA with poly-(lysine) grafted with hydrophilic polymers. Biochim. Biophys. Acta ,1998, 1380, 354-368.
10. Dubruel, P., and Schacht, E. H., Effect of polyethylene oxide blocks or grafts on the physicochemical properties of poly-(2-N-(dimethylaminoethyl)methacrylate) DNA complexes of polycations and DNA. Bioact. Compat. Polym. 2000, 15, 279-296.
11. Lemieux, P., Vinogradov, S. V., Gebhart, C. L., Guerin, N., Paradis, G., Nguyen, H. K., Ochietti, B., Suzdaltseva, Y. G., Baratakova, E. V., Bronich, T. K., St-Pierre, Y., Alakhov, V. Y., and Kabanov, A. V., Block and graft copolymers and NanoGel copolymer networks for DNA delivery into cell. J. Drug Target. 200, 8 (2), 91-105.
12. Gebhart, C. L., Sriadibhatla, S., Vinogradov, S., Lemieux, P., Alkahov, V., and Kabanov, V. A., Design and formulation of polyplexes based on Pluronic-polyethyleneimine conjugates for gene transfer. Bioconjugate Chem. 2002, 13 (5), 937-944.
13. Ochietti, B., Lemieux, P., Kabanov, A. V., Vinogradov, S., St-Pierre, Y., and Alakhov, V., Inducing neutrophil recruitment in the liver of ICAM-1-deficient mice using polyethyleneimine grafted with Pluronic P123 as an organ-specific carrier for transgenic ICAM-1. Gene Ther. 2002, 14, 939-945.
14. Ochietti, B., Guerin, N., Vinogradov, S. V., St-Pierre, Y., Lemieux, P., Kabanov, A. V., and Alakhov, V. Y., Altered organ accumulation of oligonucleotides using polyethyleneimine grafted with poly(ethylene oxide) or pluronic as carriers. J. Drug Target., 2002, 2, 113-121.
15. Belenkov, A. I., Alakhov, V. Y., Kabanov, A. V., Vinogradov, S. V., Panasci, L. C., Monia, B. P., and Chow, T. Y., Polyethyleneimine grafted with pluronic P85

enhances Ku86 antisense delivery and the ionizing radiation treatment efficacy in vivo. Gene Ther., 2004, 11 (22), 1665-1672.

16. Gene therapy- An Overview, Biotechnology in Perspective, Washington, DC.: Biotechnology Industry Organization, 1990.
17. J. E. Duncan, J. A. Whitsett, and A. D. Horowitz. Pulmonary surfactant inhibits cationic liposome-mediated gene delivery torespiratory epithelial cells in vitro. Hum. Gene Ther. 8:431–438 (1997)
18. N. Ernst, S. Ulrichsko¨tter,W. A. Schmalix, J. Ra¨dler, R. Galneder, E. Mayer, S. Gersting, C. Plank, D. Reinhardt, and J. Rosenacker. Interaction of liposomal and polycationic transfection complexes with pulmonary surfactant, J.Gen.Med,1999, 1(5), 331-340
19. M.X. Tang and F.C. Szoka, The influence of polymer structure on the interactions of cationic polymers with DNA and morphology of the resulting complexes. Gene Ther. 4 (1997), pp. 823–832.
20. De Smedt , S.C., Joseph Demeester, J., and Hennink W.E., Pharm. Res., 2000, 17(2), 113-126
21. Merdan,T. T., Kopeekb, J., and Kissel, T., Advanced Drug Delivery Reviews, 2002
22. Volume 54, Issue 5, 13, Pages 715-758
23. van de Wetering, P., Zuidam, N. J., van Steenbergen, M. J., van der Houwen, O. A. G. J., Underberg, M. J. M., and Hennink, W. E., A mechanistic study of hydrolytic stability of poly(2-dimethylamino)ethyl methacrylate). Macromolecules, 1998, 31, 8063-8068.
24. Tauer, K., Antonietti, M., Rosengarten, L. and Miller, H. (1998) Initiators based on poly(ethylene glycol) for starting heterophase polymerizations: generation of block copolymers and new particle morphologies, Macromol. Chem. Phys., 199, 897-890.
25. Tauer, P. , Westbroek, J,, De Strycker, P., Dubruel, P. , Temmerman, E., and Schacht, E.H. (2002) Flow-through cell for on-line amperometric determination of Ce(IV) during polymerization reactions, Anal. Chem., 74, 915-920.
26. Dubruel, P., and Schacht, E. H. (2000) Effect of polyethylene oxide blocks or grafts on the physicochemical properties of poly-(2-N-(dimethylaminoethyl)methacrylate) DNA complexes of polycations and DNA, Bioact. Compat. Polym., 15, 279-296.

27. Tauer, K., Antonietti, M., Rosengarten, L. and Miller, H. (1998) Initiators based on poly(ethylene glycol) for starting heterophase polymerizations: generation of block copolymers and new particle morphologies, Macromol. Chem. Phys., 199, 897-890.
28. Tauer, P. , Westbroek, J,, De Strycker, P., Dubruel, P. , Temmerman, E., and Schacht, E.H. (2002) Flow-through cell for on-line amperometric determination of Ce(IV) during polymerization reactions, Anal. Chem., 74, 915-920.
29. Nagarajan, S., Sabdham, K. and Spinivasan, V. (1995) Redox polymerization process: an efficient tool for the synthesis of block copolymers, J. Polym. Sci., Polym. Chem., 33, 2925-2933.
30. Vamvakaki, M., Billingham, N. C., and Armes, S. P. (1999) Synthesis of controlled structure water-soluble diblock copolymers via oxyanionic polymerization, Macromolecules, 32 (6), 2088 –2090.
31. Rungsardthong, U., Deshpande, M., Bailey, L., Vamvakaki, M., Armes, S.P., Garnett, M.C., and Stolnik, S. (2001) Copolymers of amine methacrylate with poly(ethylene glycol) as vectors for gene therapy, J. Control. Release, 73(2-3), 359-380.
32. Bromberg, L., Temchenko, M., and Hatton, T. A. (2003) Smart microgel studies: Polyelectrolyte and drug-absorbing properties of microgels from polyether-modified poly(acrylic acid). Langmuir 19 (21), 8675-8684.
33. Bromberg, L., Temchenko, M., and Hatton, T. A. (2003) Smart microgel studies. Polyelectrolyte and drug-absorbing properties of microgels from polyether-modified poly(acrylic acid). Langmuir 19 (21), 8675-8684.
34. van de Wetering, P., Zuidam, N. J., van Steenbergen, M. J., van der Houwen, O. A. G. J., Underberg, M. J. M., and Hennink, W. E. (1998) A mechanistic study of hydrolytic stability of poly(2-(dimethylamino)ethyl methacrylate). Macromolecules,31, 8063-8068.
35. Pr˘a´dny, M., and Sÿ evc˘ik, S. (1987) Precursors of hydrophilic polymers, 7. Potentiometric properties and structure of copolymers of 2-dimethylaminoethyl methacrylate. Makromol.Chem. 188 (2), 227-238.
36. Batrakova, E., Lee, S., Li, S., Venne, A., Alakhov, V., and Kabanov, A. (1999) Fundamental relationships between the composition of pluronic block copolymers

and their hypersensitization effect in MDR cancer cells. Pharm. Res. 16 (9),1373-1379.

37. Kozlov, M. Y., Melik-Nubarov, N. S., Batrakova, E. V., and Kabanov, A. V. (2000) Relationship between pluronic block copolymer structure, critical micellization concentration and partitioning coefficients of low molecular mass solutes. Macromolecules,33 (9), 3305-3313
38. Zhang, R., Liu, J., Han, B., He, J., Liu, Z., and Zhang, J. (2003) Recovery of nanoparticles from $(EO)_8(PO)_{50}(EO)_8$/pxylene/ H2O microemulsions by tuning the temperature. Langmuir,19 (21), 8611-8614.
39. An, S. W., Thomas, R. K., Baines, F. L., Bullingham, N.C., Armes, S. P., and Penfold, J. (1998) Neutron reflectivity of an adsorbed water-soluble block copolymer at the air/water interface: the effects of pH and ionic strength. J. Phys. Chem.B 102, 5120-5126.
40. Krylova, O. O., Melik-Nubarov, N. S., Badun, G. A., Ksenofontov, A. L., Menger, F. M., and Yaroslavov, A. A. (2003) Pluronic L61 accelerates flip-flop and transbilayer doxorubicin permeation. Chemistry 9 (16), 3930-3936.
41. Deshpande, M. C., Garnett, M. C., Vamvakaki, M., Bailey, L., Armes, S. P., and Stolnik, S. (2002) Influence of polymer architecture on the structure of complexes formed by PEGtertiary amine methacrylate copolymers and phosphorothioate oligonucleotide. J. Controlled Release 81 (1-2), 185-199.
42. Nguyen, H. K., Lemieux, P., Vinogradov, S. V., Gebhart, C. L., Guerin, N., Paradis, G., Bronich, T. K., Alakhov, V. Y., and Kabanov, A. V. (2000) Evaluation of polyether-polyethyleneimine graft copolymers as gene transfer agents. Gene Ther. 7 (2), 126-138.
43. Tauer, K., Antonietti, M., Rosengarten, L., and Miller, H. (1998) Initiators based on poly(ethylene glycol) for starting heterophase polymerizations: generation of block copolymers and new particle morphologies. Macromol. Chem. Phys. 199,897-890.
44. Allahham, A.; Stewart, P.; Marriott, J.; Mainwaring, D.E. Int. J. Pharm. 2004, 270, 139-148.
45. Vinogradov, S.V.; Bronich, T.K.; Kabanov, A.V. Bioconjug Chem. 1998, 9, 805-812.

46. Barreiro-Iglesias, R.; Alvarez-Lorenzo, C.; Concheiro, A. Int. J. Pharm. 2003, 258, 165–177.
47. Barreiro-Iglesias, R.; Alvarez-Lorenzo, C.; Concheiro, A. Int. J. Pharm. 2003, 258, 179-191.
48. Nisha, C.K.; Manorama, S.V.; Ganguli, M.; Maiti, S.; Kizhakkedathu, J.N. Langmuir 2004, 20, 2386-2396.
49. Lobo, B.A.; Davis, A.; Koe, G.; Smith, J.G.; Middaugh, C.R. Arch. Biochem. Biophys. 2001, 386, 95-105.
50. Prokop, A.; Kozlov, E.; Moore, W.; Davidson, J.M. J. Pharm. Sci. 2002, 91, 67-76.
51. Mumper, R.J.; Duguid, J.G.; Anwer, K.; Barron, M.K.; Nitta, H.; Rolland, A.P. Pharm. Res. 1996, 13, 701-709.
52. Barreleiro, P.C.A.; Olofsson, G.; Alexandridis, P. J. Phys. Chem. 2000, 104, 7795-7802.
53. Choosakoonkriang, S.; Lobo, B.A.; Koe, G.S.; Koe, J.G.; Middaugh, C.R. J. Pharm. Sci. 2003, 92, 1710-1722.
54. Rungsardthong, U.; Ehtezazi, T.; Bailey, L.; Armes, S.P.; Garnett, M.C.; Stolnik, S. Biomacromolecules 2003, 4, 683-690.
55. Guo, Y.; Sun, Y.; Li, G.; Xu, Y. Molecular Pharm. 2004, 1, 477-482.
56. Gebhart, C.L.; Kabanov, A.V. J. Control. Rel. 2001, 73, 401-416.
57. Gebhart, C.L.; Sriadibhatla, S.; Vinogradov, S.; Lemieux, P.; Alakhov, V.; Kabanov, A.V. Bioconj. Chem. 2002, 13, 937-944.
58. Liu, T.; Nace, V.N.; Chu, B. Langmuir 1999, 15, 3109-3117.
59. Prokop, A.; Kozlov, E.; Moore, W.; Davidson, J.M. J. Pharm. Sci. 2002, 91, 67-76.
60. Mumper, R.J.; Duguid, J.G.; Anwer, K.; Barron, M.K.; Nitta, H.; Rolland, A.P. Pharm. Res. 1996, 13, 701-709.
61. Lampela, P., Soininen, P., Urtti, A., Ma¨nnisto¨, P. T., and Raasmaja, A. (2004) Synergism in gene delivery by small PEIs and three different nonviral vectors. Int. J. Pharm. 270,175-184.
62. Nguyen, H. K., Lemieux, P., Vinogradov, S. V., Gebhart, C. L., Guerin, N., Paradis, G., Bronich, T. K., Alakhov, V. Y., and Kabanov, A. V. (2000) Evaluation of polyether-polyethyleneimine graft copolymers as gene transfer agents. Gene Ther. 7 (2), 126-138.

63. Kuo, J.-H. S. (2003) Effect of Pluronic block copolymers on the reduction of serum-mediated inhibition of gene transfer of polyethyleneimine-DNA complexes. Biotechnol. Appl. Biochem.37, 267-271.
64. Kuo, J.-H. S. (2003) Effect of Pluronic block copolymers on the reduction of serum-mediated inhibition of gene transfer of polyethyleneimine-DNA complexes. Biotechnol. Appl. Biochem 37, 267-271.

Chapter 7
Conclusions and Future work

7.1 Summary of Research

Amphiphilic nonionic copolymers of 4-methacryloyloxyazobenzene and N,N-dimethylacrylamide (MOAB-DMA) were synthesized by simple synthesis method. The copolymers are strongly surface active, an uncommon observation for random copolymers, and exhibit pronounced photoviscosity effects at higher concentrations. An order of magnitude changes in photoviscosity in aqueous medium which was difficult to obtain in aqueous medium[1,2] was seen here. The concentration dependence of the kinetic parameters for the reversible polymer rearrangement upon photoisomerization, as determined by electronic absorption spectroscopy, was seen and attributed to steric hindrances. *Trans*-to-*cis* isomerization under UV light leads to partial dissociation of the azobenzene aggregates that cross-link the polymers, thereby significantly affecting the polymer solution rheology, with a consequent loss of viscoelasticity upon irradiation, especially in concentrated polymer solutions.

In the attempt to enhance the photoviscosity effect further, physical blends of Pluronic F127 and MOAB-DMA were made. The nonionic surface-active polymer MOAB-DMA was seen to interact strongly with the triblock copolymer Pluronic F127. This is a surprising observation in the sense that under normal circumstances it is generally accepted that nonionic surface-active polymers have little or no affinity toward nonionic polymers, particularly at room temperature.[3,4] But the strong interaction is due to the azobenzene solubilizing in the PPO core of the Pluronic F127 micelles. The light-induced trans-cis isomerization of MOAB-DMA alters the interaction of this copolymer with F127 micelles and, as a consequence, modifies the sol-gel temperature of the system. Therefore, it is possible to prepare a liquid system of low viscosity in the dark and to increase the viscosity rapidly when UV light is applied at room temperature. The

dual light- and temperature-responsiveness of the MOAB-DMA:F127 blend can be used as matrix for delivery as well as for separations.

The electrophoretic mobility of solutes were studied in both sol and gel system. The reduction in the electrophoretic mobility of solute in the gel was found to range from 0.75 to 0.3 times depending on the size of the solute for solute size in range of 2 to 6nm. The reduction in the electrophoretic mobility was less as compared to the viscosity changes on gelation as given by Stokes' law. Hence a theoretical prediction of electrophoretic mobility of solutes in both sol and gel system was obtained and compared with experimental data. The blend matrix system containing of micelles was modeled as spheres in different configurations and the solute properties were studied. The model helps to predict the change in electrophoretic mobility for different solute size. The use of the model can be extended to similar sol-gel system such as different Pluronic systems or Pluronic-PAA systems.[5]

The numerical simulations were done to see the effect of change in solute transport properties on the resolution and yield of solute as compared to the conventional non-modulating matrix. The three dimensionless independent parameters defining the separation process were identified. The parameters are Peclet number, the ratio of the velocity of two solutes in the matrix in sol state and the ratio of change in velocity on application of stimuli. The theoretical predictions of the performance variables i.e. yield and resolution were done for different ranges of the parameters. It was seen that the performance variables for parameter ranges studied improved over the conventional non-modulated matrix when proper velocity of light front was used to obtain selective gelation of the matrix for hindering only one of the solute. The improvement ratio was seen to be higher in cases where the peaks are not well resolved to begin with. The numerical simulations were promising to show that alongwith the fact that the responsive matrix can be easily loaded/replaced in microchannels, the separation can be carried out in shorter time or length with improved efficiency using dynamic modulation of the matrix. Separation experiments were done for the proof of concept. For the same length of column and time of electrophoretic separation, the resolution of separation is seen to

be improved over the non-modulating matrix as well as conventional method using polyacrylamide.

Another self-assembling system containing triblock copolymer Pluronic was synthesized for the application in gene therapy. The careful design modification (attaching cationic polymer pDMAEMA) and selection of Pluronics (L92) was done to obtain surface active properties as compared to commonly researched PEO-based polycations. A simple synthetic route was developed for easier and cleaner preparation of polymer for transfection studies. Pluronic L92 polycationic copolymer showed to have similar transfection efficiency as cationic lipid industrial marker Lipofectamine®. In the polyplexes, the neutral pDMAEMA-DNA complexes and PPO segments can form a core; the PEO and protonized pDMAEMA segments being oriented towards the aqueous interface. The presence of Pluronic P123 promotes the interaction process and further enhances the solubility of the polyplexes alongwith reduction of serum-mediated inhibition of DNA transfer. Hence the addition of Pluronic P123 to Pluronic L92-DMAEMA improves the DNA transfection efficiacy even higher than the current industrial marker.

7.2 Future work

The concept of using dynamically modulated system can be further extended to improve the resolution. The electric field can also be modulated such that after a certain resolution is obtained, the polarity of electric field is changed. The stimulus is applied now after electric field reversal to solute 2 such that it is within gel matrix and its velocity is hindered causing a further enhancement in the resolution. The frequency with which the electric field needs to be modulated can be theoretical predicted using numerical simulations. This concept can be applied to magnetic field responsive particles. The chaining of magnetic particles can be brought out by turning on the magnetic field as demonstrated by Singh et. al.[6] The chained magnetic field can form as obstruction barrier for the transport of solutes. If this is done selectively for only one of the solute, this can lead to enhancement of separation. Electromagnets can be used for this purpose as then the control of magnetic field will be easier. The matrix in this case will be of lower

volume fraction and can be potentially used for separation of particles of sizes above 100nm.

7.3 References

1. Irie, M., and Ikeda, T., Photoresponsive polymers. In K.Takemaoto P.M. Ottenbrite, M. Kamachi (Eds.), Functional monomers and polymers, New York: Marcel Dekket, 1997, pp. 665.
2. Irie, M., Adv. Polym. Sci., 1990, 94, 27-67.
3. Goddard, E. D. Interactions of Surfactants with Polymers and Proteins; Goddard. E. D., Ananthapadmanabhan, K. P., Eds.; CRC Press: Boca Raton, FL, 1993.
4. Saito, S.; Anghel, D. F. In Polymer-Surfactant Systems; Kwak, J. C. T., Ed.; Surfactant Science Series Vol. 77; Marcel Dekker: New York, 1998; pp 357-408.
5. Ho, A.K., Bromberg, L.E., O'Connor, A.J., Perera, J.M., Stevens, G.W., Hatton, T.A, Langmuir, 17 (12), 3538 -3544, 2001.
6. Singh, H., Laibinis,P. E. , Hatton T.,A., Langmuir, 2005, 21, 24, pp. 11500-11509